EXCITATION CONTROL OF SYNCHRONOUS GENERATORS IN ELECTRICAL POWER SYSTEMS : DESIGN USING POLE-PLACEMENT AND INVERSE NYQUIST ARRAY TECHNIQUES

Peter Kenneth Muttik, B.E.(Hons), B.Sc.

Department of Electrical Engineering
University of Adelaide

Submitted for the degree of Doctor of Philosophy
in October 1979

TABLE OF CONTENTS

Appendix Page

SUMMARY

This thesis deals with the problem of determining the gains for the terminal voltage and subsidiary feedback signals applied to the excitation systems of synchronous generators in an electric power system. Gain settings which produce satisfactory dynamic behaviour for the generators need to be found.

Conventional excitation control employs fixed feedback gains which are independent of the steady-state operating point. The dynamic performance of a generator with this type of controller varies considerably over the range of possible loading conditions. In the literature there have been a number of proposals for adaptive or adjustable-gain controllers which sense operating point and accordingly adjust the feedback gains for optimum performance.

It is demonstrated that, for the single-machine infinite-bus case, pole-placement using a low-order model of the generator is a straightforward design method for fixed-gain controllers. In addition, such pole-placement can form the basis for simple adjustable-gain control strategies. The effectiveness of various control strategies is assessed over a wide range of steady-state loading conditions with a high-order generator model. The dynamic behaviour of the single-machine infinite-bus system is examined following various minor disturbances and also following serious

three-phase line-to-ground faults near the generator terminals. The effect of modelling and operating point measurement errors on the performance with adjustable-gain controllers is considered.

In order to apply the knowledge gained from the single-machine infinite-bus studies to the design of controllers for multimachine power systems, eigenvector analysis is introduced and used to investigate the changes in behaviour which result from the electrical coupling between generators. A second analysis technique, based on the Inverse Nyquist Array, is developed to provide useful engineering insight into the effect of changes in feedback gain on the dynamic behaviour of the multimachine system.

It is proposed that the design of the excitation controllers for a multimachine power system can proceed in two stages:

(a) Each generator is treated as if it is connected only to an infinite-bus by a reactive tieline. Nominal values for the feedback gains are calculated using pole-placement with a low-order model.

(b) The performance of the multimachine power system with the nominal controller gains is assessed by the computation of eigenvalues and time responses for a detailed model. If the performance needs to be improved, the Inverse Nyquist Array is used to provide guidance as to which feedback gains need to be modified.

The design procedure above is applied to a number of examples involving a four machine power system. It is demonstrated that the pole-placement controllers provide good small-signal performance in a multimachine environment. It is shown that modifications to improve dynamic performance can be easily found using analysis based on the eigenvectors and the Inverse Nyquist Array.

In a multimachine power system it is desirable that the effects of disturbances be localised and prevented from affecting distant generators. The Inverse Nyquist Array provides information concerning the interaction between the generators in a power system. The setting of feedback gains to localise disturbances on the basis of this information is explored.

STATEMENT

This thesis contains no material which has been accepted for the award of any other degree or diploma in any university, and to the best of my knowledge and belief, it contains no material previously published or written by another person, except where due reference is made in the text.

P.K. Muttik

ACKNOWLEDGEMENTS

The author sincerely thanks his supervisor, Dr. M.J. Gibbard, for his valuable advice and guidance throughout the course of this project. The author also thanks Dr. A.M. Parker for his encouragement and acknowledges his aid in providing digital computer programmes for the computation of time responses. The financial support of the Electrical Research Board in the purchase of computing facilities is gratefully acknowledged.

NOTATION

α	real part of a complex pole
β	real pole
ω	imaginary part of a complex pole
ω_1	scale factor in a standard form
ω_s	shaft speed
δ	rotor angle
δ_g	angle between q-axis and terminal voltage
$a_1, a_2, a_3, \ldots$	coefficients in a standard form
D	damping coefficient in rotor equation of motion
f_F	field voltage feedback gain
f_p	electrical power output feedback gain
f_s	shaft speed feedback gain
f_v	terminal voltage feedback gain
f_o	nominal supply frequency in Hz
H	generator inertia constant
$H(s)$	closed-loop transfer function matrix with elements $h_{ij}(s)$
i_d, i_q	direct- and quadrature-axis currents
f_g	governor gain
$K_1, K_2, K_3, K_4, K_1', K_3'$	linearization constants of third-order SMIB model
p	derivative operator d/dt
P	electrical power output
P_m	mechanical power input
Q	reactive electrical power output
$Q(s)$	open-loop transfer function matrix with elements $q_{ij}(s)$

v_a armature resistance

v_e tieline resistance

s Laplace operator

T effective time-constant for generator field winding

T_D direct-axis amortisseur time-constant

T_{ex} exciter time-constant

T'_{do}, T'_{qo} direct- and quadrature-axis transient time-constants

T''_{do}, T''_{qo} direct- and quadrature-axis subtransient time-constants

T_t time-constant in a first-order turbine-governor model

T_{SM}, T_{SR}, T_{CH} servo motor, speed relay and steam chest time-constants in a third-order turbine-governor model

T_w washout network time-constant

V_b infinite-bus voltage

V_{ref} terminal voltage set-point reference voltage

v_d, v_q direct- and quadrature-axis components of terminal voltage

v_t terminal voltage

v'_d, v''_d, v'_q, v''_q voltages proportional to d- and q-axis fluxes

x_d, x'_d, x''_d direct-axis synchronous, transient and transient reactances

x_e tieline reactance

x_q, x'_q, x''_q quadrature-axis synchronous, transient and subtransient reactances

"$^{-}$" denotes the pseudo steady-state value of a variable

"Δ" denotes the perturbation from a steady-state value

(e.g. instantaneous value of power output, $P = \Delta P + \bar{P}$).

Matrices are denoted by letters in italic script.

^ is used to denote an inverse matrix (e.g. $Q\hat{Q} = \hat{Q}Q = I$) or the elements of an inverse matrix (e.g. $\hat{Q}$ has elements $\hat{q}_{ij}$).

CHAPTER 1

INTRODUCTION

This thesis investigates methods for the design of excitation control systems for synchronous generators in electric power systems. The design is an iterative process because the excitation controller must perform satisfactorily in several diverse operating states; the control requirements following events such as the occurrence of a transmission system fault or full load rejection are quite different from the control requirements during normal operation. In this thesis, in keeping with common practice, the excitation controller is designed on the basis of performance for the small perturbations following minor disturbances during normal operation, because linear control theory may be applied under such conditions. The suitability of the resulting design is then assessed for other operating states.

Designing the excitation control system for normal operating conditions involves finding a suitable compromise between the dynamic response of terminal voltage and the damping of electromechanical oscillations following small disturbances (Quazza [1]). Typical minor disturbances are the changing of the terminal voltage set-point, V_{ref}, and small changes in the external power system resulting from switching operations, small load changes, or transformer tap-changing operations.

The design problem is complicated by the fact that the small signal behaviour of a generator is dependent on its steady-state real and reactive power output. If the excitation controller is designed such that the dynamic performance of the generator is optimum at some nominal load, then in general the performance deteriorates as the load is changed from the design value. One way to lessen this deterioration is to make a compromise between high performance and low sensitivity to load changes (Elmetwally [2]).

A few researchers (Outhred [3], Irving [4]) have investigated the possibility of applying model-reference adaptive control to overcome the above problem. The design of such a controller is an involved process - Irving states that the parameters for the reference model and the adaptation process must be chosen with due regard to the variations in the system variables. Extensive testing of this class of nonlinear time-varying controllers is necessary to ensure that they perform suitably for all possible operating circumstances.

A number of authors have proposed somewhat simpler open-loop adaptive control schemes in which measurements are made to determine the generator operating point and then adjustments made to the excitation control in order to maintain optimum performance. This type of controller is termed "adjustable" in this thesis because there is some controversy whether they should be called "adaptive" since they do not actually measure the performance of the system.

The simplest adjustable-gain strategy is that proposed by Venkata Rao [5,6] in which a measurement of the change in generator load angle is used within a Taylor series expansion for the feedback gain. The coefficients of the Taylor series are evaluated at a nominal operating point. This controller offers improved performance over a fixed-gain design but clearly cannot maintain optimum performance when the load is greatly different from the nominal.

Several authors have proposed the measurement of the real and reactive output and the application of linear optimal control theory to calculate controller parameters for best performance. One difficulty in this method is that the time required to solve the resulting matrix Riccati equation rules out real-time computation. Bartlett [7] and Abdel-Magid [8] suggest off-line calculation of the optimal gains at operating points on a grid covering the complex power plane, and the storage of the resulting values inside the controller. Raman [9] proposes the fitting of exponential functions of real and reactive power to the off-line computed gains and the implementation of an electronic controller which calculates its gains using these functions.

A further problem in the application of optimal control is that it is difficult to relate the choice of the elements of the weighting matrix in the quadratic performance index to the physical behaviour of a system. Moussa and Yu [10] choose the elements of the weighting matrix by shifting the dominant eigenvalues of the system. The necessity for this procedure suggests that pole-placement (Jameson [11], Seraji [12]) may result in a simpler, more straight-forward design method than optimal control.

This thesis investigates the design of controllers whose parameters are calculated by assigning the poles of a low-order model of the generator to specified locations. This method is developed in Chapters 2, 3 and 4, and may be applied to design a fixed-parameter controller at a nominal operating point. It can also form the basis for an adjustable parameter control strategy because the calculations are simple enough for real-time computation. The effectiveness of the pole-placement designed controllers is demonstrated by the comparison of their performance with controllers designed by other methods.

The performance of fixed and adjustable parameter controllers is examined over a wide range of operating points in order to determine the loading conditions where the use of an adjustable-gain controller offers a significant improvement in dynamic performance. Operating points for real power outputs between 0.1 and 1.2 p.u. are considered, with reactive power outputs between 1 p.u. lagging and 1 p.u. leading. This range of operation is much wider than that currently feasible because of constraints such as stator end-winding heating at leading power-factor (p.f.), rotor heating at lagging p.f. and security (i.e. transient stability) considerations. Figure 1 shows both the range of operating points which are studied and a somewhat arbitrarily chosen range of "normal" operating points. Current trends such as: increasing difficulty in obtaining transmission line easements, the use of cables in urban areas, and the increasing size of unit ratings mean that in the future there may be advantages to operation at loads which are presently considered abnormal.

Although in general excitation controllers are designed on the basis of the dynamic performance of the generator following small disturbances, the controller has an important role in a number of other diverse operating circumstances. A comprehensive list of the conditions under which the system must operate is given by Glavitsch [13]. With a fixed parameter controller it is important to ensure that the generator behaves satisfactorily in each of the operating states in this list. It is likely that an adjustable control strategy will need to be implemented with the aid of an on-line digital computer; this will also allow a much greater degree of flexibility in designing the performance for each operating mode because the controller parameters can be modified suitably when a change in operating conditions is detected.

Some authors, for example Galiana [14] and Arnold [15] have proposed controllers in which gains are modified during a disturbance, according to its size, in order to implement alternative control characteristics for small and large

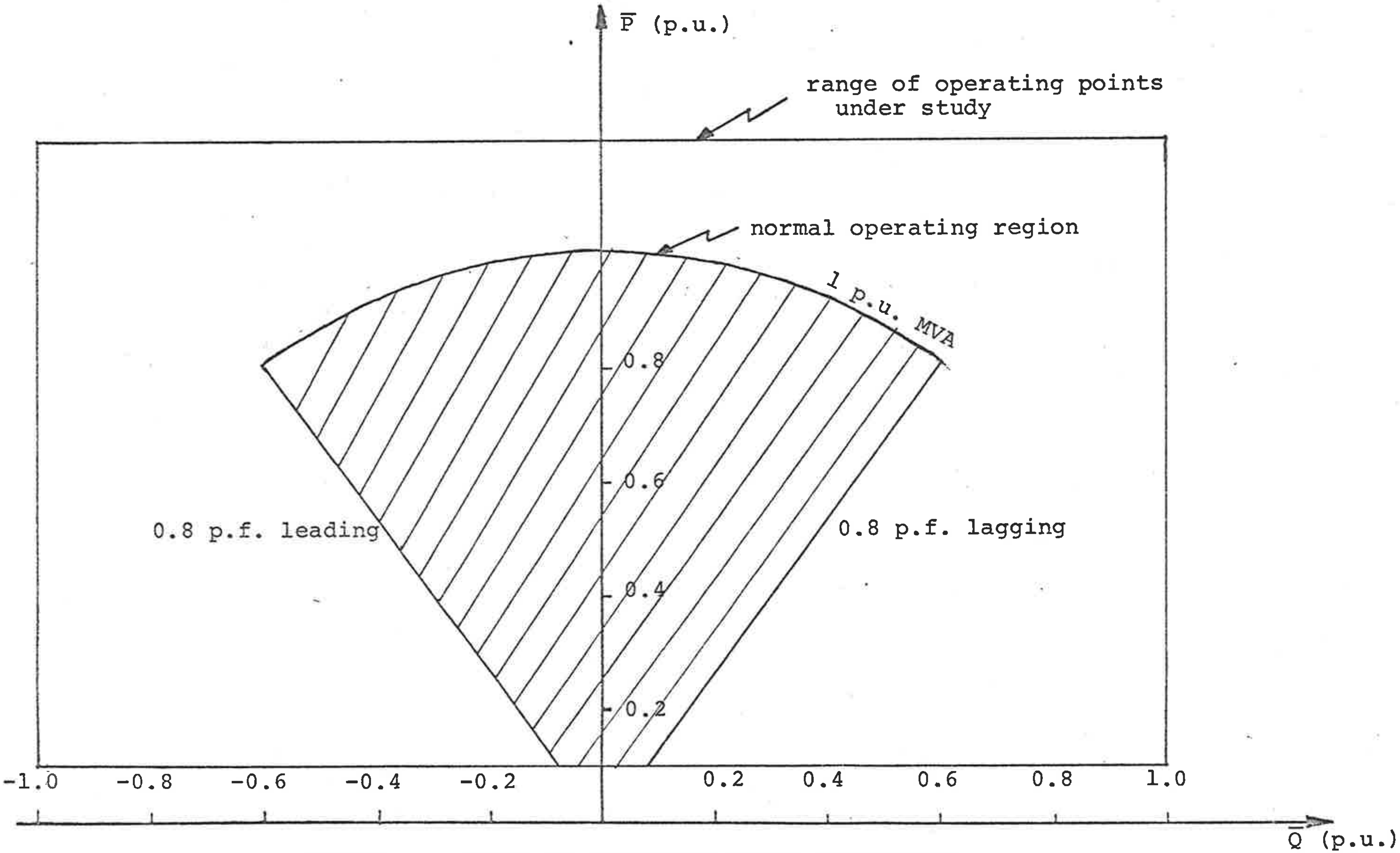

FIGURE 1 RANGE OF OPERATING LOADS CONSIDERED

disturbances. A completely different approach is adopted in this thesis - it is assumed that the adaptation process which adjusts the feedback gains according to steady-state operating points is sufficiently slow that these gains may be considered fixed during any transients. It is shown in Chapter 5 that the pole-placement designs provide suitable control action following major transmission system faults, even if the post-fault tie-line reactance changes due to the non-reclosure of a faulted line.

For the purpose of excitation control system design, it is often assumed that the generator is adequately represented by a simple third-order model ([16], [17]). The errors resulting from the simplifying assumptions used to derive this model are examined in Chapter 5 and the dynamic performance of the pole-placement strategies is assessed with a more accurate model. It is demonstrated that significant errors result at low leading power-factor if the quadrature-axis of the rotor is incorrectly represented.

In common with most controller design methods, the proposed pole-placement method is based on a single-machine infinite-bus (SMIB) model. In practice, the behaviour of a generator is influenced by interaction with generators electrically coupled to it. In Chapter 6 the dynamic behaviour of a simple two-machine infinite-bus system is examined to demonstrate the effects of interaction when two SMIB designs are combined. The philosophy which is adopted is that of using the SMIB model to provide an initial controller design. The performance of the generator in the multimachine situation is then analysed to determine its acceptability and whether improved performance is possible by modifying the controller parameters.

Various methods have been developed to analyse the performance of controllers in multimachine power systems; these are briefly discussed below:

(a) The most direct method is to determine the time-domain response of variables of interest following disturbances to the system. The response may be determined by analogue computation (Aldred [18]), digital computation (Johnson [19], Humpage [20]), tests on a model power system (Evans [21]), or specially designed electronic circuits (Blanch [22]). This method of analysis generally has the advantage that the time taken to determine the performance is relatively short and that it is easy to observe the effect of a change in a controller parameter by repeatedly applying a disturbance and slowly varying the parameter. Although observing the system time response is an effective way of determining whether a proposed design is acceptable, it is not an efficient design technique because the optimum parameter settings can only be found by trial and error.

(b) Analysis of the synchronising and damping torques acting on the generator over the band of possible rotor oscillation frequencies (De Mello [24]) proves to be valuable in providing insight necessary to explain the behaviour of the SMIB pole-placement strategies. Moussa [26] has extended this method to allow the analysis of the interaction between generators in a multimachine power system. However, synchronising and damping torque analysis is not suited to the optimisation of performance because there is no rule for the optimum values of synchronising and damping torque. According to Hamdan [27], a further disadvantage is that there is a nonlinear relationship between the controller parameters and the components of electrical torque.

(c) The analysis of the poles (or eigenvalues) provides insight into the behaviour of a multimachine power system (Undrill [28]). If only one parameter is to be varied in a design process, the root-locus technique (Stapleton [29]) allows the best value to be chosen. Yu [30] and Craven [31] have applied the domain separation technique to power system analysis to show the effect of simultaneously varying two parameters on the real part of the poles of the system. A disadvantage of eigenvalue analysis is that as the order of the model is increased by the introduction of detailed generator and controller models, the number of eigenvalues becomes large and often it is not clear which modes have the greatest effect on the performance. Eigenvector analysis is widely used in certain branches of mechanical and electrical engineering (Goldstein [32], Desoer [33]), but has seldom been applied to the analysis of electrical power systems. Wilson [34] demonstrated its use in attributing the various modes of oscillation to specific generators. A brief resumé of eigenvector theory is included in Chapter 6 where it is applied to analyse the behaviour of the two-machine infinite-bus system.

(d) The Nyquist method of using a polar plot of open-loop frequency response to view the effect of feedback gain has been applied to the design of controllers for SMIB systems (Messerle [35], Jacovides [36]). In recent years much effort has been devoted to extending classical control techniques valid for single-input single-output systems to multivariable systems (MacFarlane [35]). For certain classes of multivariable systems, Rosenbrock [37] has developed a design method based on the Inverse Nyquist Array (INA), a set of Nyquist plots based on the inverse transfer function matrix. This method has been used to design coordinated governor and excitation controllers for a SMIB system (Hughes [27], Ahson [38]). To the best of the author's knowledge, this method has been applied to multimachine power system problems only by Bumby [39] and Muttik [40]. Both papers dealt with a simple two-machine infinite-bus system. Bumby showed that if the generators are made non-interacting for small-signals by the application of cross feedback, the performance following major fault is improved. Muttik showed that interaction between generators may be reduced using only local feedback signals. The INA is a valuable tool in analysing performance because it concisely displays the effect of simultaneously varying parameters in several controllers. Chapter 7 in this thesis is devoted to the application of INA theory to the analysis of power system dynamic behaviour.

The performance of pole-placement designed controllers is investigated in Chapter 8 with a four generator power system incorporating detailed generator models. The performance is examined using eigen-analysis, INA techniques and the computation of time responses.

Significant contributions to knowledge concerning the design of excitation controllers for synchronous generators are made by this thesis:

(a) Simple fixed-gain and adjustable-gain control strategies are developed. These strategies are derived by the application of pole-placement techniques to a low-order single-machine infinite-bus model.

(b) The dynamic behaviour of the SMIB system with the pole-placement control strategies is assessed. The behaviour following small and large magnitude disturbances is examined for a comprehensive range of steady-state loading conditions. Errors arising from simple mathematical modelling of the SMIB system are investigated, especially those due to the omission of rotor iron effects. The effects of errors in the measurement of the steady-state operating condition on the dynamic performance of an adjustable-gain controller are considered.

(c) An approach to the design of excitation controllers for multimachine power systems is developed which utilises the knowledge available for SMIB systems. Initial controller designs are made using the SMIB system pole-placement technique which is developed in this thesis. (A study of simple two-machine infinite-bus power systems in Chapter 6 provides insight into the value of tieline reactance which should be used in this SMIB design.) The dynamic performance of the multimachine system with the initial controller designs is assessed using eigenvector analysis and the computation of the time response following disturbances. If the performance is not satisfactory, then examination of Inverse Nyquist Arrays, together with the eigenvectors provides engineering insight into the modifications in feedback gain settings necessary to improve performance. This use of the eigenvectors extends their usefulness in the analysis of power system dynamic behaviour beyond that suggested by other authors. The effectiveness of the above design approach is illustrated by its application to a three-machine infinite-bus power system.

(d) Multivariable control theory based on the Inverse Nyquist Array is applied to the analysis of power system dynamic behaviour. This theory has not been applied previously to the design of local controllers for multimachine power systems. The INA provides information concerning the effect of changing feedback gains on damping at various oscillation frequencies. It is demonstrated that the Gershgorin bands in the INA give guidance to the gain settings which tend to minimise the dynamic interaction between generators and hence reduce the effects of a disturbance to any generator on electrically distant generators.

CHAPTER 2

POLE-PLACEMENT DESIGN OF EXCITATION CONTROLLERS USING A SIMPLE THIRD-ORDER SMIB MODEL

2.1 PRELIMINARY REMARKS

This chapter describes the development of strategies, based on a simple model of a generator and its control systems, which may be used to adjust the parameters of the excitation control system so that poles of the system lie in specified locations. In this study, for the case where the excitation controller parameters are to be adjusted with changing load to maintain the specified performance, the parameters which are chosen to be adjustable are the gains associated with various feedback signals.

The pole-placement design method is used most simply when the order of the mathematical model of a system is less than or equal to the number of feedback gains which are able to be adjusted independently. Under these conditions, provided the system is controllable, the poles may be assigned to any arbitrary positions (Jameson [11], Fallside [40]). To ensure that an excessive number of feedback signals is not required, it is desirable that the generator and its controllers be represented by the simplest possible models which give an adequate description of their behaviour.

In this chapter, sections 2.2 and 2.3 describe the plant and controller models which are used in the design and list some of the more important assumptions inherent in their use. In sections 2.4 and 2.5 the specification of the position of the system poles is discussed and algebraic expressions are derived for the feedback gains necessary to achieve these positions.

2.2 PLANT MODEL

The plant under consideration consists of two interconnected parts: firstly, the synchronous generator for which the excitation controller is to be designed and secondly, the high-voltage power transmission system and network of loads and generators to which the generator supplies power. For the purpose of this method of controller design the simplest possible model, a Thévenin equivalent circuit, is chosen for the external network; it is assumed the generator may be considered connected to an infinite inertia system by a tieline whose resistance is negligibly small compared to its reactance. The magnitude and angle of the voltage at the "infinite bus" are unaffected by disturbances to the generator. This configuration is often termed a single-machine infinite-bus (SMIB) and has been used for simplicity by many authors (Heffron [41], Regianni [17]).

A synchronous generator is accurately modelled by a large set of non-linear algebraic and differential equations (Shackshaft [42], Reichert [43]). However, it has been found by a number of authors (Outhred [16], Yu [44]) that a linearised third-order model is adequate to describe the small-signal behaviour for the purpose of controller design. The process of deriving such a model for the single generator tieline system is described in the appendices to Reggiani [17]; his model is used in the analysis below. A similar model, which has been used in a number of papers dealing with controller design (DeMello [24], [45]; Yu [44]), is that derived by Heffron [41]. The simple expressions which relate the linearization constants of the Heffron model to those of the Regianni model are listed in Appendix 10.1, so that any expressions derived below in terms of the Regianni linearization scheme may be converted to the more commonly used Heffron form if desired.

A block diagram showing the combined plant and controller models used in this chapter is shown in Figure 2.1. Although the more important assumptions inherent in this SMIB model are given by Regianni, the following list will serve to highlight the extent of the simplification made; it is assumed that:

(1) Speed deviation from synchronous is small so that any variation in terminal voltage due to speed may be neglected. This also means that electrical or mechanical torque is numerically equal to electrical or mechanical power.

(2) The effects of the amortisseur windings may be neglected or compensated for by a damping term proportional to speed in the equation of motion for the rotor. This damping term can be used to account also for positive or negative damping from the speed governor and steam turbine.

(3) The effects of saturation of the iron in the generator are negligible and that the values of time constants and reactances used to describe the behaviour of the plant are sufficiently accurate under all operating conditions.

Transfer functions derived from the 3rd order SMIB model

$$\frac{\Delta v_t}{\Delta v_{ref}} = \frac{f_v(2HK_4 s^2 + DK_4 s + 2\pi f_o(K_1'K_4 + K_3'K_2))}{x}$$

$$\frac{\Delta P}{\Delta v_{ref}} = \frac{f_v(2HK_2 s^2 + DK_2 s)}{x}$$

$$\frac{\Delta \delta}{\Delta v_{ref}} = \frac{-2\pi f_o f_v K_2}{x}$$

$$\frac{\Delta v_t}{\Delta P_m} = \frac{(f_s K_4 - 2\pi f_o K_3' T)s + 2\pi f_o(f_p(K_1'K_4 + K_2K_3') - K_3)}{x}$$

$$\frac{\Delta p}{\Delta p_m} = \frac{(f_s K_2 + 2\pi f_o K_1' T)s + 2\pi f_o(K_1 + f_v(K_1'K_4 + K_2K_3'))}{x}$$

$$\frac{\Delta \delta}{\Delta P_m} = \frac{2\pi f_o Ts + 2\pi f_o(1 + f_v K_4 - f_p K_2)}{x}$$

where $x = 2HTs^3 + (TD + 2H(1 + f_v K_4 - f_p K_2))s^2 + (2\pi f_o TK_1' +$

$f_s K_2 - D(1 + f_v K_4 - f_p K_2))s + 2\pi f_o(K_1 + f_v(K_1'K_4 + K_2K_3'))$

NOTE: K_1, K_2, K_3, K_4, K_1' and K_3' are constants which depend on the terminal voltage and real and reactive power output of the generator (see Appendix 10.3).

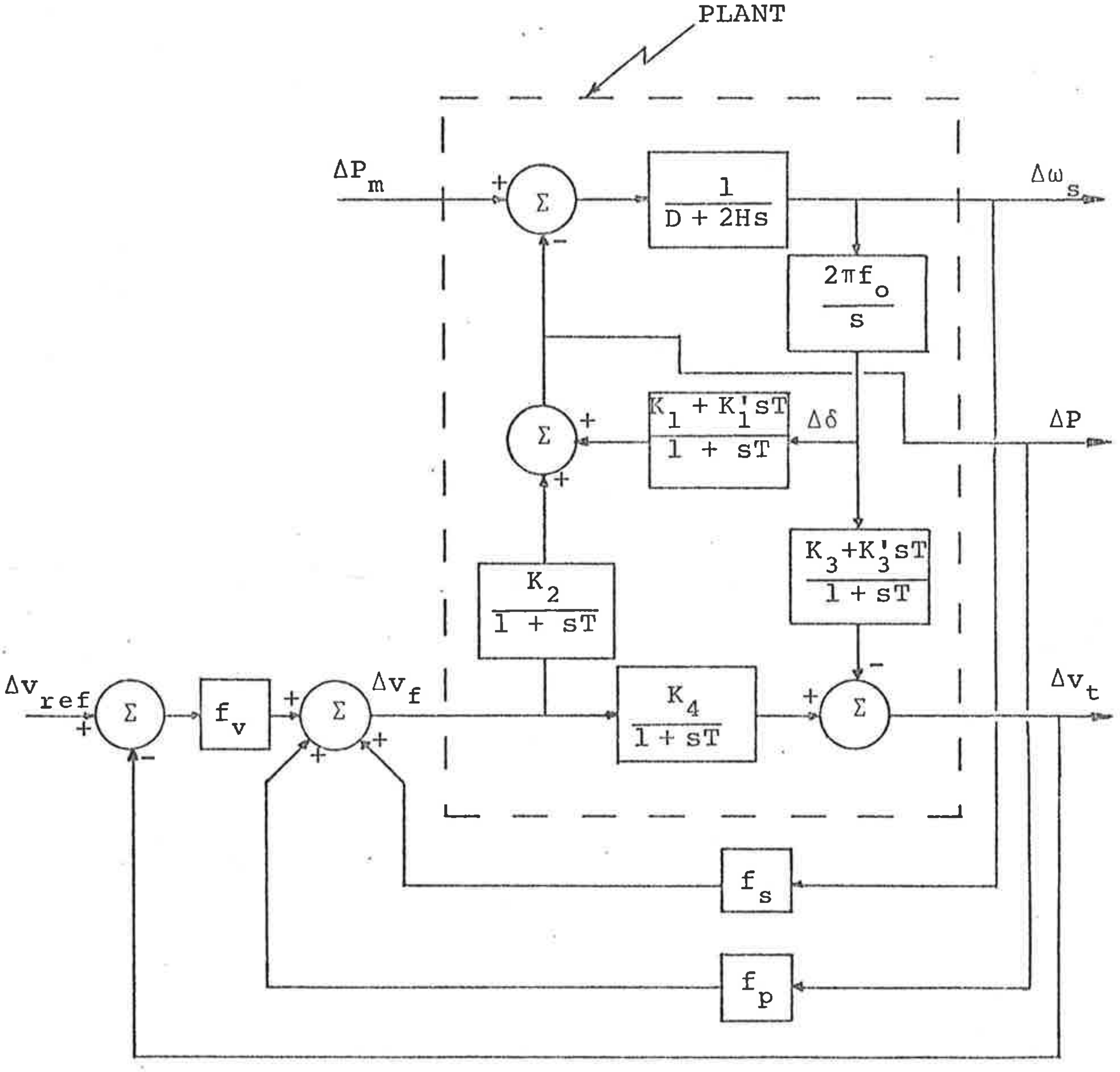

FIGURE 2.1 BLOCK DIAGRAM OF A LINEARISED THIRD-ORDER SMIB MODEL

(4) The quadrature-axis transient reactance equals the quadrature axis synchronous reactance because there is no field winding in this axis.

(5) The external network may be replaced by a Thévenin equivalent circuit.

(6) Transients resulting from changes in the flux linkages in the stator and in the external network reactance decay too quickly to affect dynamic behaviour significantly.

(7) The voltage drops across the resistances of the stator and tieline are small compared with those across the reactances and may be ignored.

2.3 CONTROLLER MODELS

It is usually considered that a synchronous generator has two input quantities - the mechanical torque supplied to its shaft and the field voltage. It is assumed in the following analysis that:

(a) The time constants associated with the behaviour of the speed governor and steam turbine are sufficiently long that the mechanical power or torque may be considered constant.

(b) The time constants of the feedback transducers and amplifiers used in the excitation system are sufficiently short that each feedback loop and the exciter may be represented by a pure gain.

(c) Any filters used to improve voltage regulation, such as lag-lead filters to increase static voltage gain or washout filters to remove steady-state components, have negligible effect on dynamic behaviour.

For simplicity of analysis and design, it is supposed, as stated in Chapter 1, that the adaptation process, which adjusts the feedback gains as the steady state operating point changes, is sufficiently slow that these gains may be considered as constants in calculating the dynamic behaviour of the system.

The block diagram of the plant and controllers is shown in Figure 2.1. It should be noted that the gains f_v, f_s and f_p represent the total gains in the terminal voltage, shaft speed, and electrical power feedback loops respectively.

In practice the signals from the various transducers would be added together at a low power level in amounts determined by the respective loop gains and the sum applied to a high gain exciter in the forward loop.

One important point is that, because one per unit speed has been chosen to be synchronous speed, speed deviations ($\Delta\omega_s$) expressed in per unit tend to be numerically small; consequently the feedback gain f_s is generally large. The value of f_s should be divided by $2\pi f_o$ if speed is to be expressed in radians/second rather than in the per unit form used in this work.

2.4 DERIVATION OF EXPRESSIONS FOR THE FEEDBACK GAINS NECESSARY FOR SPECIFIED POLES

By applying block diagram manipulation techniques to Figure 2.1, it is possible to derive a number of transfer functions describing the perturbations in system variables such as speed, angle or terminal voltage in response to changes in the mechanical power input or the voltage set point. A table in Figure 2.1 lists a number of such transfer functions. The characteristic equation for the closed loop system is found by equating the denominator, which is the same in each case, to zero as shown in equation (2.1).

$$2HTs^3 + (TD + 2H(1 + f_vK_4 - f_pK_2))s^2 + (2\pi f_oTK_1' + f_sK_2 + f_vK_4 + D(1 + f_vK_4 - f_pK_2))s + 2\pi f_o(K_1 + f_v(K_1'K_4 + K_2K_3')) = 0 \tag{2.1}$$

The three roots of the above equation are the poles or characteristic frequencies of the third order model and describe its transient performance. Because the coefficients of s in equation (2.1) are real numbers, the poles will either consist of a pair of complex conjugate roots and a real root, or three real roots. It is assumed below that the former is the case; the derivation of relationships for the case when there are three real roots is similar to that below.

Suppose that the poles of the system are specified to lie at $s = -\beta$ and $s = -\alpha \pm j\omega$ so that the response consists of an exponential component with time constant $1/\beta$ together with an oscillatory component whose damped frequency of oscillation is ω and whose amplitude decays with time constant

$1/\alpha$. An alternative form of the characteristic equation derived from the pole positions is

$$s^3 + (2\alpha + \beta)s^2 + (\alpha^2 + 2\alpha\beta + \omega^2)s + \beta(\alpha^2 + \omega^2) = 0 \qquad (2.2)$$

By equating of the coefficients of powers of s in equations (2.1) and (2.2), equations (2.3), (2.4) and (2.5) are derived. The equations relate the feedback gains f_v, f_s and f_p to the parameters α, β and ω characterizing the pole locations.

$$f_v = \frac{\beta T(\alpha^2 + \omega^2)\left(\frac{H}{\pi f_o}\right) - K_1}{K_1'K_4 + K_2K_3'} \qquad (2.3)$$

$$f_p = \frac{1 + T(D/2H - 2\alpha - \beta) + f_vK_4}{K_2}$$

$$= \frac{1 + T(D/2H - 2\alpha - \beta)}{K_2} + \frac{\beta T(\alpha^2 + \omega^2)\left(\frac{H}{\pi f_o}\right) - K_1}{\frac{K_2}{K_4}(K_1'K_4 + K_2K_3')} \qquad (2.4)$$

$$f_s = \frac{2HT(\alpha^2 + 2\alpha\beta + \omega^2) - 2\pi f_o TK_1' + TD(D/2H - 2\alpha - \beta)}{K_2} \qquad (2.5)$$

D, H, T and f_o are machine constants, independent of operating point. The variables K_1, K_2, K_3, K_4, K_1' and K_3' characterize the operating point; expressions for these variables in terms of the steady-state output are listed in Appendix 10.3.

2.5 THE CHOICE OF POLE LOCATIONS FOR OPTIMUM PERFORMANCE

2.5.1 The relationship between standard forms and poles

The theory of standard forms as developed by Whiteley [46], Graham [47] and in the discussion to Graham's paper, may be adapted to aid in the choice of pole positions for optimum performance.

Suppose the step-response of a third order system is optimised by the minimisation of an integral function of the error between input and output. The resulting characteristic equation may be expressed in the form,

$$s^3 + a_1\omega_1 s^2 + a_2\omega_1{}^2 s + \omega_1{}^3 = 0 \tag{2.6}$$

where ω_1 is a scale factor depending on the size of the coefficient of s^o and the values of a_1 and a_2 show the relative sizes of the coefficients of the higher powers. Standard form theory states that for some classes of transfer functions, if some change is made to the system and the step-response re-optimised using the same error function, it is found that although in general the value of the scale factor is changed, the values of a_1 and a_2 are always the same as before.

If the coefficients of like powers of s are equated in equations (2.2) and (2.6), expressions may be derived relating the coefficients of the standard form for an optimised system to the locations of the poles, as follows:

$$a_1 = \frac{2\alpha + \beta}{[\beta(\alpha^2 + \omega^2)]^{1/3}} \tag{2.7}$$

$$a_2 = \frac{\alpha^2 + 2\alpha\beta + \omega^2}{[\beta(\alpha^2 + \omega^2)]^{2/3}} \tag{2.8}$$

$$\omega_1{}^3 = \beta(\alpha^2 + \omega^2) \tag{2.9}$$

It is easily shown that if the poles for optimum performance are $s = -\alpha_n \pm j\omega_n$ and $s = -\beta_n$ when $\omega_1 = 1$, then, as ω_1 varies, the pole positions for optimum response are at $s = -(\alpha_n \pm j\omega_n)\omega_1$ and $s = -\beta_n\omega_1$. Thus the relative positions of the poles do not change, only the distance from the origin changes proportionally to ω_1. The damping ratio of the complex pair of poles is independent of ω_1. The value of ω_1 may be considered to be a measure of the speed of response of the system; changing ω_1 does not alter the shape of the time response but merely changes its time scale, with large ω_1 producing a short-lived transient. By the comparison of the coefficients of like powers of s in equations (2.1) and (2.6), expressions for the gains f_v, f_s and f_p may be derived in terms of the standard form parameters a_1, a_2 and ω_1, rather than α, β and ω as follows:

$$f_v = \frac{\omega_1{}^3 T\left(\frac{H}{\pi f_o}\right) - K_1}{K_1' K_4 + K_2 K_3'} \tag{2.10}$$

$$f_p = \frac{1 + T(D/2H - a_1\omega_1) + f_v K_4}{K_2}$$

$$= \frac{1 + T(D/2H - a_1\omega_1)}{K_2} + \frac{\omega_1{}^3 T\left(\frac{H}{\pi f_o}\right) - K_1}{\frac{K_2}{K_4}(K_1' K_4 + K_2 K_3')} \tag{2.11}$$

$$f_s = \frac{2HTa_2\omega_1{}^2 - 2\pi f_o TK_1' + TD(D/2H - a_1\omega_1)}{K_2} \tag{2.12}$$

2.5.2 The choice of standard form

Graham investigated a number of integral criteria and found that the integral of time multiplied by absolute-error (ITAE) criterion has high selectivity and leads to a fast well-damped response. In the following work, the pole locations which are specified are those which result in the characteristic equation corresponding to an ITAE standard form.

The values of the standard form parameters a_1 and a_2 which correspond to the minimum ITAE depend on the numerator of the transfer function as well as the denominator. The denominator determines the poles of the system and hence the frequency and damping of the modes in the response, but the size and shape of the response depends also on the relative amplitudes and phase shifts of the modes; these are determined by the numerator.

The zero position-error standard forms investigated by Graham minimise the ITAE for transfer functions which have a numerator independent of s and are of the form

$$\omega_1{}^n/(s^n + a_1\omega_1 s^{n-1} + a_2\omega_1{}^2 s^{n-2} + \ldots + a_{n-1}\omega_1{}^{n-1}s + \omega_1{}^n).$$

Kabriel [48] used this type of standard form to choose the gains for the proportional and derivative signals in a fixed-gain voltage regulator. He found that despite the fact that the numerator of the transfer function between the terminal voltage output and the reference input is frequency dependent, the zero position-error standard form gave a suitable step-response.

Graham gives the coefficients a_1 and a_2 for the third-order zero position-error ITAE standard form to be 1.75 and 2.15 respectively. A hybrid computer test, described in Appendix 10.2, is used to check that these values give the optimum ITAE voltage response for the excitation control system using subsidiary feedback signals. The use of these values for a_1 and a_2 in equation (2.6) shows that the poles lie at $s = -0.71\ \omega_1$ and $s = -0.52\ \omega_1 \pm j\ 1.07\ \omega_1$.

Quazza [1] states a major problem in the design of controllers for small signal conditions is to find a suitable compromise between the speed of voltage response and the damping of electromechanical rotor oscillations. The effective field time constant of the generator is related closely to the position of the real pole, β, whereas the movement of the rotor is identified with the complex poles (Outhred [16]). Extensive tests described in section 3.3.3 show that the zero position-error ITAE pole configuration results in a suitable compromise between damping and voltage response.

2.5.3 The choice of control strategy

(i) Fixed gains - PP/3/FG

Pole-placement may be used to design a conventional fixed-gain excitation control system. A nominal operating point is chosen and the values of f_v, f_s and f_p which give the desired pole locations are calculated. These values are subsequently used at all operating points. This strategy is denoted PP/3/FG to indicate Pole-Placement using a 3rd-order model by the choice of Fixed Gains at a nominal operating point.

Kabriel found that the use of an ITAE standard form in designing a fixed-gain voltage regulator gave a wide limit for dynamic stability and good performance over a wide range of loading conditions.

(ii) Constant pole locations - PP/3/AG/FP

If a_1, a_2 and ω_1 are constants independent of operating point, then the poles of the system do not change with operating point. Equations (2.10) to (2.12) show the way in which f_v, f_s and f_p must be adjusted to achieve this. This strategy is denoted PP/3/AG/FP to indicate Pole-Placement for a 3rd-order model by using Adjustable Gains to achieve Fixed Pole-positions.

(iii) Constant voltage gain and fixed relative pole positions - PP/3/AG/Ff$_v$

When equation (2.7) is rearranged into the form

$$\omega_1{}^3 = \frac{K_1 + f_v(K_1'K_4 + K_2K_3')}{T(H/\pi f_o)} \tag{2.13}$$

an alternative adjustable-gain control strategy is evident. Suppose f_v is held at a fixed value independent of operating point, then ω_1 is determined only by equation (2.13). Because ω_1 is proportional to the cube root of the right hand side of this equation, changes in operating point have a relatively small effect on ω_1. Provided f_s and f_p are varied according to equations (2.11) and (2.12), with ω_1 as determined by equation (2.13), the poles will lie in the correct relative positions for the optimum response at every operating point. This strategy is denoted PP/3/AG/Ff$_v$ to signify Pole-Placement using a 3rd-order model and Adjustable Gains but with a Fixed gain for the terminal voltage feedback loop (f_v).

An advantage of this strategy compared to the fixed pole-position strategy is that only the two subsidiary feedback gains, f_s and f_p, need to be adjustable so that cost may be reduced and the reliability increased.

2.5.4 A summary of the 3rd-order model based pole-placement control strategies

Table 2.2 summarises and compares the three control strategies developed in this chapter. The design stage is shown as the specification of pole positions because the strategies may be used with any desired pole configuration although in this thesis the poles are chosen so that the resulting characteristic equation corresponds to an ITAE standard form.

		PP/3/FG	PP/3/AG/FP	PP/3/AG/Ff$_v$
Design: specify		(a) design operating point. (b) pole locations in terms of α, β, ω or the parameters a_1, a_2 and ω_1.*	(a) pole locations in terms of α, β, ω or the parameters a_1, a_2 and ω_1.*	(a) voltage gain f_v. (b) relative pole positions or the parameters a_1 and a_2.*
Effect of changes in operating point	f_v	none - fixed value.	adjusted according to equation (2.10) or (2.3).	none - fixed value.
	f_s	none - fixed value.	adjusted according to equation (2.12) or (2.5).	adjusted according to equation (2.12).
	f_p	none - fixed value	adjusted according to equation (2.11) or (2.4).	adjusted according to equation (2.11).
	a_1	a_1, a_2: vary, in general do not correspond to any known standard form except at nominal load.	none - fixed value.	none - fixed value.
	a_2		none - fixed value.	none - fixed value.
	ω_1	varies according to equation (2.13).	none - fixed value.	varies according to equation (2.13).
	α	α, β, ω: vary, may be calculated from equation (2.1).	none - fixed value	proportional to ω_1
	β		none - fixed value	proportional to ω_1
	ω		none - fixed value	proportional to ω_1

* Whenever these strategies are used in this thesis the poles are specified to be in positions such that the characteristic polynomial corresponds to a third-order zero-position-error ITAE standard form ($a_1 = 1.75$, $a_2 = 2.15$).

TABLE 2.2 SUMMARY OF CONTROL STRATEGIES BASED ON A THIRD ORDER MODEL

CHAPTER 3

PERFORMANCE OF THE THIRD-ORDER POLE-PLACEMENT STRATEGIES ASSESSED WITH LOW-ORDER SMIB MODELS

3.1 PRELIMINARY REMARKS

In Chapter 2, three strategies for adjusting the feedback gains of an excitation control system are devised by the application of pole-placement methods. This chapter investigates whether the gains required by these strategies are reasonable and compares their performance with that resulting from the use of controllers designed by other methods. For simplicity, only low-order models are employed in this chapter; the effects of more detailed generator and controller modelling are discussed in Chapter 5.

In this chapter, section 3.2 investigates the feedback gains required to implement the pole-placement controllers and examines how these vary with operating point. The effect of various control strategies on the small signal behaviour of the linearised 3rd-order SMIB model of Chapter 2 is examined in section 3.3. The performance after major transmission system faults is investigated in section 3.4 using a non-linear third-order model described in Appendix 10.4.

It may be noted that controllers designed for different sets of system data are used as examples in various parts of this chapter. The reasons for this are to demonstrate that the strategies perform well for a range of parameters, and to allow comparison with other controllers' designs which have appeared in the literature.

3.2 APPLICATION OF THE POLE-PLACEMENT STRATEGIES

3.2.1 The specification of ω_1

The main problem in the design of a controller which maintains the system poles in positions corresponding to the zero position-error ITAE standard form is the choice of the scale parameter ω_1. Several values of ω_1, and the corresponding feedback gains required, are shown in Table 3.1 for a typical case.

The values of ω_1 and the voltage gain f_v are closely related, as shown by equation (2.13). Synchronizing and damping torque concepts (DeMello [24]) may be applied to give a qualitative explanation for the corresponding subsidiary feedback gains required. Consider the different effects of speed and power feedback on rotor oscillations. Ideally a signal proportional to shaft speed deviation added to the field voltage should produce only an electrical damping torque in phase with speed oscillations. However, because of the time constant associated with changes in field flux linkages, the resulting torque not only has a damping component but also a synchronising torque component which is in phase with the oscillations in rotor angle. It can be shown that the increase in synchronizing torque raises the frequency of rotor oscillations. A similar argument may be used to demonstrate that negative feedback of electrical power will also damp rotor oscillations but will tend to reduce their frequency.

row no.	Scale Factor ω_1	Real Pole β (Np/s)	Complex Poles α (Np/s)	ω (rad/s)	Feedback Gains f_v (p.u.)	f_s (p.u./100)	f_p (p.u.)
1	2.5	1.78	1.3	2.68	4.93	-11.9	-13.7
2	5	3.55	2.6	5.35	38.4	2.74	-25.9
3	5.5	3.88	2.85	5.85	50.0	6.57	-27.6
4	7.5	5.33	3.9	8.03	129	27.2	-31.8
5	10	7.10	5.2	10.7	306	61.4	-28.3
6	12.5	8.88	6.5	13.4	597	105.4	-12.3

NOTES:

(a) Because the poles are placed so that the characteristic polynomial is an ITAE standard form, α, β and ω are directly proportional to ω_1 with constants of proportionality 0.52, 0.71 and 1.07 respectively (see section 2.5.2).

(b) When there is no excitation control, ($f_v = f_s = f_p = 0$), the system is unstable and α, β and ω are 0.24, -0.01 and 6.04 respectively.

Operating point: $\overline{P} = 1$ p.u., $\overline{Q} = -0.3$ p.u., $\overline{v}_t = 1$ p.u.

System data: Abdel-Magid parameters (row 3 of Table 3.2).

TABLE 3.1 VARIATION OF FEEDBACK GAIN WITH CHOICE OF ω_1

Because the closed-loop damped frequency of oscillation (ω) is proportional to ω_1, in cases when ω_1 is small such as those near the top of Table 3.1, the excitation controller must cause a reduction in oscillation frequency from the open-loop value. The above discussion shows that this reduction may be achieved together with improved damping by the use of negative power feedback. However, the use of power feedback alone in row 1 of Table 3.2 would result in heavier damping than required, so part of the negative synchronising torque is supplied by a negative speed feedback signal. The damping torque component from such a speed feedback tends to destabilise the system. This is clearly undesirable because the loss of the power feedback signal may cause instability at a normally stable operating point. A similar argument may be used to show that if ω_1 is excessively large the necessary increase in rotor oscillation frequency is obtained by heavy positive speed feedback and on undesirable positive power feedback.

In deciding what value of ω_1 to specify for a given system, several factors must be taken into account:

(1) The closed-loop poles should be large enough to give a fast response, but not so large as to invalidate the third order model. (Outhred [16])

(2) The value of f_v should be large enough to cause ceiling voltage during major system faults, but not so large as to invalidate the third order model. (See section 4.1)

(3) There should be no negative damping torques associated with the speed or the power feedback signals.

(4) The speed and the power feedback gains should not be so large as to cause undue modulation of the terminal voltage during small disturbances. (Quazza [1])

If a suitable compromise between the pole positions and the feedback gains can not be found, it is necessary to review the choice of relative pole positions. If a_1 and a_2 are changed, the relative pole positions and the feedback gains f_s and f_p required for a given ω_1, all take on new values. However, controllers have been successfully designed using ITAE pole-placement for each of the sets of data in Table 3.2. Choosing a value of ω_1 of approximately six gives a closed-loop damped frequency of oscillation near 1 Hz ($\omega \approx 2\pi$ rad/s) and a settling time of the order of 1 second for the voltage response. Typically, this requires a value of f_v in the range 40-100 p.u.

3.2.2 Variation in the feedback gain requirements with load

Section 3.2.1 describes the factors which must be taken into account when applying the pole-placement design method. This section investigates the way in which the feedback gains required to implement the adjustable gain strategies depend on operating point. The PP/3/FG strategy uses fixed gains and is discussed in section 3.3.1.

Consider again the example used in the previous section,

Row	x_d (p.u.)	x_q (p.u.)	x'_d (p.u.)	T'_{do} (sec.)	x_e (p.u.)	H (p.u.)	D (p.u.)	f_o (Hz)	f_v (p.u.)	Source
1	2.65	2.65	0.45	4.2	0.3	2.73	5.46	50	30,50	Outhred [16]
2	1.75	1.68	0.285	3.68	0.3	3.82	2.26	60	50,70 200	Dandeno [56], Wilson [52], Raina [46]
3	1.6	1.55	0.32	6.0	0.4	5.0	0	60	50	Abdel Magid [8]
4	2.2	2.1	0.44	6.05	0.6	2.65	0	50	60	Reichert [44] with x_e increased from 0.3 to 0.6
5	1.8	1.7	0.3	5.0	0.5	3.5	0	50	70	formed from typical parameters

TABLE 3.2 SMIB SYSTEM DATA FROM VARIOUS SOURCES

which shows the feedback gains necessary to implement pole-placement at a nominal operating point ($\bar{P}$ = 1 p.u., $\bar{Q}$ = -0.3 p.u.). The feedback gains and poles in row 3 of Table 3.1 satisfy all of the requirements listed in section 3.2.1.

(a) Fixed pole-positions

Suppose the PP/3/AG/FP strategy is employed to maintain the poles at s = -3.88 and s = -2.85 ± j 5.85 for all operating points, then Figure 3.1 shows the necessary feedback gains as functions of load. The speed and power feedback gain requirements are quite differently from that of the voltage gain. Analysis of equations (2.10) to (2.12) reveals that the gain variations are mainly due to changes in the denominator functions. The denominator of the voltage gain expression is $(K_1'K_4 + K_2K_3')$ but that of the speed and power gain expressions is simply K_2. The values of $(K_1'K_4 + K_2K_3')^{-1}$ and $K_2{}^{-1}$ are plotted as functions of load in Figure 3.2.

Comparison of Figures 3.1(a) and 3.2(a) confirms the fact that the behaviour of the voltage gain is governed mainly by $(K_1'K_4 + K_2K_3')^{-1}$. The value of $(K_1'K_4 + K_2K_3)$ is related to the change in electrical torque produced by a perturbation in rotor angle. It is small under low excitation conditions, which occur when the real power output is small and the reactive power is approximately equal to $\frac{-\bar{V}_t{}^2}{x_q}$.

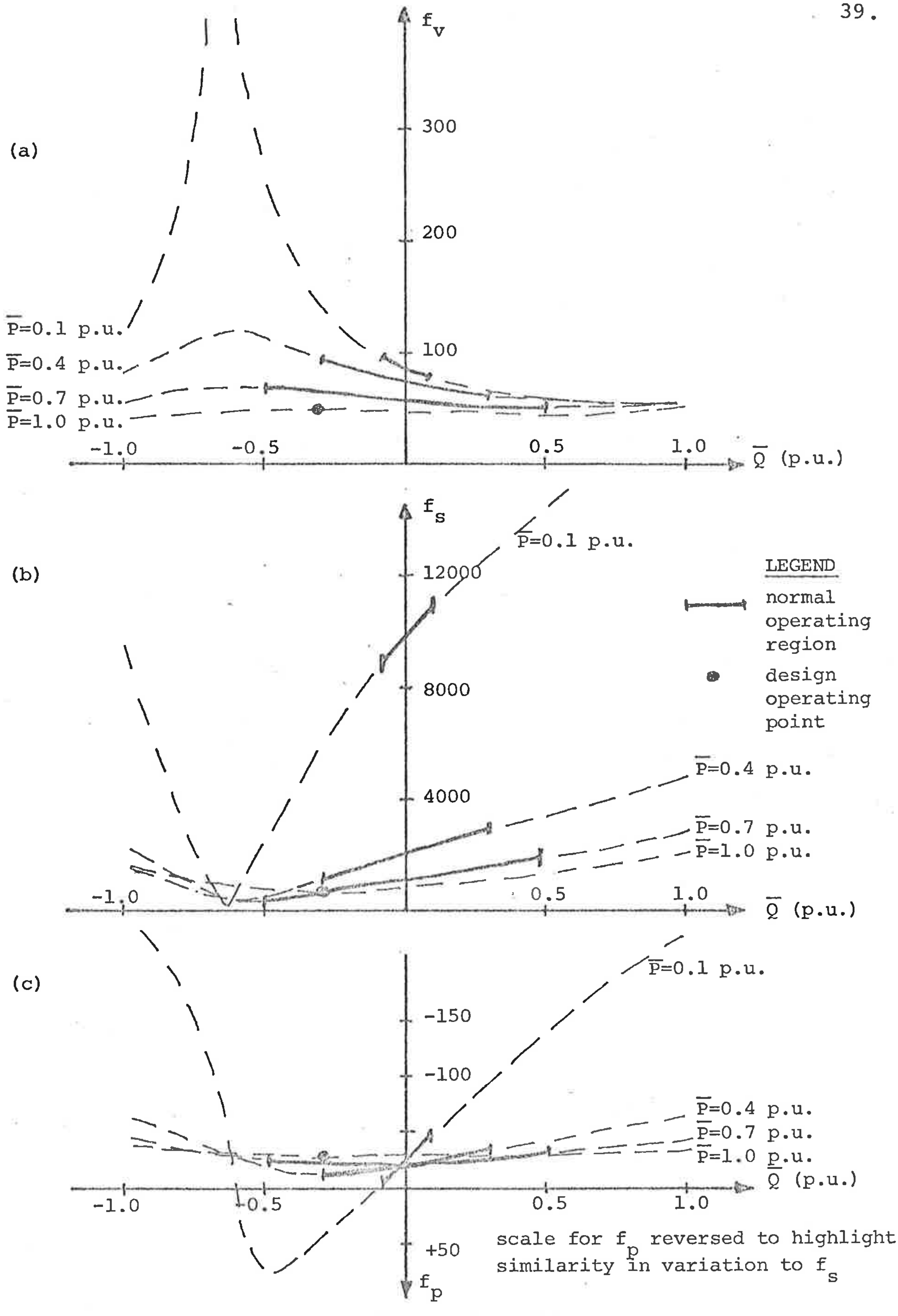

FIGURE 3.1 TYPICAL VARIATION IN FEEDBACK GAIN WITH LOAD FOR THE PP/3/AG/FP STRATEGY

(gains calculated to maintain poles at $s = -2.85 \pm j5.85$ and $s = -3.88$ for system having data in row 3 of Table 3.2)

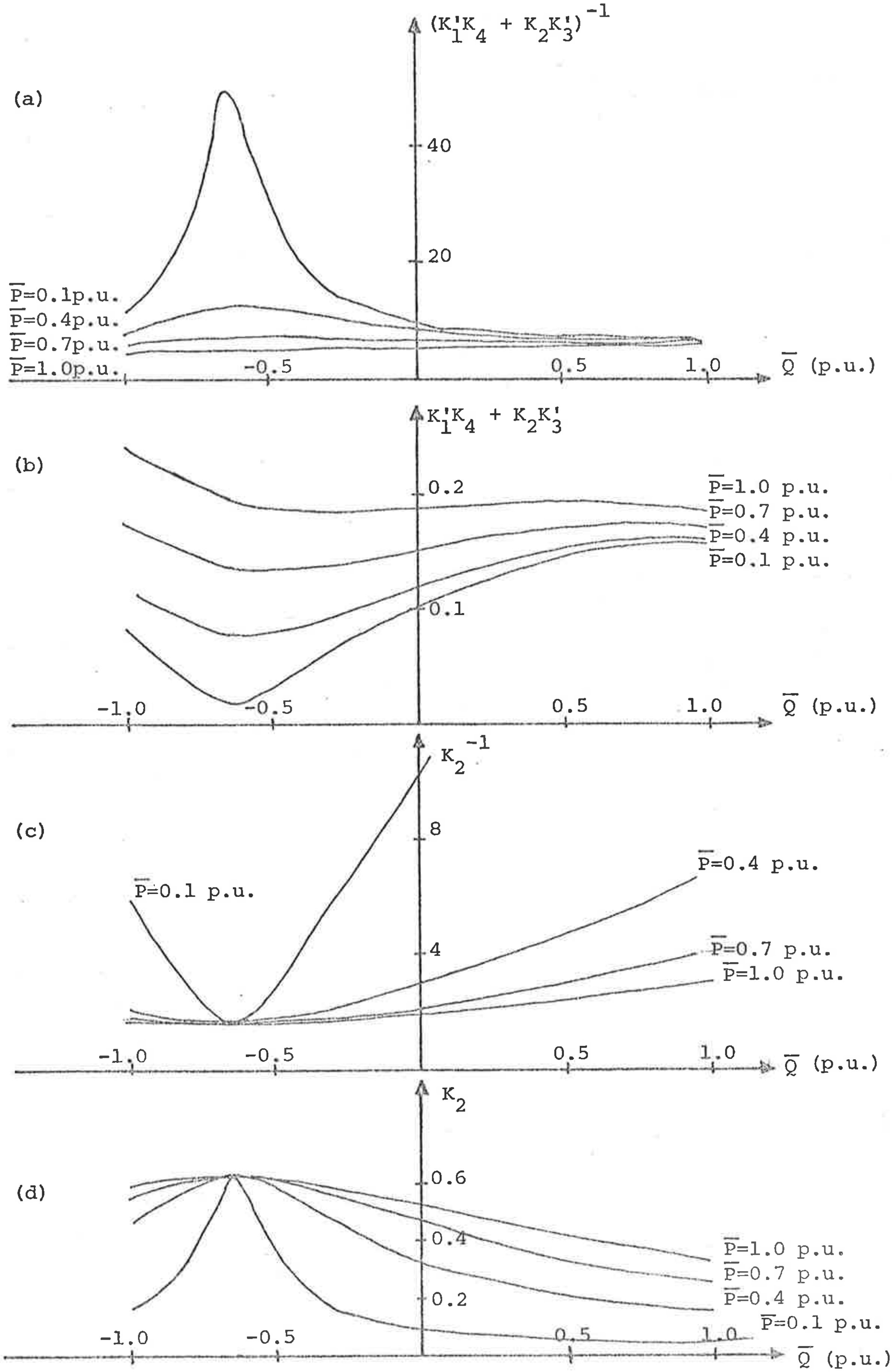

FIGURE 3.2 TYPICAL VARIATION IN THE VALUES OF OPERATING POINT DEPENDENT PARAMETERS

(calculated for system with data in row 3 of Table 3.2)

Comparison of Figures 3.1(b) and (c) with Figure 3.2(c) confirms the fact that the behaviour of the subsidiary gains is governed mainly by K_2^{-1}. The value of K_2 describes the change in electrical torque produced by a change in field voltage. It depends on cos δ_g, where δ_g is the angle between the terminal voltage and the quadrature axis, and is small for low lagging power factor loads.

(b) Fixed relative pole-positions and fixed voltage gain

Suppose the PP/3/AG/Ff_v strategy is employed with the voltage gain (f_v) chosen to be 50 as in row 3 of Table 3.1. The relative positions of the poles do not change, but their distance from the origin depends on ω_1. In part (iii) of section 2.5.3 it is argued that the value of ω_1 should not vary greatly with load. Figure 3.3(a) shows that this is true except for operation at low excitation. Equation (2.13) suggests that ω_1 depends mainly on $(K_1'K_4 + K_2K_3')$, and comparisons of Figures 3.2(b) and 3.3(a) shows a similar load dependence.

The subsidiary feedback gains required by the PP/3/AG/Ff_v strategy are plotted as a function of load in Figures 3.3(b) and (c); comparison with Figures 3.1(b) and (c) shows that the values are similar to those required by the PP/3/AG/FP strategy. This is not surprising since equations (2.11) and (2.12) are used in both strategies. For the fixed-pole strategy the value of ω_1 substituted into these equations is a constant and for the other strategy it is not heavily dependent on load.

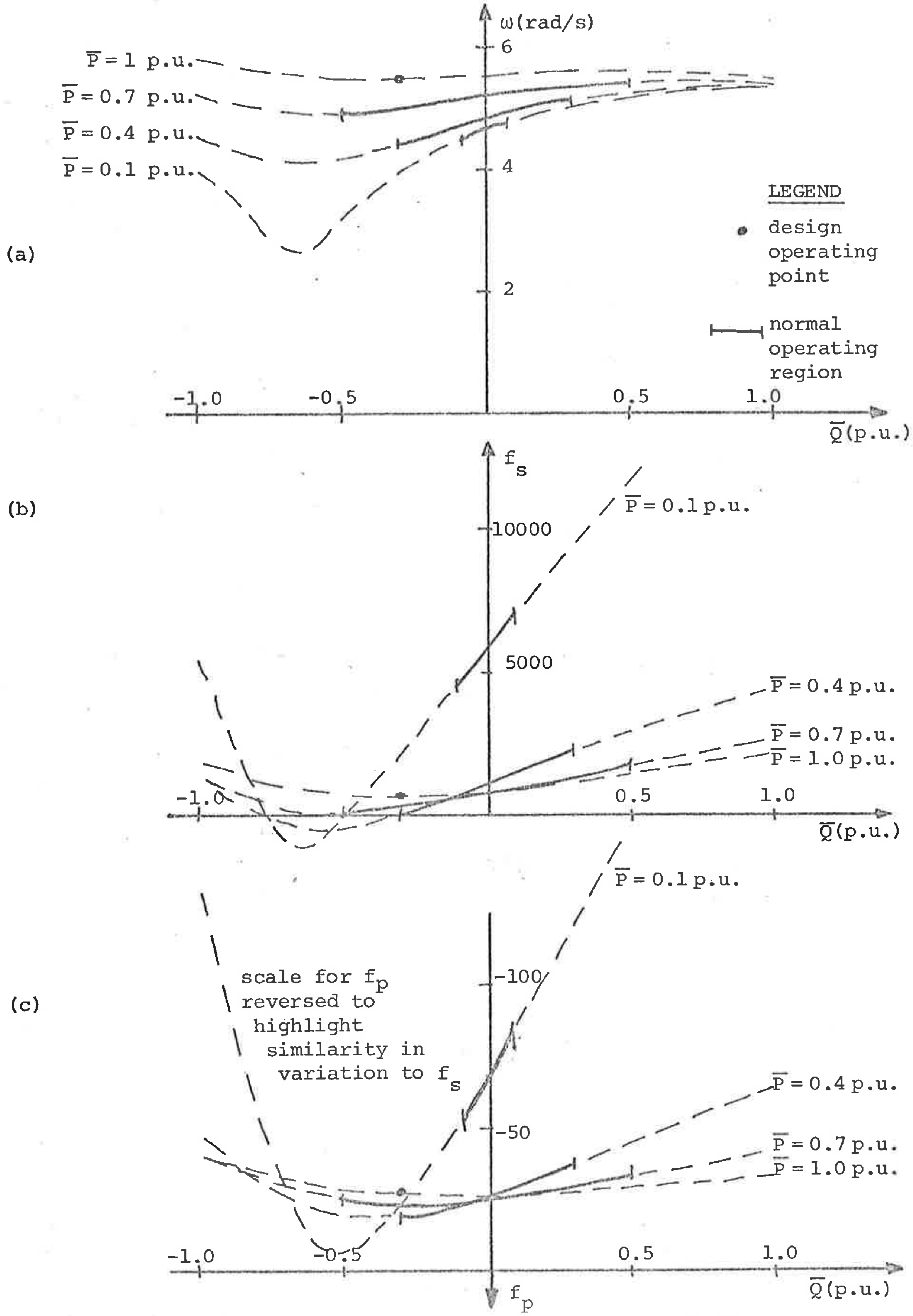

FIGURE 3.3 TYPICAL VARIATION IN THE FEEDBACK GAINS WITH LOAD FOR THE PP/3/AG/Ff$_v$ STRATEGY

(system data in row 3 of Table 3.2, controller designed to maintain ITAE pole configuration with $f_v = 50$)

(c) The strong effect of K_2 and $(K_1'K_4 + K_2K_3')$ on the feedback gains necessary for optimum performance is not unique to the pole-placement design method, similar behaviour may be noted in the following cases:

(a) Bartlett [7] applied linear optimal control theory to the design of an adjustable feedback gain controller. Similar trends to those in Figure 3.1 are evident in his plots of the resulting feedback gains.

(b) Abdel-Magid [8] designed a controller in which the voltage gain is fixed, and the gain and time constant of a filter producing a power-based stabilising signal are adjusted so as to minimise an integral performance criterion. (For further details see part (ii) of section 3.3.2) The values of his time constant (T_{AM}) and gain (K_{AM}) are plotted as functions of load in Figure 3.4; the gain clearly varies in a similar fashion to the subsidiary gains in Figure 3.3 and K_2^{-1} in Figure 3.2.

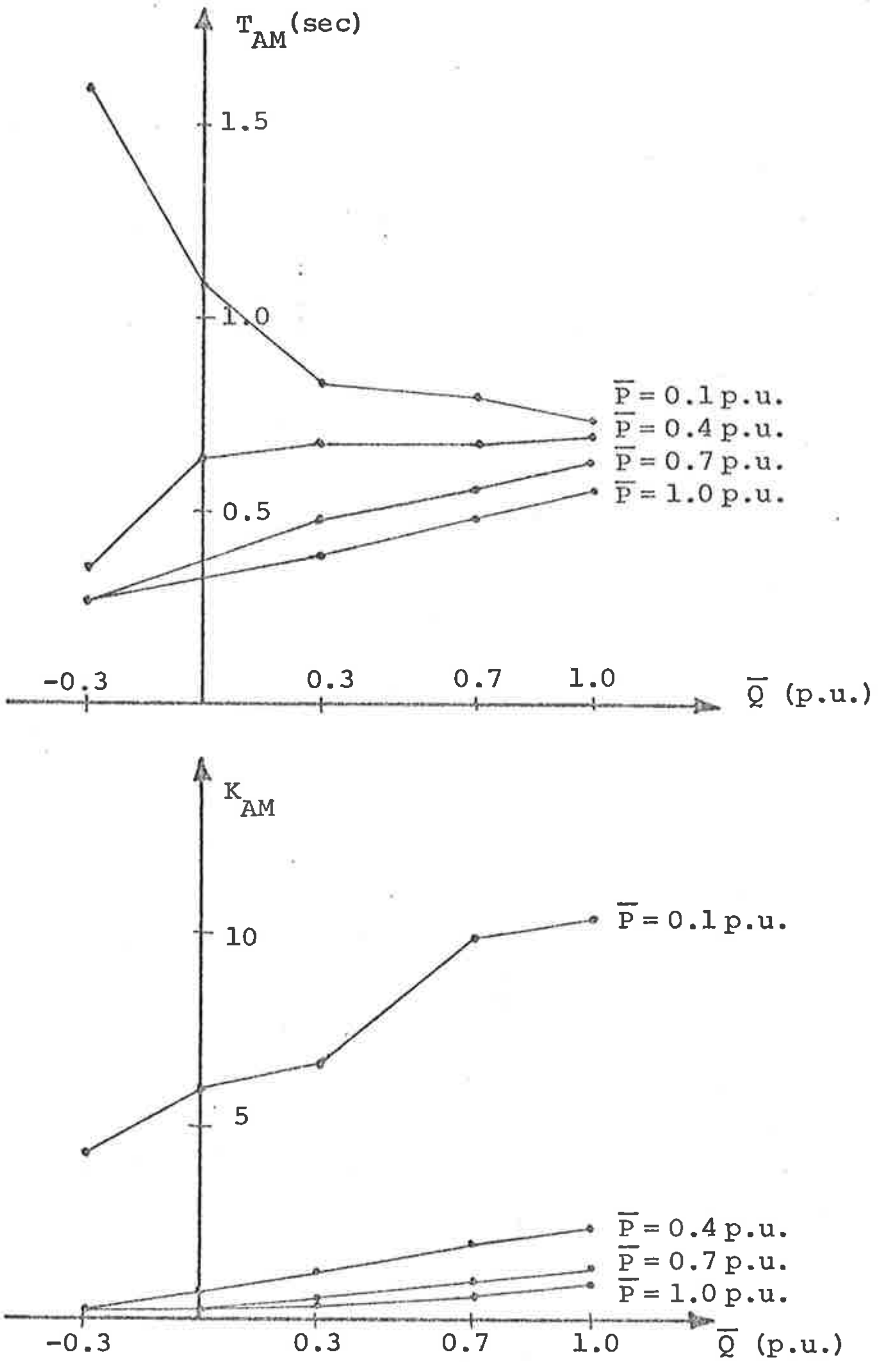

FIGURE 3.4 TIME-CONSTANT AND GAIN SETTINGS FOR ABDEL-MAGID'S CONTROLLER

(points marked • denote values listed in [8])

3.3 SMALL-SIGNAL BEHAVIOUR OF THE SMIB SYSTEM

3.3.1 PP/3/FG and other fixed-gain excitation controller designs

A study was undertaken to determine the effect of changing real and reactive load on the dynamic performance of generators equipped with fixed-gain excitation systems. The aims of the study were:

(i) To identify the operating points at which there is a significant deterioration in performance when a controller is designed simply on the basis of operation near rated-load.

(ii) To investigate the suitability of the PP/3/FG pole-placement strategy for designing fixed-gain excitation systems.

The method employed was to calculate the poles at a grid of operating points covering the rectangular study region in Figure 1. Table 3.2 lists the different sets of system parameters which were tried. Controllers designed by PP/3/FG pole-placement and several other methods ([16], [61]) were studied. Moderately low values of voltage gain were chosen in most cases because the third order model is not valid for high f_v (see section 4.1). Only controllers which give heavy damping of rotor oscillations by the use of subsidiary feedback signals were considered in this study.

The results of the study may be illustrated by the comparison of the behaviour of a SMIB system resulting from the use of two different controller designs. Figure 3.5

shows the effect of varying load on a controller which was designed by Outhred [16] to give wide stability limits and heavily damped rotor oscillations. The positions of the poles are plotted in Figure 3.6 for the same system when the feedback gains are chosen instead by PP/3/FG pole-placement with a design operating point with $\overline{P} = 0.9$ p.u. and $\overline{Q} = 0.1$ p.u. Figure 3.7 compares the response of these designs following a step in voltage set-point.

(i) Deterioration in performance with load

Despite the fact that the pole locations and step-responses in these two cases are quite different, comparison of Figures 3.5 and 3.6 shows that the movements of the poles resulting from changes in load are similar.

At leading power factor there is a tendency for the real pole to move towards the imaginary axis so that the time constant of the exponential mode increases. The exponential mode is at its slowest when the reactive load is approximately $\dfrac{-\overline{v}_t^{\,2}}{x_q}$.

The leading power factor stability limit lies well outside the normal operating region. Except for a small region at very low power, stability is lost by growing oscillations. At lagging power factor there is a steady decline in the damping of the oscillatory mode as the reactive load increases. However, the stability limit lies well outside the normal operating region and often outside

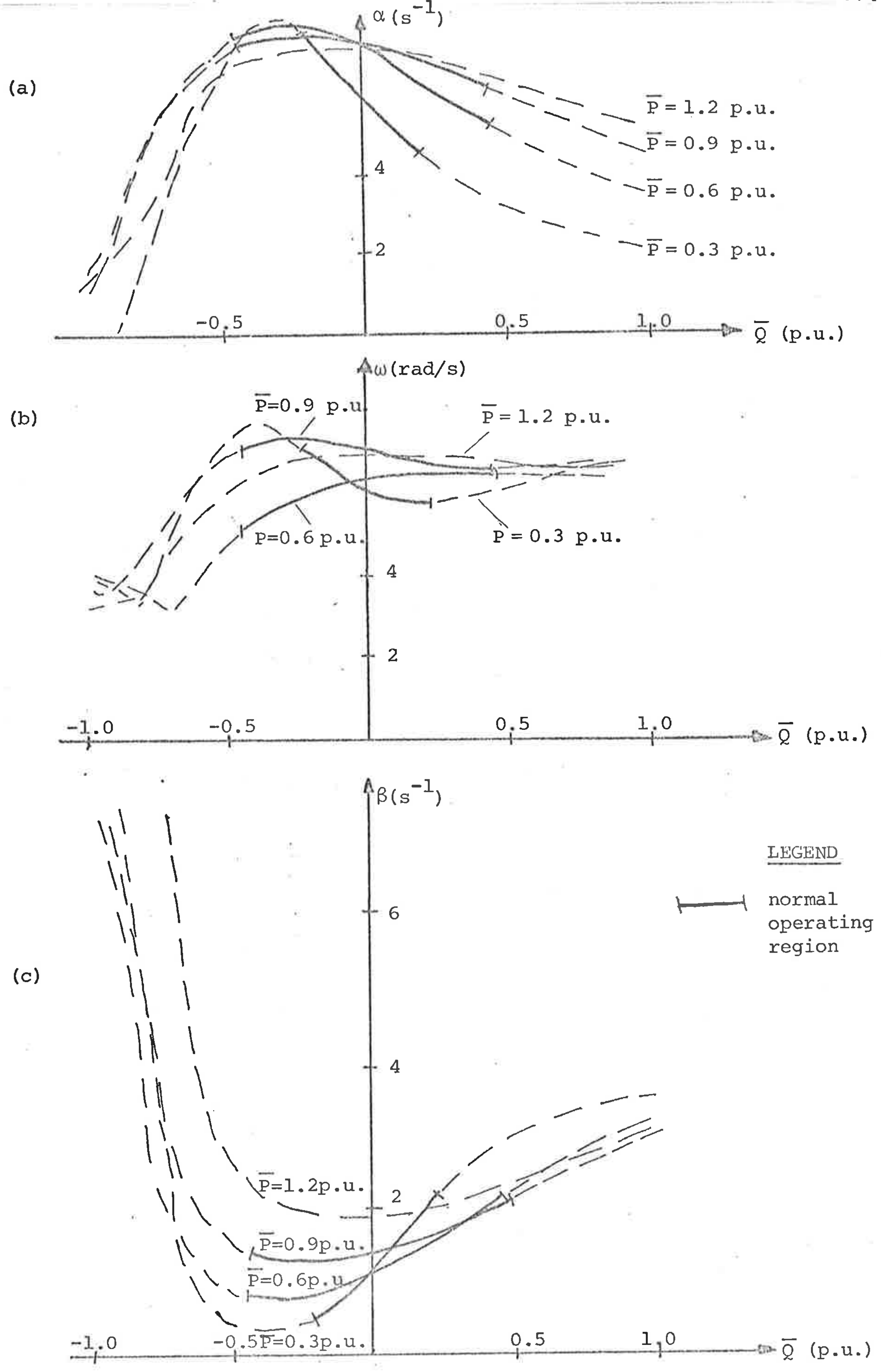

FIGURE 3.5 EFFECT OF LOAD ON THE POLE-POSITIONS WITH OUTHRED'S FIXED-GAIN CONTROLLER DESIGN

(system data in row 1 of Table 3.2, $f_v = 30$, $f_s = 722$, $f_p = -40.3$, $\bar{v}_t = 1$ p.u.)

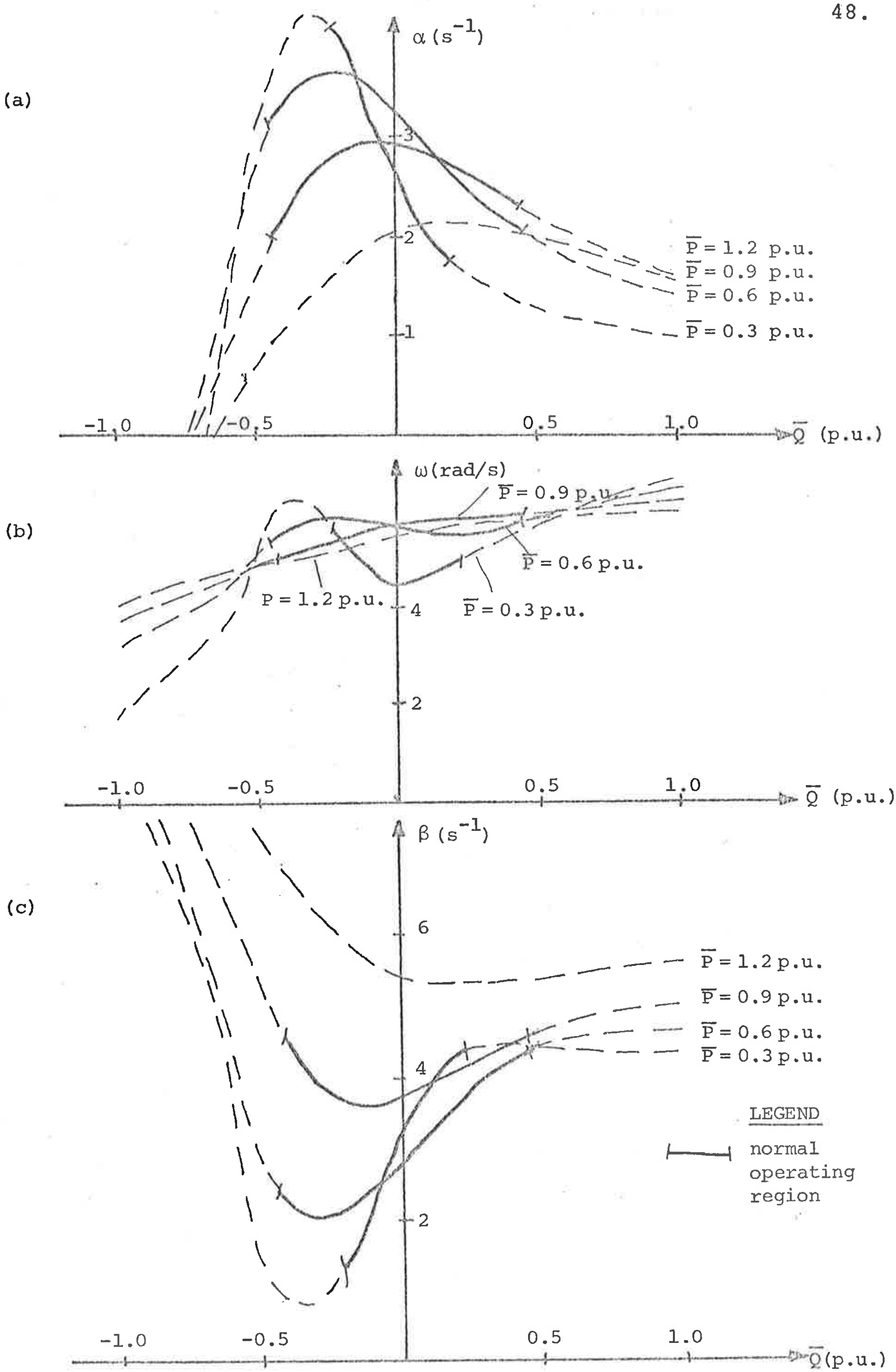

FIGURE 3.6 EFFECT OF LOAD ON THE POLE POSITIONS WITH A PP/3/FG FIXED-GAIN CONTROLLER

(system data in row 1 of Table 3.2, $f_v = 30$, $f_s = -222$, $f_p = -19.7$, $\overline{v}_t = 1$ p.u. Controller designed to have $\alpha = 2.8$, $\beta = 3.8$, $\omega = 5.8$ $\overline{P} = 0.9$ p.u. and $\overline{Q} = 0.1$ p.u.)

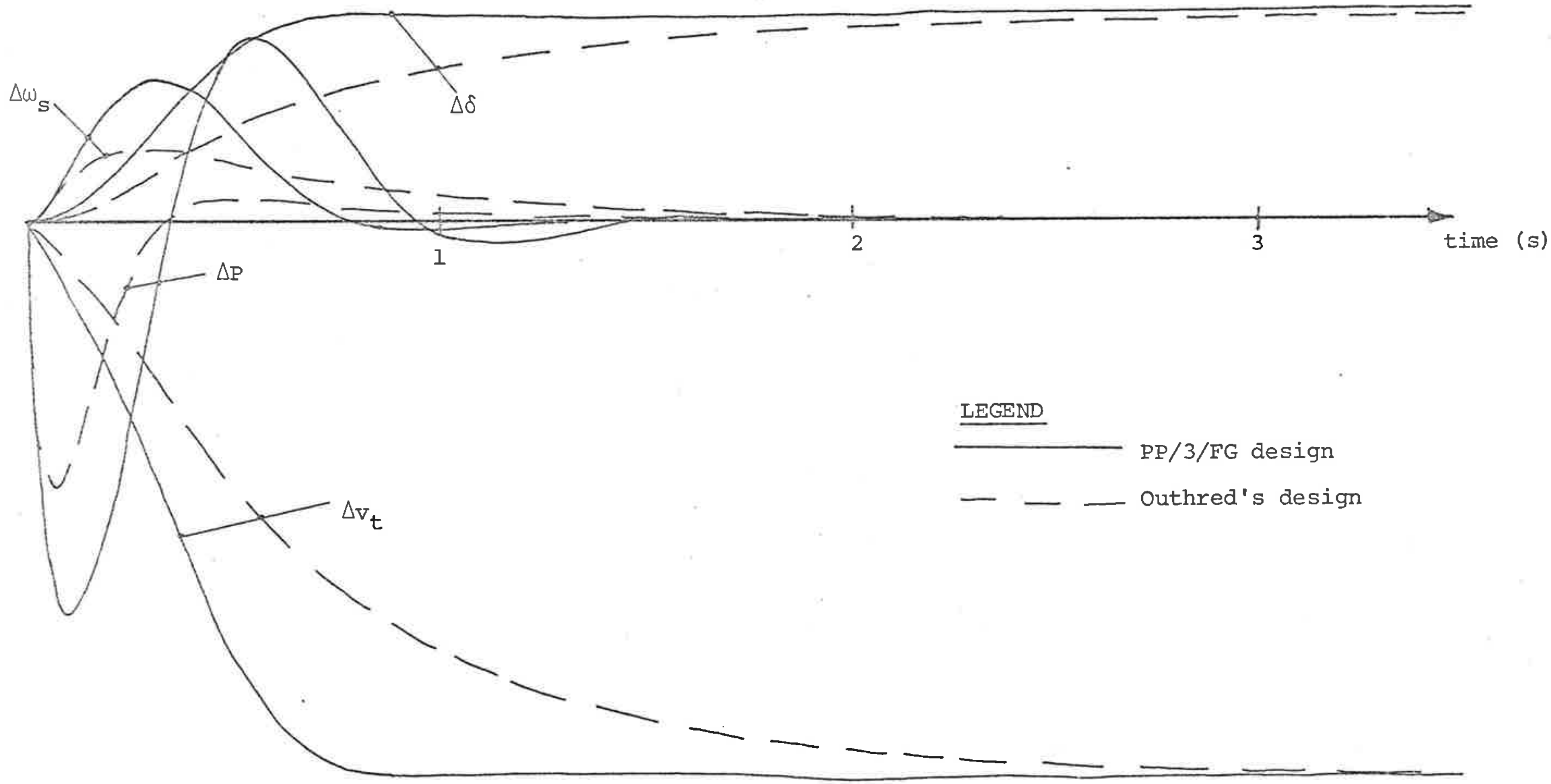

FIGURE 3.7 COMPARISON OF RESPONSES FOLLOWING A STEP-CHANGE IN VOLTAGE SET-POINT

(System data is given in row 1 of Table 3.2. Generator load is $\overline{P} = 0.9$ p.u. and $\overline{Q} = 0.1$ p.u. Outhred's controller uses $f_v = 30$, $f_s = 722$, $f_p = -40.3$ to place system poles at $s = -7.15 \pm j7.04$ and $s = -1.56$. PP/3/FG controller uses $f_v = 30$, $f_s = -222$, $f_p = -10.1$ to place the poles at $s = -2.85 \pm j5.76$ and $s = -3.82$.)

the study region defined in Figure 1. For both leading and lagging p.f., as the real power output is reduced, a given change in reactive load results in increasingly large changes in pole positions.

These trends are evident in every case which was studied, and may be attributed mainly to variations in K_2 and $(K_1'K_4 + K_2K_3')$ changing the effect of the feedback gains f_v, f_s and f_p on the coefficients in the characteristic equation (2.1). The effect of the changes in pole position on the time domain behaviour is illustrated by Figure 3.8 in which a PP/3/FG fixed-gain controller is applied to Abdel-Magid's system (row 3, Table 3.2). The synchronous reactances are lower than in Outhred's system, so the poorly damped real pole and the stability limit occur at higher reactive loading.

It may be concluded that the deterioration in performance of fixed-gain controllers only becomes significant at low real power output or at extremely high reactive loads.

(ii) Comparison of pole-placement and Outhred's design

Comparison of Figures 3.5(a) and 3.6(a) reveals that the controller designed by Outhred results in wider stability limit and heavier damping of oscillations than the PP/3/FG design controller. However, Figure 3.7 shows that the lightly damped real pole of the Outhred controller leads to a sluggish voltage response. The pole-placement controller gives an improved speed of response but this requires an increase in the amplitude in the perturbations to shaft speed and the electrical power output. The two design methods offer different solutions to the compromise necessary between damping and voltage response.

(iii) Summary

PP/3/FG pole-placement may be applied to design controllers for each of the systems in Table 3.2. In each case the calculated gains are not excessive and result in:

(a) Stability limits well outside the normal operating region,

(b) A reasonable compromise between damping and voltage response for all operating points inside the normal operating region, except those at low load.

Typical performance resulting from the PP/3/FG fixed gain pole-placement strategy is shown in Figure 3.8. It may be concluded that placing the poles in positions corresponding to the ITAE standard form appears to be the simple way of designing effective fixed-gain controllers.

3.3.2 Adjustable gain pole-placement strategies - PP/3/AG/FP and PP/3/AG/Ff$_v$

(i) Time responses for the third-order SMIB model

In order to observe the performance of the adjustable gain pole-placement strategies in the time domain, a third-order linearised model of the SMIB system was implemented with the aid of an analog-digital hybrid computer. The

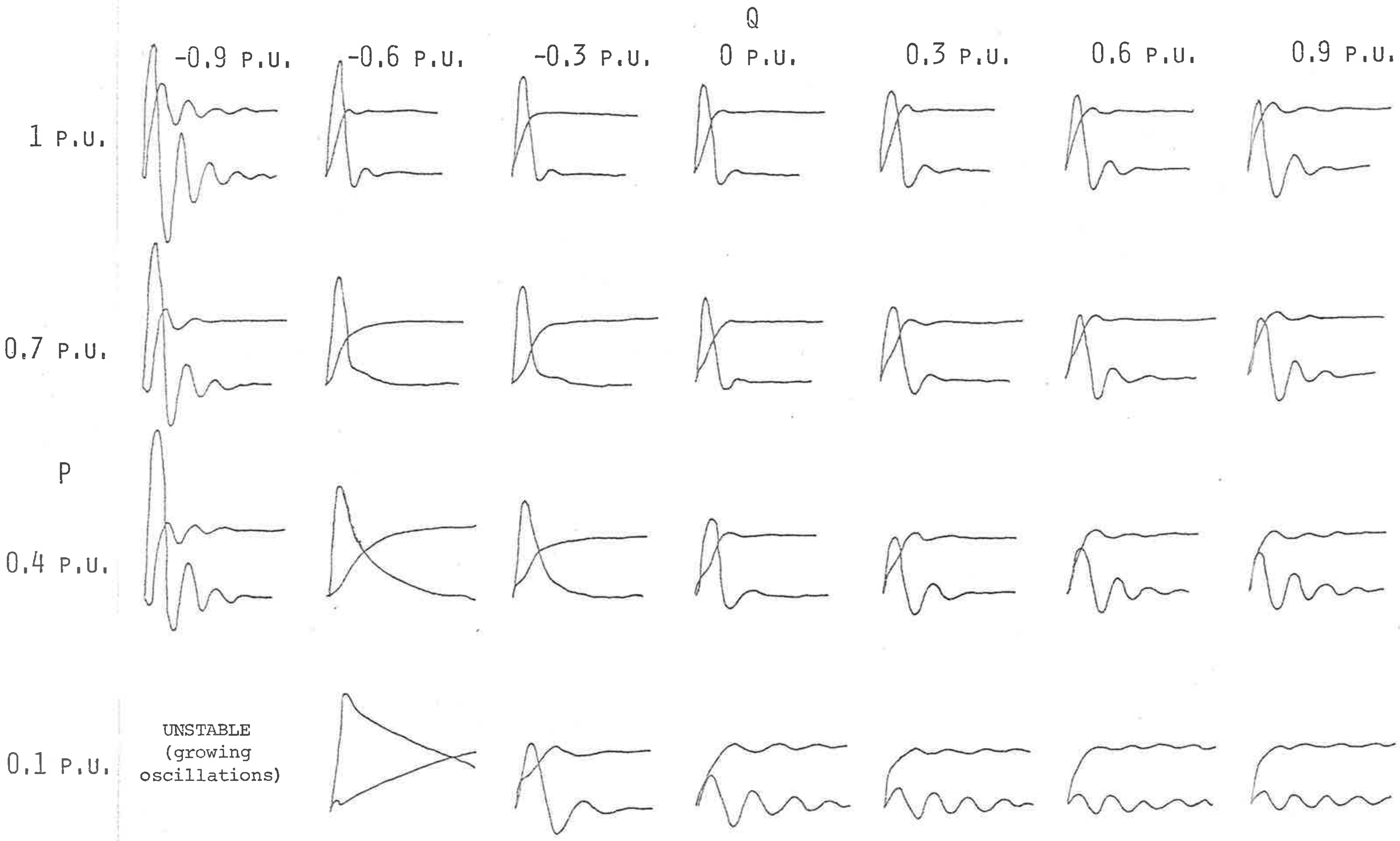

FIGURE 3.8 RESPONSES FOLLOWING A STEP IN V_{ref} WITH A PP/3/FG CONTROLLER

(System data: row 3 of Table 3.2; Controller Design: $f_v = 50$, $f_s = 657$, $f_p = -27.6$. nominal op. pt. $\overline{P} = 1$ p.u., $\overline{Q} = -0.3$ p.u.)

perturbations to the electrical power output, shaft speed, rotor angle and terminal voltage were observed following step-changes in either voltage set-point or mechanical power input. Observations were made over a wide range of operating points. Controllers using the adjustable-gain strategies have been designed for each of the systems in Table 3.2 and in each case the performance is similar.

Typical results for the PP/3/AG/FP and the PP/3/AG/Ff$_v$ strategies are shown in Figures 3.9 and 3.10 respectively. Because the PP/3/AG/FP poles are independent of load, Figure 3.9 illustrates the fact that the terminal voltage response depends not only on the locations of the poles but also on those of the zeroes. The transfer function for the angle response to voltage reference input has no finite zeroes, and that for the speed response has a single zero at the origin (Figure 2.1); therefore the shape of the speed and angle response with both PP/3/AG controllers is independent of operating point - changes to the operating point only change the magnitude of the responses in the fixed pole case. The time scale of the responses for the fixed voltage gain case depend on the scale parameter, ω_1, and their magnitudes are dependent on ω_1 and the operating load.

(ii) Comparison of the pole-placement adjustable-gain controllers with Abdel-Magid's design

Abdel-Magid [8] has proposed an excitation control system which has a fixed gain for the terminal voltage loop

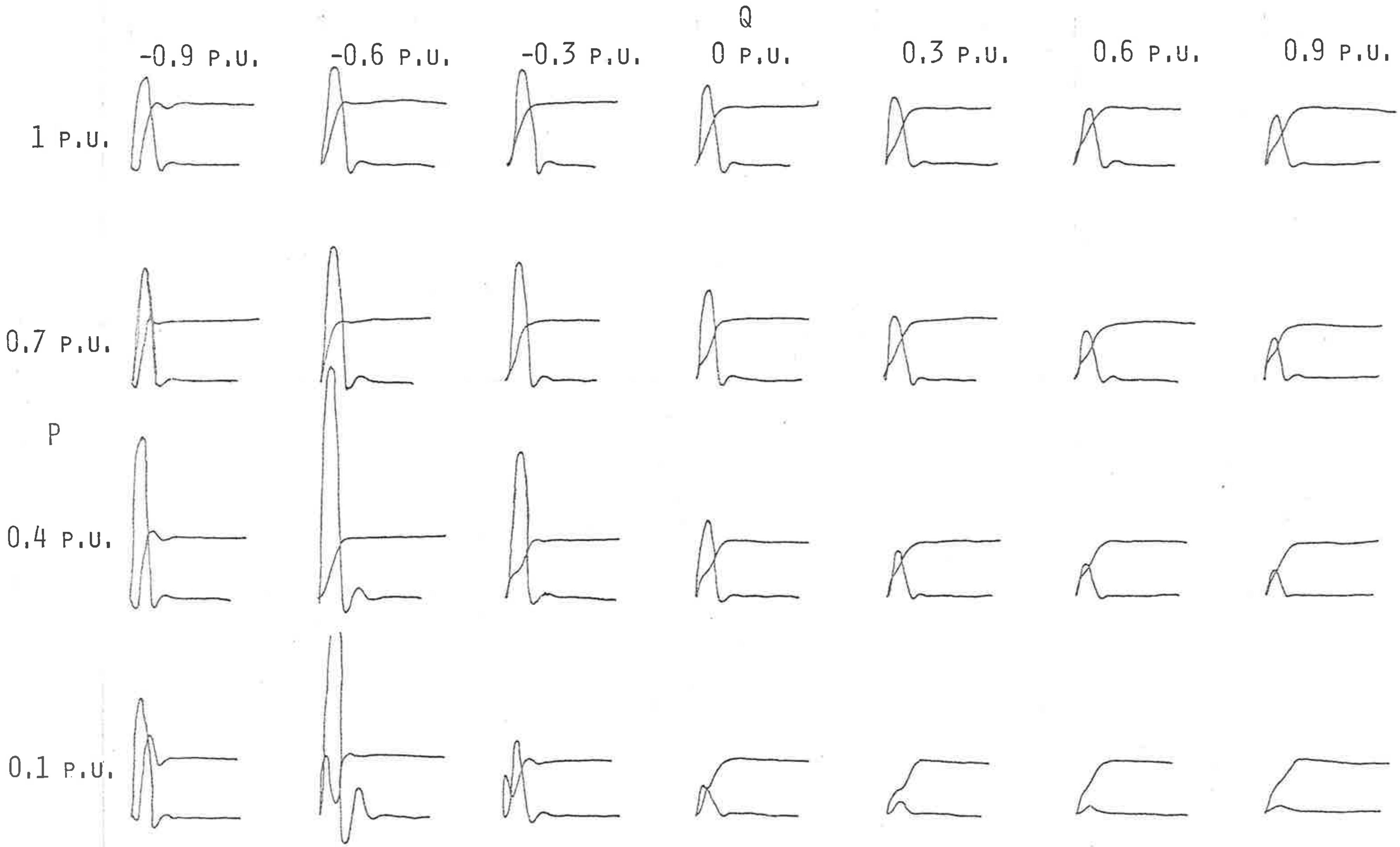

FIGURE 3.9 RESPONSES FOLLOWING A STEP IN V_{ref} WITH A PP/3/AG/FG CONTROLLER

(System data: row 3 of Table 3.2; Controller design: poles at $s = -2.85 \pm j5.85$, $s = -3.88$, $\omega_1 = 5.46$)

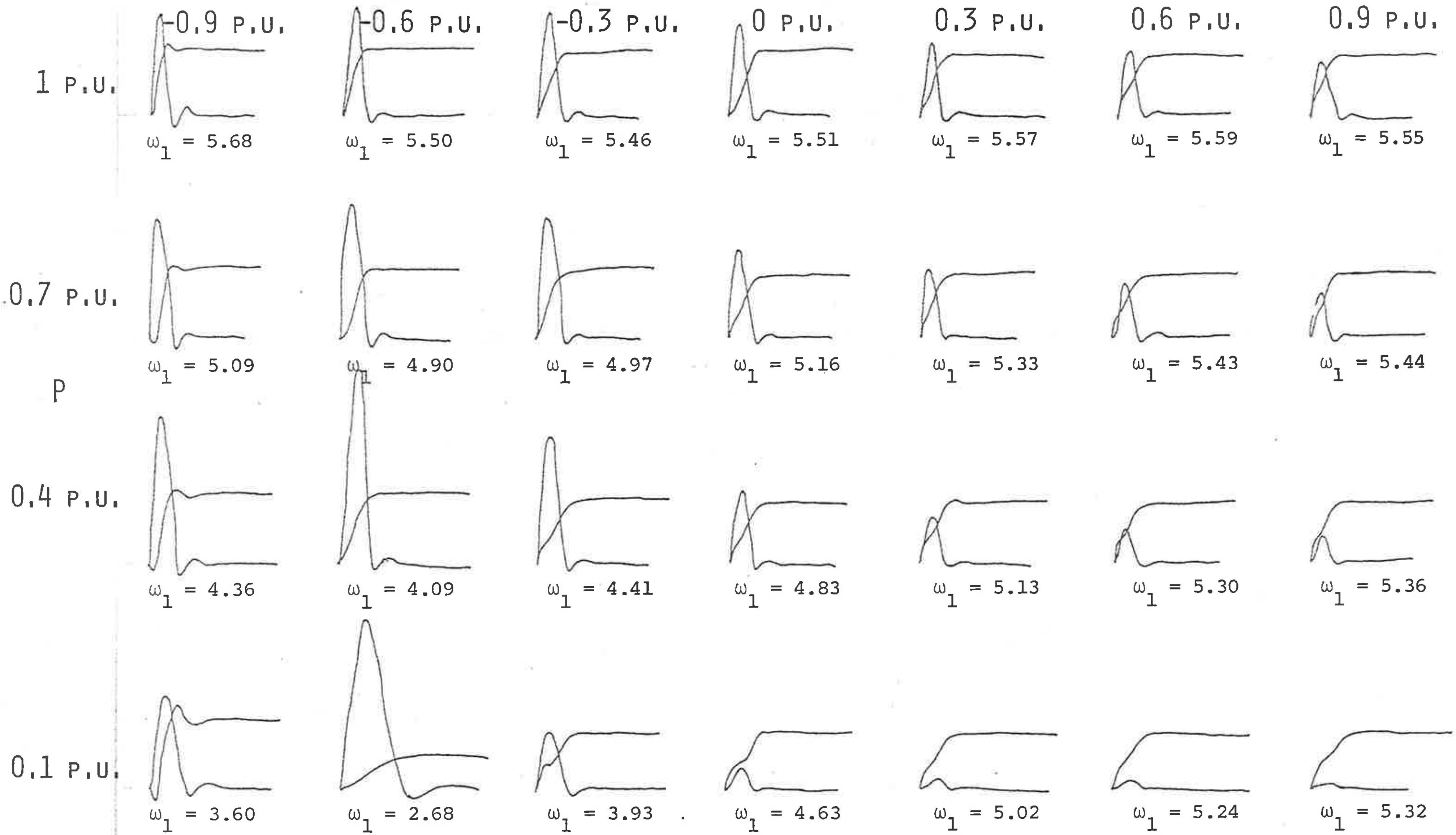

FIGURE 3.10 RESPONSE FOLLOWING A STEP IN V_{ref} WITH A PP/3/AG/Ff_v CONTROLLER

(System data: row 3 of Table 3.2; Controller design: $f_v = 50$, poles at $s = -0.52\,\omega_1 \pm j1.07\,\omega_1$, $s = -0.71\,\omega_1$)

and a stabilising signal based on the electrical power output. The stabilising signal is passed through a filter with transfer function $\frac{K_{AM}s}{(1 + sT_{AM})^2}$. The gain K_{AM} and the time constant T_{AM} are adjusted to maintain optimum performance at all generator loading conditions. The optimum values are calculated by minimising a performance index based on the square of the shaft speed deviation following a step in mechanical power input.

In order to compare the performance of the pole-placement designed controllers with that of Abdel-Magid's, a short exciter time constant was added to the SMIB model in order to duplicate his model. In order to avoid the introduction of steady-state error in terminal voltage following a change in steady-state mechanical power input, a washout network was included in the electrical power feedback loop of the pole-placement designs; the time constant of the network was arbitrarily set to 1.5 seconds. Both PP/3/AG/FP and PP/3/AG/Ff_v controllers are designed to use the same voltage gain (f_v = 50) as Abdel-Magid at his nominal operating point ($\overline{P}$ = 1 p.u., $\overline{Q}$ = -0.3 p.u.). (These designs are employed as examples in section 3.2.2 and Figures 3.1 and 3.3.)

Consider the effect of the more detailed excitation system model on the poles of the system; Table 3.3 lists the specified pole positions and those calculated using the higher order modél at the nominal load.

PP/3 design pole locations	PP/3 actual pole locations	Abdel-Magid pole locations
-2.85 ± j 5.85	-3.44 ± j 4.16	-0.85 ± j 8.64
-3.88	-6.80 ± j 8.31	-1.68 ± j 3.50
	-0.65	-1.89
		-20.9

TABLE 3.3 POLE LOCATIONS FOR CONTROLLERS AT NOMINAL OPERATING POINT IN ABDEL-MAGID'S SYSTEM

The introduction of the exciter time constant increases the damping of rotor oscillations and reduces their frequency. The poles associated with the exciter and the field flux linkages combine to form a heavily damped pair of complex conjugate poles. The small real pole corresponds to the action of the washout network. The reasons for the effect of the exciter time constant are examined in the next chapter. However, investigation has shown that at all operating points, the behaviour of this system is similar to that predicted by the third-order pole-placement design model.

The poles resulting from the use of Abdel-Magid's design are listed in Table 3.3. It is evident that the associated system dynamic performance is inferior to that of the pole-placement designs. This is confirmed by Figure 3.11 which shows the time responses following a step change in the mechanical power input. The main defect of the pole-placement controllers is the slow return of terminal

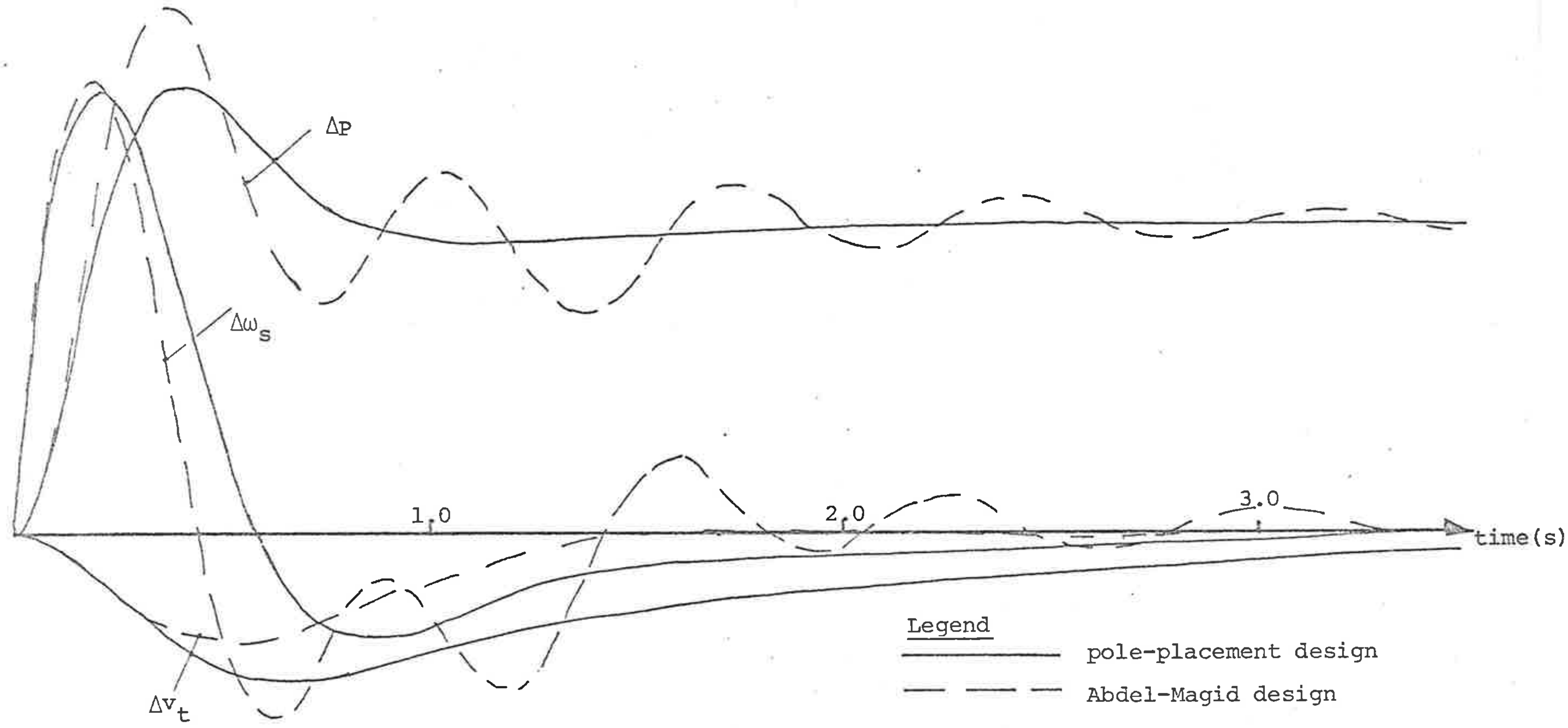

FIGURE 3.11 COMPARISON OF RESPONSES FOLLOWING A STEP-CHANGE IN MECHANICAL POWER INPUT

(Generator output: $\overline{P}$ = 1 p.u., $\overline{Q}$ = -0.3 p.u. System data: See row 3 of Table 3.2. The pole-placement controller uses gains calculated using a third-order SMIB model: f_v = 50, f_s = 657, f_p = -27.6 but has a washout network with a 1.5 second time-constant included in the power feedback loop.)

voltage to its steady state value resulting from the action of the washout network. However, this is not a serious problem because the step in mechanical power is an unrealistic disturbance - investigation showed that the steady-state error to be removed following realistic disturbances is much smaller than that for mechanical power steps.

Figure 3.12 compares the performance of various controller designs at a low load operating point where the real power is 0.1 p.u. and the reactive load is -0.3 p.u. The effect of using the same designs as at the nominal operating point is shown in Figure 3.12(a) - the performances of both Abdel-Magid's design and the pole-placement design deteriorate in the way predicted in section 3.3.1. Figure 3.12(b) shows the behaviour of three adjustable controller designs: PP/3/AG/Ff_v, PP/3/AG/FP and Abdel-Magid's. The heaviest damping is given by the fixed pole strategy. Despite a severe dip during the voltage response, the voltage rise time for this strategy is also the fastest. The damping and the voltage response of the PP/3/AG/Ff_v design is not as high as that of the PP/3/AG/FP because ω_1 has fallen from 5.46 to 3.93, but the performance of this design is superior to that of Abdel-Magid's. Abdel-Magid's adjustable design offers better damping than his fixed design, but at this operating point not only the adjustable but also the fixed gain pole-placement controllers offer superior performance.

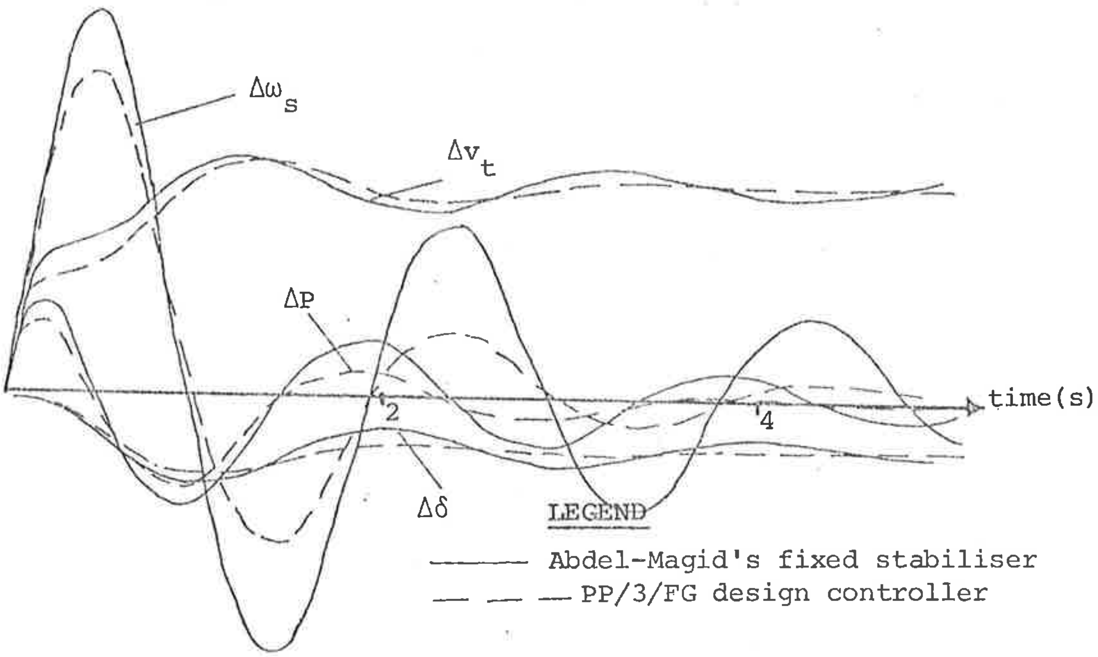

(a) fixed-gain controllers

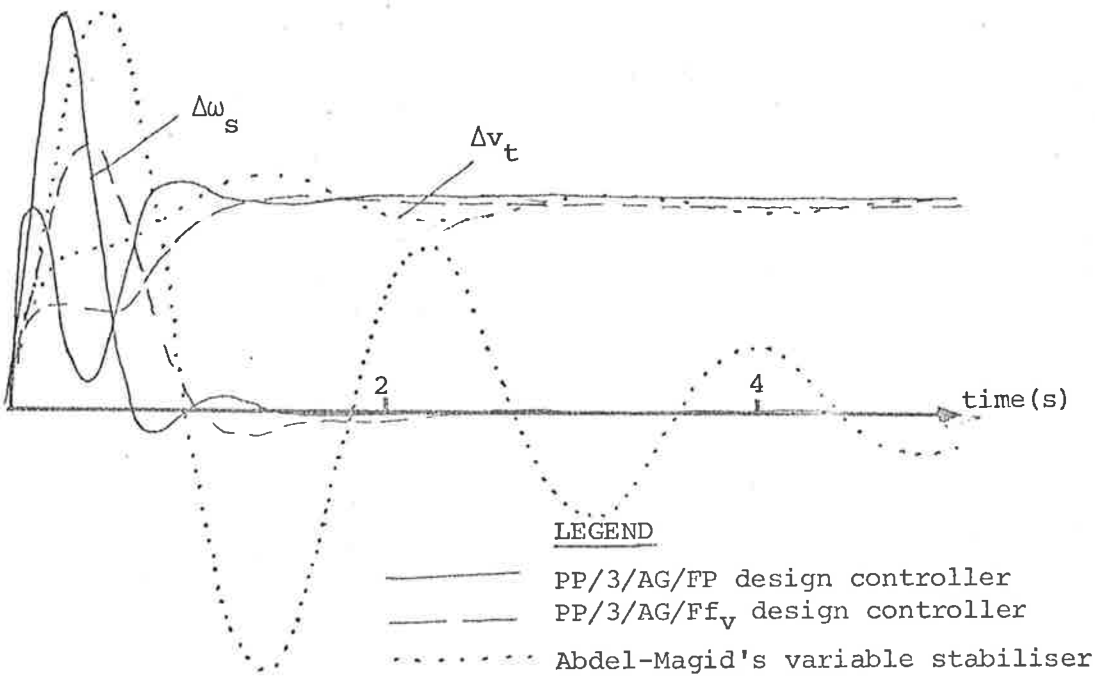

(b) adjustable-gain controllers

FIGURE 3.12 RESPONSE OF SMIB SYSTEM TO A STEP IN VOLTAGE SET-POINT

(System operating with $\overline{P}$ = 0.1 p.u. and Q = -0.3 p.u.; system data listed in row 3 of Table 3.2. Model includes 0.05 sec exciter time-constant. Pole-placement controllers have a washout network in the power feedback loop with time-constant set to 1.5 s. At the operating point shown, PP/3/AG/FP controller uses $f_v = 142$ and has $\omega_1 = 5.46$, PP/3/AG/Ff$_v$ controller uses $f_v = 50$ and has $\omega_1 = 3.93$. PP/3/FG designed at $\overline{P} = 1$ p.u., $\overline{Q} = -0.3$ p.u. with $f_v = 50$.)

The behaviour of the three adjustable controllers has been compared at each of the operating points where Abdel-Magid lists his values of gain and time-constant; in each case the performance of both pole-placement strategies is clearly superior to his. The performance of Abdel-Magid's controller could be improved significantly by the use of a performance index which penalises deviations in other states as well as speed during the design calculations.

3.3.3 Sensitivity of adjustable gain controller performance to operating point measurement errors

In order to apply the adjustable gain strategies it is necessary to determine on-line the steady-state operating point. This could be found, for example, by low pass filtering measurements of the terminal voltage and the real and reactive power output in order to obtain "pseudo steady-state" values of these quantities (Phung [49]). Appendix 10.3 shows how these values, together with an estimate of the tie-line reactance, may be used to calculate the necessary feedback gains for real-time control. Clearly there will be small errors in each of these quantities describing the operating point; the aim of this section is to determine the severity of the degradation in performance due to such errors.

Kasturi [50] describes a method by which the sensitivity of the poles of a power system to changes in a parameter may be determined. His method is applied to find the sensitivity of the values of α, β and ω to changes in the values of $\overline{P}$, $\overline{Q}$ $\overline{v}_t$ and x_e. Two minor modifications are made to his method:

(a) Kasturi describes a complex pair of poles in terms of the natural frequency of oscillation and the damping ratio. In keeping with the preceding work, the complex pair is here described by the real part, α, and the damped frequency of oscillation, ω.

(b) Kasturi defines the sensitivity of one variable, say "a", with respect to variations in another, say "b", as: $\frac{\partial \ell na}{\partial \ell nb} = \frac{\partial a}{\partial b} \cdot \frac{b}{a}$. In this work the term "sensitivity" is defined by the unnormalised form $\frac{\partial a}{\partial b}$. For example, the sensitivity of the real root β to an error in sensing $\overline{P}$ is $\frac{\partial \beta}{\partial \overline{P}}$. With this form, a simple calculation reveals the movement in the s-plane resulting from a given error (e.g. when $\frac{\partial \beta}{\partial \overline{P}}$ is -20, the effect of a +0.05 p.u. error in sensing $\overline{P}$ is to displace the real pole by 1 unit towards the right half s-plane.

The sensitivities of the pole-placement controllers have been examined over a wide range of real and reactive load for systems with data in rows 2, 4 and 5 of Table 3.2. The results in each case are similar in form and typical values are shown in Figures 3.13 and 3.14. The sensitivities of the adjustable gain controllers have been compared with those of fixed gain controllers; the overall trends are the

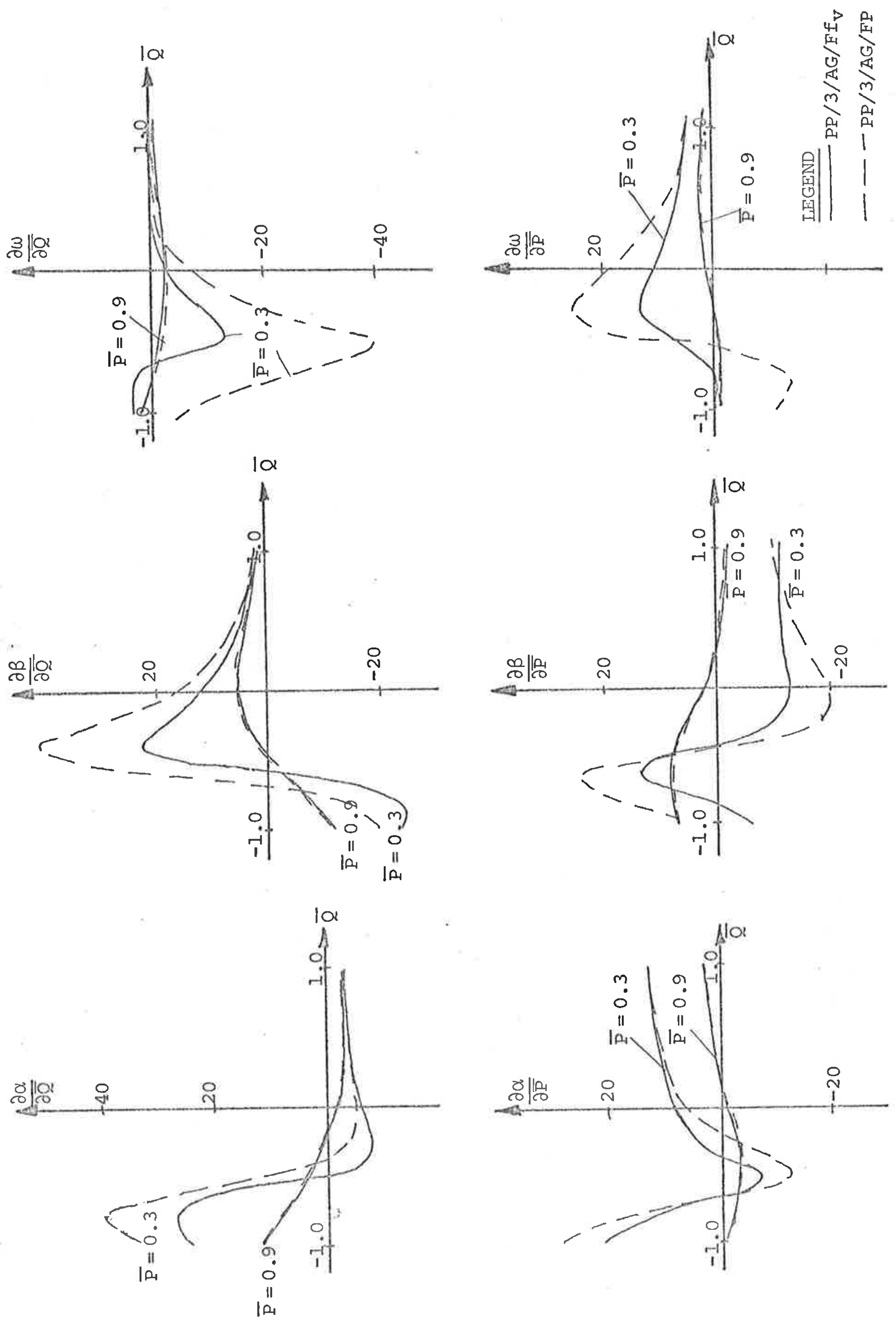

FIGURE 3.13 RATES OF CHANGE OF POLE POSITIONS WITH LOAD
($\overline{P}$ and $\overline{Q}$ are expressed in per unit, α and β are in s^{-1} and ω is in radians/s. Values are calculated for the system in row 2 of Table 3.2, with a PP/3/AG/Ff$_V$ controller using $f_V = 50$ and a PP/3/AG/FP controller with $\omega_1 = 7$.)

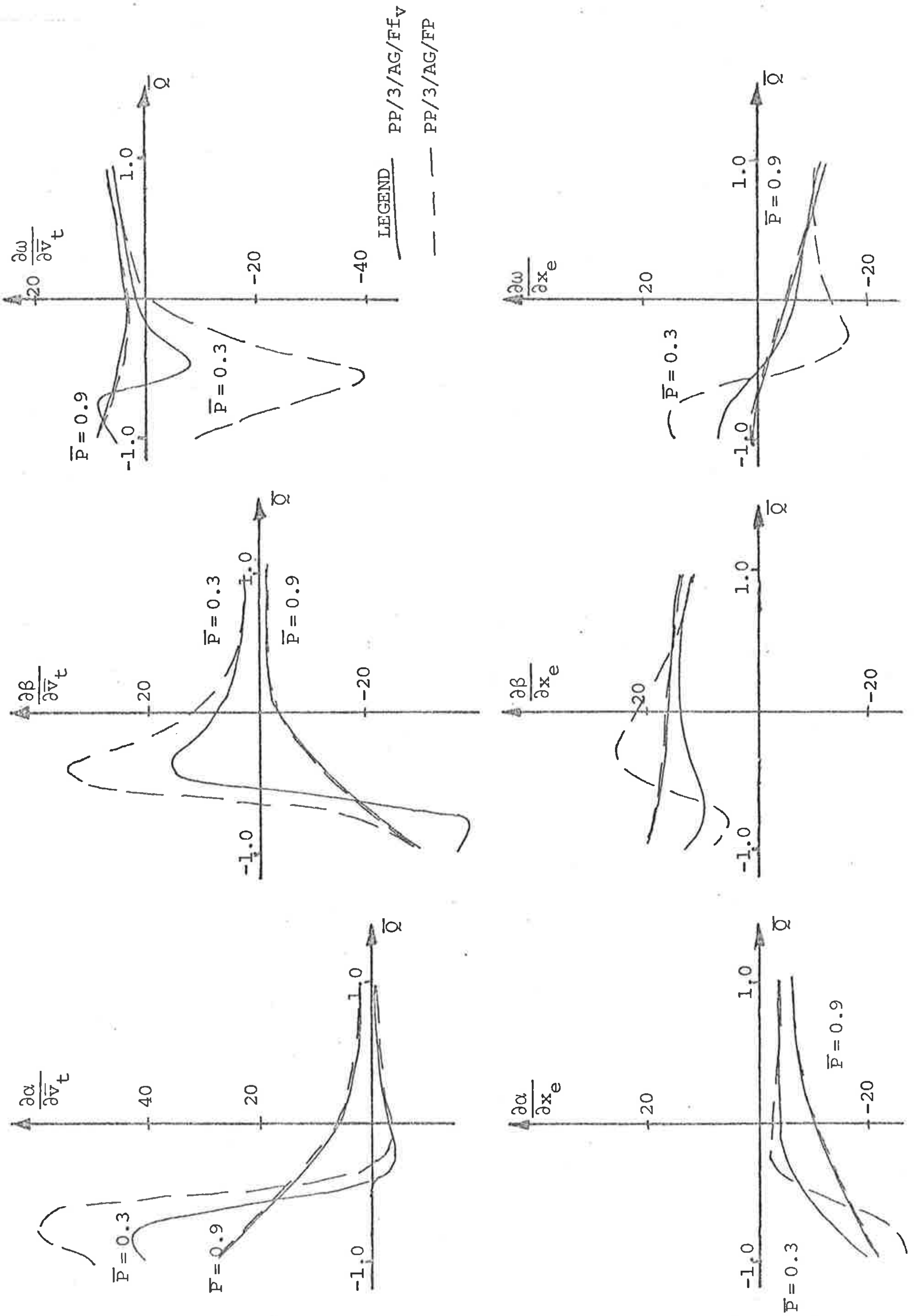

FIGURE 3.14 RATES OF CHANGE OF POLE POSITIONS WITH OPERATING POINT

($\bar{P}$ and $\bar{Q}$ are expressed in per unit, α and β are in s^{-1} and ω is in radians/s. Values are calculated for the system in row 2 of Table 3.2 with a PP/3/AG/Ff$_V$ controller using $f_V = 50$ and a PP/3/AG/FP controller with $\omega_1 = 7$.)

same but the sensitivities with adjustable gains are somewhat higher.

Increased sensitivity at low load is mentioned by Bartlett - this is common to all controller designs and is related to the high rate of change of angle with loading at low excitation levels. Figures 3.13 and 3.14 indicate that this is in fact the only region of the complex power plane, where sensitivity to operating point measurement errors presents problem with the pole-placement strategies. It may be seen that the PP/3/AG/Ff_v strategy is less sensitive to such errors than the PP/3/AG/FP strategy. The greatest sensitivity is that associated with terminal voltage and reactive load measurements.

Although the investigation into the effect of measurement errors has been brief and has only considered the effect of an error in a single measurement, the results give some indication of the degradation in performance due to these errors. It should be noted that in the cases where there is a high sensitivity, the degradation may not be as severe as predicted - for large parameter changes the rate of change of the sensitivity should be considered.

3.4 LARGE SIGNAL BEHAVIOUR OF THE SMIB SYSTEM

3.4.1 Preamble

Although the pole-placement control strategies are based on a linearised model which is only valid for small perturbations, a practical controller must provide damping during the large amplitude oscillations following a major fault in the power transmission system. The behaviour of the PP/3/FG, PP/3/AG/FP and PP/3/AG/Ff_v designs was investigated at a wide range of operating points using a third-order non-linear SMIB model (Appendix 10.4). Time responses were calculated by a digital computer program utilising a Runge-Kutta integration procedure. In order to simulate the effect of the exciter ceiling limits, the field voltage was limited so that 5.5 p.u. $\geqslant v_f \geqslant$ -5.5 p.u.

The performance was investigated for two different sets of system parameters:

(1) Wilson [51] designed a controller for the SMIB system in row 2 of Table 3.2 on the basis of large signal response. The field voltage in his controller is calculated by the non-linear expression:

$$v_f = f_v(V_{ref} - v_t) + f_1\Delta\omega_s + f_2\Delta P + f_3\Delta P\cdot\Delta\omega_s$$

$$+ f_4(\Delta\omega_s)^2 + f_5(\Delta P)^2 \qquad (3.1)$$

The values of the gains f_v, f_1, f_2, f_3, f_4 and f_5 are independent of operating point. Wilson specified the voltage gain, f_v, to be 200 and then used a third-order non-linear SMIB model to choose values for the other gains on the basis of the large signal performance under two different operating circumstances.

For comparison, controllers using fixed and adjustable gain strategies were designed on the basis of ITAE pole-placement at Wilson's nominal operating point, ($\overline{P}$ = 0.96 p.u., $\overline{Q}$ = 0.096 p.u.). The considerations listed in section 3.2.1 suggested that a suitable design would result from the choice of ω_1 corresponding to $f_v = 50$ (poles at $s = -3.7 \pm j\,7.5$ and -5.0 with $f_v = 50$, $f_s = 565$, $f_p = -15.6$).

(2) In order to investigate the large signal performance of pole-placement designed controllers under more severe operating conditions, a system with a higher tie-line reactance and a lower short-circuit ratio was chosen (row 5 of Table 3.2). In this case designs were based on pole-placement at an arbitrarily chosen operating point ($\overline{P}$ = 0.9 p.u. and $\overline{Q}$ = 0.1 p.u.), where $f_v = 60$ gave suitable pole positions with reasonable subsidiary feedback gains (poles at $s = -3.4 \pm j\,6.9$ and -4.5 with $f_v = 60$, $f_s = 1400$, $f_p = -45$).

A problem in comparing the post-fault performance of various controllers is that there is no simple figure of merit which may be used to determine which response is best. The criterion which is applied below to assess the relative merits of different designs is the rate of decay of the perturbation in rotor angle. It is seen that markedly different responses may be deemed equally desirable by this criterion.

3.4.2 Results of studies

(a) Wilson's system

The performance of the pole-placement designed controllers was compared with that of Wilson's design over the wide range of operating points in Table 3.4. Two sets of tests were computed in which three phase line-to-ground faults are applied near the generator terminals. In the first set the tie-line reactance is returned to the prefault value as soon as the fault is removed. In the second set, the postfault tie-line reactance is increased to 0.55 p.u. in order to simulate the non-reclosure of a faulted line.

no.	1	2	3	4	5	6	7	8	9
$\overline{P}$	0.96	1.2	0.8	0.5	0.9	0.9	0.5	0.5	0.9
$\overline{Q}$	0.096	0.203	0.05	0.5	-0.135	-0.3	-0.3	-0.5	0.661
$\overline{V}_t$	0.985	0.994	0.981	1.0	0.989	1.0	1.0	1.0	1.216
x_e	0.3	0.3	0.3	0.3	0.3	0.3	0.3	0.3	1.0

TABLE 3.4 TEST OPERATING POINTS WITH WILSON'S SYSTEM

(i) Faults with reclosure

At every operating point in Table 3.4 all four designs provide substantial damping; typical results are shown in Figure 3.15. The performance of the PP/3/AG/FP and PP/3/AG/Ff_v adjustable gain strategies is slightly better than that of the PP/3/FG fixed-gain pole-placement design at operating points 4 and 8, and somewhat superior to that of Wilson's design at operating points 7 and 8 (Figure 3.16).

(ii) Faults without reclosure

These tests are of particular interest because the increased postfault tieline reactance means that the steady-state operating point is different from that before the fault. If the adaptation process modifying the feedback gains is slow, the controller must operate for a time with gains calculated at the prefault loading conditions and using the prefault value of x_e. Throughout these tests the gains were held at the prefault value. Tests were performed with initial operating points 1 to 8. In each case, Wilson's controller gave the best damping; this appears to be a consequence of his design method which was based on choosing a compromise between performance at a "normal" operating point (1) and a "long-line" operating point (9). However, despite the change in tie-line reactance, the pole-placement controllers gave strong damping as shown in Figure 3.17.

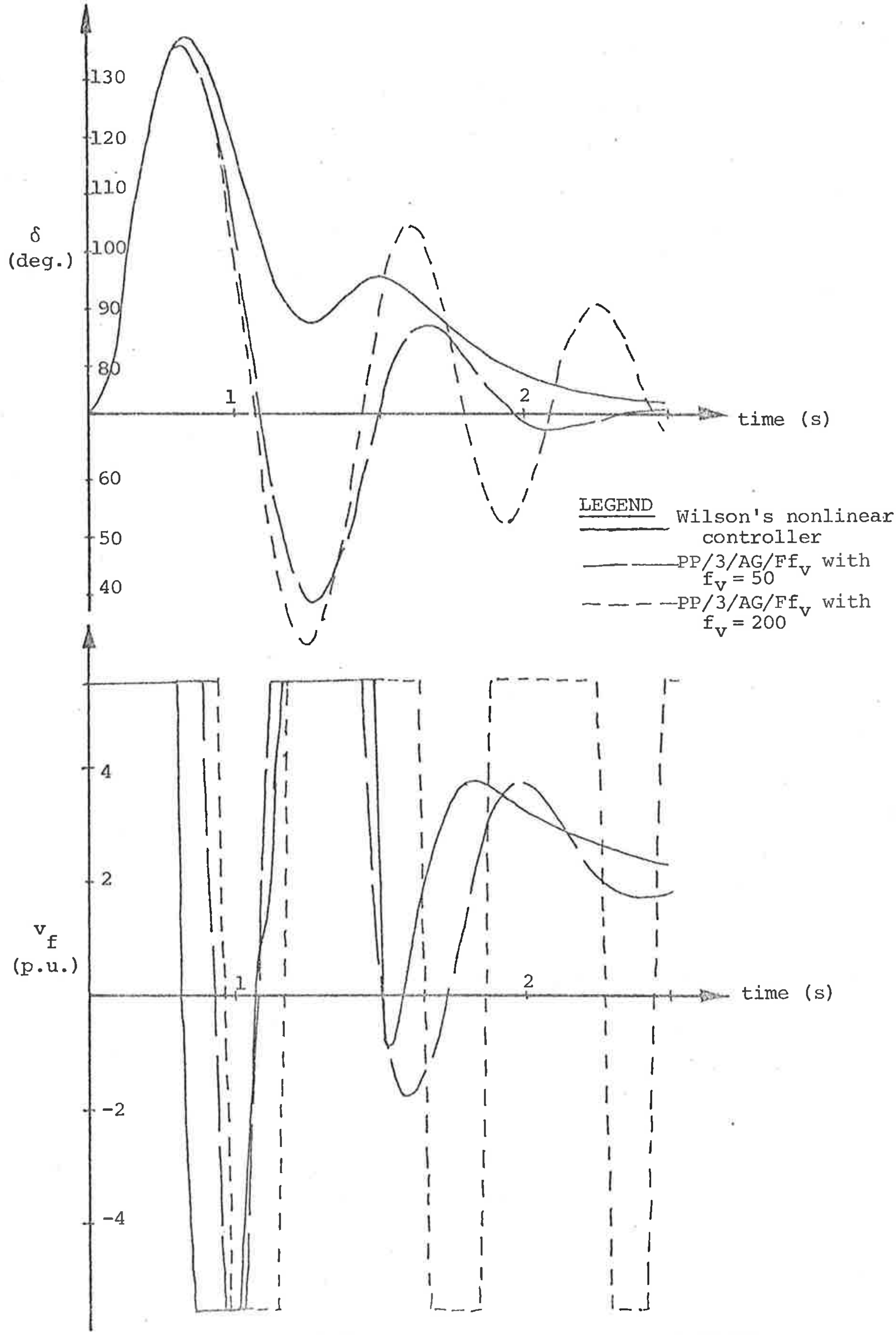

FIGURE 3.15 COMPARISON OF POST-FAULT PERFORMANCE

(System and fault are as in Wilson's nominal case [52] with $\overline{P}$ = 0.96 p.u., $\overline{Q}$ = 0.096 p.u.)

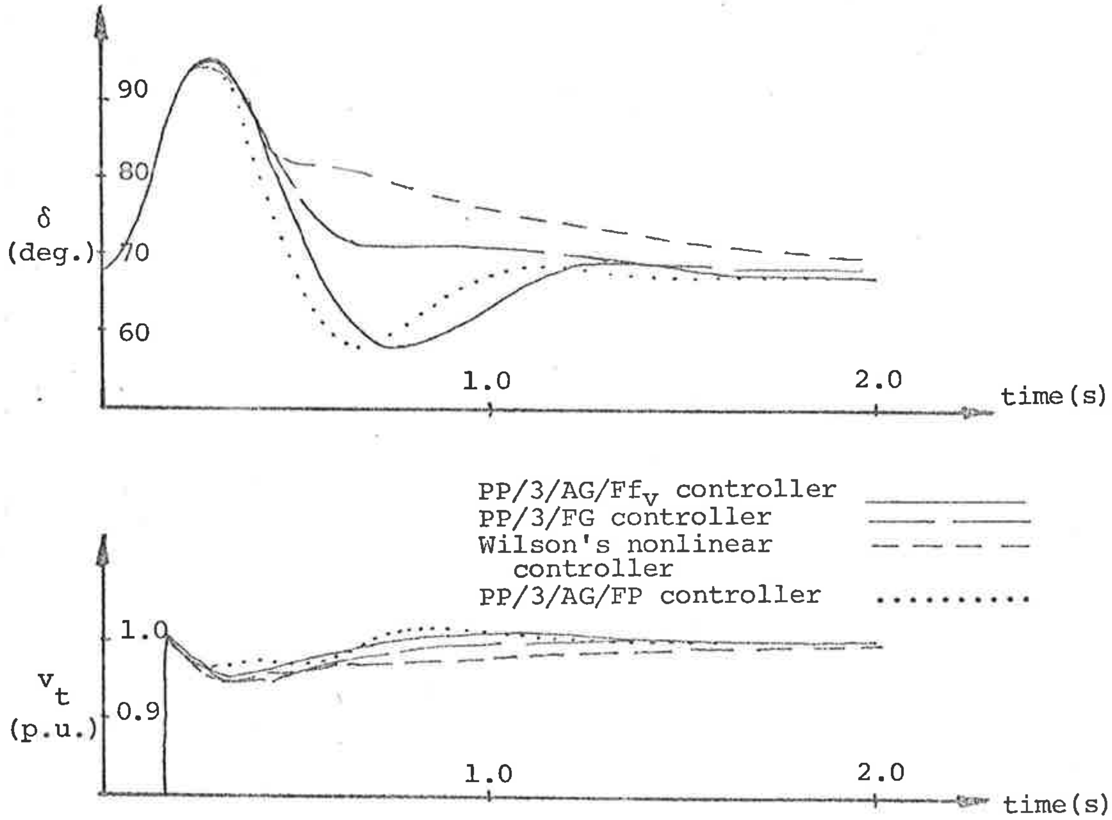

FIGURE 3.16 COMPARISON OF POST-FAULT RESPONSES

(System data in row 2 of Table 3.2. Fault applied at h.v. bus for 0.15 seconds with $\overline{P}$ = 0.5 p.u. and $\overline{Q}$ = -0.3 p.u. PP/3/AG/Ff$_V$ design uses f_V = 50, PP/3/AG/FP design uses ω_1 = 7.)

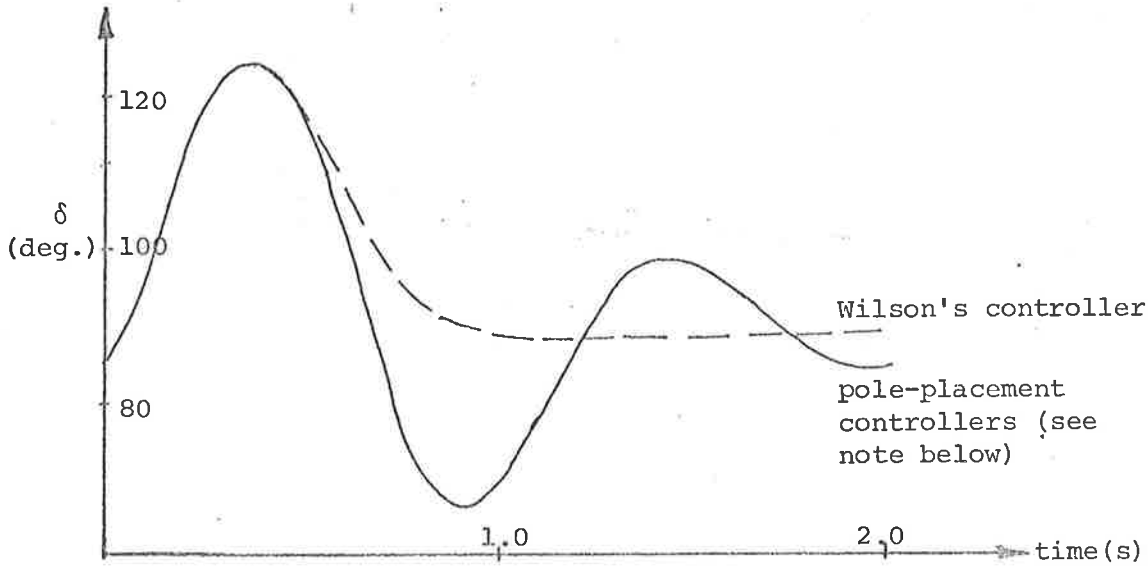

FIGURE 3.17 COMPARISON OF POST-FAULT RESPONSES

(System data listed in row 2 of Table 3.2 Fault near h.v. bus cleared after 0.06 seconds by line switching which results in an increased value of x_e equal to 0.55 p.u. For the load used, $\overline{P}$ = 0.9 p.u. and $\overline{Q}$ = -0.135 p.u., the performances of the PP/3/FG, PP/3/AG/Ff$_V$ and PP/3/AG/FP controllers is almost identical. For clarity only the response of the PP/3/AG/Ff$_V$ design which has f_V = 50, f_s = 377, f_p = -15.5 is shown.)

Overall, at normal operating points, the pole-placement controllers and Wilson's design offer similar performance for the third-order SMIB model. The simplest design is the PP/3/FG strategy because it requires only fixed gain linear feedback signals. Following Wilson, one way to improve the behaviour in the event of non-reclosure after a fault could be to choose a compromise between the pole-placement designs at a normal operating point and one with high x_e.

(b) Second system

The performance of pole-placement controllers was studied with the second set of system parameters (row 5 of Table 3.2), over a similar range of loading conditions to those in Table 3.4. As before, all of the pole-placement designs resulted in substantial postfault damping. The adjustable gain strategies again gave slightly heavier damping than the fixed-gain strategy for loads distant from the design operating point (taken to be $\overline{P} = 0.9$ p.u., $\overline{Q} = 0.1$ p.u.). A set of tests with the postfault tie-line reactance increasing to 1 p.u. once more showed that the pole-placement designs provide significant damping despite the changed steady state operating point.

3.4.3 The effect of high voltage gain on pole-placement controller performance

Under small signal conditions, the damping of a pole-placement controller depends on ω_1, which is determined by the value of f_v. Designs which have high voltage gains have the highest oscillation frequencies and the best damping. However, under large signal conditions the effect of the exciter voltage limits must be taken into account, as shown by the example in Figure 3.15. The pole-placement design incorporating a voltage gain of 50 has better performance than Wilson's controller. The pole-placement design with a substantially higher voltage gain has significantly poorer damping.

The deterioration in performance is most noticeable at high load and lagging power factor because the steady state value of field voltage is then closest to the positive limit. When the PP/3/AG/FP strategy is used to adjust the feedback gains, high voltage gains occur in the low power, leading power factor region of operation, even with moderate values of ω_1. However, excitation levels are low under these conditions and the deterioration in performance due to the field voltage limit is not significant.

It has been found that as a general rule, controllers designed by ITAE pole-placement at design operating points near rated load, should use voltage gains less than about 120 to avoid deterioration of large signal performance due to limiting effects.

3.4.4 Summary

Although an extensive study was made of the large signal performance of the third-order SMIB system, the results are not discussed in great length because subsequent investigation showed that significant errors can result from the use of such a simple model to compute large signal performance (see section 5.6). To illustrate this point, Figure 3.18 illustrates the behaviour of Wilson's design with the design model and a more detailed model. The higher frequency mode of oscillation evident in the field voltage response results from the neglect of the exciter time constant in the design of regulators with high f_v (see Chapter 4.1). Figure 3.19 compares the performance of a pole-placement controller using the design and the more detailed model.

The following general observations were made during the course of the large signal studies with the third-order SMIB model. Subsequent investigations in Chapter 5 show that they are valid despite the errors in the actual responses computed:

(1) The pole-placement strategy results in heavy postfault damping, provided ω_1 and hence f_v are not too high. The designs are not sensitive to changes in network reactances after the fault.

(2) Although the use of adjustable gains does result in some improvement in performance with large reactive loads (e.g. $|Q| > 0.5$ p.u.), the improvement in performance in the normal operating region is negligible.

(3) The critical clearing time is very short for operation at high initial values of rotor angle, so that for practical operation under these conditions, special

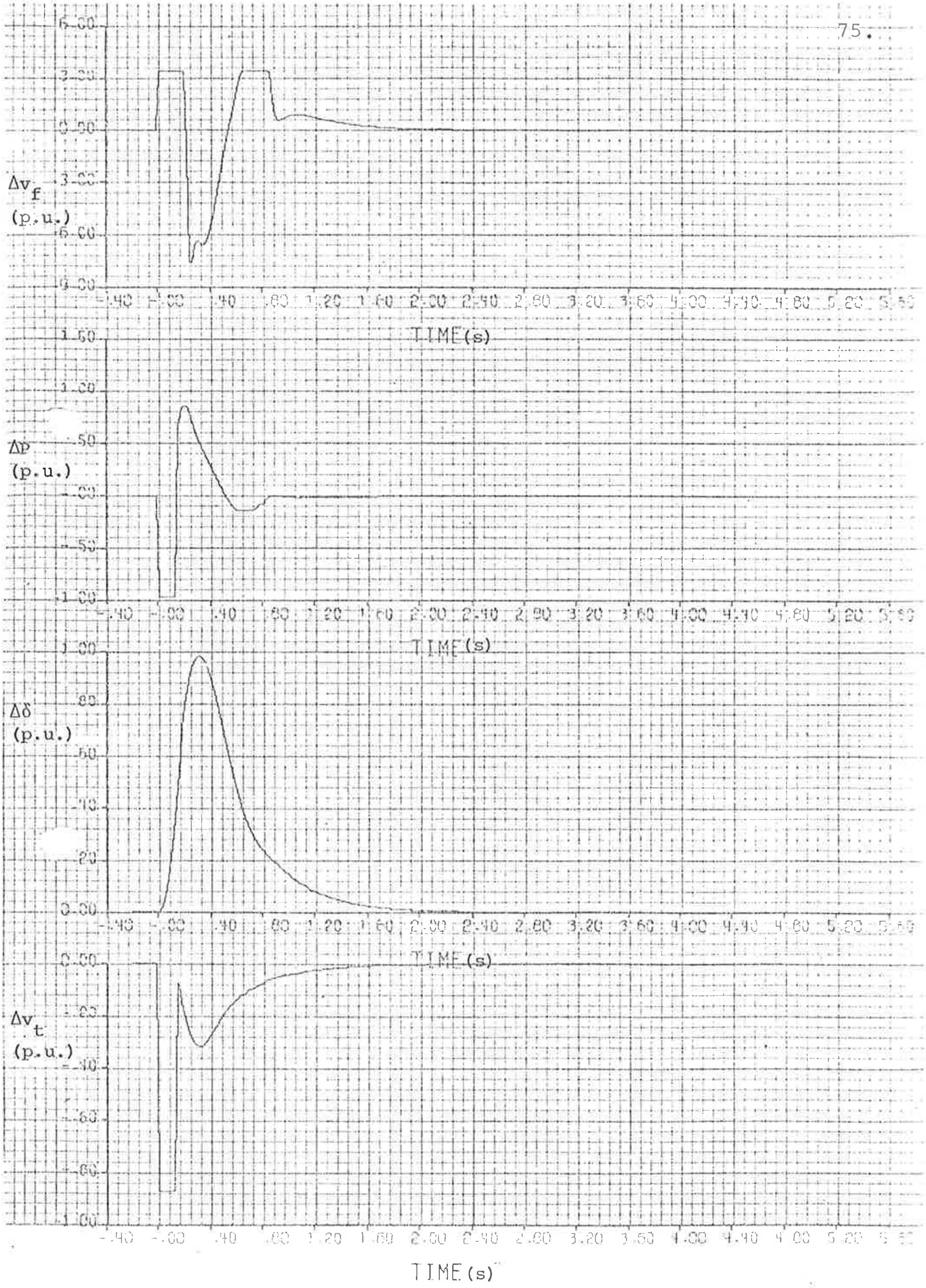

FIGURE 3.18(a) LARGE-SIGNAL RESPONSE WITH WILSON'S CONTROLLER AND A THIRD-ORDER SMIB MODEL

(Operating point 1 of Table 3.4; 0.14 s fault followed by reclosure. Only rotor winding in generator model is the d-axis field winding. No exciter time-constant.)

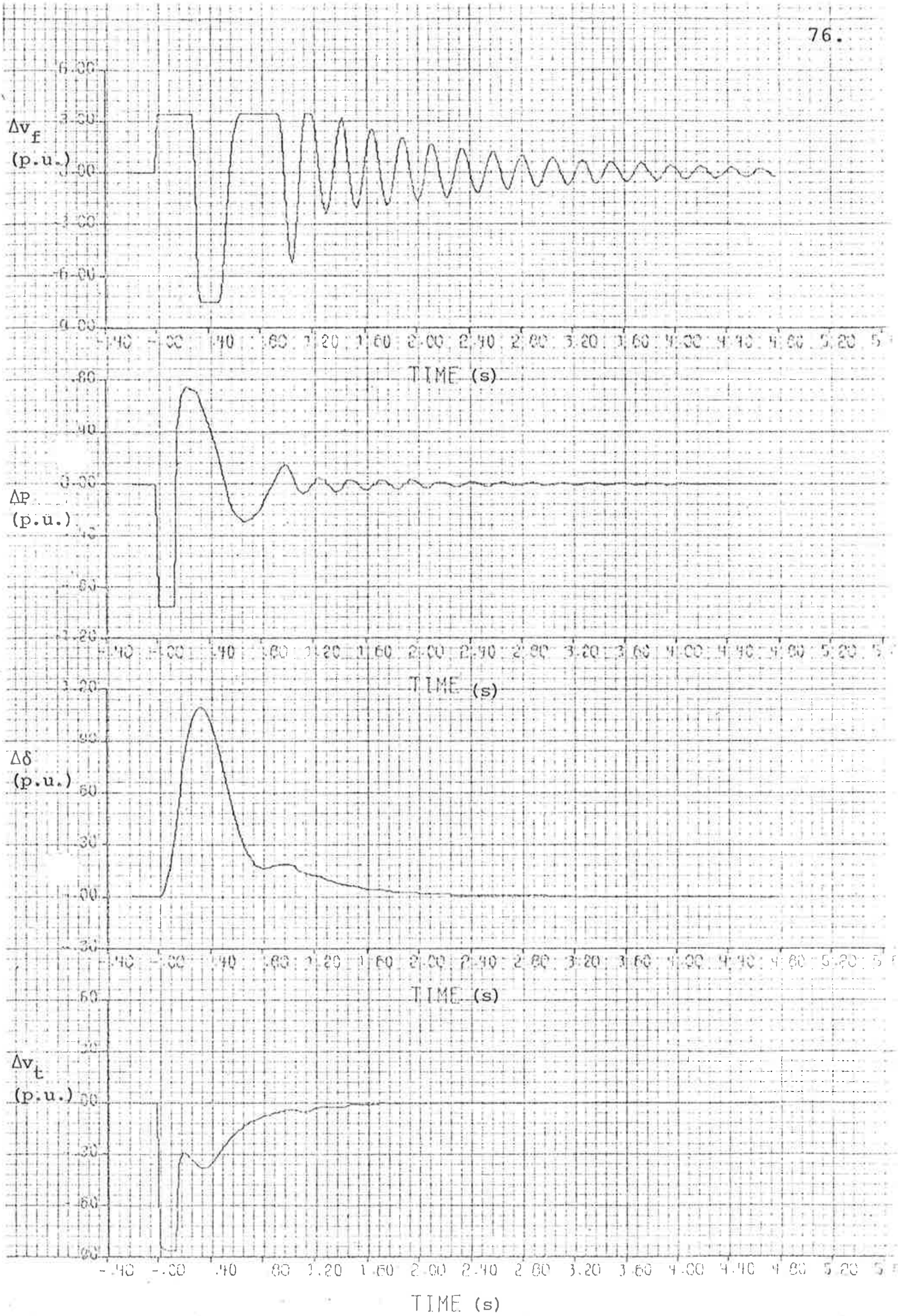

FIGURE 3.18(b) LARGE-SIGNAL RESPONSE WITH WILSON'S CONTROLLER AND AN EIGHTH-ORDER SMIB MODEL

(Operating point 1 of Table 3.4; 0.14 s fault followed by reclosure. Generator model has 2 d-axis and 2 q-axis rotor windings. Exciter time constant T_{ex} = 0.05 s)

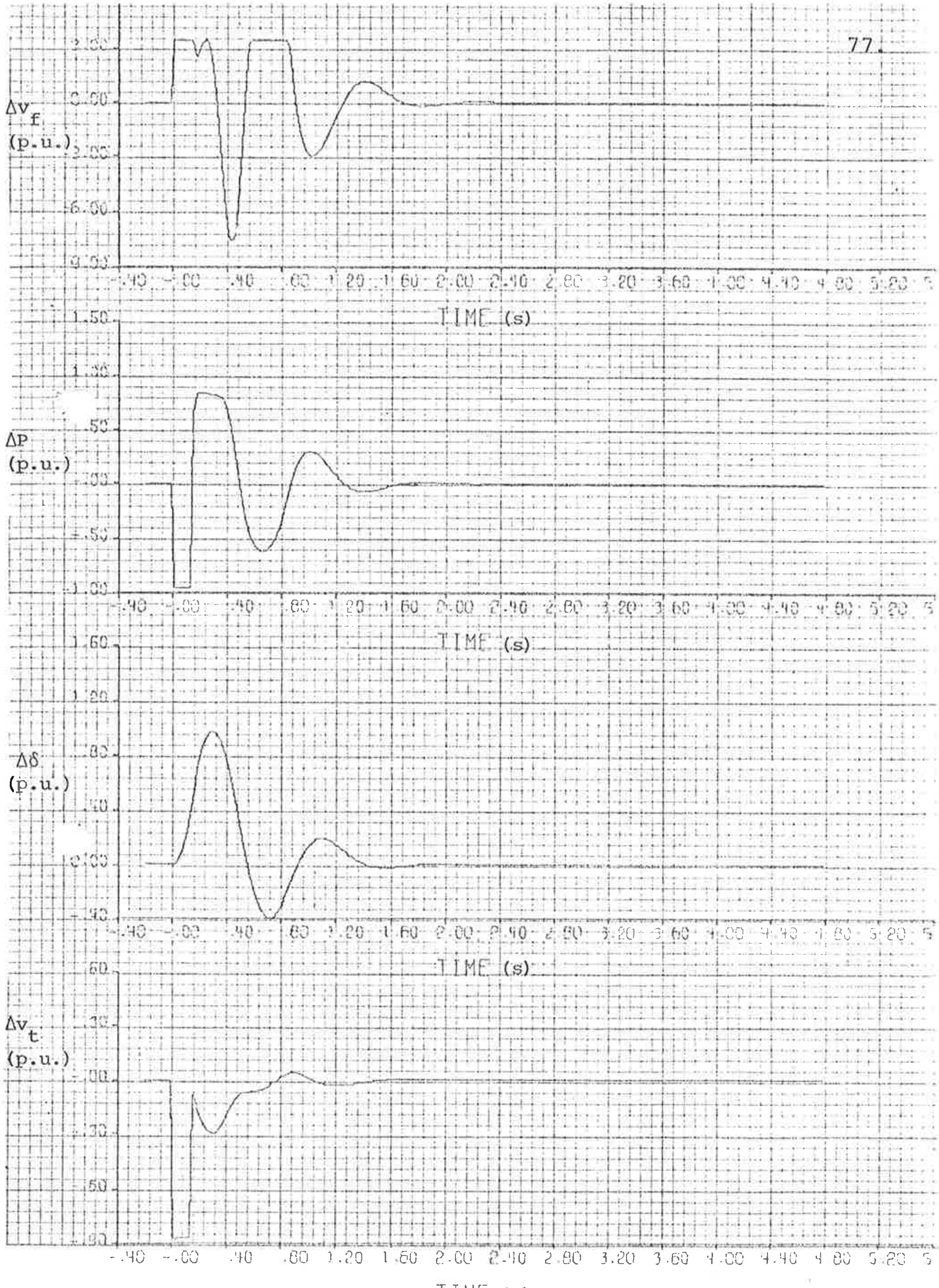

FIGURE 3.19(a) LARGE-SIGNAL RESPONSE WITH A POLE-PLACEMENT CONTROLLER AND A THIRD-ORDER MODEL

(Operating point 1 of Table 3.4; 0.14 s fault followed by reclosure. Only generator rotor winding is the d-axis field winding. No exciter time-constant. Controller designed for ITAE pole positions and $f_v = 50$)

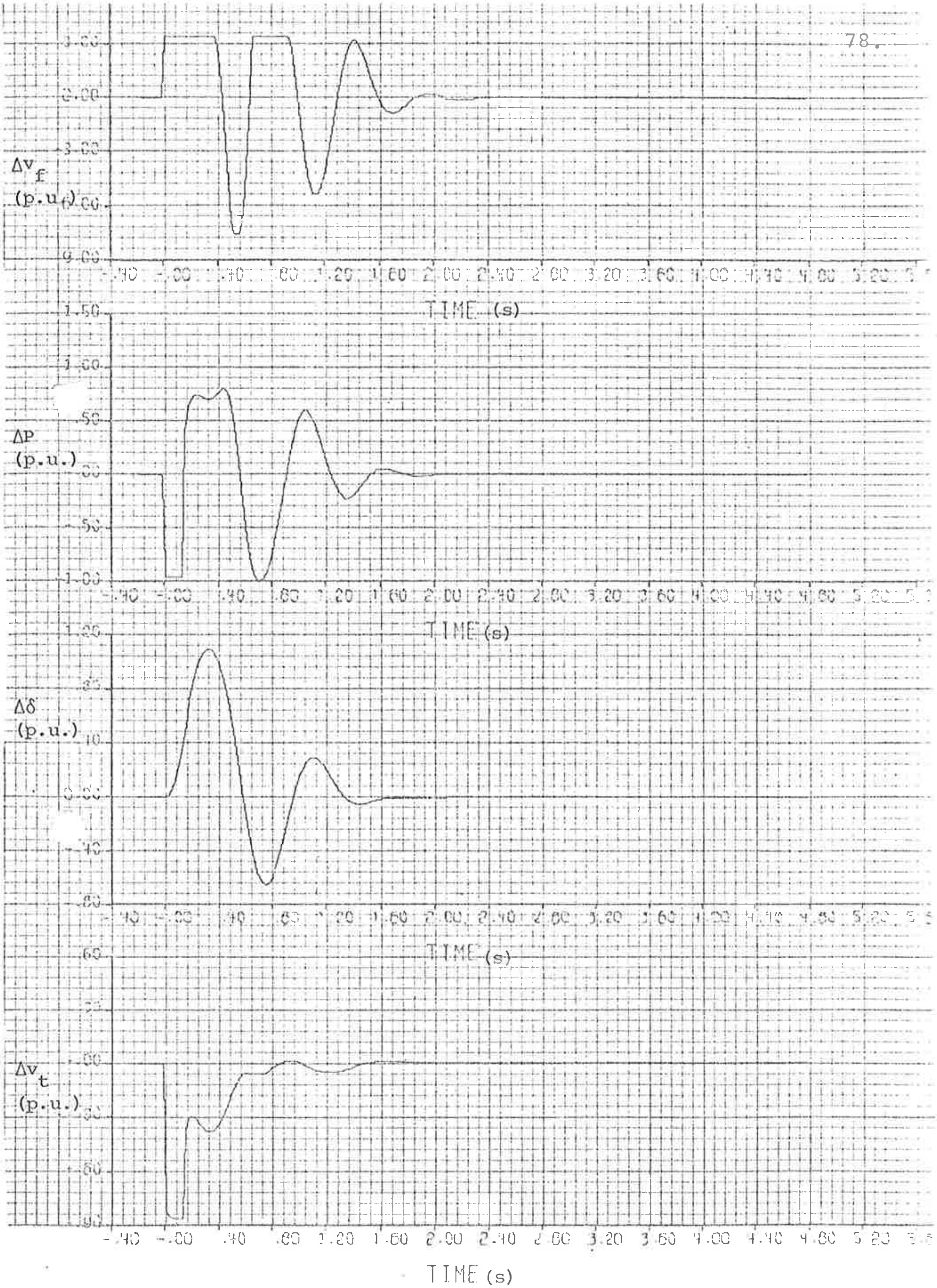

FIGURE 3.19(b) LARGE-SIGNAL RESPONSE WITH A POLE-PLACEMENT CONTROLLER AND AN EIGHTH-ORDER SMIB MODEL

(Operating point 1 of Table 3.4; 0.14 s fault followed by reclosure. Generator model has 2 q-axis and 2 d-axis rotor windings. Exciter time-constant 0.05 s. Same controller as for Figure 8.19(a), designed by pole-placement with $f_v = 50$)

measures to improve transient stability are necessary (e.g. braking resistors or fast valving).

This section completes Chapter 3 which shows that the placing of the poles of the SMIB system into positions corresponding to the third-order zero position-error ITAE standard form can be achieved with realistic feedback gains. The small and large signal performance which results is competitive with that resulting from other more complicated design procedures; this performance is, however, assessed using simple models which involve many assumptions. Pole-placement control strategies which take account of some of these simplifications are developed in the following chapter.

CHAPTER 4

POLE-PLACEMENT DESIGN USING A THIRD-ORDER SMIB MODEL AND A FIRST-ORDER EXCITATION SYSTEM MODEL

4.1 PRELIMINARY REMARKS

One limitation of the pole-placement control strategies which are investigated in Chapters 2 and 3 is that the third-order model represents the entire excitation control system by pure gains, ignoring all delays in the transducers, filters and amplifiers.

The effect of this assumption on the poles of the system is illustrated in Figure 4.1 by the introduction of a simple first-order exciter model. When the time constant, T_{ex}, is very small the dominant poles consist of one real pole and a pair of complex conjugate poles in the positions computed from the third-order model of Chapters 2 and 3. As the size of T_{ex} is increased, the damping initially improves; this effect has been noted by Aldred [52] and Stapleton [29]. When the time constant becomes sufficiently large, the poles associated with the exciter and the field flux linkages merge to form a second complex pair of poles. With further increase in T_{ex}, the damping of both oscillatory modes deteriorates. The point at which the second mode of oscillation becomes significant depends on the controller gains and time constant, and also on the time constant of

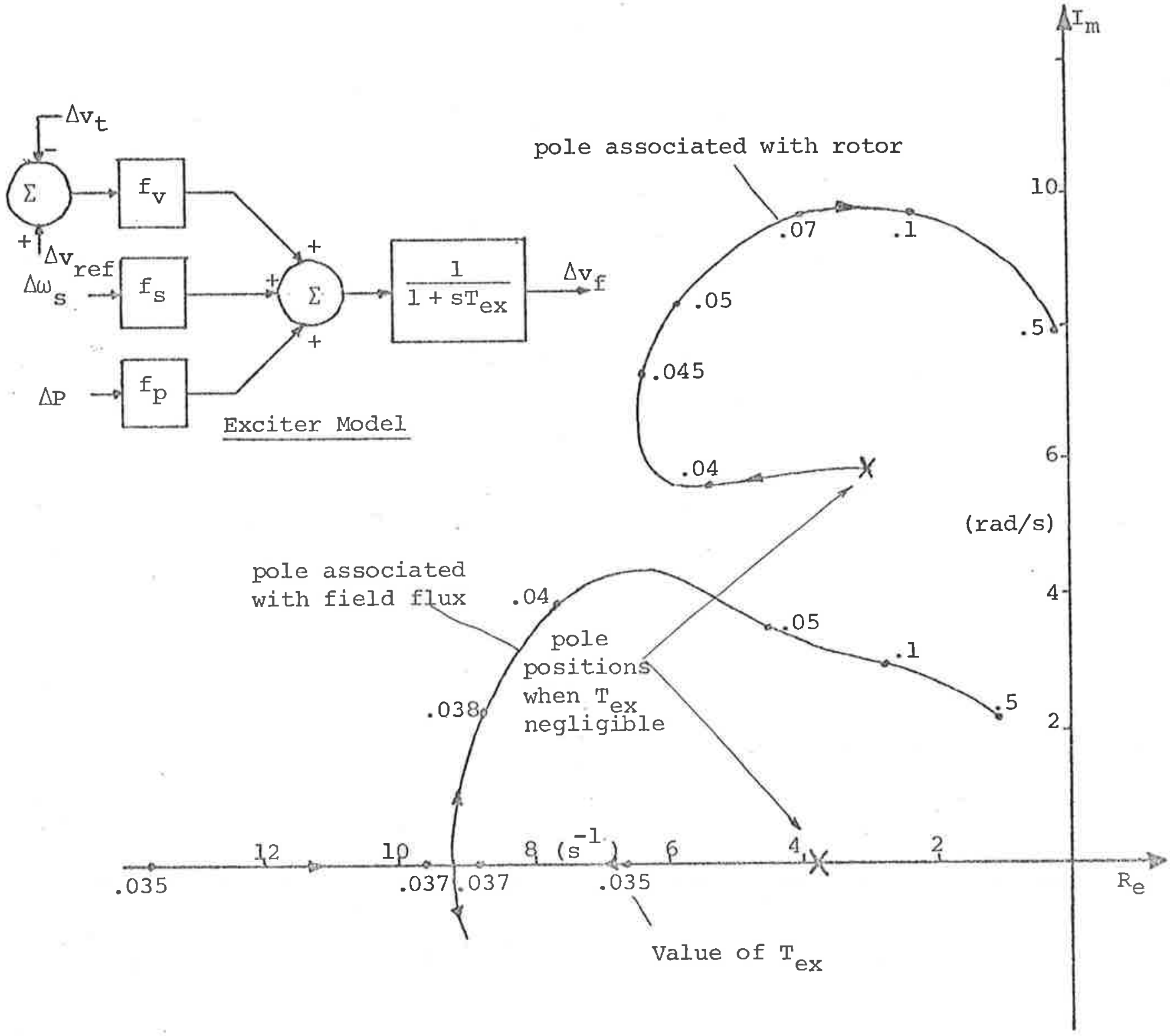

FIGURE 4.1 EFFECT OF INTRODUCING AN EXCITER TIME-CONSTANT ON THE POLES OF THE SMIB SYSTEM

(The exciter model shown is added to the third-order SMIB model used in Chapters 2 and 3. System data is listed in row 3 of Table 3.2. Controller gains are set to $f_v = 50$, $f_s = 657$, $f_p = -27.6$ as described in section 3.2 with the generator load being $\overline{P} = 1.0$ p.u., $\overline{Q} = -0.3$ p.u.)

the generator field winding. On the basis of performance when the generator is unloaded, DeMello [23] claims that in order to maintain good damping the voltage gain, f_v, should be less than $\frac{T'_{do}}{2T_{ex}}$. Outhred [16] states that for controller design using a third-order model to be valid, the poles need to be "of reasonably low frequency".

The aim of this chapter is to develop control strategies which maintain their designed performance with changing steady-state operating point, for those cases where the third-order SMIB model is not valid. A number of authors (DeMello [24], Yu [44], Abdel-Magid [8]) have modelled thyristor-type excitation systems by a single forward loop time constant; the SMIB model of Chapter 2 is supplemented by such a first-order controller model, resulting in a fourth-order model for the system. In order to assign pole locations arbitrarily, four adjustable parameters are required. It is assumed that the perturbation in field voltage is fed back to the exciter in addition to the terminal voltage, shaft speed and electrical power signal used previously. The feedback gain for this signal is denoted "f_F". Figure 4.2 shows the changes which are made to the model used in previous chapters.

A commonly used value for T_{ex} in designing thyristor-type excitation controllers is 0.05 seconds. This value is used in the majority of the calculations described in this thesis, but a few results have been computed using larger values to demonstrate that the pole-placement strategies are applicable to slower excitation systems.

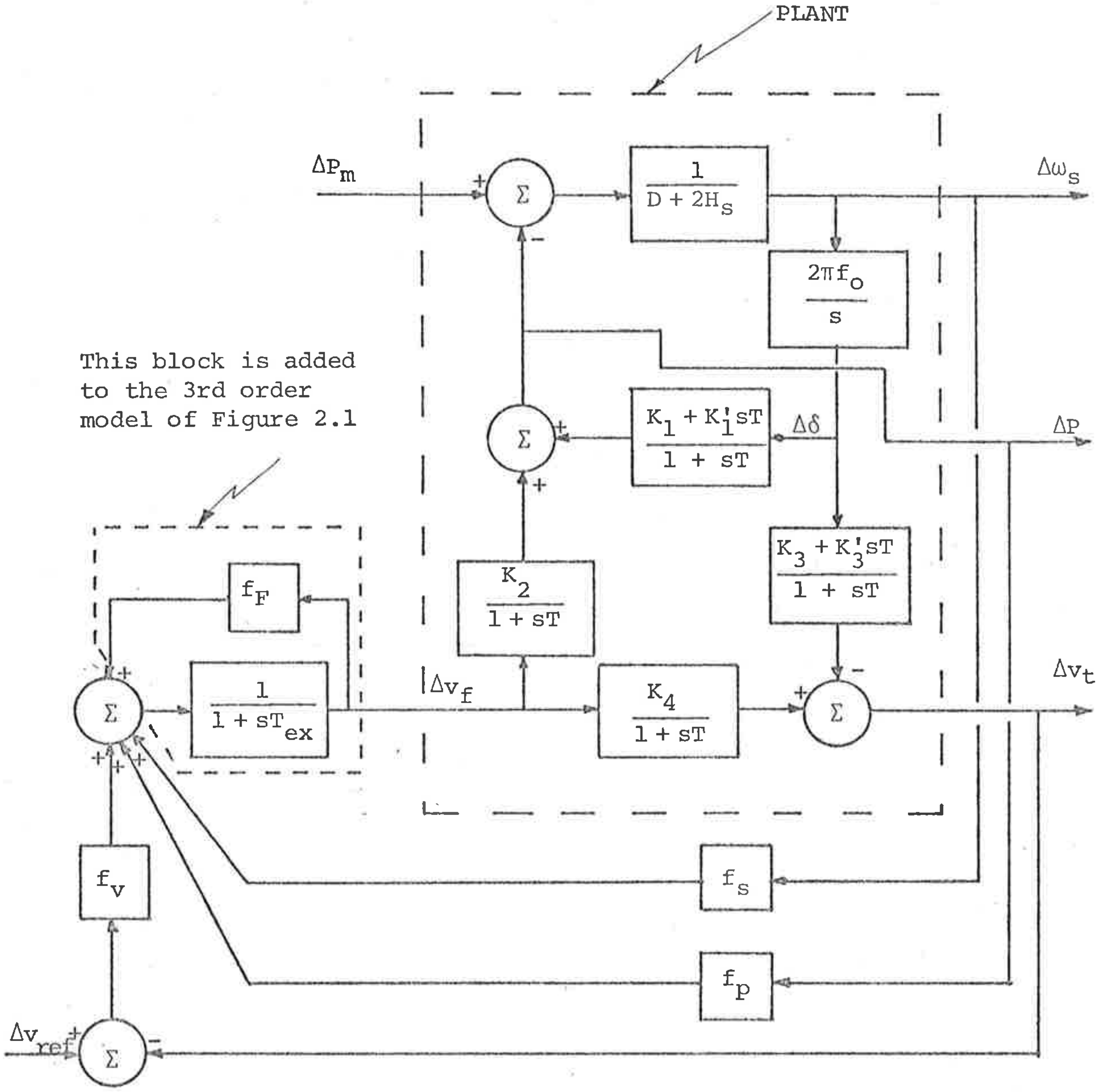

FIGURE 4.2 BLOCK DIAGRAM OF A FOURTH-ORDER LINEARISED SMIB MODEL

4.2 POLE-PLACEMENT CONTROL STRATEGIES BASED ON A FOURTH-ORDER SYSTEM MODEL

4.2.1 Derivation of expressions for the feedback gains

The characteristic equation of the system may be derived by block diagram manipulation of Figure 4.2:

$$s^4 + \left(\frac{1-f_F}{T_{ex}} + \frac{1}{T} + \frac{D}{2H}\right)s^3 + \left(\frac{1-f_F}{T_{ex}} \cdot \left(\frac{1}{T} + \frac{D}{2H}\right) + \frac{f_v K_4 - f_p K_2}{TT_{ex}} + \frac{D}{2HT} + \frac{\pi f_o K_1'}{H}\right)s^2$$

$$+ \left(\frac{1-f_F}{T_{ex}} \cdot \left(\frac{D}{2HT} + \frac{\pi f_o K_1'}{H}\right) + \frac{f_s K_2 + D\cdot(f_v K_4 - f_p K_2)}{2HTT_{ex}} + \frac{\pi f_o K_1}{HT}\right)s$$

$$+ \left(\frac{1-f_F}{T_{ex}} \cdot \left(\frac{\pi f_o f_v}{HT}\right) + \frac{f_o f_v (K_1' K_4 + K_2 K_3')}{HTT_{ex}}\right) = 0 \qquad (4.1)$$

Suppose the controller is designed so that the characteristic polynomial corresponds to a fourth-order standard form. As discussed in section 2.5.1, the relative pole positions are governed by the constants a_1, a_2 and a_3; the time scale of the response is determined by ω_1. An alternative form of the characteristic equation is then:

$$s^4 + a_1\omega_1 s^3 + a_2\omega_1^2 s^2 + a_3\omega_1^3 s + \omega_1^4 = 0 \qquad (4.2)$$

By comparison of the coefficients of the powers of s in equations (4.1) and (4.2), four equations are derived for the gains in terms of the standard form parameters and constants describing the system and its operating point:

$$f_F = 1 + T_{ex}(1/T + D/2H - a_1\omega_1) \quad (4.3)$$

$$f_v = \frac{(H/\pi f_o)TT_{ex}\omega_1^4 + (f_F - 1)K_1}{K_1'K_4 + K_2K_3'} \quad (4.4)$$

$$f_p = \frac{T_{ex}(D/2H + T((\pi f_o/H)K_1' - a_2\omega_1^2)) + f_vK_4 + (1 - f_F)(1 + TD/2H)}{K_2} \quad (4.5)$$

$$f_s = \frac{T_{ex}(2HTa_3\omega_1^3 - 2\pi f_oK_1) + 2H(f_F - 1)(D/2H + (\pi f_o/H)K_1'T) - D(f_vK_4 - f_pK_2)}{K_2} \quad (4.6)$$

4.2.2 The choice of control strategy

The three strategies used with the third-order model may also be applied to the fourth-order case.

(1) Fixed-gain controllers - PP/4/FG

The gains necessary to achieve an ITAE pole configuration at a nominal steady-state operating point may be computed by equations (4.3) to (4.6). If the gains are fixed at these values for all loading conditions, the resulting control strategy is denoted by PP/4/FG to denote Pole-Placement using a 4th-order model with Fixed-Gains.

(2) Controllers with fixed pole locations - PP/4/AG/FP

When pole positions independent of load are required, the values of a_1, a_2, a_3 and ω_1 are constants in equations (4.3) to (4.6) and variations in generator output change only the values of K_1, K_1', K_2, K_3' and K_4. Inspection of equation (4.3) reveals that the value of f_F is independent of load; only three adjustable-gains are required to implement a controller which maintains fixed pole positions using the fourth-order model. The controllers which use Pole-Placement for a 4th-order model to choose Adjustable-Gains which result in Fixed Pole-positions independent of generator load are denoted PP/4/AG/FP.

(3) Controllers with fixed voltage gain - PP/4/AG/Ff_v

In Chapters 2 and 3 it is shown that when the voltage gain, f_v, is fixed, it is possible by using two adjustable subsidiary feedback gains to maintain the poles of a third-order model of the system in an optimum configuration. Furthermore, changes in load have a relatively small effect on the scale factor, ω_1, and hence in the speed and damping of the response. An equation expressing ω_1 in terms of f_v is derived for the fourth-order system by the substitution of equation (4.3) into equation (4.4):

$$\omega_1^{\,4} - \left(\frac{\pi f_o}{H} \cdot \frac{a_1 K_1}{T}\right)\omega_1 - \left(\frac{\pi f_o}{H} \cdot \left[\frac{f_v (K_1' K_4 + K_2 K_3')}{TT_{ex}} + \frac{K_1}{T}\left(\frac{D}{2H} + \frac{1}{T}\right)\right]\right) = 0 \qquad (4.7)$$

When the PP/3/AG/Ff_v strategy is considered in Chapter 2, it is evident from equation (2.13) that ω_1 for the third-order model varies as the cube root of $(K_1' K_4 + K_2 K_3')$. In the present case, the dependence of ω_1 on operating point is not as clear cut. It is found, however, that irrespective of the system parameters used, the variation in ω_1 with operating point is smaller for the fourth-order model than for the PP/3/AG/Ff$_v$ strategy; as might be expected from equation (4.7) the variations depend approximately on $(K_1'K_4 + K_2K_3')^{\frac{1}{4}}$.

When f_v is fixed, the value of ω_1 is dependent on load; equation (4.3) shows that unlike for the fixed pole case, the feedback f_F needs to be adjusted with operating point in order to maintain the relative pole positions. Thus with the fourth-order model, the use of the fixed voltage gain strategy requires the same number of adjustable-gains as that of fixed pole positions. The Adjustable-Gain strategy utilising Fixed voltage gain f_v for Pole-Placement with a 4th order system model is denoted PP/4/AG/Ff$_v$.

4.2.3 The choice of pole positions

In view of the success in Chapter 3 of controllers designed by placing poles so that the characteristic polynomial corresponds to a third-order zero position-error ITAE standard form, this pole-placement method is applied to the fourth-order system. Graham [48] lists the values of a_1, a_2 and a_3 to be 2.1, 3.4 and 2.7 respectively; the corresponding pole positions are $s = -0.42\ \omega_1 \pm j\ 1.26\ \omega_1$ and $s = -0.63\ \omega_1 \pm j\ 0.41\ \omega_1$. Controllers which are designed to have their poles in this configuration are denoted by the letter "A", for example PP/4/FG/A or PP/4/AG/FP/A.

In the example in Figure 4.1, increases in the time lag due to the regulator improve the damping of the system while there is one pair of complex poles. However, soon after the second complex pair of poles emerges, further increases in the lag cause deterioration in damping. It is shown in Chapter 5 that one effect of the amortisseur windings, which are omitted in the fourth-order model, is to increase the lag in the regulator loop. This additional lag results in a degradation in performance for the 'A' strategies which have the poles in 2 complex pairs.

Suppose that the system is designed to have three dominant poles in positions corresponding to the third-order zero position-error ITAE standard form, and a fourth non-dominant pole deeper in the left half of the s-plane. Because there is only one pair of complex poles, the effect of neglected lags should be reduced. The relative pole positions are chosen to be $s = -0.40\ \omega_1 \pm j\ 0.81\ \omega_1$, $-0.54\ \omega_1$ and $-2.28\ \omega_1$ in order to place the exciter pole near its open loop value, ($s = -1/T_{ex}$ for $T_{ex} \approx 0.05$ sec.), for typical rotor oscillation frequencies. As discussed in section 2.5.1, the relative pole positions and the standard form constants are interrelated because a_1, a_2 and a_3 simply describe the relative sizes of the coefficients of the characteristic equation. The values of the standard form constants a_1, a_2 and a_3 corresponding to the new pole configuration are 3.61, 4.27 and 3.27 respectively. Controllers designed to have their poles in this configuration are denoted the letter "B".

4.2.4 A summary of the fourth-order model based pole-placement control strategies

The pole-placement control strategies developed in this chapter are summarized in Table 4.1. In this thesis the values of a_1, a_2 and a_3 are chosen to be either 2.1, 3.4 and 2.7 respectively corresponding to the "A" strategies or 3.61, 4.27 and 3.27 corresponding to the "B" strategies. The pole-placement strategies may, however, be used with any pole configuration or standard form by substituting the appropriate values for a_1, a_2 and a_3.

		PP/4/FG/A PP/4/FG/B	PP/4/AG/FP/A PP/4/AG/FP/B	PP/4/AG/Ff$_v$/A PP/4/AG/Ff$_v$/B
Design –		Specify: (a) design operating point, (b) a_1, a_2, a_3 and ω_1 or the positions of the 4 poles (at the design operating point).	(a) a_1, a_2, a_3 and ω_1 or the the locations of the 4 fixed poles.	(a) voltage gain f_v, (b) a_1, a_2 and a_3 or the relative positions of the 4 poles.
Effect of Changes in Operating Point	f_v	none - fixed value	adjusted according to equ.(4.4)	none - fixed value
	f_p	none - fixed value	adjusted according to equ.(4.5)	adjusted according to equ.(4.5)
	f_s	none - fixed value	adjusted according to equ.(4.6)	adjusted according to equ.(4.6)
	f_F	none - fixed value	none - fixed value	adjusted according to equ.(4.3)
	a_1	vary, in general do not correspond to a known standard form except at nominal load	none	none
	a_2		none gains adjusted to keep these constant	none gains adjusted to keep these constant
	a_3		none	none
	ω_1	varies according to equ.(4.7)	none	varies according to equ.(4.7)
poles		vary, calculated from equ.(4.1)	fixed	proportional to ω_1

TABLE 4.1 SUMMARY OF POLE-PLACEMENT CONTROL STRATEGIES BASED ON FOURTH-ORDER MODEL

In this thesis

the "A" strategies have $a_1 = 2.1$, $a_2 = 3.4$, $a_3 = 2.7$ resulting in poles at $s = -0.42\ \omega_1 \pm j\ 1.26\ \omega_1$ and $s = -0.63\ \omega_1 \pm j\ 0.41\ \omega_1$.

the "B" strategies have $a_1 = 3.61$, $a_2 = 4.27$, $a_3 = 3.27$ resulting in poles at $s = -0.40\ \omega_1 \pm j\ 0.81\ \omega_1$, $-0.54\ \omega_1$ and $-2.28\ \omega_1$.

4.3 FEEDBACK GAIN REQUIREMENTS OF THE POLE-PLACEMENT STRATEGIES BASED ON THE FOURTH-ORDER SMIB MODEL

4.3.1 Dependence on the choice of ω_1

In the previous section, two different pole configurations are proposed for use with the pole-placement strategies based on the fourth-order model. Investigation shows that the feedback gains necessary to achieve these pole positions are not excessive. Typical requirements in the normal operating region are illustrated by Table 4.2. Synchronising and damping torque concepts may be applied, as in section 3.2.1, to explain the way the subsidiary feedback gains f_s and f_p vary with ω_1. The effect of the field voltage feedback may be explained by noting that it reduces the effective values of T_{ex}, f_v, f_s and f_p by a factor $(1 - f_F)$. When f_v is low the system tends to have only one pair of complex poles; in order to achieve two pairs as required in fourth-order ITAE pole-placement, positive feedback of field voltage ($f_F > 0$) is used to increase the effective exciter time constant and voltage gain. When f_v is high the system tends to have two pairs of complex poles; negative feedback of field voltage ($f_F < 0$) is used to suppress the regulator oscillatory mode in the case of the standard form with one pair of complex poles.

Pole-placement using the two standard forms has been investigated for different sets of system parameters. In each case a solution which offers reasonable damping and frequency of oscillation with acceptable feedback gains was found.

f_v	f_s	f_p	f_F	ω_1	poles
50	959	-18.0	+0.24	7.48	$-3.17 \pm j\ 9.47,\ -4.66 \pm j\ 3.12$
100	2290	-22.8	+0.09	8.88	$-3.78 \pm j\ 11.22,\ -5.56 \pm j\ 3.68$
150	3513	-23.8	-0.01	9.82	$-4.17 \pm j\ 12.39,\ -6.16 \pm j\ 4.06$
200	4663	-22.9	-0.08	10.55	$-4.47 \pm j\ 13.37,\ -6.56 \pm j\ 4.39$
300	6810	-17.7	-0.20	11.67	$-4.94 \pm j\ 14.76,\ -7.29 \pm j\ 4.84$

(a) poles in configuration "A"

f_v	f_s	f_p	f_F	ω_1	poles
50	433	-27.6	-0.33	7.51	$-2.98 \pm j\ 6.09,\ -4.06,\ -17.0$
100	1909	-36.3	-0.58	8.90	$-3.54 \pm j\ 7.22,\ -4.81,\ -20.2$
150	3298	-40.4	-0.75	9.84	$-3.90 \pm j\ 7.99,\ -5.30,\ -22.4$
200	4619	-42.1	-0.88	10.56	$-4.19 \pm j\ 8.58,\ -5.69,\ -24.0$
300	7108	-41.3	-1.09	11.68	$-4.60 \pm j\ 9.49,\ -6.24,\ -26.8$

(b) poles in configuration "B"

gains and pole positions at $(\overline{P},\overline{Q}) = (0.9,\ 0.0)$ for system with $x_d = 1.6$, $x_d' = 0.32$, $x_q = 1.55$, $x_e = 0.4$, $T'_{do} = 6.0$ (row 3 of Table 3.2) and $T_{ex} = 0.05$ secs.

TABLE 4.2 FEEDBACK GAINS AND POLE POSITIONS FOR THE FOURTH-ORDER POLE-PLACEMENT STRATEGIES

4.3.2 Variation of feedback gain requirements with load

The way the gains required to implement the pole-placement strategies vary with operating point has been investigated for several sets of system parameters and various values of ω_1. As for the PP/3/AG/FP and the PP/3/AG/Ff$_v$ strategies (section 3.2.2), it is found that the dominant effects are due to the denominator of the expressions for feedback gain (equations (4.3) to (4.6)).

The voltage gain f_v for the constant pole position strategies PP/4/AG/FP/A and PP/4/AG/FP/B depends mainly on $(K_1'K_4 + K_2K_3')^{-1}$, and is large when excitation levels are small. The speed and power feedback gains f_s and f_p are dependent on K_2^{-1} and become large under low power, low power-factor conditions. The value of f_F required for constant pole positions does not change with load. Figures 4.3 and 4.4 show the gains required to implement the PP/4/AG/FP strategies for the example used in section 3.2.2. These may be compared with those for the PP/3/AG/FP strategy in Figure 3.3.

When the constant voltage gain strategies PP/4/AG/Ff$_v$/A and PP/4/AG/Ff$_v$/B are applied, as stated in section 3.2.2, the value of ω_1 varies less than for the third-order model based PP/3/AG/Ff$_v$ strategy. However, the speed and the power feedback gains still depend mainly on K_2^{-1}. The value of f_F depends only on ω_1 and hence varies according to its value. Figures 4.5 and 4.6 show the gains necessary to implement the PP/4/AG/Ff$_v$ strategies which may be compared with those in Figure 3.4 for the PP/3/AG/Ff$_v$ case.

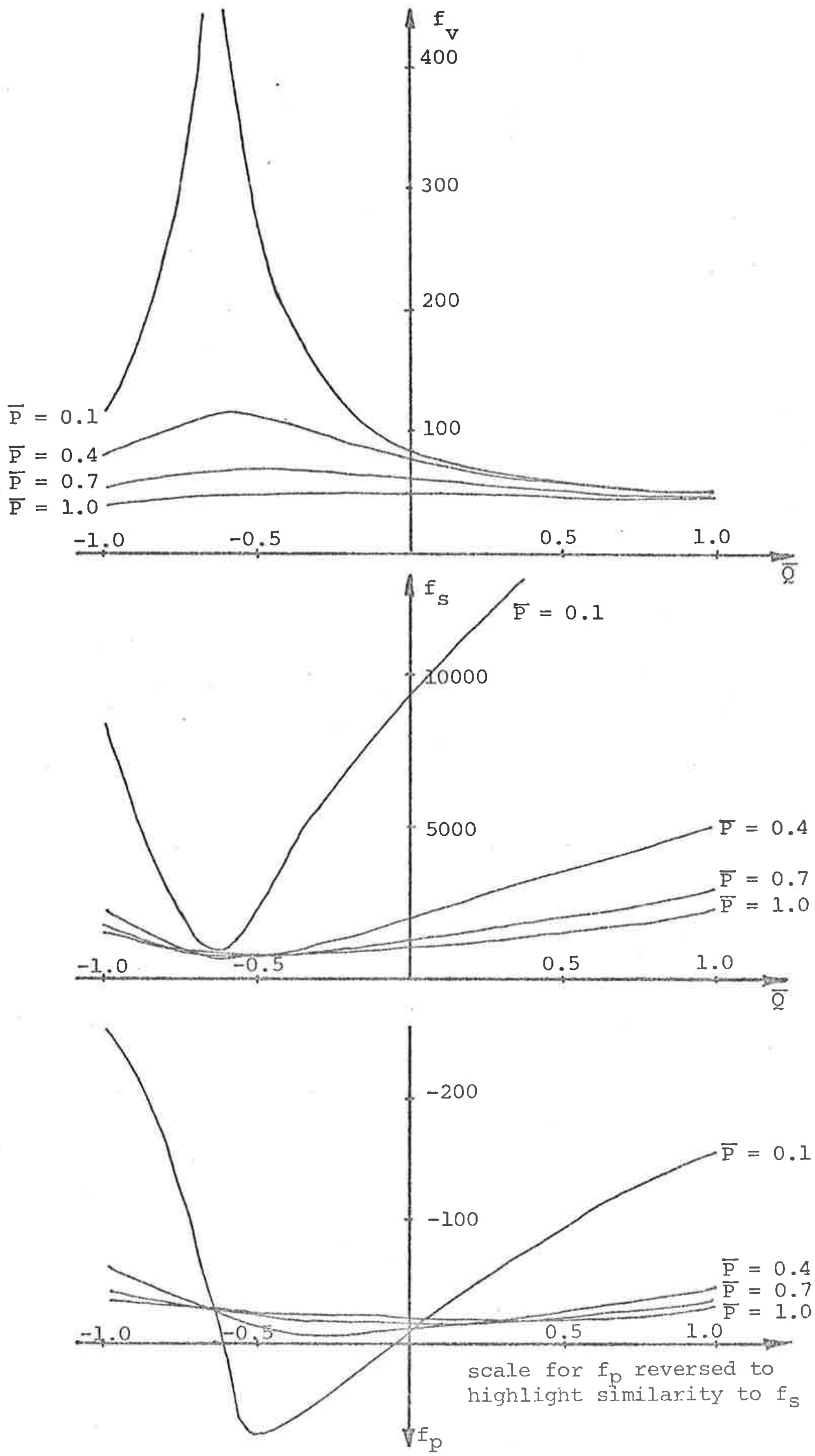

FIGURE 4.3 ADJUSTMENT OF FEEDBACK GAIN NECESSARY TO IMPLEMENT STRATEGY PP/4/AG/FP/A

(System data in row 3 of Table 3.2, T_{ex} = 0.05 s. Poles specified to lie at s = -3.22 ± j 9.60, s = -4.7 ± j 3.13.)

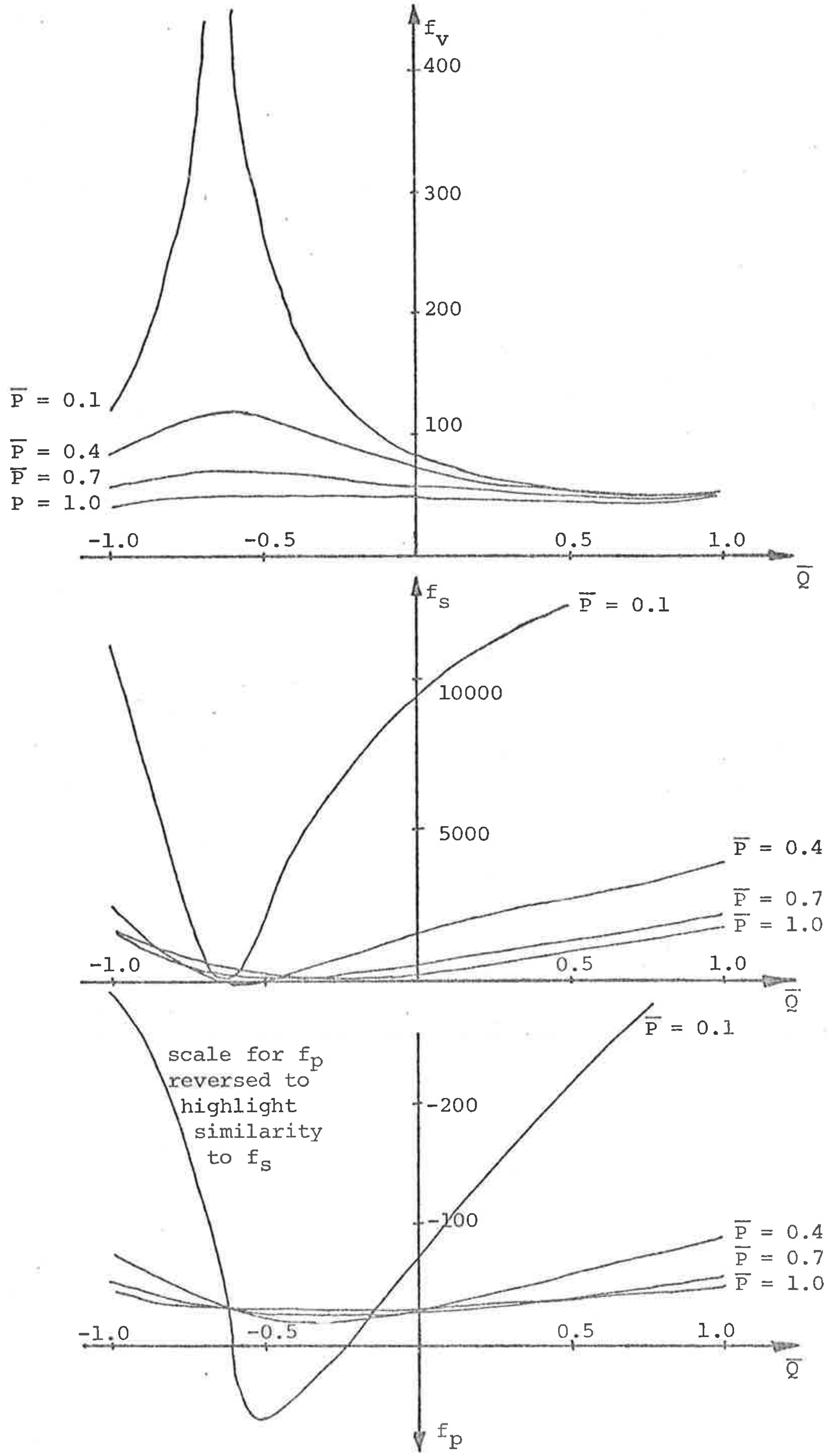

FIGURE 4.4 ADJUSTMENT OF FEEDBACK GAIN NECESSARY TO IMPLEMENT STRATEGY PP/4/AG/FP/B

(System data in row 3 of Table 3.2, T_{ex} = 0.05 s. Poles specified to lie at s = -2.85 ± j 5.85, s = -3.88 and s = -20.0.)

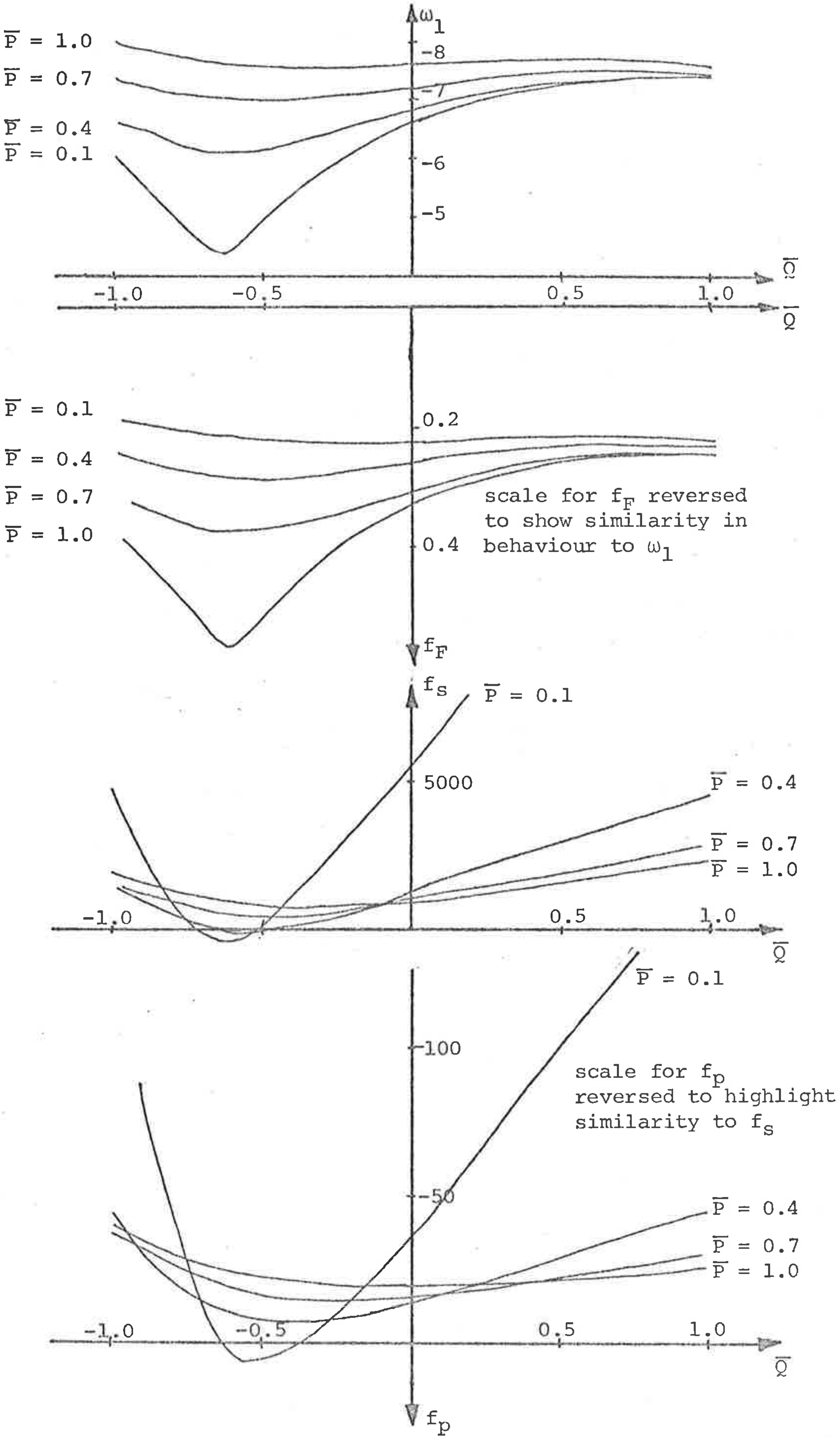

FIGURE 4.5 ADJUSTMENT OF FEEDBACK GAIN NECESSARY TO IMPLEMENT STRATEGY PP/4/AG/Ff_v/A AND THE VARIATION IN ω_1

(System data in row 3 of Table 3.2, T_{ex} = 0.05 s. Voltage gain, f_v fixed at 50; a_1 = 2.1, a_2 = 3.4, a_3 = 2.7.)

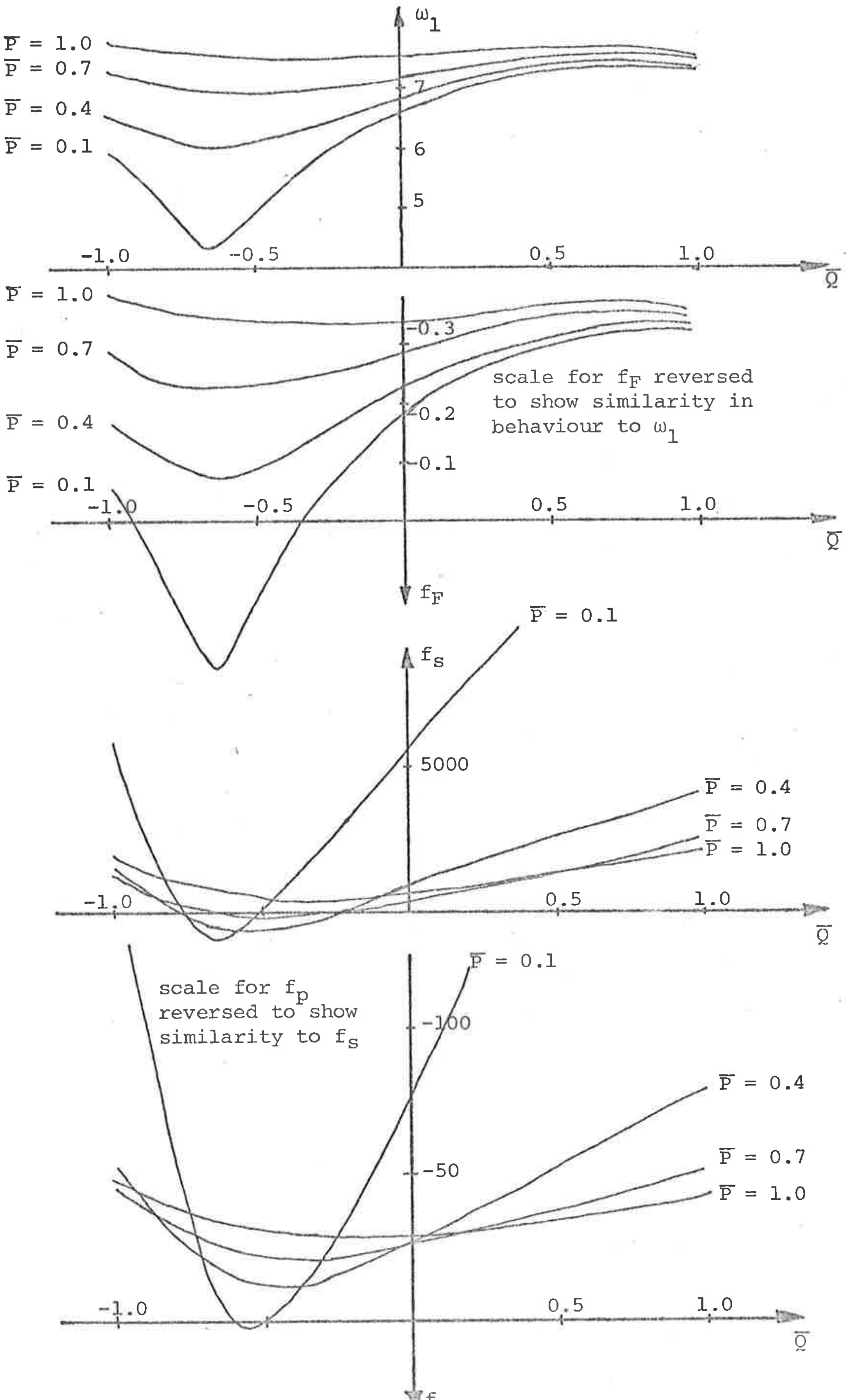

FIGURE 4.6 ADJUSTMENT OF FEEDBACK GAIN NECESSARY TO IMPLEMENT STRATEGY PP/4/AG/Ff_v/B AND THE VARIATION IN ω_1

(System data in row 3 of Table 3.2, T_{ex} = 0.05 s. Voltage gain fixed at 50; a_1 = 3.61, a_2 = 4.27, a_3 = 3.27.)

It has been found that when the exciter time constant is short (typically 0.05 secs.), the gains required by the strategies based on the fourth-order model do not differ greatly from those for the strategies based on the third-order model. As the exciter time constant, T_{ex}, is increased, larger feedback gains are required to achieve comparable performance. Irrespective of the value of T_{ex}, the way the gains must be adjusted with load depends mainly on the denominator terms of the gain expressions.

4.4 A PRELIMINARY COMPARISON OF THE PERFORMANCE OF POLE-PLACEMENT STRATEGIES BASED ON THIRD AND FOURTH ORDER MODELS

In Chapter 3 it is shown that the PP/3/AG/FP and PP/3/AG/Ff$_v$ strategies give improved performance over Abdel-Magid's design, despite the fact that performance is compared using his model which includes an exciter time constant and a washout filter not allowed for in the pole-placement design. This same model is used to compare the performance of the PP/4/AG/Ff$_v$/A, PP/4/AG/Ff$_v$/B and PP/3/AG/Ff$_v$ strategies.

Figure 4.7 shows the performance of the three strategies when a medium value of f_v equal to 50 is chosen and the exciter time constant has a value of 0.05 seconds. The fastest response and best damping is given by strategy PP/4/AG/Ff$_v$/A having the poles in the fourth-order ITAE positions but this leads to the largest swing in electrical power. Although the nominal position of the poles of the PP/3/AG/Ff$_v$ strategy are very close to those of the PP/4/AG/Ff$_v$/B dominant poles, it may be seen that the effect of the short exciter time constant has been to improve slightly the damping and speed of response.

Figure 4.8 shows the behaviour of controllers using the 3 strategies when f_v is increased to 200. The PP/4/AG/Ff$_v$/A strategy again leads to the best response. However, contrary to the previous case, because the voltage gain f_v is higher, the exciter time constant causes a slight deterioration in the performance of the PP/3/AG/Ff$_v$

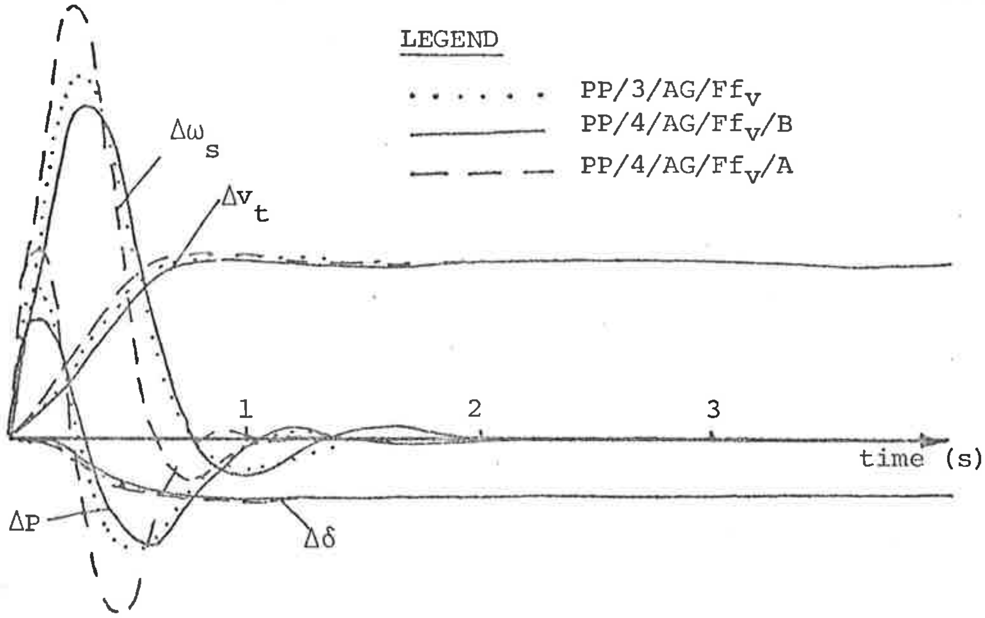

FIGURE 4.7 COMPARISON OF RESPONSES WITH $f_v = 50$ AND $T_{ex} = 0.05$ SECONDS

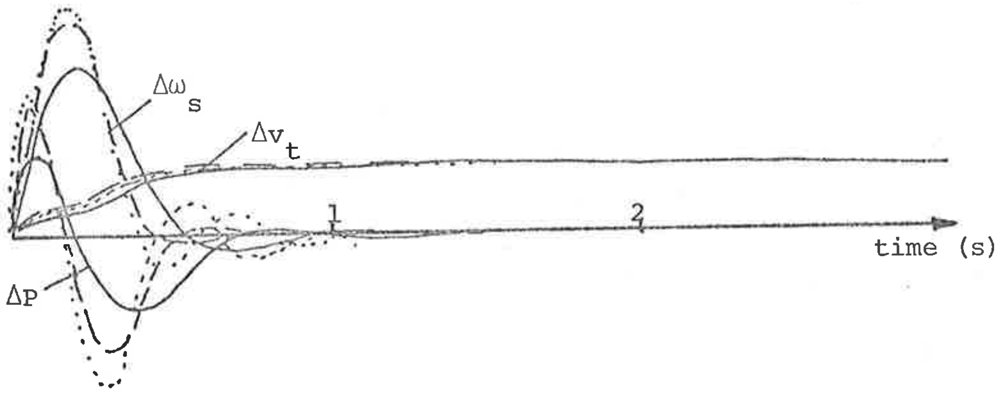

FIGURE 4.8 COMPARISON OF RESPONSES WITH $f_v = 200$ AND $T_{ex} = 0.05$ SECONDS

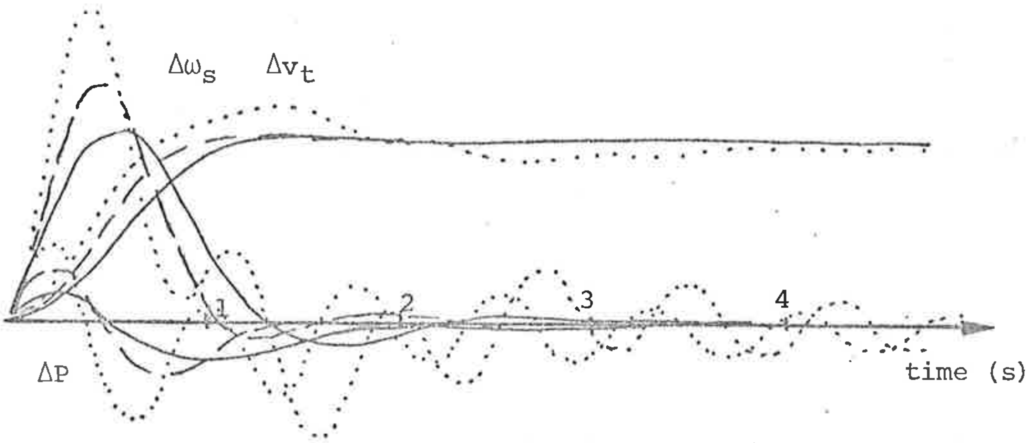

FIGURE 4.9 COMPARISON OF RESPONSES WITH $f_v = 50$ AND $T_{ex} = 0.5$ SECONDS

(For Figures 4.7, 4.8 and 4.9, system data is listed in row 3 of Table 3.2 and the controller includes a washout filter with a 1.5 s time-constant in the power feedback loop. The disturbance applied in each case is a step change in the terminal voltage set-point.)

	f_s	f_p	f_F	f_s	f_p	f_F	f_s	f_p	f_F
PP/3/AG/Ff$_v$	657	-27.6	-	4220	-31.6	-	657	-27.6	-
PP/4/AG/Ff$_v$/A	829	-20.2	0.23	4167	-38.6	-0.10	-3348	-14.5	-3.23
PP/4/AG/Ff$_v$/B	314	-28.2	-0.34	4075	-55.3	-0.91	-7949	-37.0	-6.41
	FIG 4.7			FIG. 4.8			FIG. 4.9		

controller; it may be seen that the oscillation frequency is higher and damping poorer than of the PP/4/AG/Ff_v/B controller which has dominant poles in the specified positions.

Figure 4.9 shows the responses when the voltage gain f_v is 50 but the exciter time constant is increased to 0.5 seconds. The use of the PP/3/AG/Ff_v strategy with the assumption of negligible exciter time constant is clearly not valid and leads to poorly damped oscillatory behaviour. The PP/4/AG/Ff_v/A and PP/4/AG/Ff_v/B strategies both give acceptable responses with the former controller having faster response but requiring larger deviations in speed and power to achieve this.

The above examples demonstrate that a short exciter time constant does not cause deterioration to the performance of the strategies developed in Chapter 3 provided only moderate voltage gain is used. The pole-placement strategies developed in this chapter are superior when the time constant is not negligible or when a large voltage gain and high speed of response (ω_1) are required.

Further comparison of all of the pole-placement strategies is made in the next chapter using a more realistic system model. For this reason, no conclusions are drawn at this stage concerning the relative merits of various strategies.

CHAPTER 5

THE PERFORMANCE OF POLE-PLACEMENT STRATEGIES WHEN APPLIED TO HIGHER-ORDER SMIB MODELS

5.1 REVISED PLANT AND CONTROLLER MODELS

As discussed in section 2.1, the plant model describing the generator and transmission system which is used for the pole-placement design of excitation controllers involves a large number of simplifying assumptions. This chapter examines the errors in pole-placement resulting from the inclusion of some of these neglected effects. The performance of all the pole-placement strategies are compared in order to determine the best strategies.

Until recently it was thought that the rotor was adequately represented in the q-axis by one rotor circuit describing the effect of the amortisseur winding with a single subtransient time constant; the inadequacy of this representation was demonstrated by Shackshaft [53]. Subsequent work by Schulz [54], Dandeno [55], Wilson [56] and others has resulted in the recognition of the importance of flux variations deep in the q-axis rotor iron, especially under leading power-factor conditions. For the following studies, in keeping with current practice [57], the generator rotor is represented by a field winding and a damper winding in the d-axis, and two damper windings in the q-axis. (The details of the model are discussed in Appendix 10.4.)

In this thesis the term "damper winding" is used to mean a rotor circuit which unlike the field winding, includes no voltage source. The term "amortisseur winding" is reserved for damper windings which model the subtransient effects produced by currents flowing near the surface of the rotor and in the rotor cage bars; the single d-axis damper winding and one of the q-axis damper windings are such windings. The behaviour of the flux in the q-axis rotor iron is described by a single damper winding which produces a transient time-constant for this axis.

Most controller designs appearing in the literature have been assessed with models having at most one q-axis damper winding; it is demonstrated that significant errors in the performance predicted near the leading power-factor stability limit result from the neglect of the q-axis rotor iron effects.

In order to ensure that the results of this investigation into the effects of generator modelling do not depend on the choice of generator parameters, the three different sets of data listed in Table 5.1 are employed.

In the previous chapters it is assumed that the mechanical power input is constant, thus the effect of governor action is ignored. In this chapter a third-order representation of the turbine and its speed-governor is included in the plant model in order to investigate its effect on performance. The turbine and governor model,

	MODEL			
	DA	DM	BB	
f_o (Hz)	60	60	50	
x_d (p.u.)	1.75	1.75	2.2	
x_d' (p.u.)	0.285	0.285	0.44	
x_d'' (p.u.)	0.24	0.24	0.324	
T'_{do} (sec.)	3.68	5.20	6.05	
T''_{do} (sec.)	0.029	0.011	0.041	Data derived
T_D (sec.)	0.016	0.006	0.012	from references
x_q (p.u.)	1.68	1.68	2.1	[43] and [55]
x_q' (p.u.)	0.47	0.47	0.64	
x_q'' (p.u.)	0.24	0.24	0.282	
T'_{qo} (sec.)	0.54	1.96	1.54	
T''_{qo} (sec.)	0.053	0.053	0.110	
D (p.u.)	0.0	0.0	0.0	
H (p.u.)	3.82	3.82	2.65	
r_a (p.u.)	0.003	0.003	0.003	
x_e (p.u.)	0.3	0.3	0.6	
T_{ex} (sec.)	0.05	0.05	0.05	
T_W (sec.)	2.0	2.0	2.0	Data selected
T_{CH} (sec.)	0.3	0.3	0.3	by author
T_{SM} (sec.)	0.2	0.2	0.2	
T_{SR} (sec.)	0.1	0.1	0.1	
r_e (p.u.)	0.03	0.03	0.06	
f_g	-25	-25	-25	

NOTES:

(1) BB parameters correspond to an 1500 MVA turbogenerator (Reichert [43]).

(2) Parameters DA and DM both refer to the same 800 MVA turbogenerator (Dandeno [55]). Set DA is derived from conventional ANSI tests but set DM is obtained by considering the frequency response of the direct and quadrature-axis operational impedances.

TABLE 5.1 PARAMETERS USED IN STUDIES WITH HIGHER-ORDER MODELS which is chosen for its simplicity, is taken from an IEEE Committee report [58] and represents a non-reheat turbine with a mechanical-hydraulic type governor. Comparison of performance with and without the inclusion of this model indicates the maximum error likely to stem from the neglect of the governor loop; for conventional steam turbines the long reheater time-constant reduces the effect of the governor on rotor oscillations.

A first-order model with a single exciter time-constant equal to 0.05 seconds is used to represent the excitation system. A washout filter with an arbitrarily chosen time-constant of 2 seconds is included in the electrical power feedback loop.

Figure 5.1 shows the block diagram for a linearised model of the entire SMIB system. The original set of nonlinear equations is used at the end of the chapter to investigate performance after major transmission system faults and is presented in Appendix 10.4.

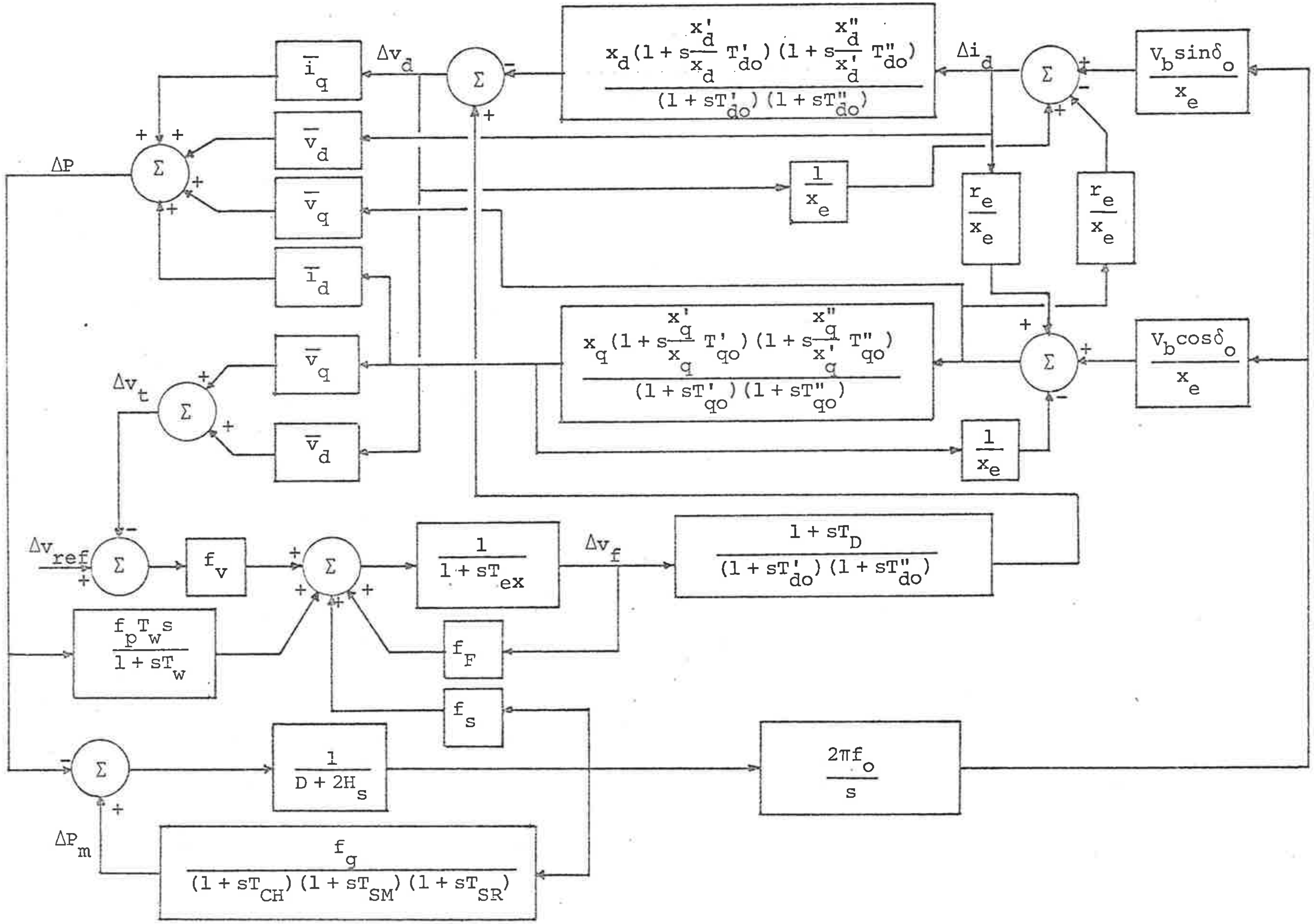

FIGURE 5.1 A LINEARISED MODEL OF THE SMIB SYSTEM EMPLOYING DETAILED GENERATOR AND CONTROLLER REPRESENTATION

5.2 THE EFFECT OF MODELLING ASSUMPTIONS ON THE POLES OF THE SMIB SYSTEM

5.2.1 Comparison of the effects with a fixed load

The effects of various simplifying assumptions on the poles of a generator, governor and excitation system are shown in Table 5.2(a). To confirm these results, similar studies have been carried out with different generator and controller parameters, but are not presented in this work. In order to illustrate the differences which may result from such changes, Table 5.2(b) shows the results for the same generator when the values of T'_{do}, T'_{qo} and T''_{do} are changed as suggested by Dandeno [55]. Figure 5.2 graphically displays the results of Tables 5.2(a) and (b). It appears that the largest changes occur in columns 2, 5, 6 and 8, but it should be noted that:

(a) The values in column 8 are obtained by inserting a large value of D in the rotor equation of motion. In general, the mechanical damping due to friction and windage is small so that errors resulting from its neglect are much smaller than those indicated.

(b) Column 6 shows that the governor loop reduces the damping of rotor oscillations. In general, the effect will be less than that indicated because the time constant of the reheater used with large turbo-alternators results in an attenuation of the effect of speed variations on the outputs of the LP and IP stages of the turbine.

1 full m/c model	2 rotor iron effects in q-axis neglected	3 q-axis amortisseur neglected	4 d-axis amortisseur neglected	5 d-axis and q-axis amortisseurs neglected	6 governor effects neglected	7 tie-line resistance neglected	8 insertion of damping in the eq. of motion (D = 2H)	9 washout filter neglected	
$-3.24\pm j6.30$	$-1.99\pm j5.40$	$-3.07\pm j6.63$	$-2.90\pm j6.68$	$-2.68\pm j6.90$	$-4.43\pm j7.21$	$-3.26\pm j6.75$	$-4.03\pm j5.63$	$-3.66\pm j6.41$	*a*
			-19.6	-19.6					
$-11.20\pm j3.73$	$-11.1\pm j3.39$	$-11.2\pm j3.99$	-11.5	-11.5	$-10.32\pm j4.99$	$-11.96\pm j3.20$	$-11.5\pm j3.37$	$-11.5\pm j3.40$	*b*
- 4.42	-	- 4.68	- 4.42	- 4.68	- 2.20	- 4.44	- 4.42	- 4.42	*c*
- 0.55	- 0.54	- 0.55	- 0.55	- 0.55	- 0.50	- 0.55	- 0.57		*d*
- 1.06	- 1.26	- 1.06	- 1.06	- 1.06	-	- 1.07	- 0.98	- 1.19	*e*
$-7.81\pm j5.83$	$-8.98\pm j6.49$	$-7.75\pm j5.13$	$-6.83\pm j4.29$	$-6.77\pm j3.95$	-	$-7.08\pm j5.10$	$-7.24\pm j6.90$	$-7.03\pm j5.73$	
-27.9	-68.5	-	-27.9	-	-27.9	-27.9	-27.8	-27.9	*f*
-43.4	-43.4	-43.4	-	-	-43.4	-43.2	-43.4	-43.4	

a poles due to equation of rotor motion
b poles due to field winding and exciter
c pole due to q-axis iron
d pole due to washout filter
e governor poles
f poles due to d- and q-axis amortisseur windings

<u>System Parameters:</u> Dandeno et al. ANSI data (DA: $T'_{do} = 3.68$, $T''_{do} = 0.029$, $T'_{qo} = 0.54$)

<u>Controller:</u> $f_v = 50$, $f_s = 103$, $f_p = -18.7$, $f_p = 0.586$ (PP/4/AG/FP/A)

<u>Operating Point:</u> $\overline{P} = 0.5$, $\overline{Q} = 0.0$, $\overline{V}_t = 1.0$

<u>TABLE 5.2(a) EFFECT OF MODELLING ASSUMPTIONS ON THE POLES OF THE SMIB SYSTEM</u>

1 full model	2 rotor iron effects in q-axis neglected	3 q-axis amortisseur neglected	4 d-axis amortisseur neglected	5 both d-axis and q-axis amortisseurs neglected	6 governor effects neglected	7 tie-line resistance neglected	8 damping term inserted in the eq. of motion (D = 2H)	9 washout filter neglected	
-2.03±j8.19	-2.09±j6.75	-1.76±j8.15	-1.95±j8.15	-1.68±j8.12	-2.40±j8.39	-1.88±j8.28	-2.67±j8.25	-2.07±j8.31	*a*
-0.54±j0.10	-	-0.54±j0.10	-0.54±j0.10	-0.54±j0.10	-0.66	-0.54±j0.10	-0.53±j0.12	-0.60	*b*
	-0.55				-0.49				
-2.01	-1.12	-2.03	-2.00	-2.03	-	-2.03	-1.98	-2.08	
-9.83	-9.82	-9.85	-9.73	-9.74	-	-9.73	-9.84	-9.77	*c*
-5.69±j2.85	-5.71±j3.25	-5.73±j2.80	-5.70±j2.72	-5.73±j2.67	-4.09	-5.68±j2.64	-5.56±j2.92	-5.59±j2.67	
-23.6	-23.5	-23.5	-24.9	-28.9	-23.5	-23.9	-23.6	-23.6	*d*
-26.8	-68.6	-	-26.8	-	-26.8	-26.9	-26.8	-26.8	*e*
-99.5	-99.5	-99.6	-	-	-99.5	-99.5	-99.5	-99.5	

a pole due to rotor equation of motion
b poles due to the q-axis iron effect and washout filter
c poles due to the governor and field winding
d exciter pole
e poles due to d- and q-axis amortisseurs

System Parameters: Dandeno et al. modified data (DM: $T'_{do} = 5.2$, $T''_{do} = 0.011$, $T'_{qo} = 1.96$)

Controller: $f_v = 50$, $f_s = 103$, $f_p = -18.7$, $f_F = 0.586$ (PP/4/AG/FP/A)

Operating Point: $\overline{P} = 0.5$, $\overline{Q} = 0.0$, $\overline{V}_t = 1.0$

TABLE 5.2(b) EFFECT OF MODELLING ASSUMPTIONS ON THE POLES OF THE SMIB SYSTEM

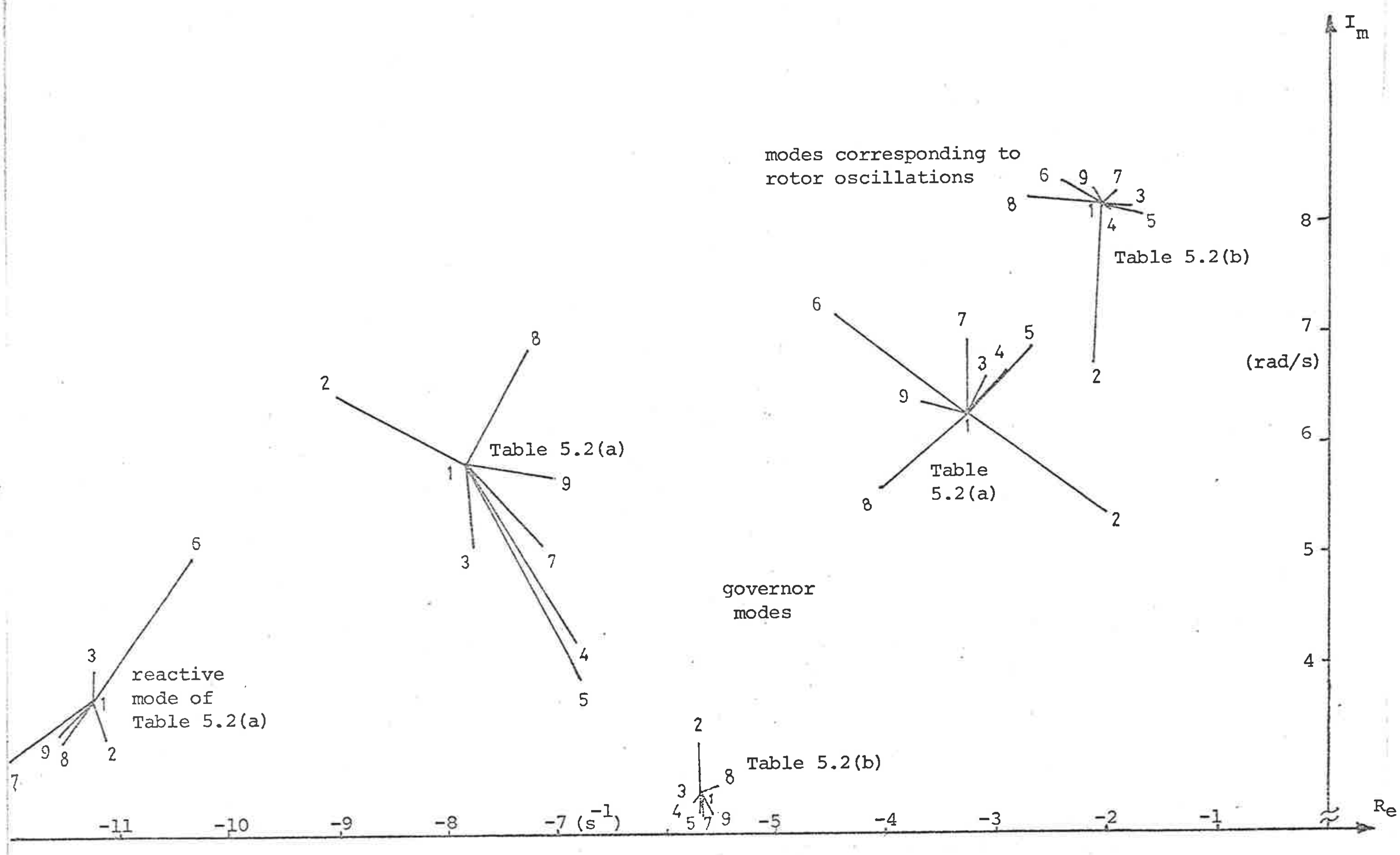

FIGURE 5.2 EFFECT OF SIMPLIFYING ASSUMPTIONS ON THE POSITIONS OF POLES FOR OSCILLATORY MODES

(1 corresponds to the pole positions for the full model and 2 - 9 show the changes in pole position associated with the assumptions in columns 2 to 9 of Table 5.2.)

(c) Column 5 corresponds to the neglect of both the d- and q-axis amortisseur windings (the effect of neglecting each separately is shown in columns 3 and 4). Dandeno investigated generator modelling for large-scale multi-machine studies and claimed that both d- and q-axis amortisseur windings can be ignored provided his method of calculating generator parameters from frequency-response tests is employed. Comparison of columns 1 and 5 in Tables 5.2(a) and (b) confirms that the error resulting from this simplification is indeed smaller for data set DM in Table 5.2(b). The reduced error may be attributed to the fact that the value of T''_{do} is lower than in the ANSI test data so that the phase lag introduced into regulator loop by the d-axis amortisseur is reduced at the frequency of rotor oscillations (see discussion in section 5.3.2).

(d) Column 2 corresponds to the neglect of the q-axis rotor iron effects. It is evident that the neglect of this effect results in much larger errors than the neglect of the q-axis amortisseur. This result is used in Chapter 8 to justify the neglect of the q-axis amortisseur in the utilisation of an existing digital computer program with provision for only one q-axis rotor winding.

5.2.2 Effect of load on the accuracy of simplified generator models

In the studies described in the previous section, it became evident that the errors resulting from reducing the number of windings in the generator model are heavily dependent on the reactive load. Table 5.3 lists the poles of an SMIB system with a PP/3/FB fixed-gain controller at various operating points - the poles resulting from four different generator models are compared. The oscillatory modes are plotted in Figure 5.3 to aid interpretation. In order to demonstrate that the results of the previous section are not unique to the generator used by Dandeno, a different machine is used.

Comparison of columns 1 and 2 reveals that effect of neglecting the d-axis amortisseur winding does not vary greatly with load; in general, its neglect leads to an optimistic estimate for the damping of rotor oscillations. The natural damping action of the amortisseur winding is negated by the effect of the phase-lag introduced into the regulator loop. The effect of the d-axis amortisseur is reduced somewhat at low lagging power-factor (p.f.).

Comparison of columns 2 and 3 shows that neglect of the q-axis amortisseur winding is only significant at low leading p.f. where it results in the damping of rotor oscillations being underestimated.

Comparison of columns 3 and 4 reveals that at lagging p.f. the q-axis rotor iron effects (T'_{qo}) produce a real pole close to the imaginary axis; the poles due to the exciter time-constant and the d-axis transient time-constant (T'_{do}) combine to form a complex conjugate pair, often called the reactive mode of oscillation (Moussa [26]). As the operating point moves towards leading p.f., the poles in the

TABLE 5.3 DOMINANT POLES RESULTING FROM DIFFERENT MODELS AT VARIOUS OPERATING POINTS

$\overline{Q}$	1 full model	2 no d-axis amortisseur	3 no d- or q-axis amortisseur	4 no q-axis rotor iron effect no d- or q-axis amortisseur
-0.8	-2.86±j10.19 -1.20±j 3.02 -5.55	-3.92±j 9.62 -1.32±j 2.95 -6.35	-1.95±j 9.24 -1.26±j 2.40 -15.4	+0.66±j 7.72 -10.88±j 0.98
-0.4	-2.28±j11.56 -2.67±j 1.28 -4.95	-3.73±j10.73 -2.41±j 1.15 -7.53	-3.22±j10.64 -2.06±j 1.29 -11.31	-2.73±j 9.85 -8.30 -6.69
0.0	-2.52±j11.62 -4.49±j 3.26 -1.38	-4.27±j10.35 -5.93±j 2.76 -1.39	-4.27±j10.35 -5.95±j 2.73 - 1.42	-3.99±j10.46 -6.24±j 2.18
0.4	-3.07±j10.72 -4.04±j 4.51 -1.27	-5.08±j 8.43 -5.32±j 5.51 -1.27	-5.35±j 8.43 -4.94±j 5.66 - 1.30	-5.40±j 8.77 -4.83±j 5.03
0.8	-4.13±j 9.46 -2.97±j 5.15 -1.31	-7.70±j 7.73 -2.61±j 5.69 -1.31	-7.71±j 7.83 -2.55±j 5.65 - 1.34	-7.61±j 7.87 -2.62±j 5.47

(a) $\overline{P} = 0.9$

$\overline{Q}$	1	2	3	4
-0.7	-1.97±j10.43 +0.01±j 1.48 -9.24	-2.68±j10.26 -0.01±j 1.49 -9.76	-1.54±j 9.92 -0.05±j 1.42 -18.7	-0.09±j 7.89 -17.9 - 2.40
-0.4	-2.04±j12.70 -9.38, -0.76 -2.03	-3.66±j12.06 -12.45±j1.13 -1.98	-3.72±j12.05 -11,57,-0.75 - 2.09	-3.78±j12.13 -11.80,-1.07
0.0	-3.01±j11.13 -4.85±j 3.91 -0.73	-4.50±j 9.57 -6.58±j 3.78 -0.73	-4.38±j 8.81 -6.18±j 4.95 - 0.73	-5.70±j 8.65 -4.52±j 2.99
0.4	-3.30±j 8.69 -4.46±j 5.97 -0.98	-2.67±j 7.22 -8.04±j 5.83 -0.98	-2.17±j 7.06 -8.27±j 6.02 - 0.98	-2.09±j 5.76 -8.13±j 6.28
0.8	-1.87±j 6.38 -5.77±j 7.38 -1.15	-1.56±j 6.24 -8.92±j 5.79 -1.15	-1.35±j 6.22 -8.99±j 5.83 - 1.17	-1.26±j 5.64 -8.96±j 5.89

(b) $\overline{P} = 0.3$

System Parameters: BB of Table 5.1
Controller: $f_v = 60$, $f_s = 1400$, $f_p = -45$, $f_F = 0$ (PP/3/FG fixed-gains designed by pole-placement at P, Q = 0.9, 0.1)

NOTE: The governor and washout filter are omitted from the model to simplify computation - it is found that the effect on each model is similar.

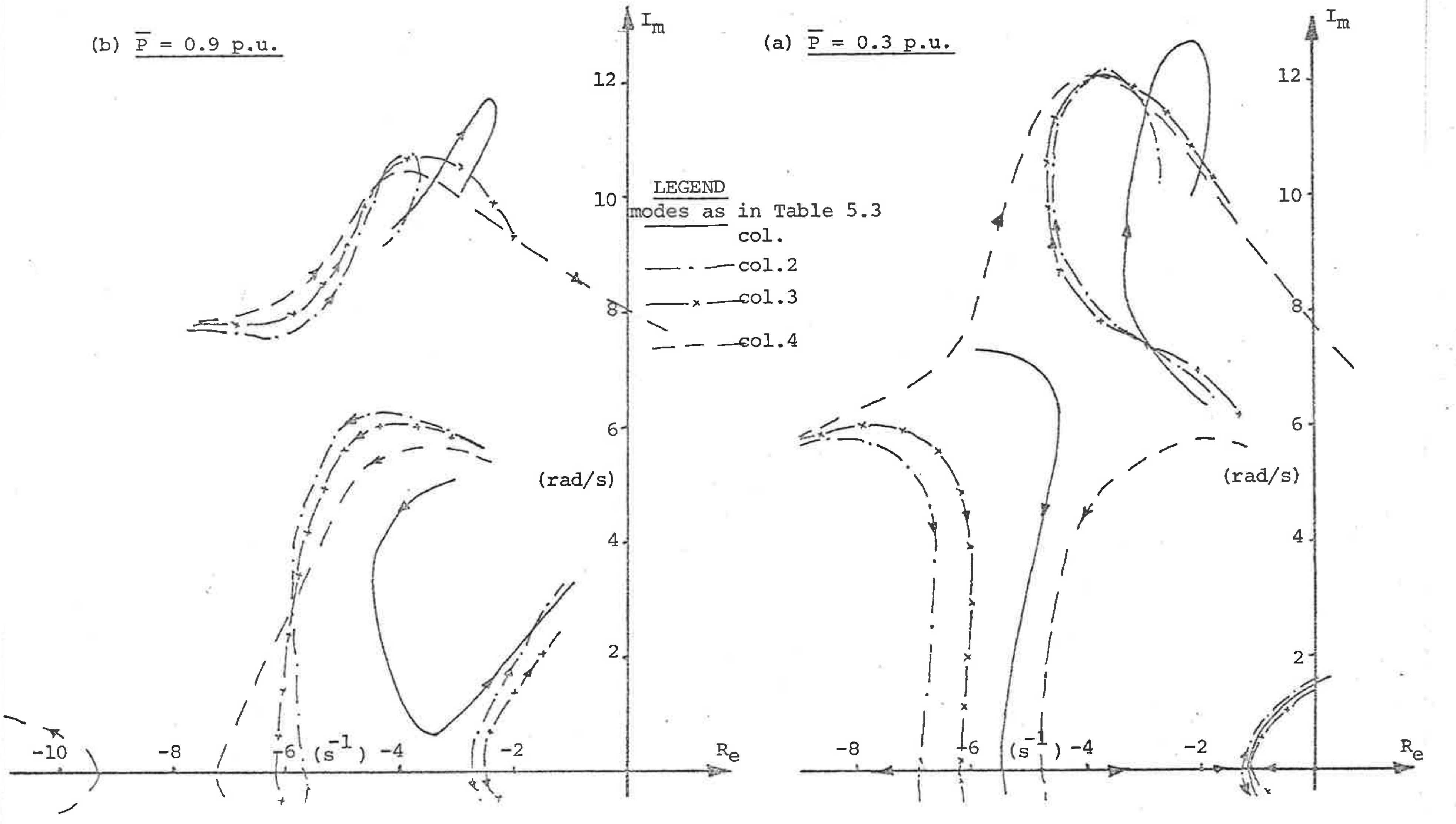

FIGURE 5.3 THE EFFECT OF REACTIVE LOAD ON THE DOMINANT OSCILLATORY MODES OF VARIOUS SMIB SYSTEM MODELS (Refer to Table 5.3)

reactive mode separate into two real poles. Further in the leading p.f. region the poles due to T'_{do} and T'_{qo} combine to form a low frequency oscillatory mode - the leading p.f. stability limit results from this mode. If the q-axis rotor iron effect is neglected the stability limit depends on a higher frequency mode of oscillation; the stability limit is then slightly optimistic at low real power output but significantly pessimistic at higher power outputs.

In order to explain the past success of controllers which have been designed in ignorance of the q-axis rotor iron effect, it should be noted that generators are usually operated near rated real power output and at lagging p.f. - this is a condition for which the load angle δ is high (e.g. $70° - 90°$). It may be deduced from Figure 5.1 that under such conditions the effect of the quadrature-axis loop is small since the torques produced in this axis depend on $\cos\delta$. Behaviour near the leading p.f. stability limit similar to that described above has been reported by Stephenson [59]. He investigated the effect of varying the damper time-constant of a generator model with only one damper in each axis.

Although the q-axis transient time-constant produces a lightly-damped real pole at lagging p.f., this mode has little effect on the behaviour of the system. Figure 5.4 illustrates the fact that with a high order system, inspection of the poles is not sufficient to determine the acceptability of performance. In order to decide whether lightly-damped

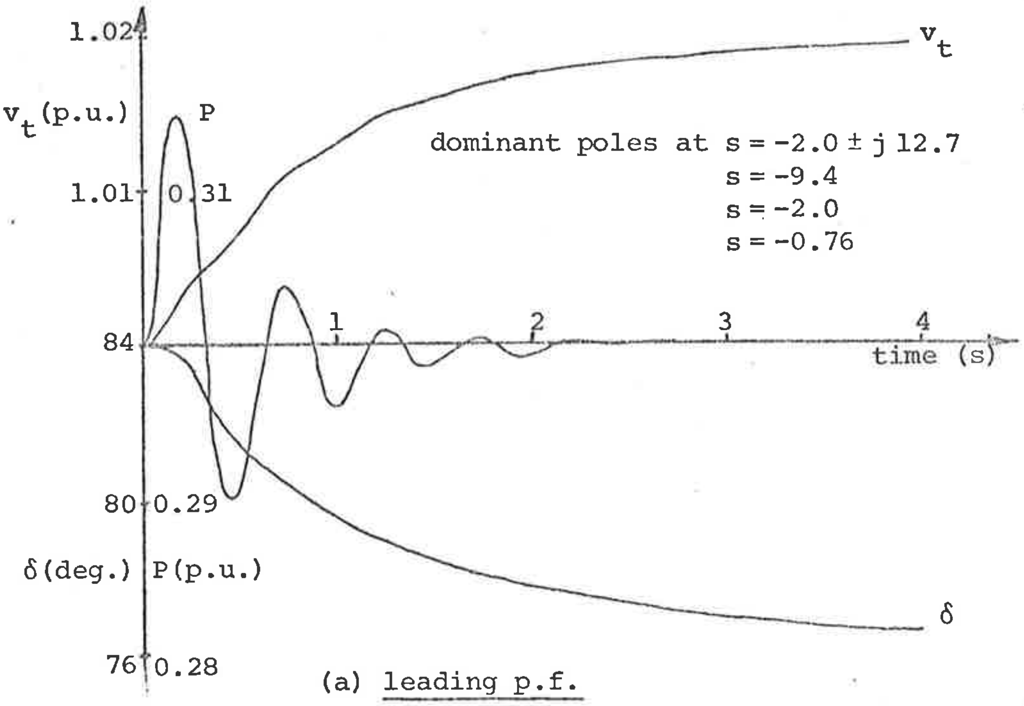

(a) leading p.f.

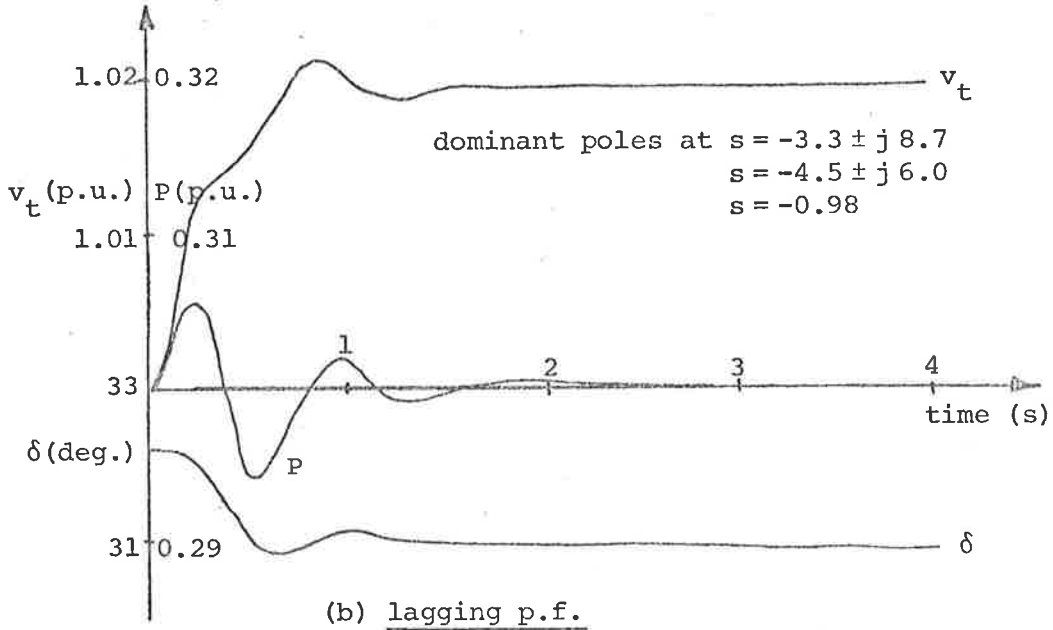

(b) lagging p.f.

FIGURE 5.4 A COMPARISON OF RESPONSES AT LEADING AND LAGGING POWER FACTOR

(System data is listed in column BB of Table 5.1.
Controller gains: $f_v = 60$, $f_s = 1400$, $f_p = -45$.
In case (a) $\overline{P} = 0.3$ p.u., $\overline{Q} = -0.4$ p.u. and in case (b) $\overline{P} = 0.3$ p.u., $\overline{Q} = +0.4$ p.u. The disturbance applied is a 2% step in voltage set-point.)

poles have a significant effect on the behaviour it is necessary either to perform eigenvector analysis or to compute the time response of the system following disturbances (see section 6.2 for further details on eigenvectors).

Results similar to those above have been obtained with each of the sets of generator data in Table 5.1.

5.3 SMALL-SIGNAL PERFORMANCE WITH POLE-PLACEMENT DESIGNED EXCITATION CONTROLLERS

5.3.1 Fixed-gain controllers

The feedback gain settings for the PP/3/FG fixed-gain design used in Table 5.3 are chosen on the basis of pole-placement for a third-order SMIB model. Following the guidelines of section 3.2.1, the poles are specified to lie at $s = -3.6 \pm j\,7.4$ and $s = -4.9$, when the load is $\overline{P} = 0.9$ p.u. and $\overline{Q} = 0.1$ p.u. Table 5.3 demonstrates that although the poles of the more detailed model are different from those predicted by the low-order model, the important features of the performance are the same:

(a) If the machine is operated at low excitation, (i.e. low $\overline{P}$ and $\overline{Q}$ near $-\frac{\overline{v}_t^{\,2}}{x_q}$), there exists a lightly-damped real pole, corresponding to the behaviour of the field flux linkages which results in poor voltage response.

(b) At low lagging p.f. the damping of rotor oscillations deteriorates as reactive load increases.

(c) The leading p.f. stability limit lies well outside the normal operating region defined in Chapter 1.

Table 5.4 compares the behaviour of three different fixed-gain controllers which are designed for a generator with data set DA in Table 5.1. For ease of interpretation, the oscillatory modes are plotted in Figure 5.5. Two controllers are designed by pole-placement, using strategies PP/3/FG and PP/4/FG, and the third is a design by Raina [61]

$\overline{Q}$	Fixed Gain Controllers 1	2	3	4 Variable Gain PP/4/AG/Ff$_v$/B
-1.0	-3.58±j 9.37 -1.32±j 4.36 -14.3	-5.55±j 7.36 -0.58±j 3.85 -19.8	-2.58±j28.03 -1.68±j 3.52 - 9.08	-6.67±j11.73 -1.37±j 2.76 -14.6
-0.4	-3.36±j12.54 -4.34±j 1.05 - 7.53	-4.49±j 8.95 -3.92±j 0.50 -15.04	-2.41±j33.15 -3.32±j 2.37 - 4.75	-5.15±j 7.29 -5.28±j 1.02 -10.29
0.0	-3.99±j12.54 -5.96±j 4.48 - 2.87	-4.24±j 8.32 -10.31±j2.28 - 2.73	-2.79±j33.09 -3.82±j 3.59 - 3.05	-4.23±j 8.32 -10.32±j2.25 - 2.73
0.4	-4.57±j11.67 -5.25±j 5.94 - 3.15	-3.30±j 7.70 -11.11±j3.93 - 3.11	-32.6±j31.81 -3.43±j 4.40 - 3.22	-4.47±j 9.15 -11.71,-9.02 - 2.74
0.8	-5.29±j10.42 -4.36±j 7.17 - 3.51	-2.47±j 7.47 -11.80±j3.69 - 3.51	-3.68±j30.38 -3.02±j 4.92 - 3.53	-4.62±j 9.52 -12.95,-7.57 - 2.96

(a) $\overline{P} = 0.9$

-1.0	-3.74±j 8.21 +0.88±j 2.92 -20.25	-4.82±j 7.56 +0.89±j 2.31 -24.1	-2.48±j18.55 -0.19±j 3.28 -15.4	-6.14±j12.74 -0.22±j 2.10 -14.9
-0.5	-3.49±j13.40 -8.66, -6.53 - 0.84	-4.91±j10.13 -15.83,-5.62 - 0.77	-2.46±j33.49 -5.28±j 2.07 - 0.85	-2.69±j 6.30 -10.01±j3.79 - 1.70
0.0	-5.45±j11.02 -5.28±j 6.04 - 1.91	-3.78±j 7.47 -11.52±j0.86 - 1.98	-4.07±j29.41 -3.85±j 4.79 - 1.80	-3.96±j 9.67 -12.6, -8.31 - 1.63
0.4	-6.87±j 9.16 -3.49±j 7.69 - 2.75	-2.50±j 7.54 -15.95,-9.06 - 2.83	-4.79±j26.95 -3.00±j 5.70 - 2.68	-4.53±j10.25 -13.70,-6.81 - 2.16
0.8	-2.30±j 7.85 -7.76±j 8.82 - 3.30	-1.79±j 7.64 -17.50,-8.47 - 3.37	-5.23±j25.5 -2.40±j 6.23 - 3.26	-4.77±j10.31 -14.05,-6.19 - 2.62

(b) $\overline{P} = 0.3$

System Data: DA, full model, no governor, no washout filter.

Controllers:

	f_v	f_s	f_p	f_F	design
1	50	565	- 15.6	0	PP/3/FG
2	50	103	- 18.7	-0.586	PP/4/FG
3	200	5573	-118.0	0	Raina
4	PP/4/AG/Ff$_v$/B				

TABLE 5.4

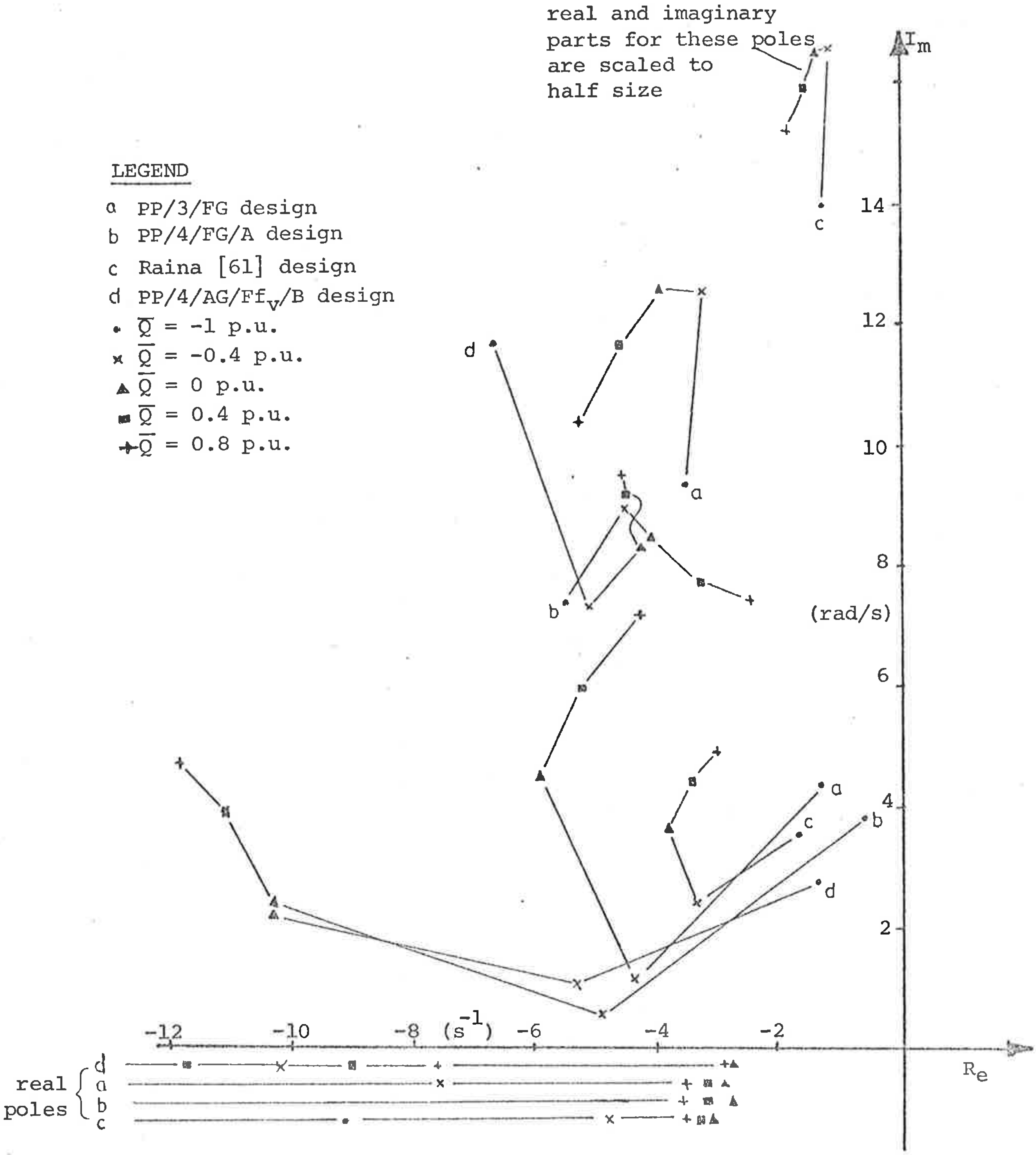

FIGURE 5.5(a) THE EFFECT OF REACTIVE LOADING ON THE SMIB SYSTEM WITH VARIOUS CONTROLLERS

(This figure shows the pole positions listed in Table 5.4(a))

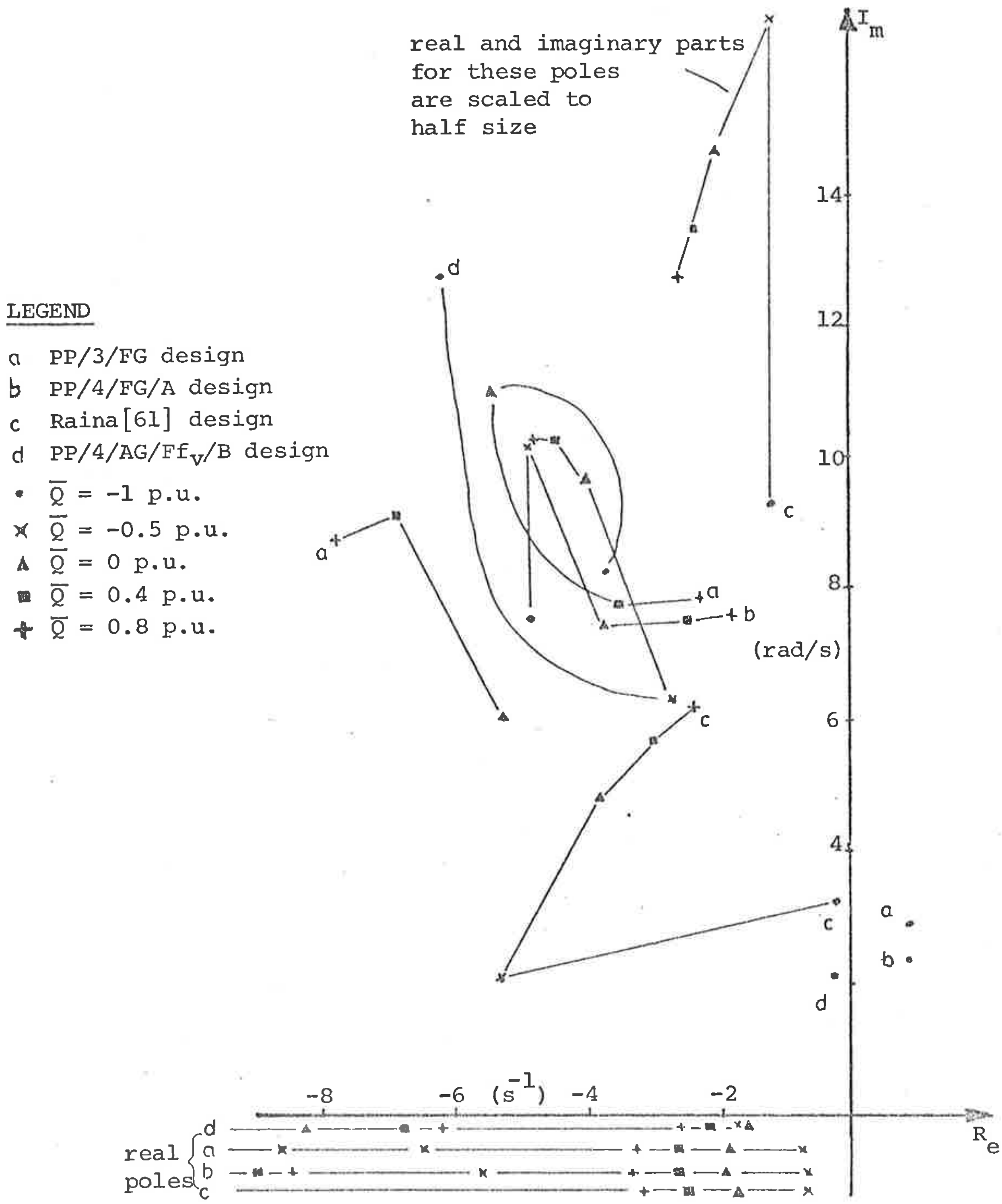

FIGURE 5.5(b) THE EFFECT OF REACTIVE LOADING ON THE SMIB SYSTEM WITH VARIOUS CONTROLLERS

(This figure shows the pole positions listed in Table 5.4(b)) based on the minimisation of a performance index for a fourth-order SMIB model. The high voltage-gain selected by Raina leads to a high frequency reactive mode of oscillation. There is little to choose between the performance of these designs. The behaviour noted above in points (a), (b) and (c) is again evident and has been observed with all fixed-gain controllers studied.

5.3.2 Comparison of adjustable-gain strategies

In Chapters 2 and 4 pole-placement concepts and simple models are used to develop a number of strategies with which to adjust the feedback gains of a controller in order to maintain heavy damping and fast speed of response with changing loading conditions. Table 5.5 shows the poles resulting from the application of these strategies at a wide range of operating points. A sixth-order generator model is used, but for simplicity, the governor and washout filter are not included because they affect each design to a similar extent. The complex poles of this table are plotted in Figure 5.6 as an aid to interpretation.

It is evident that the best damping results from the PP/4/AG/Ff_v/B and PP/4/AG/FP/B strategies and the worst from the PP/4/AG/Ff_v/A and PP/4/AG/FP/A strategies. The reason for this is the effect of the direct axis amortisseur winding on the poles due to the d-axis transient time-constant (T'_{do}) and the exciter time-constant.

The introduction of the d-axis amortisseur has a

$\overline{Q}$	1 PP/3/AG/Ff_V	2 PP/3/AG/FP	3 PP/4/AG/Ff_V/A	4 PP/4/AG/FP/A	5 PP/4/AG/Ff_V/B	6 PP/4/AG/FP/B	7 PP/4/FG/B
-0.8	-1.90±j13.73 -1.08±j 1.96 -6.87	-2.43±j13.23 -0.92±j 1.81 -6.67	-1.98±j14.70 -1.05±j 2.03 -5.99	-2.03±j14.00 -0.95±j 1.91 -5.99	-4.22±j13.16 -0.86±j 1.69 -7.26	-4.23±j12.49 -0.78±j 1.59 -7.30	-5.31±j 9.06 -0.66±j 2.86 -5.27
-0.4	-2.74±j12.42 -2.86±j 1.77 -3.30	-2.96±j12.16 -2.66±j 1.75 -3.44	-2.20±j12.62 -3.01±j 2.09 -2.83	-2.23±j12.44 -2.91±j 2.00 -2.83	-4.84±j10.52 -2.10±j 1.41 -5.76	-4.94±j10.20 -2.02±j 1.42 -5.80	-4.51±j 9.51 -2.36±j 1.42 -5.84
(p.u.) 0.0	-2.73±j11.57 -4.25±j 3.56 -1.38	-2.87±j11.47 -4.12±j 3.76 -1.38	-1.94±j11.64 -4.33±j 3.67 -1.38	-1.95±j11.64 -4.35±j 3.64 -1.38	-4.52±j 8.85 -5.34±j 3.18 -1.39	-4.61±j 8.58 -5.32±j 3.20 -1.39	*design op pt -4.52±j 8.85 -5.34±j 3.18 -1.39
0.4	-2.38±j11.06 -4.79±j 3.61 -1.27	-2.35±j11.06 -4.82±j 3.61 -1.27	-1.67±j11.36 -4.63±j 3.79 -1.27	-1.67±j11.49 -4.71±j 3.80 -1.27	-3.86±j 8.57 -6.14±j 3.02 -1.26	-3.90±j 8.42 -6.21±j 3.00 -1.26	-3.58±j 6.28 -6.52±j 5.97 -1.27
0.8	-2.18±j10.22 -5.04±j 3.11 -1.30	-1.83±j10.67 -5.33±j 3.17 -1.30	-1.52±j10.87 -4.52±j 3.49 -1.30	-1.45±j11.41 -4.79±j 3.62 -1.31	-3.41±j 8.17 -6.31±j 2.12 -1.30	-3.44±j 8.44 -6.58±j 2.10 -1.30	-1.83±j 5.32 -8.30±j 6.14 -1.31

(a) $\overline{P}$ = 0.9 p.u.

$\bar{Q}$	1 PP/3/AG/Ff$_v$	2 PP/3/AG/FP	3 PP/4/AG/Ff$_v$/A	4 PP/4/AG/FP/A	5 PP/4/AG/Ff$_v$/B	6 PP/4/AG/FP/B	7 PP/4/FG/B
-0.7	-3.47±j12.67 +0.12±j 1.45 -6.82	-2.82±j14.21 +0.27±j 1.74 -6.95	-2.35±j13.09 +0.20±j 1.57 -6.39	-2.36±j14.85 +0.33±j 1.79 -6.61	-4.31±j11.98 +0.07±j 1.36 -7.25	-4.61±j13.42 +0.16±j 1.57 -7.30	-3.37±j 9.48 +0.03±j 1.34 -9.28
-0.4	-5.21±j10.45 -2.46±j 3.30 -1.03	-3.08±j11.61 -4.36±j 4.56 -1.05	-2.29±j 9.14 -3.70±j 3.83 -1.04	-1.84±j11.39 -5.05±j 4.62 -1.05	-5.95±j 6.19 -3.46±j 4.46 -1.01	-4.26±j 7.80 -6.47±j 5.09 -1.04	-3.79±j10.93 -1.90 -0.71
(p.u.) 0.0	-2.75±j10.5 -5.31±j 4.01 -0.74	-1.53±j11.46 -6.83±j 4.73 -0.74	-1.33±j10.72 -5.36±j 4.34 -0.74	-0.96±j11.86 -6.56±j 5.10 -0.74	-3.17±j 8.93 -6.91±j 2.62 -0.74	-1.90±j 9.68 -8.73±j 2.97 -0.74	-3.62±j 8.64 -7.01±j 1.51 -0.73
0.4	-2.39±j10.97 -5.26±j 3.42 -0.94	-1.80±j11.50 -5.89±j 3.71 -0.94	-1.43±j11.24 -5.05±j 3.83 -0.94	-1.28±j11.94 -5.59±j 4.16 -0.94	-3.40±j 9.28 -6.44±j 1.94 -0.95	-3.36±j 9.63 -6.98±j 2.05 -0.94	-2.11±j 7.21 -8.44±j 1.68 -0.98
0.8	-1.39±j10.44 -5.04±j 3.01 -1.11	-1.76±j11.13 -5.63±j 3.24 -1.11	-1.45±j10.87 -4.70±j 3.45 -1.11	-1.32±j11.69 -5.20±j 3.74 -1.11	-3.37±j 8.65 -6.29±j 1.43 -1.12	-3.35±j 9.11 -6.78±j 1.52 -1.11	-1.26±j 6.23 -8.04,-10.6 -1.16

(b) $\bar{P}$ = 0.3 p.u.

System Parameters: BB of Table 5.1

Model: sixth-order generator model
no governor or washout filter

"Ff$_v$" strategies use f_v = 60

specified (PP/3/AG/FP : -3.3±j 6.8, -4.5
pole (PP/4/AG/FP/A : -3.6±j10.8, -5.4±j3.5
positions (PP/4/AG/FP/B : -3.3±j 6.8, -4.5, -20

TABLE 5.5 DOMINANT POLES FOR DIFFERENT POLE-PLACEMENT STRATEGIES

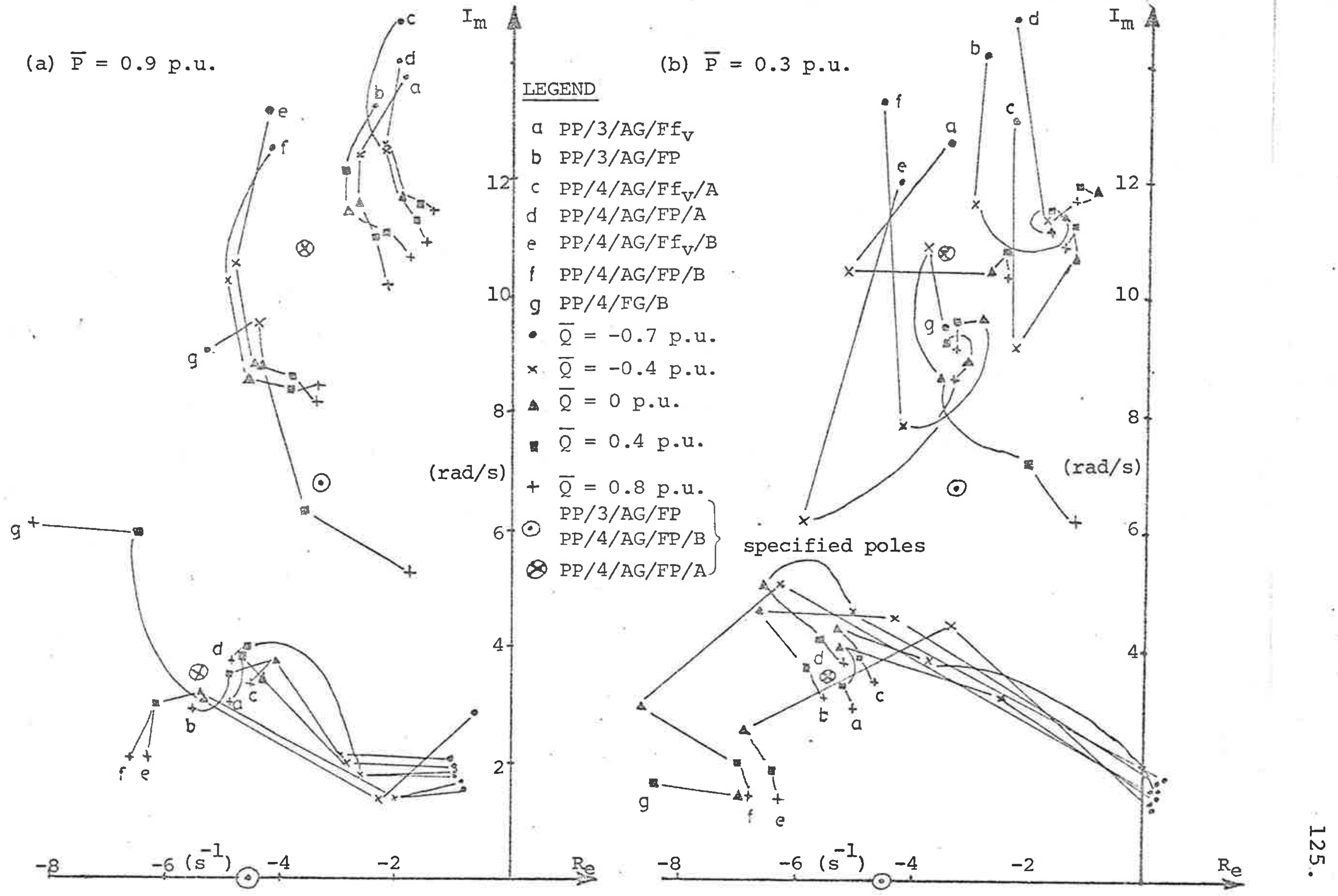

FIGURE 5.6 THE EFFECT OF REACTIVE LOADING ON THE SMIB SYSTEM WITH VARIOUS CONTROLLERS

(This figure shows the pole positions listed in Table 5.5.)

similar effect to that of changing the exciter time-constant. In order to demonstrate this, Figure 5.7 shows the effect of varying both the exciter time-constant and T_D, the d-axis damper time-constant (and hence T''_{do}) on the dominant poles of an SMIB system. Figure 4.1 shows that increasing the phase lag in the regulator loop of the PP/3/AG/FP and PP/3/AG/Ff_v designs makes the poles due to T'_{do} and the exciter time-constant move together and form a reactive mode of oscillation. Soon after the formation of this reactive mode, further increase in phase lag generally causes deterioration in the damping of both the reactive mode and the mode corresponding to rotor oscillations. The PP/4/AG/Ff_v/B and PP/4/AG/FP/B strategies take account of the phase lag due to the exciter time-constant and in addition place the T'_{do} and T_{ex} poles well apart on the real axis - this appears to offset the effect of the d-axis amortisseur. The PP/4/AG/Ff_v/A and PP/4/AG/FP/A strategies take account of the exciter time-constant but have a pole configuration in which the reactive mode is already present - the effect of the d-axis amortisseur phase lag is to cause an immediate deterioration in damping.

At lagging of the lightly-damped real pole due to the q-axis iron effect has little effect on performance, but at leading p.f. the low frequency oscillatory mode not predicted by models omitting T'_{qo} must be considered as well as the rotor oscillatory mode. The damping of this low frequency mode is similar for each of the adjustable gain strategies and they all have similar leading p.f. stability limits. It

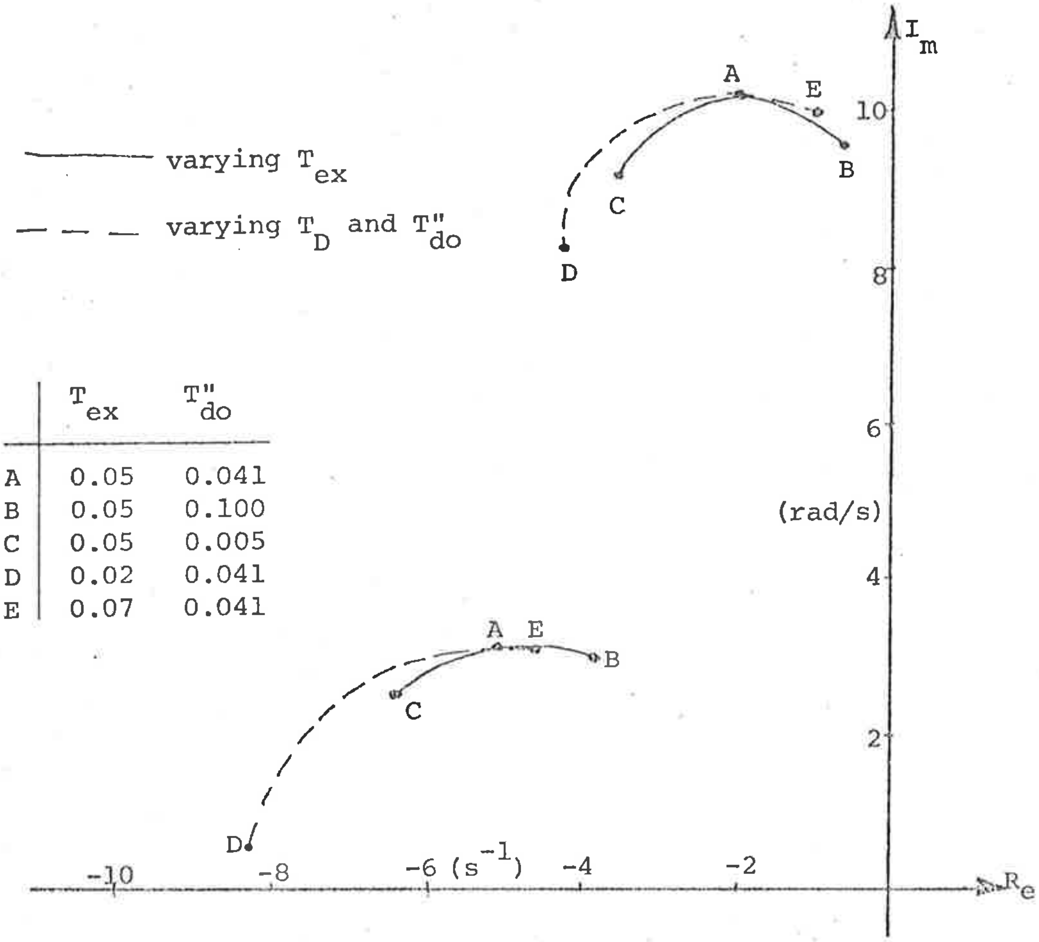

	T_{ex}	T''_{do}
A	0.05	0.041
B	0.05	0.100
C	0.05	0.005
D	0.02	0.041
E	0.07	0.041

FIGURE 5.7 A COMPARISON OF THE EFFECTS OF VARYING THE EXCITER AND d-AXIS DAMPER TIME CONSTANTS ON THE COMPLEX POLES OF A SMIB SYSTEM

must be emphasized that if the q-axis rotor iron effects and T'_{qo} are omitted from the test model, it is erroneously found that all the adjustable-gain strategies extend the stability limit to well beyond the study region defined in Figure 1.

At most operating points the performance of the PP/4/AG/FP/B and PP/4/AG/Ff_v/B strategies are similar. However, at low power output and leading p.f., the former strategy is inferior because it has a poorer stability limit and requires high voltage gain. The high f_v results in a high sensitivity to operating point measurement errors.

Based on the results of extensive tests for different sets of system parameters (the tests involving both the calculation of poles and the observation of small and large disturbance time responses), it is concluded that, as illustrated in this section, the PP/4/AG/Ff_v/B strategy is the best of the adjustable-gain strategies developed in earlier chapters.

5.3.3 Comparison of adjustable-gain strategy PP/4/AG/Ff_v/B with fixed-gain designs

In Table 5.4, comparison of the poles resulting from the PP/4/AG/Ff_v/4 strategy with those of the three fixed-gain designs shows that an improvement in performance results at all operating points from the use of the adjustable-gain strategy. This improvement is partly due to the choice of pole positions which offset the effect of the d-axis amortisseur as described in the previous section and partly due to the gain adjustment. Figures 5.8 and 5.9 illustrate the improvement in performance at two different operating points.

Besides the various adjustable-gain designs, Table 5.5 also shows the performance of a fixed-gain PP/4/FG/B controller which has its poles specified to lie in the same positions as the adjustable-gain design when the load is $\overline{P} = 0.9$ p.u. at unity p.f. It is evident that the damping of the PP/4/FG/B design is better than most of the adjustable-gain designs due to choice of pole positions which reduce errors resulting from the omission of the d-axis damper from the design model.

Comparison of the PP/4/FG/B and PP/4/AG/Ff_v/B strategies reveals that the performance is comparable for most operating points and adjustable-gains only give improved performance at low p.f. At low power, leading power-factor, all designs fail due to the omission of the q-axis transient time-constant from the design model. At higher loads and leading p.f. the use of the adjustable-gain strategy leads to a significantly improved stability limit. Figure 5.10 compares the performance of the PP/4/FG/B and PP/4/AG/Ff_v/B designs at various loads in order to illustrate the above points.

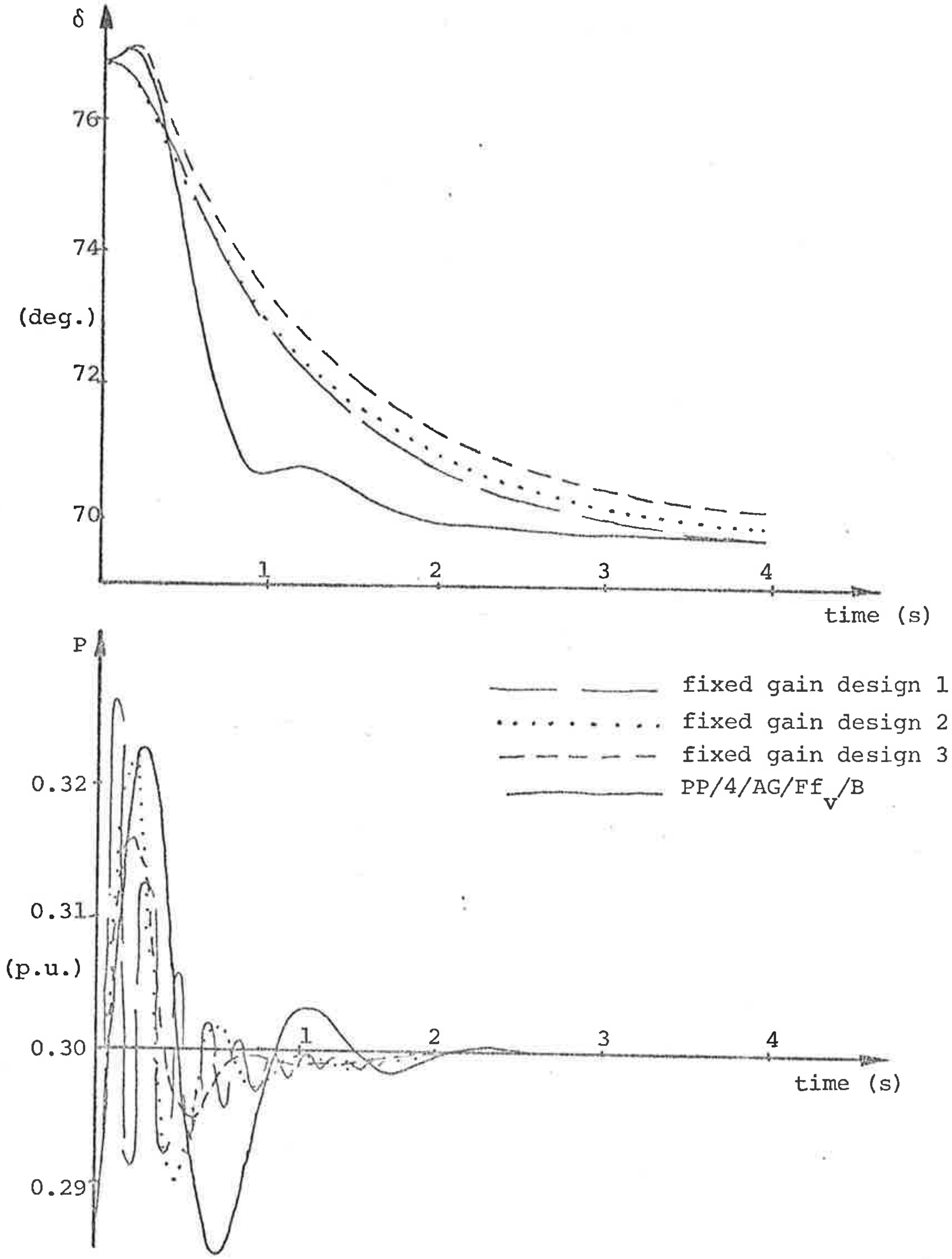

FIGURE 5.8 SMALL SIGNAL RESPONSES WITH VARIOUS CONTROLLERS AT LEADING LOAD

($\overline{P}$ = 0.3 p.u., $\overline{Q}$ = -0.5 p.u., system data listed in row DA of Table 5.1. System model comprises of a 6th order SMIB model with no governor or washout filter. Disturbance applied is a 10% increase in x_e.)

design	f_V	f_S	f_P	f_F	source
1	200	5573	-118	-	Raina [61]
2	50	565	-15.6	-	PP/3/FG
3	50	103	-18.7	-0.59	PP/4/FG/A
-	50	-601	- 5.3	-0.18	PP/4/AG/Ff$_V$/B

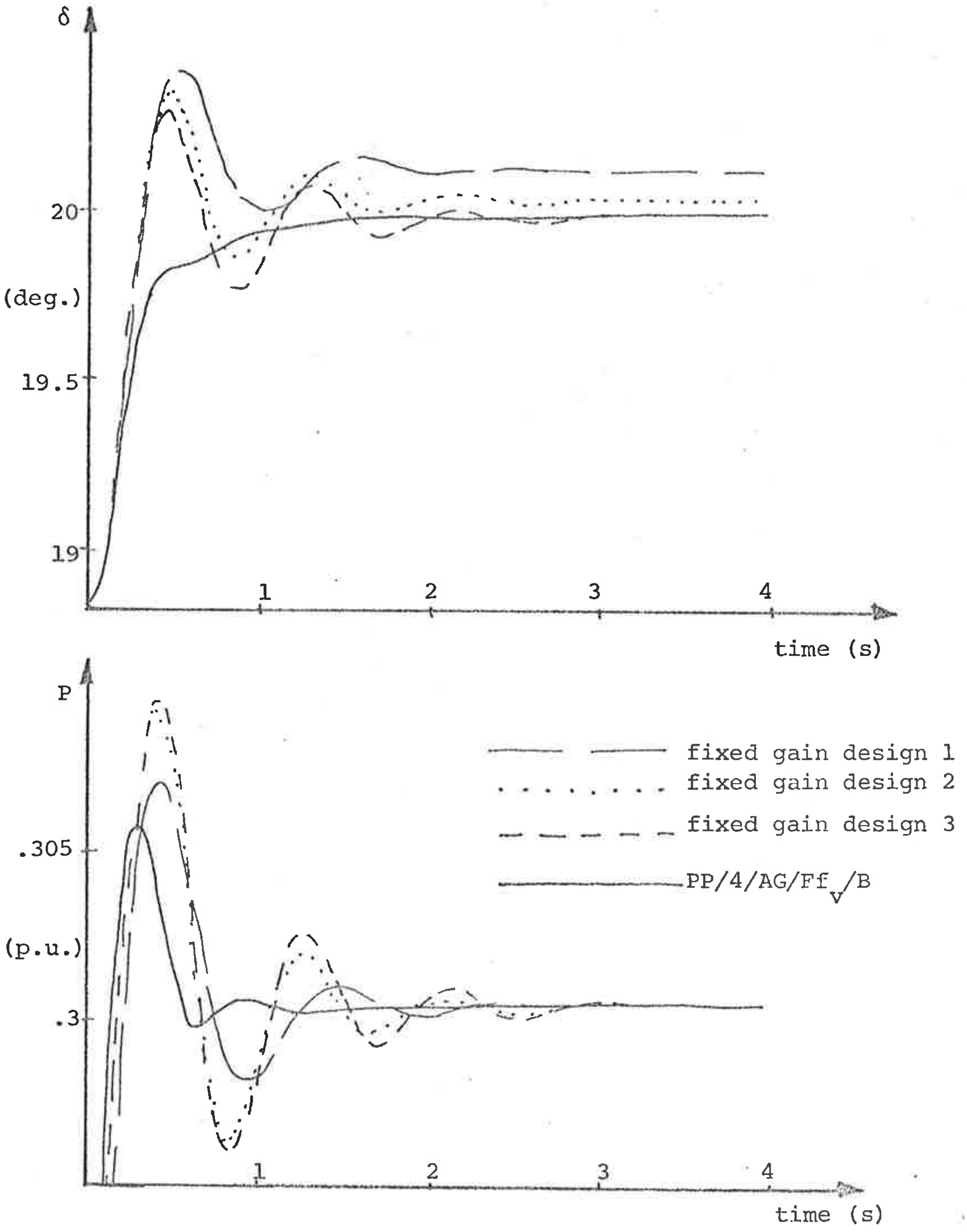

FIGURE 5.9 SMALL SIGNAL RESPONSES WITH VARIOUS CONTROLLERS AT LAGGING LOAD

($\overline{P}$ = 0.3 p.u., $\overline{Q}$ = 0.8 p.u., system data listed in row DA of Table 5.1. System model comprises of a 6th order SMIB model with no governor or washout filter. Disturbance applied is a 10% increase in x_e.)

design	f_v	f_s	f_p	f_F	source
1	200	5573	-118	-	Raina [61]
2	50	565	-15.6	-	PP/3/FG
3	50	103	-18.7	-0.59	PP/4/FG/A
-	50	3654	-69.4	-0.64	PP/4/AG/Ff$_v$/B

FIGURE 5.10 SMALL SIGNAL PERFORMANCE OF PP/4/FG/B FIXED-GAIN AND PP/4/AG/Ff$_v$/B ADJUSTABLE-GAIN CONTROLLERS

Disturbance: 5% step in v_{ref}.
System Data: set BB of Table 5.
Controllers: as for Table 5.

Case	$\overline{P}$	$\overline{Q}$	Controller gains	Comment
(a)	0.3	0.8	fixed	better damping with
(b)	0.3	0.8	adjusted	adjustable-gains
(c)	0.3	-0.4	fixed	slow voltage response with
(d)	0.3	-0.4	adjusted	fixed-gains
(e)	0.9	0.4	fixed	"normal" op region - similar
(f)	0.9	0.4	adjusted	performance
(g)	0.9	-0.8	fixed	low frequency mode evident -
(h)	0.9	-0.8	adjusted	better damping ratio for PP/4/AG/Ff$_v$/B but slower response

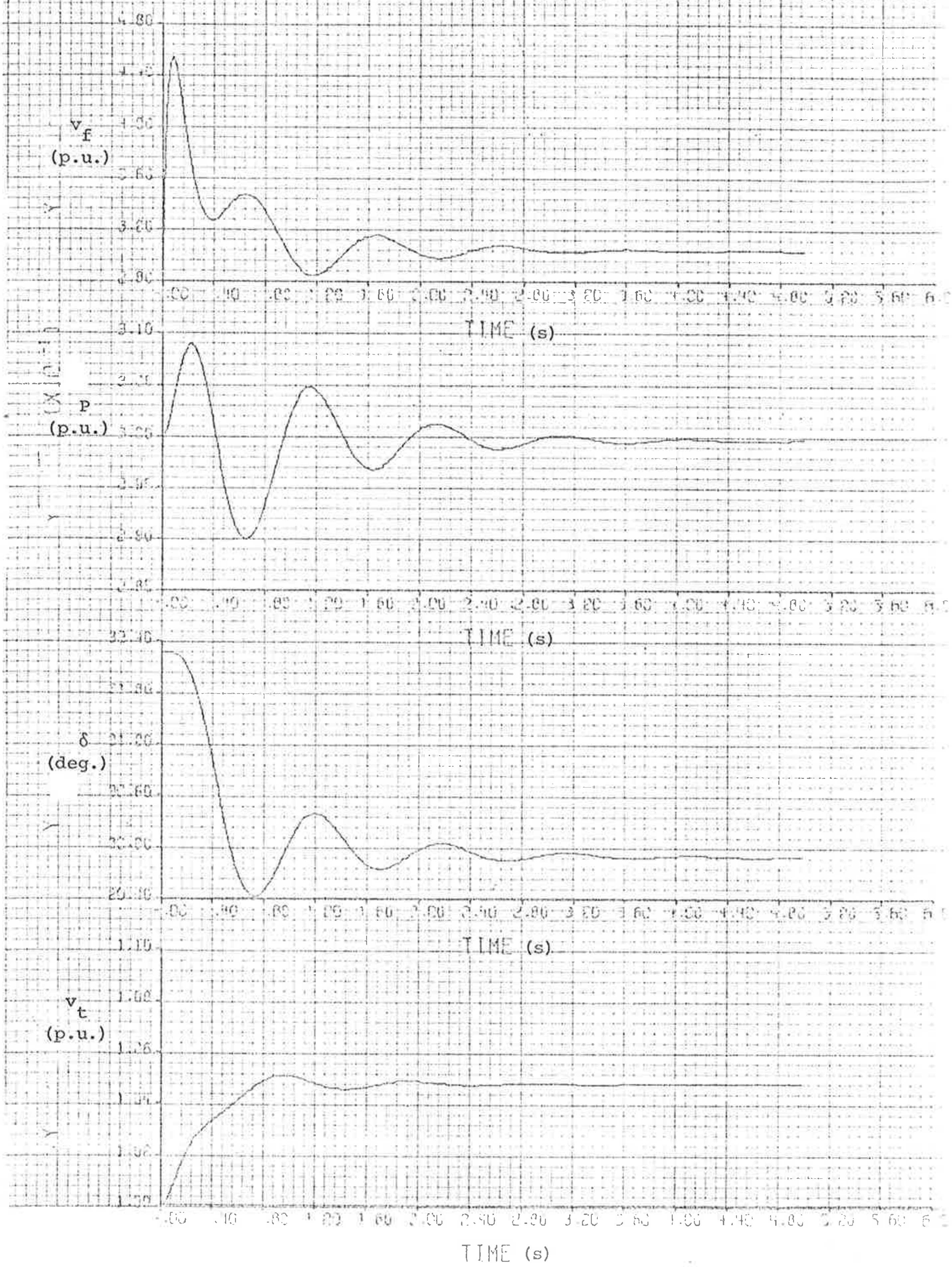

FIGURE 5.10(a) PP/4/FG/B CONTROLLER AT $\overline{P}$ = 0.3 p.u., $\overline{Q}$ = 0.8 p.u.

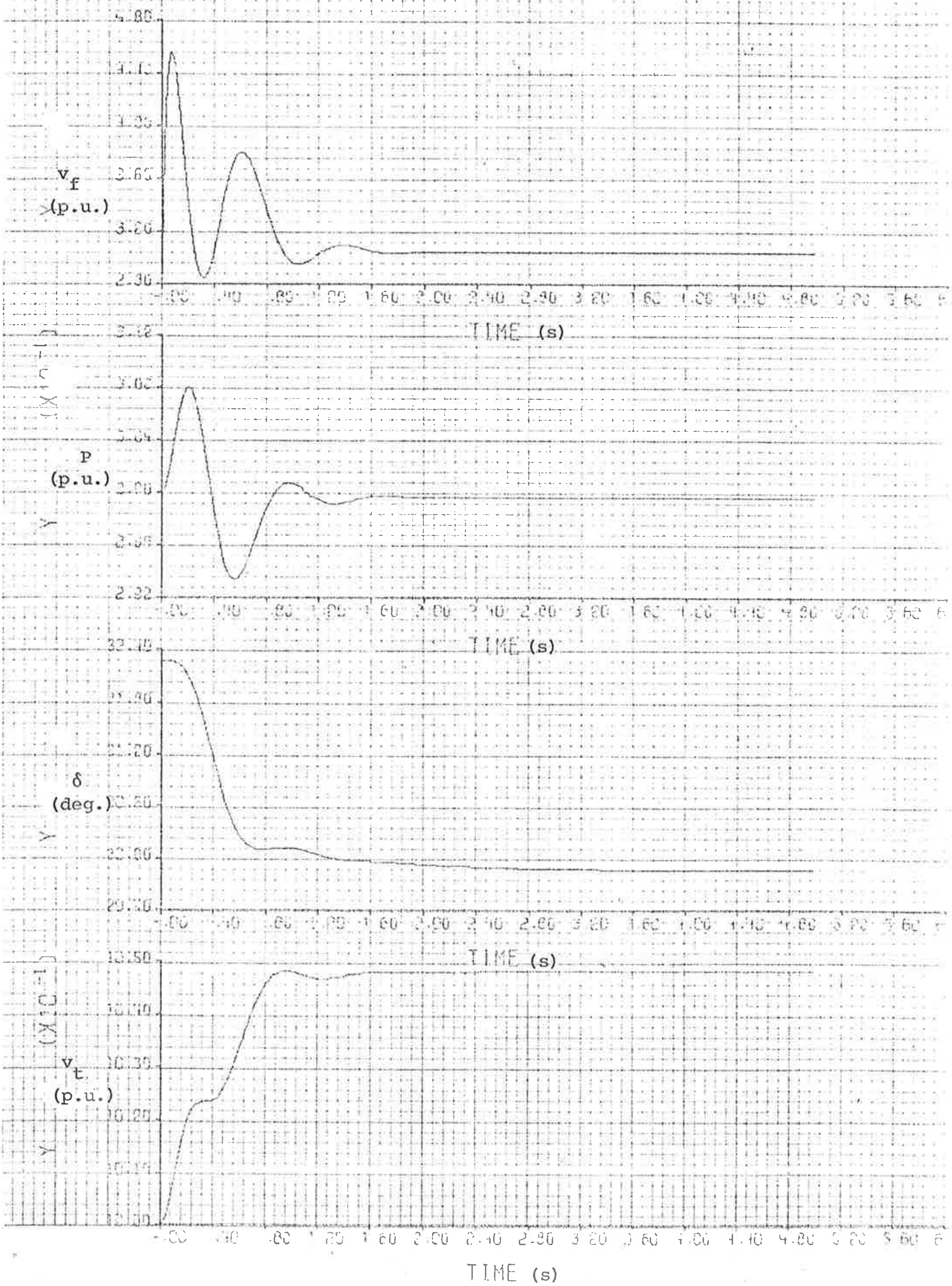

FIGURE 5.10(b) PP/4/AG/Ff_v/B CONTROLLER AT $\overline{P}$ = 0.3 p.u., $\overline{Q}$ = 0.8 p.u.

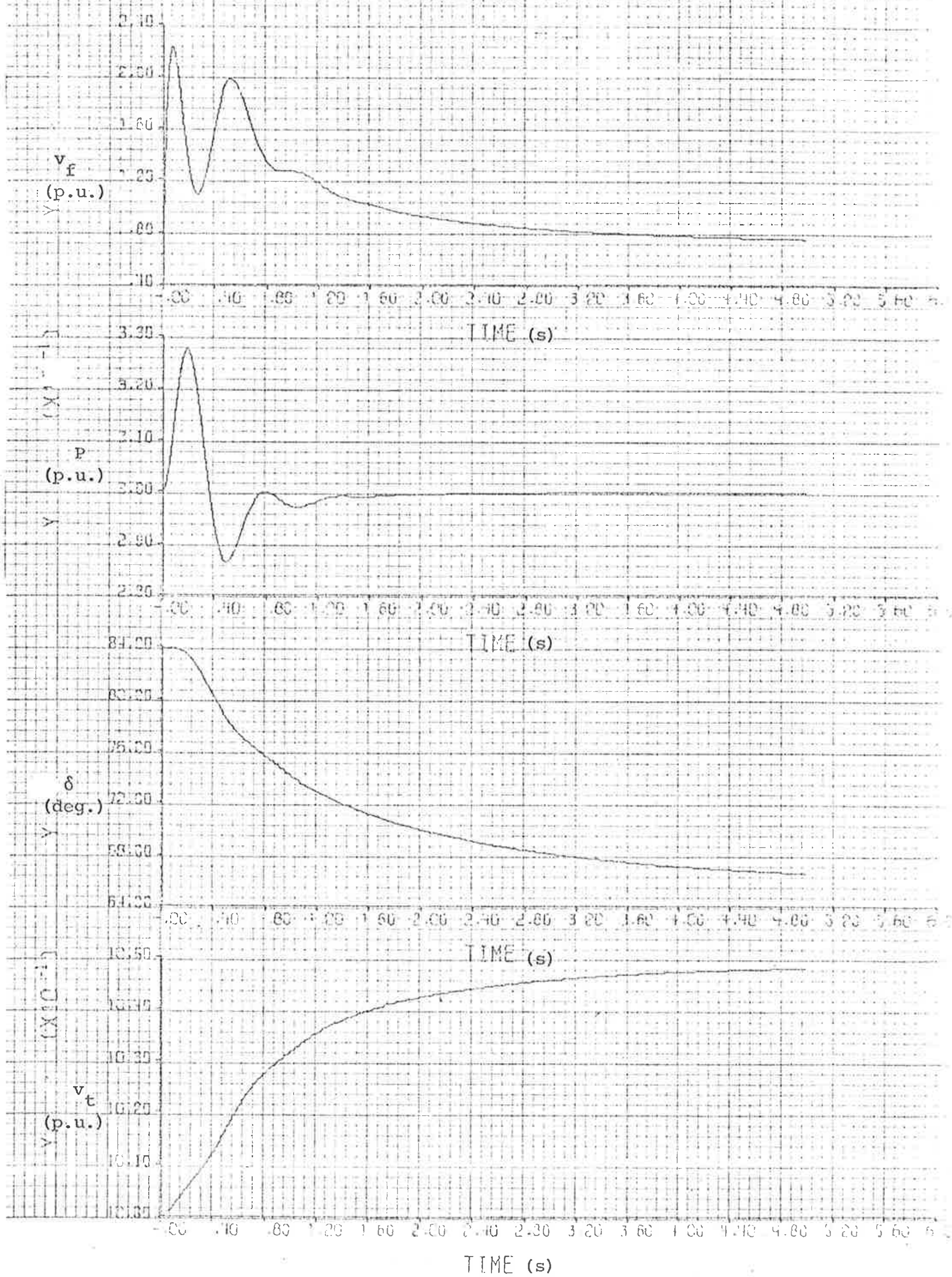

FIGURE 5.10(c) PP/4/FG/B CONTROLLER AT $\overline{P}$ = 0.3 p.u., $\overline{Q}$ =-0.4 p.u.

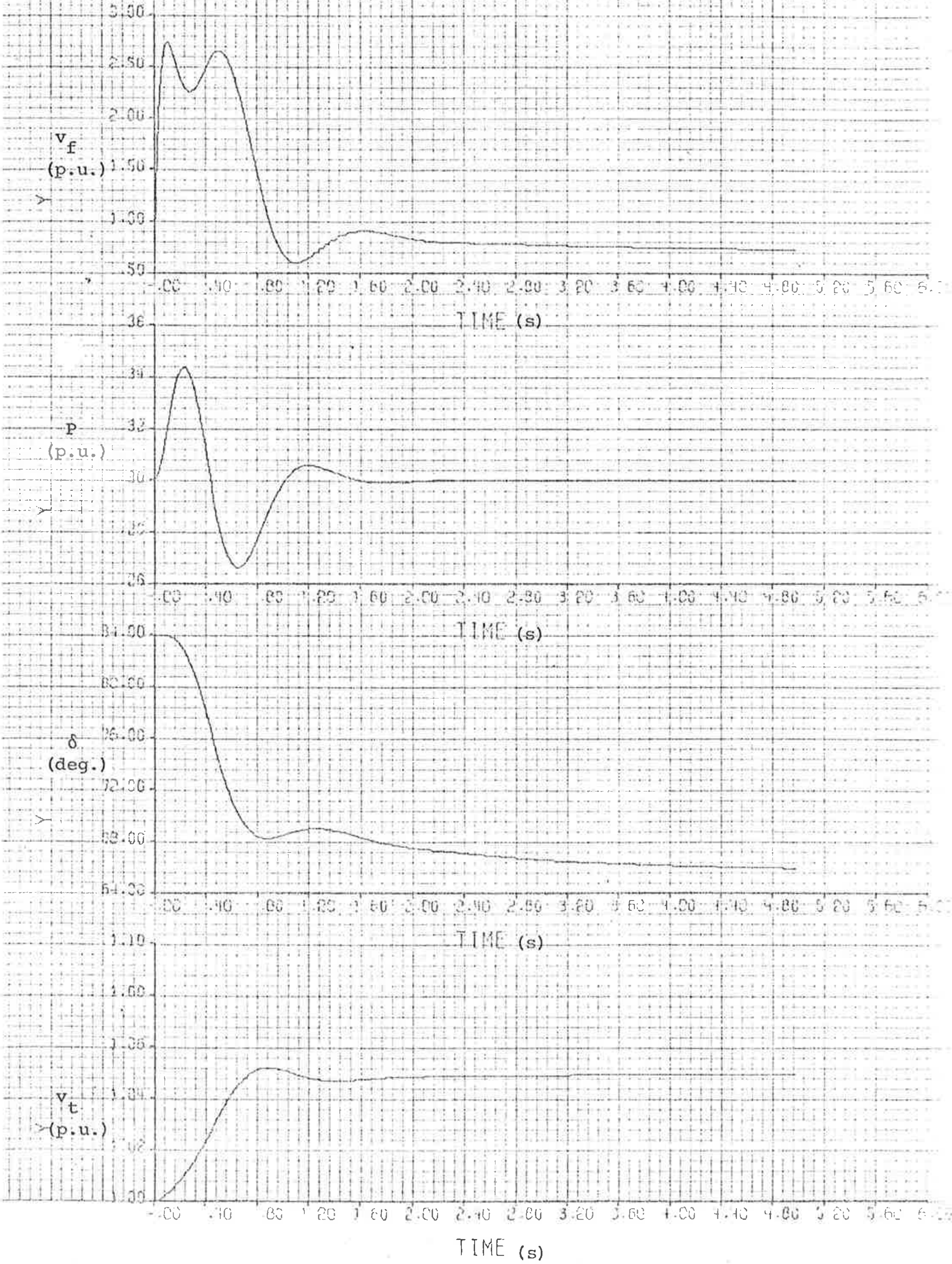

FIGURE 5.10(d) PP/4/AG/F_{fv}/B CONTROLLER AT $\overline{P}$ = 0.3 p.u., $\overline{Q}$ =-0.4 p.u.

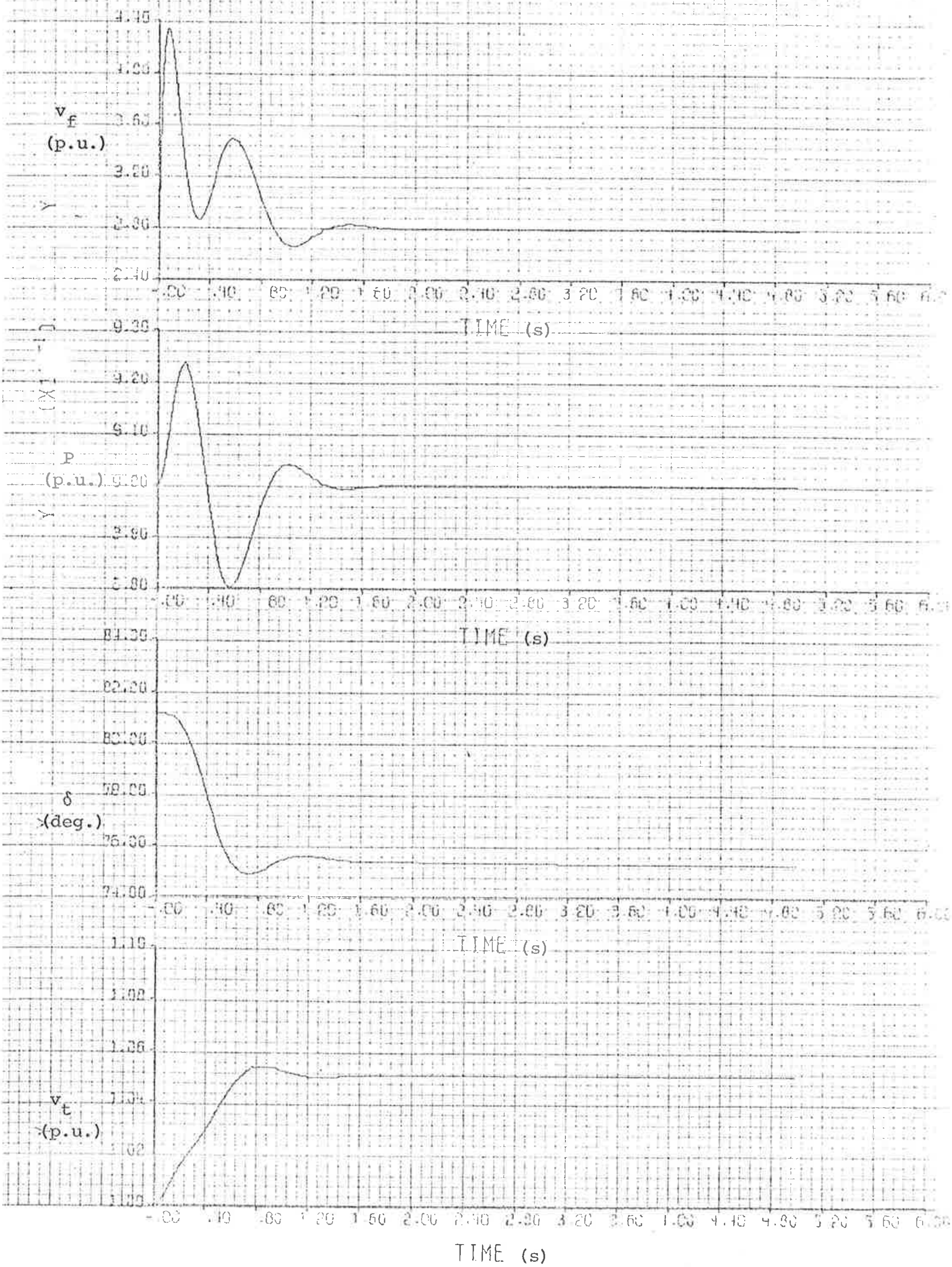

FIGURE 5.10(e) PP/4/FG/B CONTROLLER AT $\overline{P}$ = 0.9 p.u., $\overline{Q}$ = 0.4 p.u.

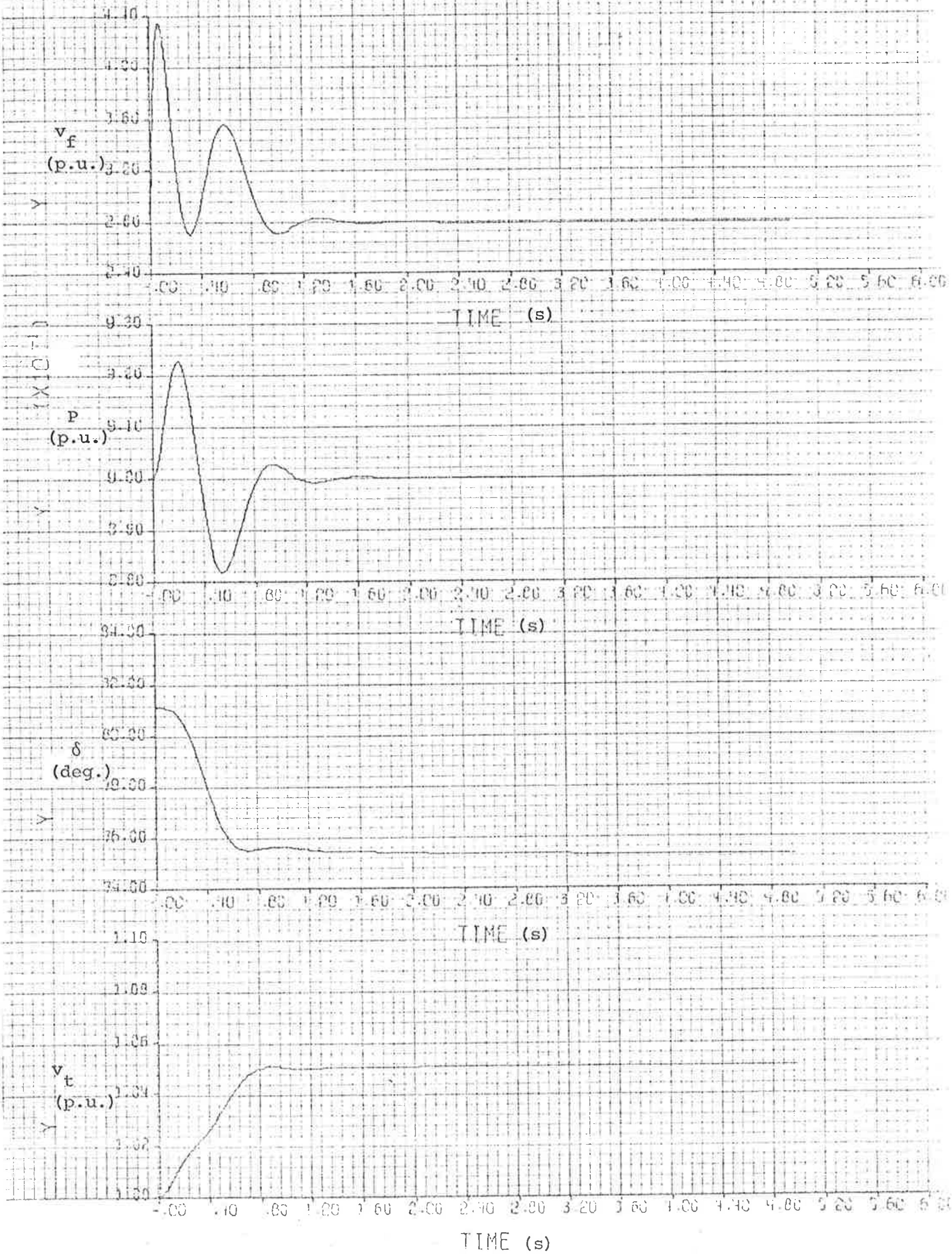

FIGURE 5.10(f) PP/4/AG/Ff$_V$/B CONTROLLER AT $\overline{P}$ = 0.9 p.u., $\overline{Q}$ = 0.4 p.u.

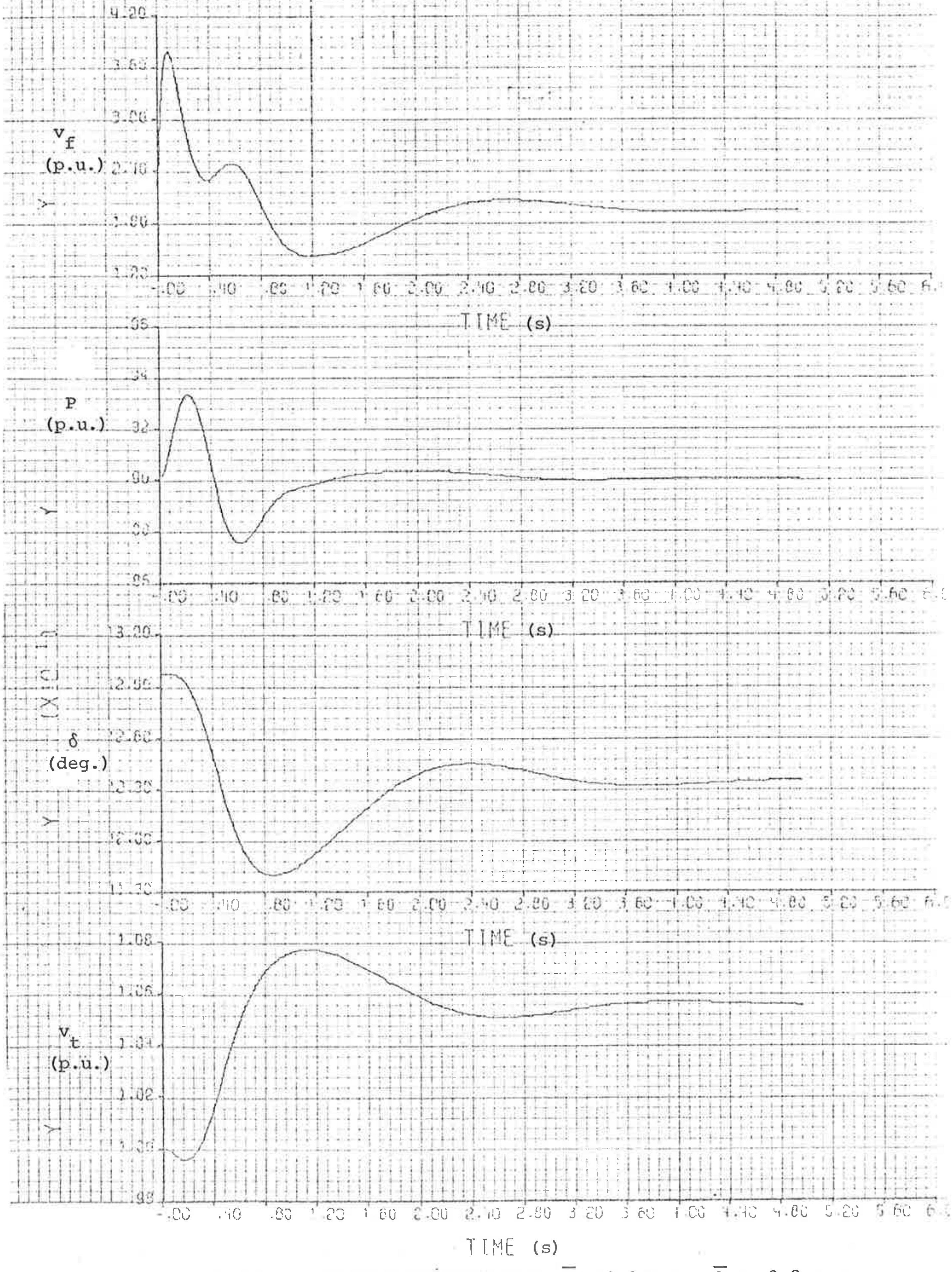

FIGURE 5.10(g) PP/4/FG/B CONTROLLER AT $\overline{P}$ = 0.9 p.u., $\overline{Q}$ = -0.8 p.u.

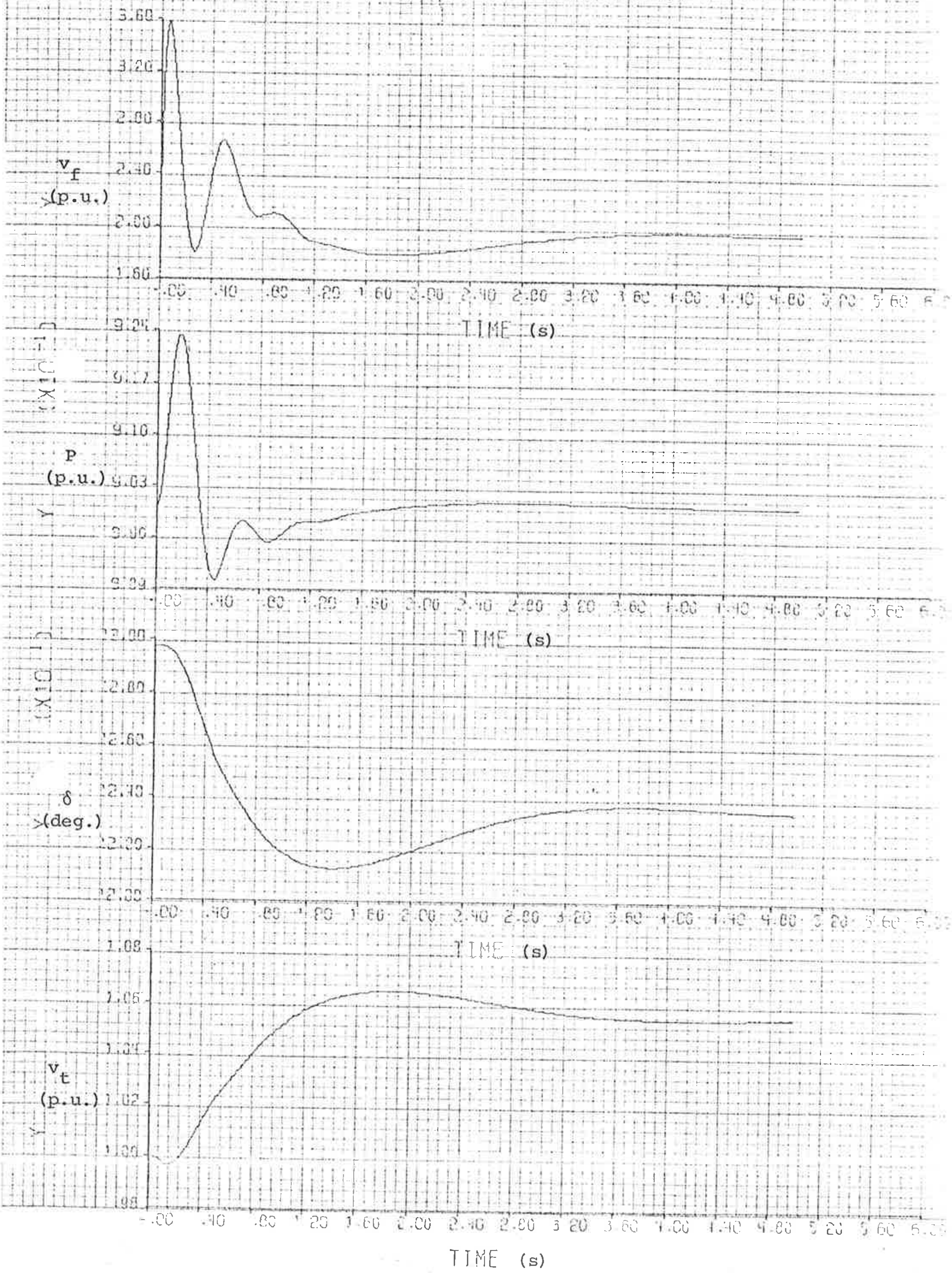

FIGURE 5.10(h) PP/4/AG/Ff_v/B CONTROLLER AT $\overline{P}$ = 0.9 p.u., $\overline{Q}$ = -0.8 p.u.

5.3.4 Sensitivity of adjustable-gain controller performance to operating point measurement error

The sensitivity of the poles of a system with a PP/4/AG/Ff$_v$/B controller to errors in measuring operating point was checked at a few different operating points. Unlike section 3.4 where the problem was investigated analytically, the method employed was simply to note the changes in the poles of the system, when the values of $\overline{P}$, $\overline{Q}$, $\overline{v}_t$ and x_e were perturbed in turn from their nominal value. The results show that the sensitivities of the damping and frequency of oscillation of the higher frequency dominant oscillatory mode are in general similar to that of α and ω for the third-order model, and that the sensitivity of the damping of the lower frequency mode is similar to that of β.

The sensitivity of the poles of the PP/4/AG/Ff$_v$/B system was compared to that of generator with a PP/4/FG/B fixed-gain excitation system. At medium and high real power output, when the gains of the two controllers do not differ greatly, the sensitivities are similar, but at low load, when the adjustable-gain controller uses high gains, its sensitivity is higher than for the fixed-gain case. At lagging power factor the largest sensitivity is for an error in sensing $\overline{P}$, but this affects mainly a heavily damped mode so it is not of great consequence. In the leading power factor region, errors in $\overline{Q}$ or $\overline{v}_t$ lead to the largest changes in performance; these errors are important because they heavily affect the critical low frequency oscillatory mode.

The above results indicate that the conclusions in section 3.3.3 are valid, namely care is needed at low excitation levels, but elsewhere error from operating point measurements should not be a problem.

5.4 LARGE SIGNAL PERFORMANCE WITH POLE-PLACEMENT DESIGNED EXCITATION CONTROLLERS

5.4.1 Preamble

A brief study was undertaken of the behaviour of the SMIB system with various controllers following a three-phase line-to-ground fault in the transmission system. The aim was to determine the effectiveness of the PP/4/AG/Ff$_v$/B adjustable feedback gain strategy, which is based on small signal considerations, when applied under large signal conditions. A digital computer program based on the nonlinear equations of Appendix 10.4 was used to calculate time responses. In order to simulate the exciter ceiling limits, the magnitude of the field voltage was constrained to be less than or equal to 5.5 p.u. Unlike some other authors (Raina [60]), the magnitudes of the subsidiary speed and power signals were not constrained.

5.4.2 Comparison of PP/4/FG/B fixed-gain and PP/4/AG/Ff$_v$/B adjustable-gain controllers

The large signal behaviour of generators with the PP/4/AG/Ff$_v$/B adjustable-gain controller does offer some improvement over the PP/4/FG/B fixed-gain controller at low lagging power-factor (see Figure 5.11(a) and (b)). The improvement is especially noticeable when the postfault reactance increases from the prefault value, which occurs on the switching out of a faulted line (see Figure 5.11(c) and (d)). At low loads the behaviour of both controllers is similar to that predicted by the small signal analysis,

FIGURE 5.11 LARGE SIGNAL PERFORMANCE OF THE PP/4/FG/B FIXED-GAIN AND PP/3/AG/Ff$_v$/B ADJUSTABLE-GAIN CONTROL STRATEGIES

System Data: as for set BB in Table 5.

Controllers: as for Table 5.

Faults: In order to simulate a three phase line to ground fault the infinite bus voltage and tie-line reactances are changed to reduced values v_{bf} and x_{ef} for the duration of the fault.

cases	fault time	v_{bf}	x_{ef}	postfault reactance x'_e
(a),(b),(e),(f)	0.1 sec.	0.0 p.u.	0.2 p.u.	0.6 p.u.
(c),(d),(g),(h)	0.1 sec.	0.0 p.u.	0.2 p.u.	1.0 p.u.
(i),(j)	0.05 sec.	0.0	0.2	0.6 p.u.
(k),(l)	0.05	0.33	0.33	0.6 p.u.

case	P	Q	Controller gains	Comments
(a)	0.3	0.8	fixed	AG slightly
(b)	0.3	0.8	adjusted	better
(c)	0.3	0.8	fixed	AG superior
(d)	0.3	0.8	adjusted	
(e)	0.3	-0.4	fixed	slow exponential
(f)	0.3	-0.4	adjusted	mode in FG
(g)	0.3	-0.4	fixed	FG superior!
(h)	0.3	-0.4	adjusted	
(i)	0.9	0.4	fixed	similar
(j)	0.9	0.4	adjusted	
(k)	0.9	-0.8	fixed	AG superior
(l)	0.9	-0.8	adjusted	

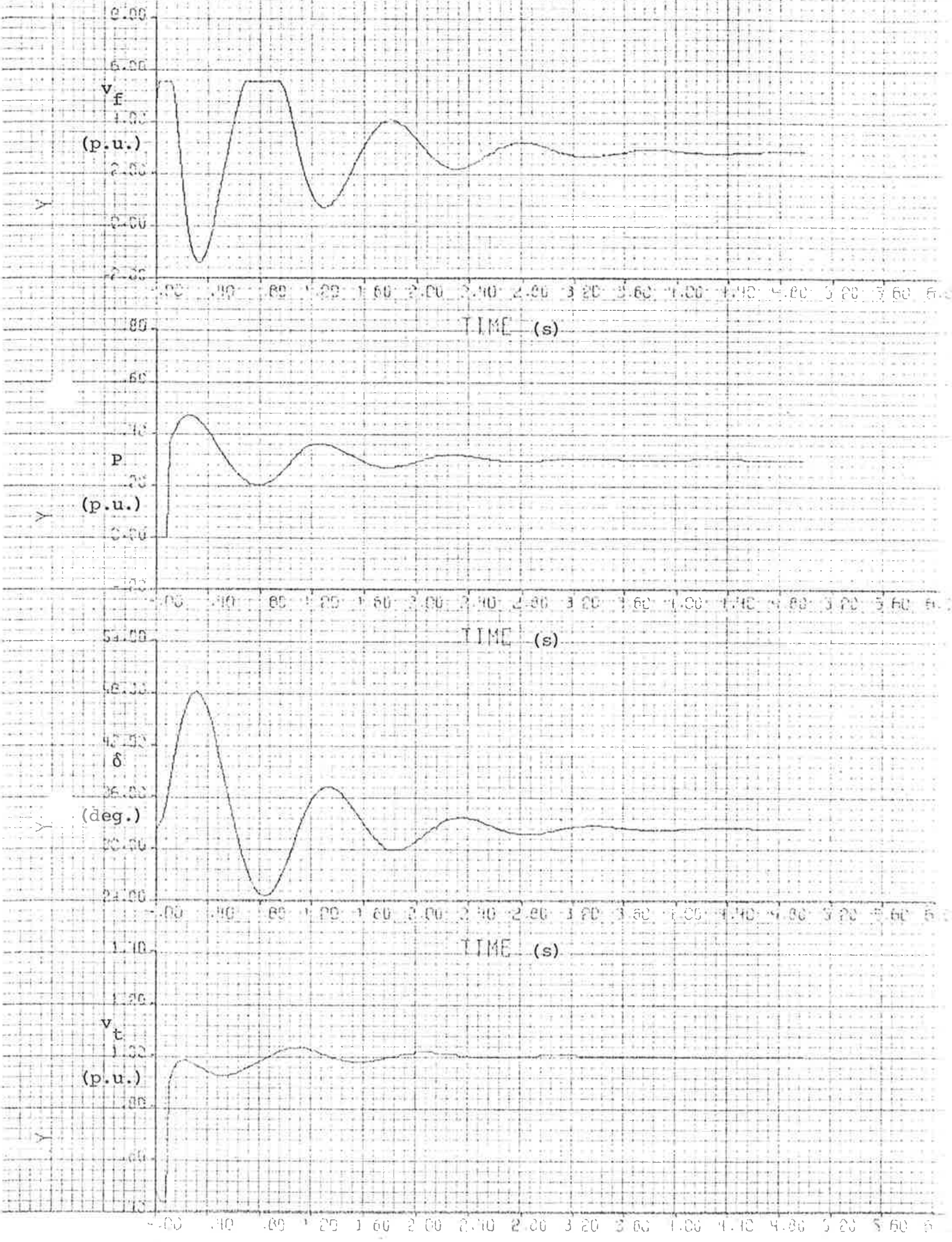

FIGURE 5.11(a) PP/4/FG/B CONTROLLER AT $\overline{P}$ = 0.3 p.u., $\overline{Q}$ = 0.8 p.u.

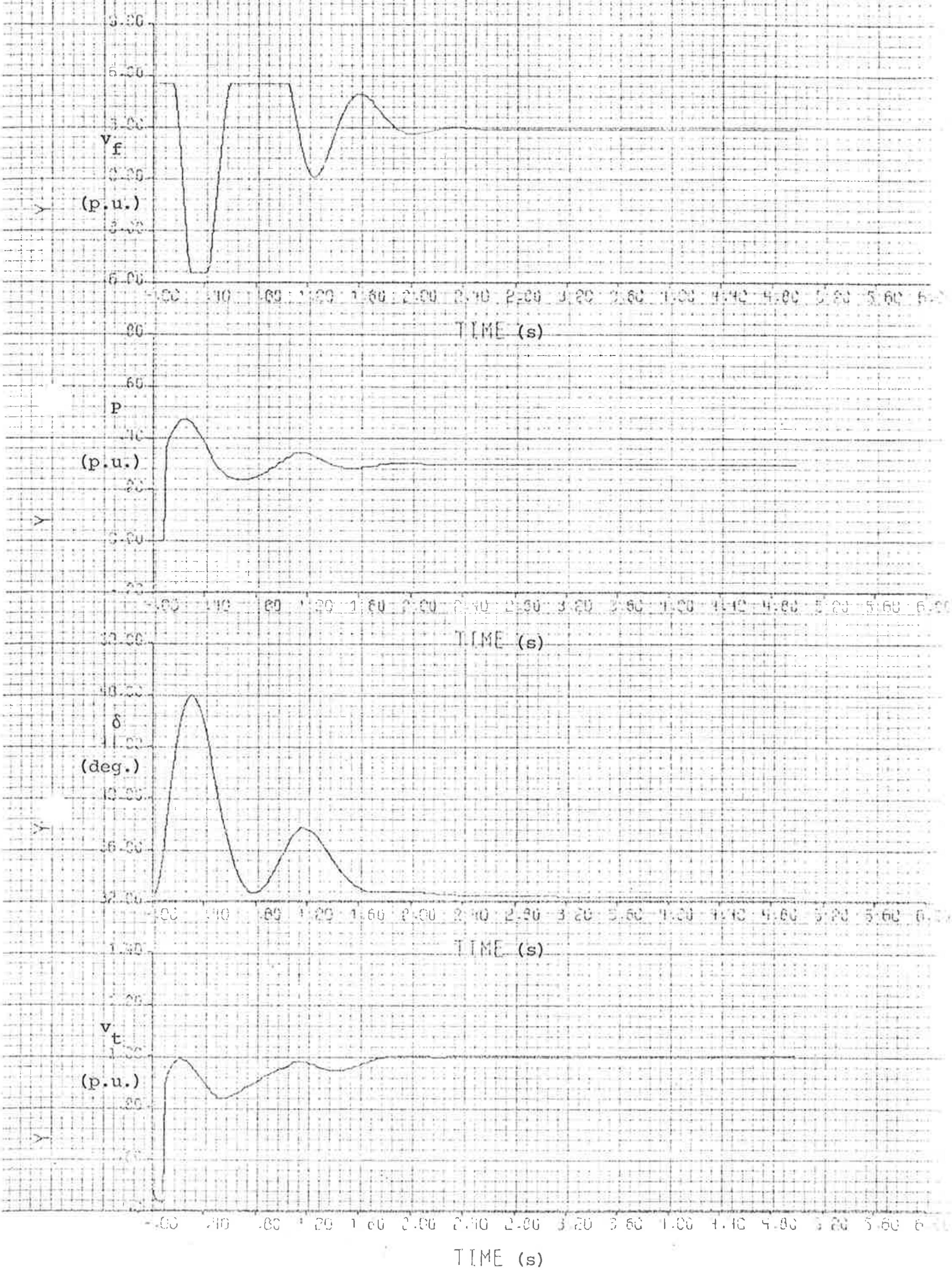

FIGURE 5.11(b) PP/4/AG/Ff_v/B CONTROLLER AT $\overline{P}$ = 0.3 p.u., $\overline{Q}$ = 0.8 p.u.

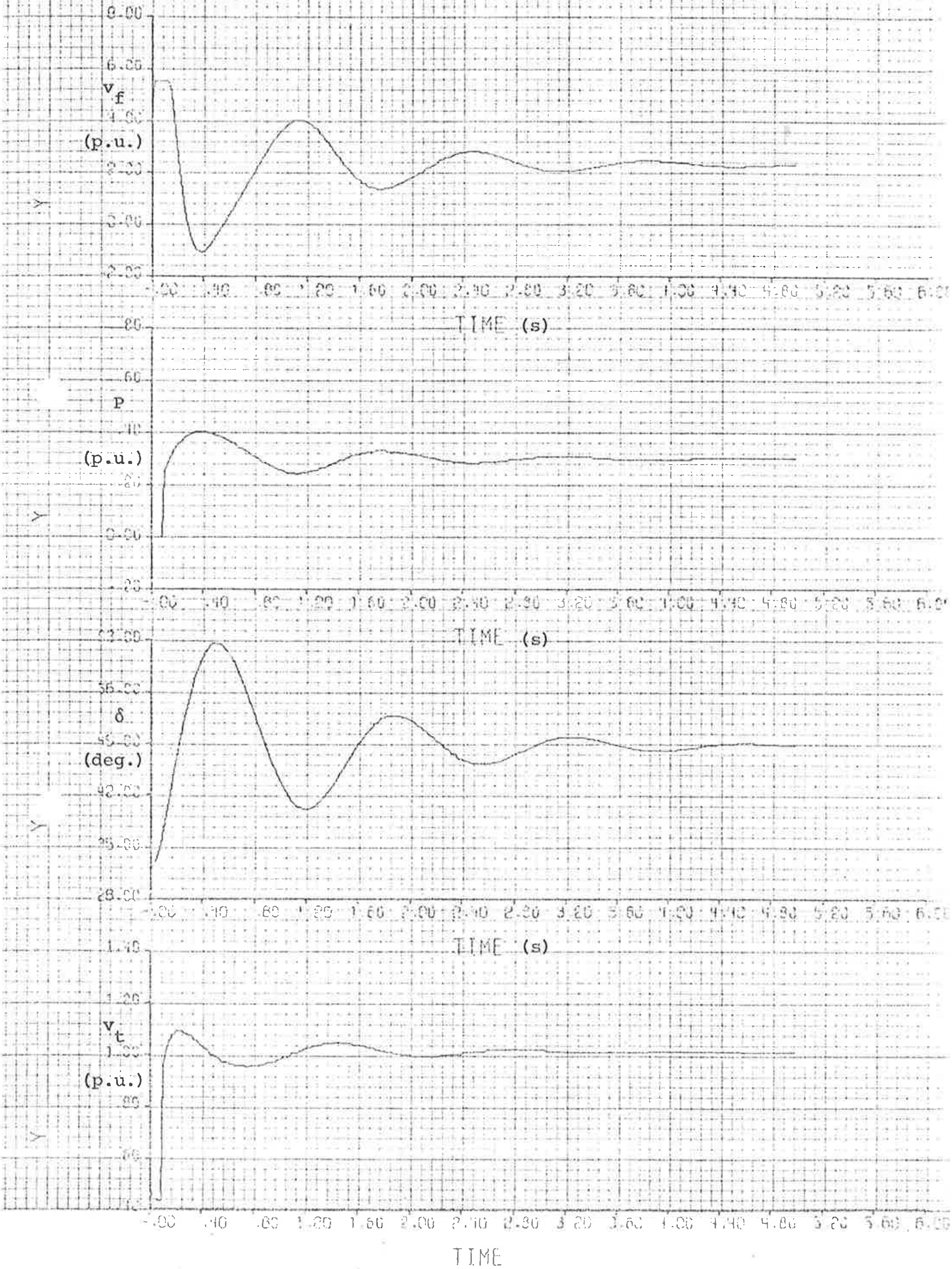

FIGURE 5.11(c) PP/4/FG/B CONTROLLER AT $\overline{P}$ = 0.3 p.u., $\overline{Q}$ = 0.8 p.u.

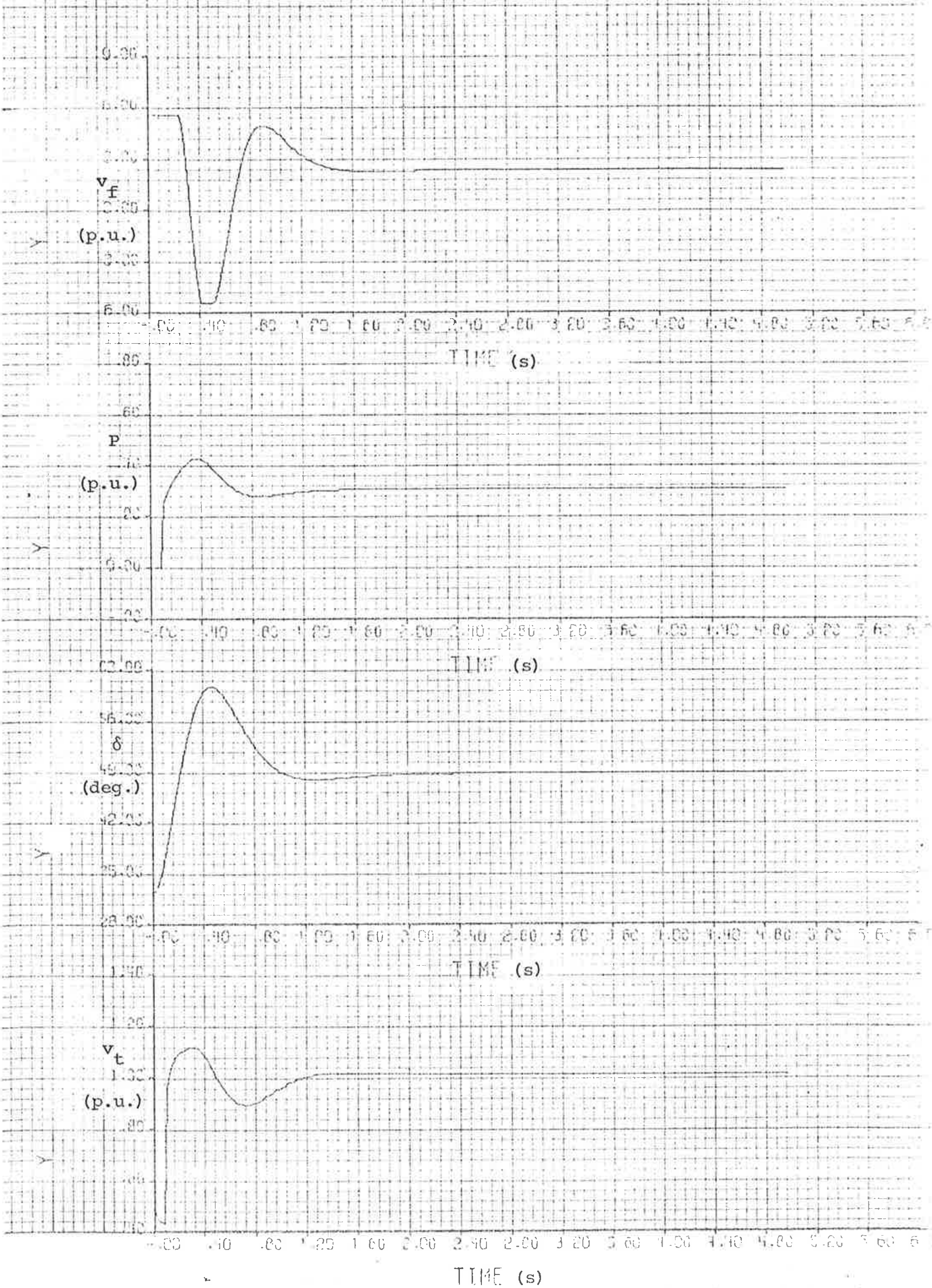

FIGURE 5.11(d) PP/4/AG/Ff_V/B CONTROLLER AT $\overline{P}$ = 0.3 p.u., $\overline{Q}$ = 0.8 p.u.

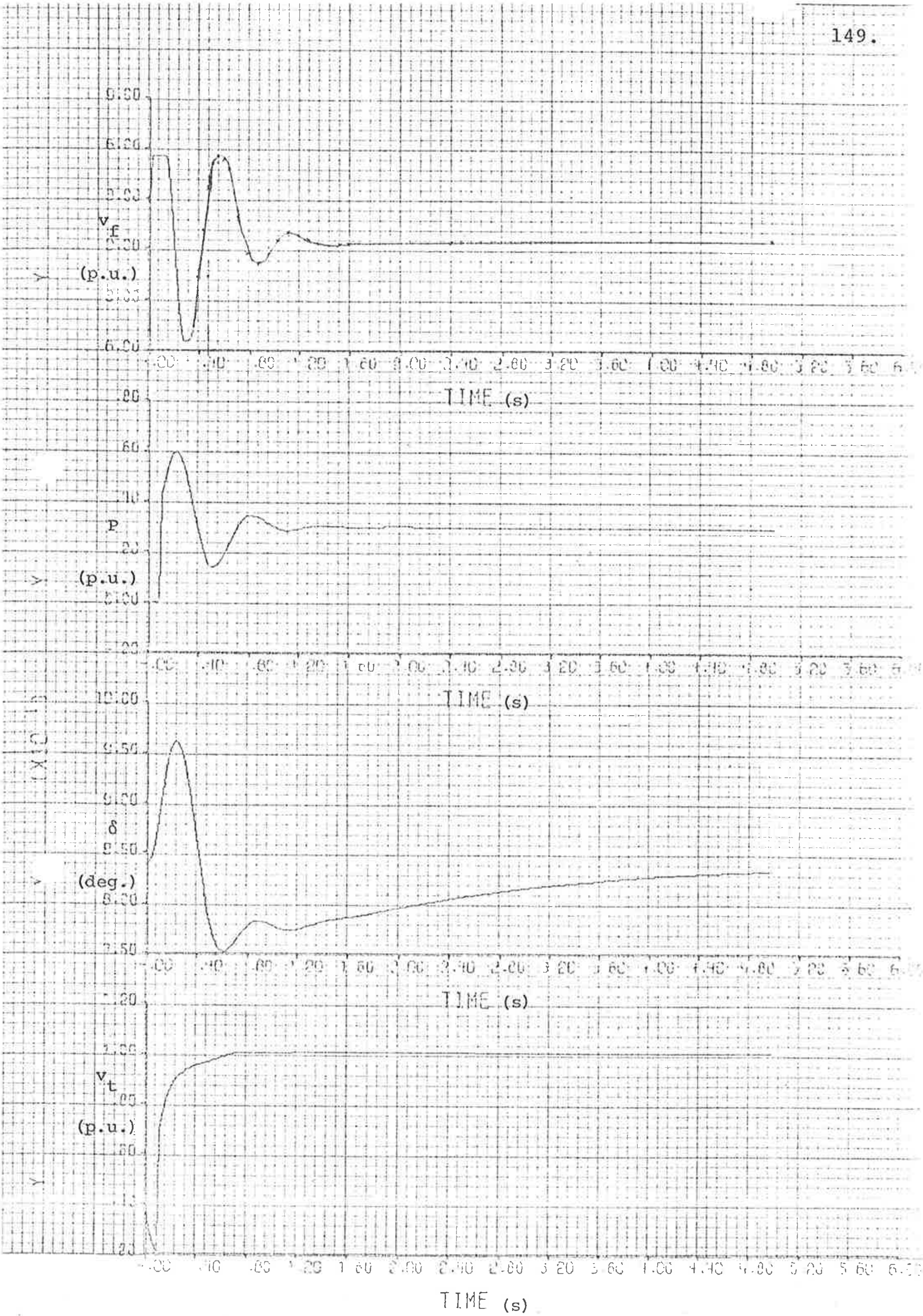

FIGURE 5.11(e) PP/4/FG/B CONTROLLER AT $\overline{P}$ = 0.3 p.u., $\overline{Q}$ = -0.4 p.u.

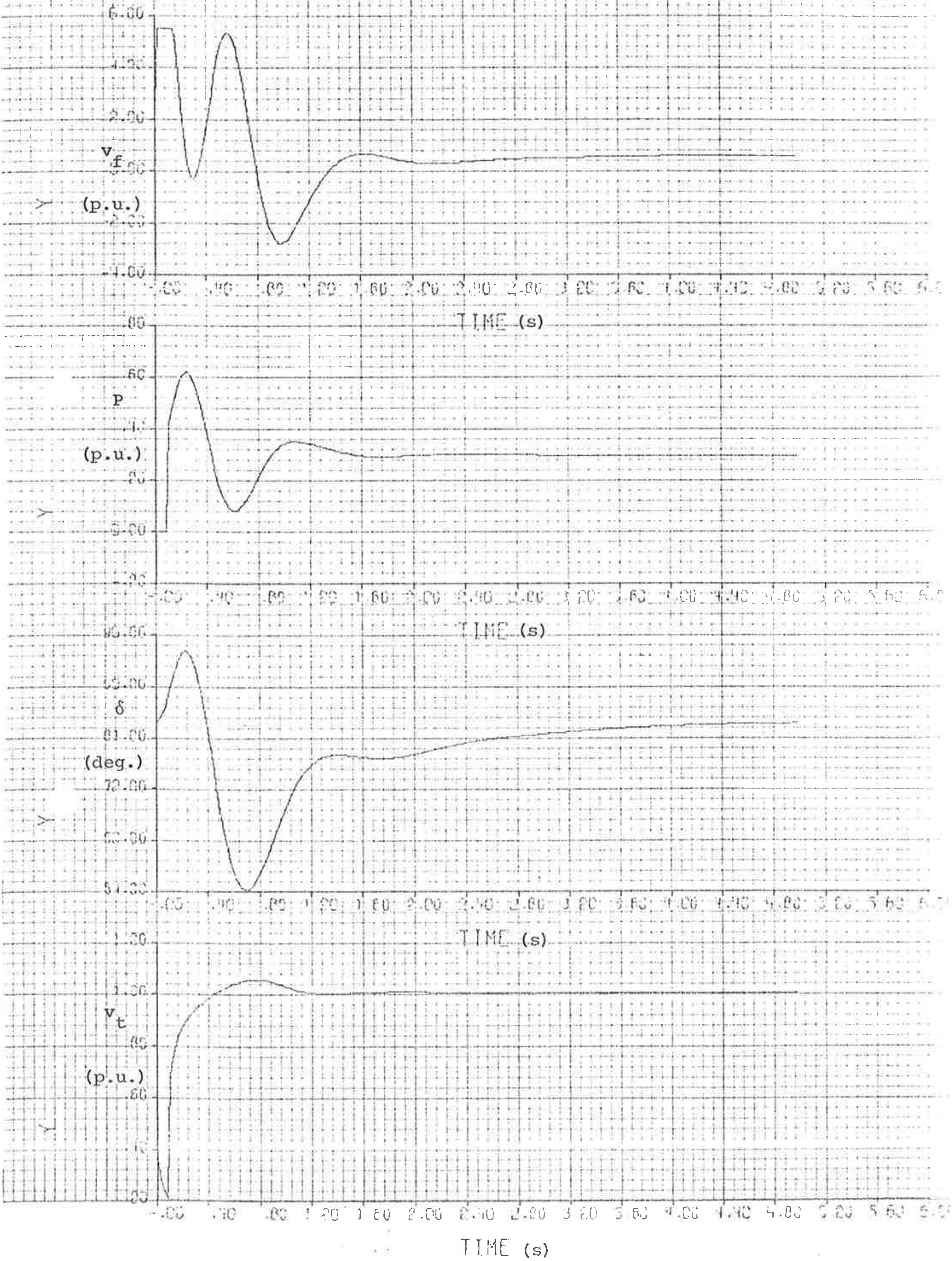

FIGURE 5.11(f) PP/4/AG/Ff_V/B CONTROLLER AT $\overline{P}$ = 0.3 p.u., $\overline{Q}$ = -0.4 p.u.

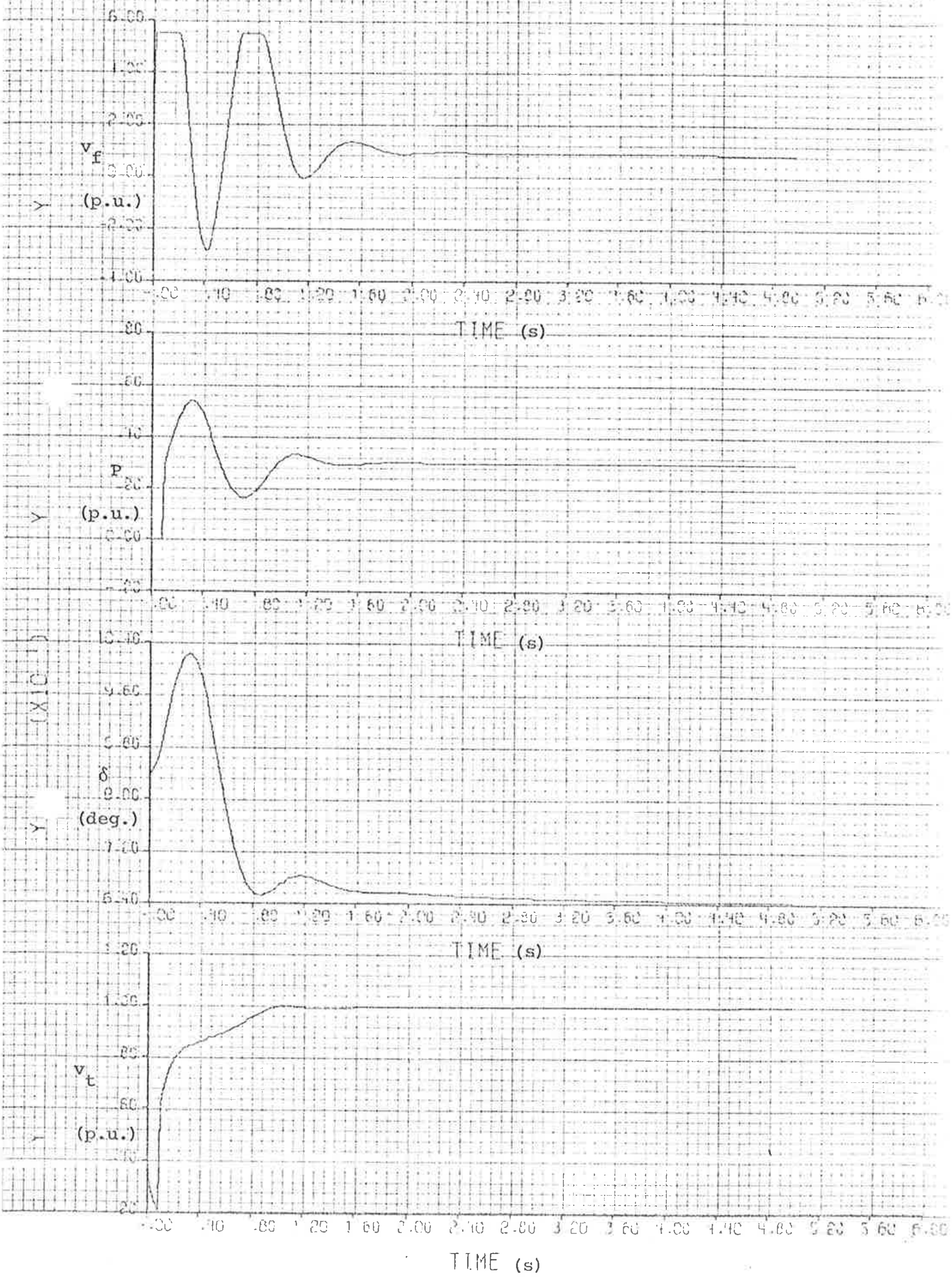

FIGURE 5.11(g) PP/4/FG/B CONTROLLER AT $\overline{P}$ = 0.3 p.u., $\overline{Q}$ = -0.4 p.u.

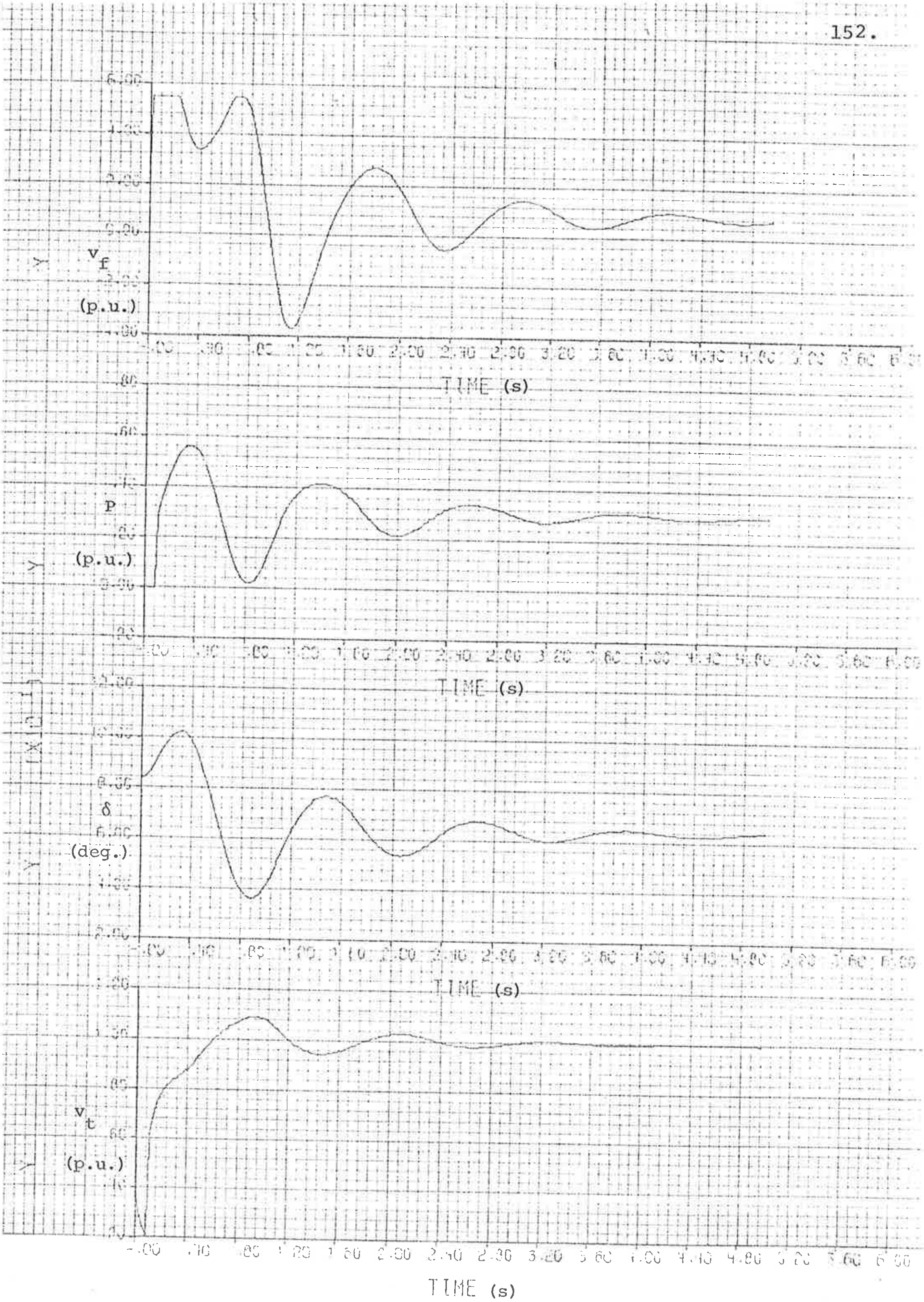

FIGURE 5.11(h) PP/4/AG/Ff$_V$/B CONTROLLERS AT $\overline{P}$ = 0.3 p.u., $\overline{Q}$ = -0.4 p.u.

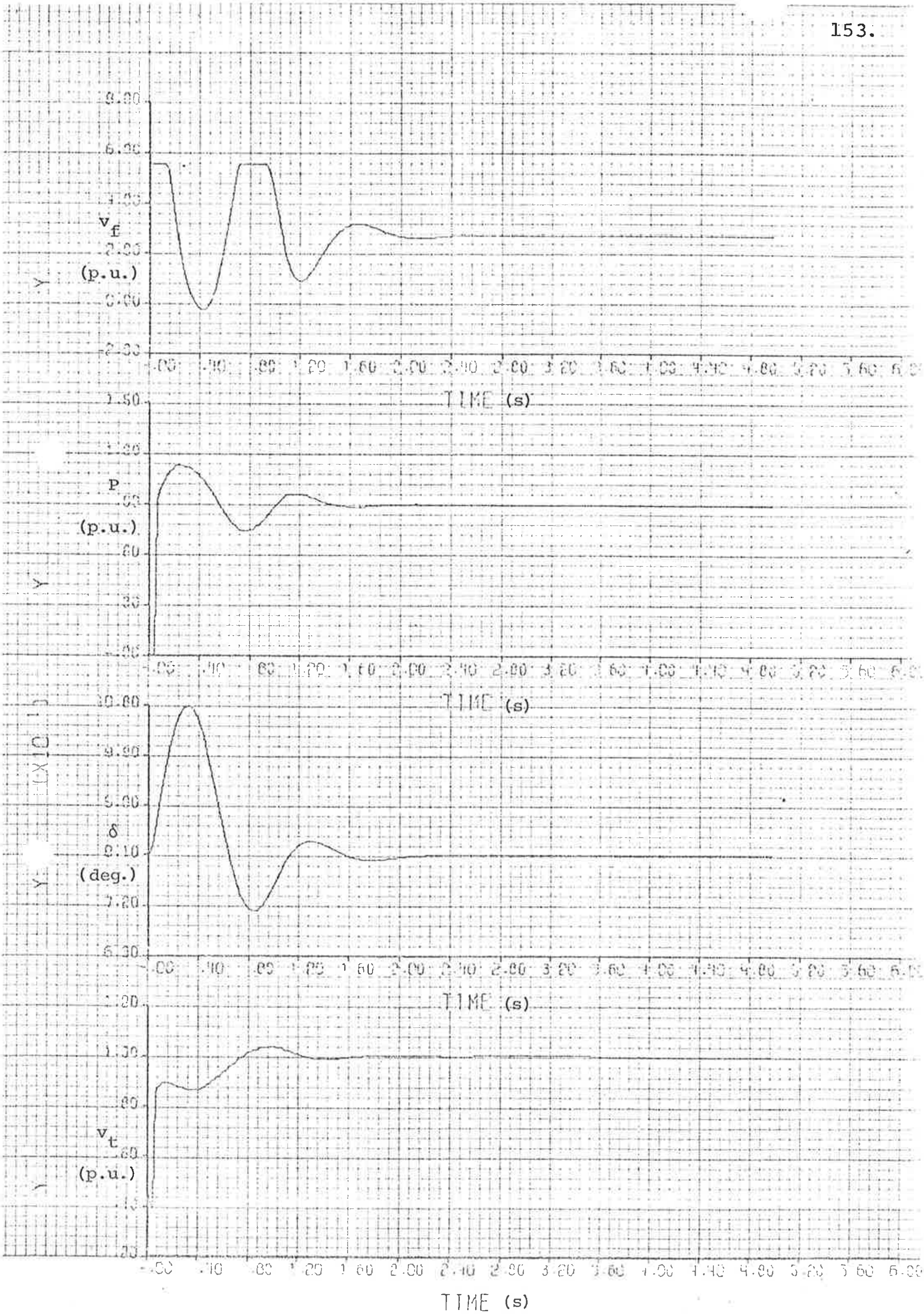

FIGURE 5.11(i) PP/4/FG/B CONTROLLER AT $\overline{P}$ = 0.9 p.u., $\overline{Q}$ = 0.4 p.u.

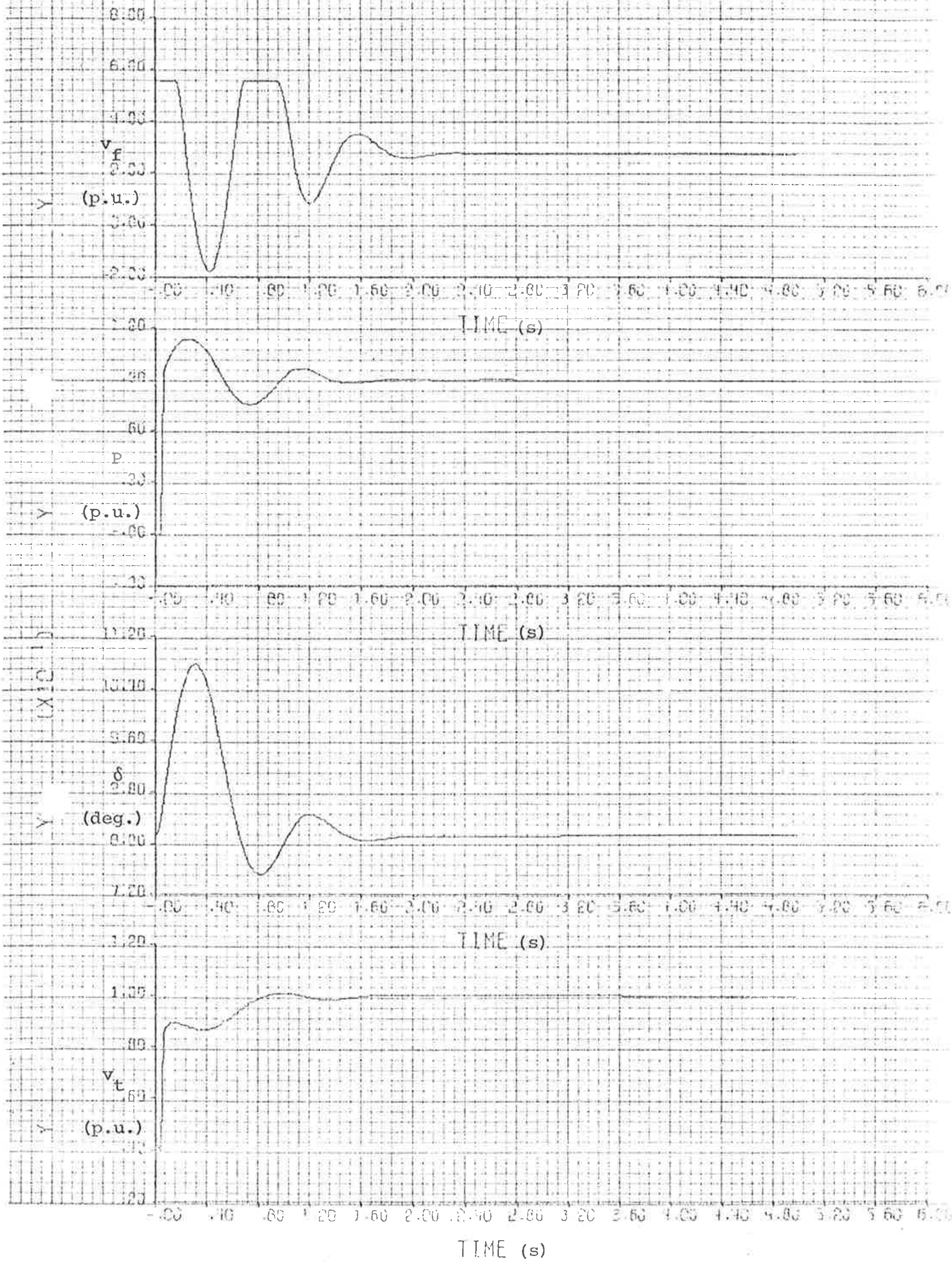

FIGURE 5.11(j) PP/4/AG/Ff_v/B CONTROLLER AT $\overline{P}$ = 0.9 p.u., $\overline{Q}$ = 0.4 p.u.

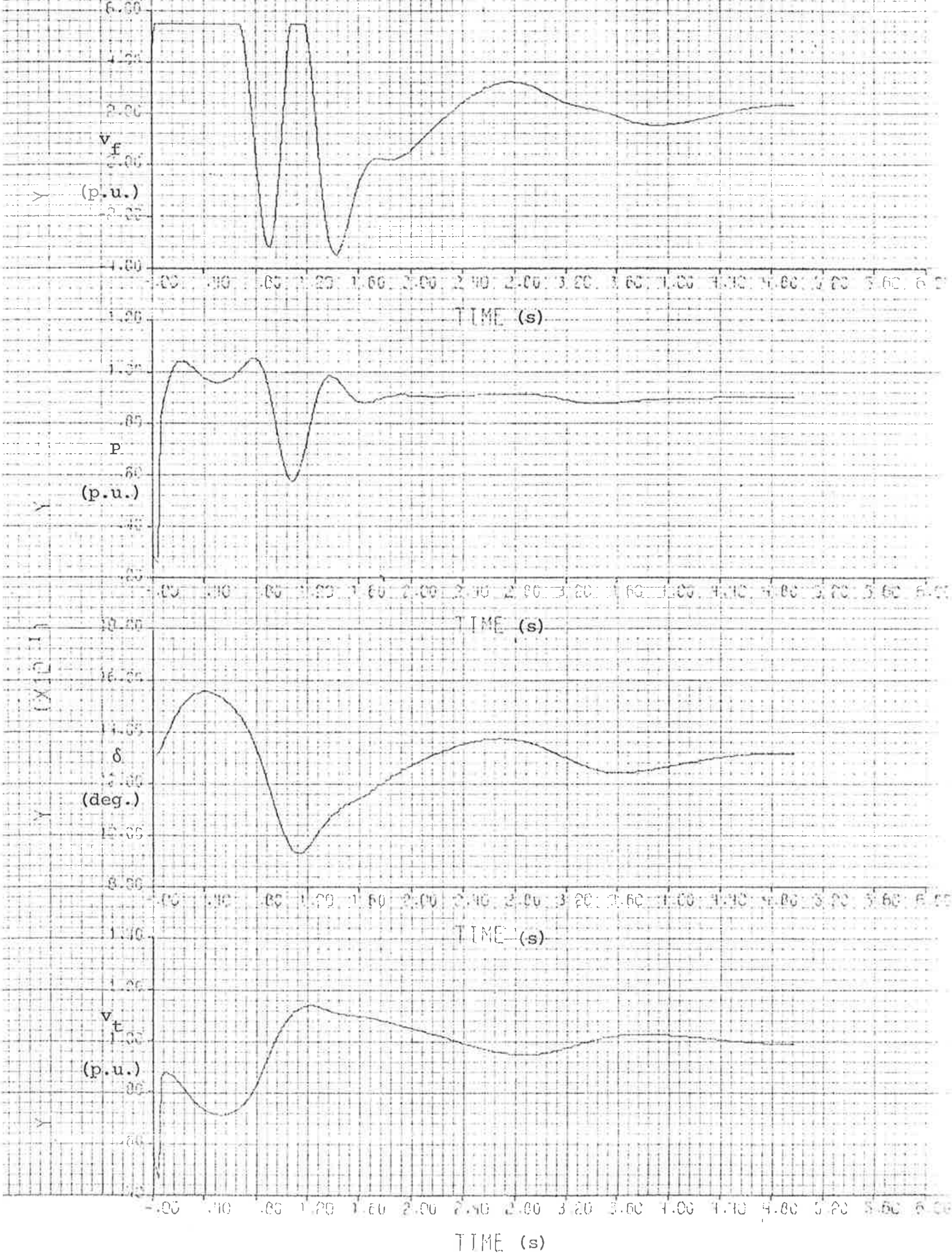

FIGURE 5.11(k) PP/4/FG/B CONTROLLER AT $\overline{P}$ = 0.9 p.u., $\overline{Q}$ = -0.8 p.u.

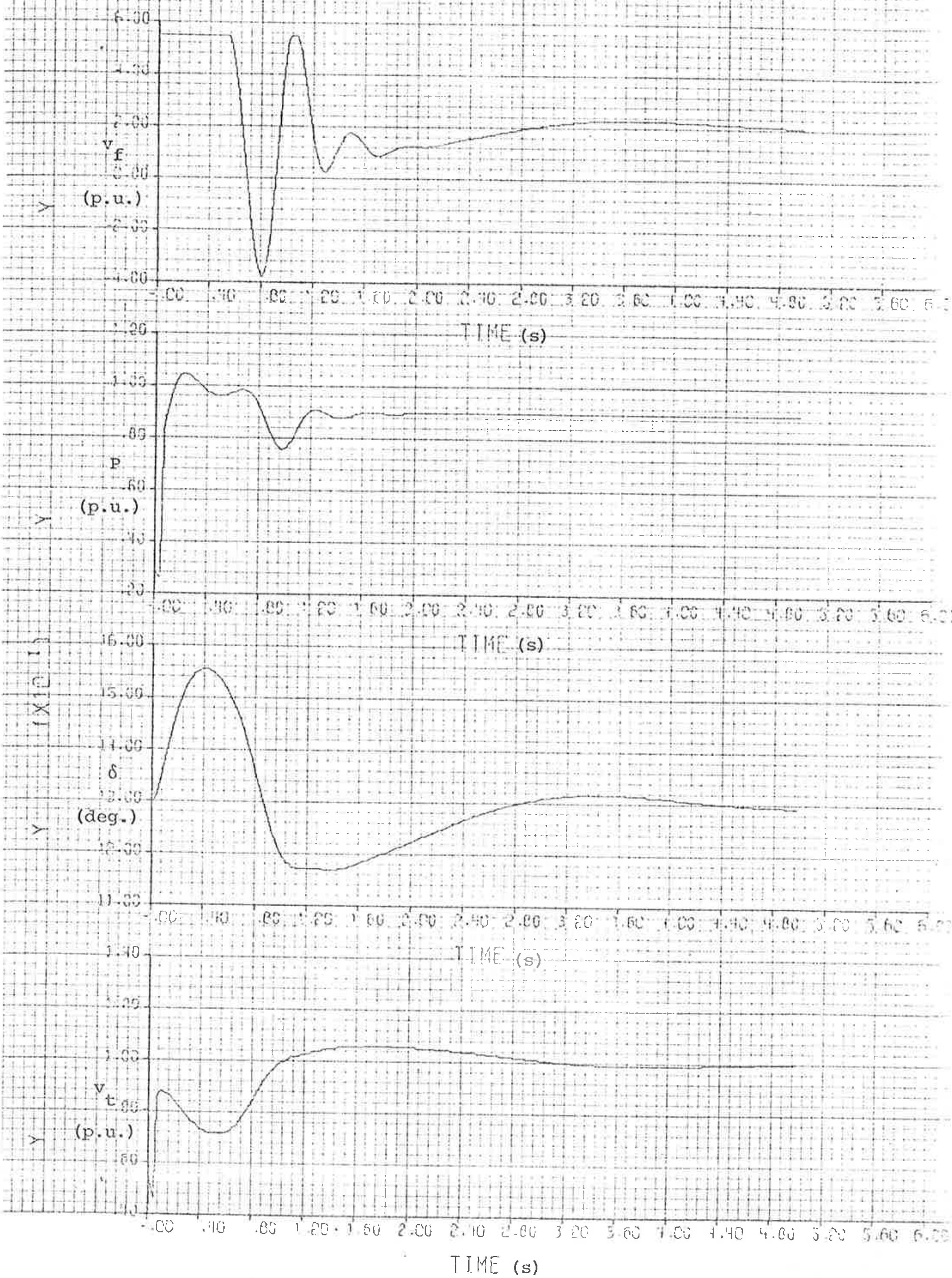

FIGURE 5.11(1) PP/4/AG/Ff$_v$/B CONTROLLER AT $\overline{P}$ = 0.9 p.u., $\overline{Q}$ = -0.8 p.u.

because with a realistic clearing time for the fault, the low accelerating power during the fault results in only a relatively small perturbation in rotor angle.

At leading power-factor, when the postfault tie-line reactance is unchanged from the initial value, the performance at low load is similar to that predicted by small signal analysis (Figure 5.11(e) and (f)). However, when the excitation at the initial operating point is low, and the postfault reactance is increased from the prefault value, the adjustable-gain controller has poorer damping than the fixed-gain controller designed for rated load (Figure 5.11(g) and (h)). The reason is that the increased reactance causes the postfault steady-state operating point to be at a considerably higher power-factor than the operating point before the fault. Figure 4.4 shows that at an initial operating point where $\overline{Q} \approx v_t^2/x_q = 0.65$, the values of the feedback gains necessary for good performance are low, but that as the value of $\overline{Q}$ tends towards zero the feedback gain necessary rises rapidly. This problem is not encountered with the PP/3/AG/Ff$_v$ strategy, because it may be seen from Figure 3.4 that the minimum value of f_p in the low power leading power-factor region is somewhat higher.

When operation at medium to high real power output and leading power-factor is considered, if typical exciter ceilings and protection operating times are used the limit set by transient stability considerations lies well inside the dynamic stability limit of the fixed-gain controller. (In order to produce Figure 5.11 (i), (j), (k) and (l), the fault severity is reduced by reducing the clearing time.) To safely utilise the extended dynamic stability limit possible with the adjustable-gain excitation control, some aid for transient stability such as braking resistors, or fast valving is necessary. It is necessary to assess the effect of such an aid on postfault damping. In the event of an electrohydraulic governor, a coordinated governor and excitation system design would probably give the best results for small and large signal conditions. A further factor which must be taken into account under leading p.f. conditions is the design of the generator itself, with respect to the permissible end core heating losses.

5.4.3 Effects of generator modelling on large signal performance

During the course of the large signal of study, in a similar way to section 5.2, the effect of modelling assumptions on the performance of the system were investigated. Dandeno investigated the effects of generator modelling on the performance of machines with conventional rotating exciters and no stabilising signals. He found that the effect of the choice of generator model decreased as the excitation level at the prefault operating point increased. In this study a similar trend is found for systems using a short exciter time-constant and stabilising signals based on pole-placement. In agreement with Dandeno's results the neglect of the amortisseur windings leads to a slightly optimistic estimate of the magnitude of the first swing.

The application of stabilising signals allows operation at significantly leading power-factor, and it is found that as in the small signal studies described in section 5.3, the neglect of the q-axis transient time-constant at such loads leads to large errors. Figure 5.12 shows the behaviour of various models at this type of operating point. The largest errors in predicting postfault damping result from omitting the effects of the quadrature axis rotor iron or the governor.

It is concluded that, provided only moderately accurate results are required, the recommendations given by Dandeno for the use of a model with a transient time-constant in each axis are also valid for thyristor type excitation systems with stabilising signals derived from shaft speed, electrical power output and field voltage.

This section concludes Chapter 5 which shows that the PP/4/FG/B and PP/4/FG/Ff_v/B strategies are the best of the pole-placement control strategies developed in Chapters 2 and 4. Although these strategies are based on a simple low order model, they provide fast voltage response and heavy damping of electromechanical oscillations when applied to a high order SMIB model. The performance is acceptable under a wide range of operating conditions and for both large and small disturbances.

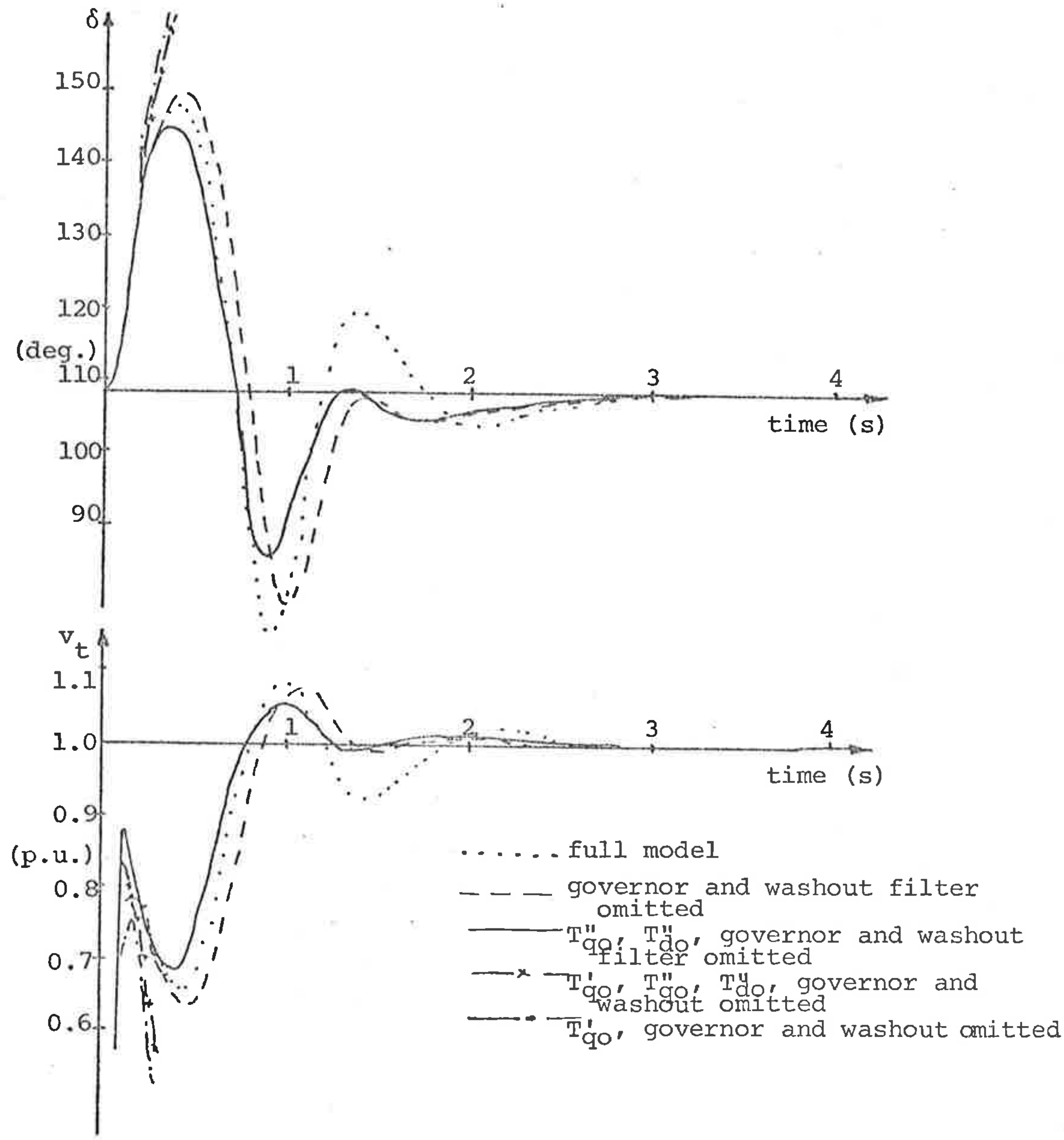

FIGURE 5.12 THE EFFECT OF MODELLING ON LARGE SIGNAL RESPONSE

(System data set BB in Table 5.1; controller gains set by $PP/4/AG/Ff_v/B$ to $f_v = 60$, $f_s = 1198$, $f_p = -63.3$, $f_F = -0.54$. To simulate fault V_b and x_e are both reduced to 0.33 for 0.1 sec. with $\overline{P} = 0.9$ p.u. and $\overline{Q} = -0.4$p.u.)

CHAPTER 6

ANALYSIS OF THE EFFECTS OF INTERACTION BETWEEN GENERATORS USING SIMPLE GENERATOR MODELS IN A TWO-MACHINE INFINITE-BUS CONFIGURATION

6.1 PRELIMINARY DISCUSSION

6.1.1 System model

In the preceding chapters dealing with the design of excitation controllers by pole-placement and the assessment of their performance, it is assumed that the generator of interest is remote from other generators in the power system. This assumption may be justified in a number of cases but in practice there is generally interaction with the other generators. In this chapter the term "interaction" simply means that the dynamic behaviour of a generator is affected by the dynamics of nearby generators coupled to it through the transmission system. The definition of interaction is discussed further in section 7.1. This chapter examines the effect of this interaction on the small signal performance of the generator and how it depends on the electrical coupling between the generators.

The example which is used to illustrate the effect of interaction between generators is a comparison of the performance of the two systems shown in Figure 6.1(a) and (b). It is assumed that:

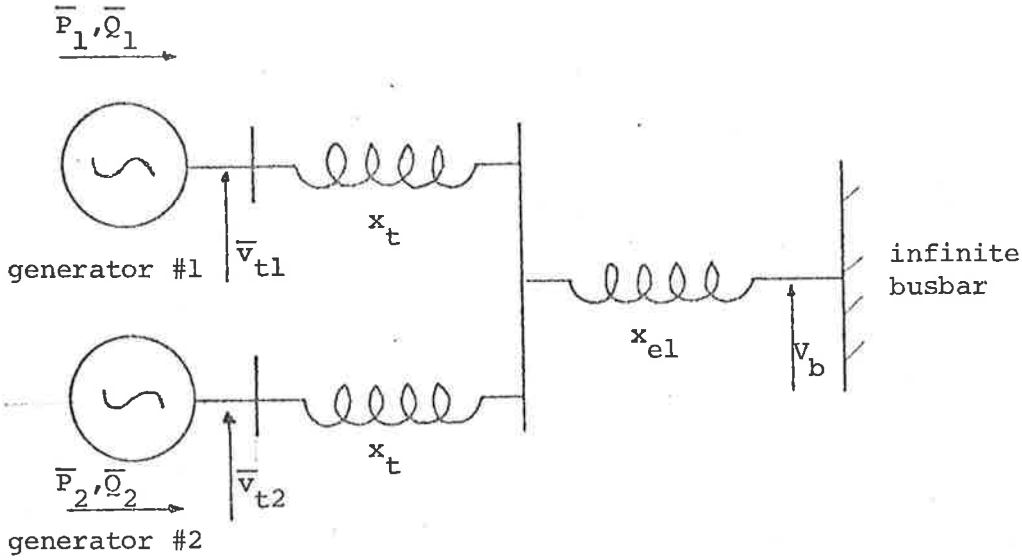

(a) A two-machine infinite-bus system

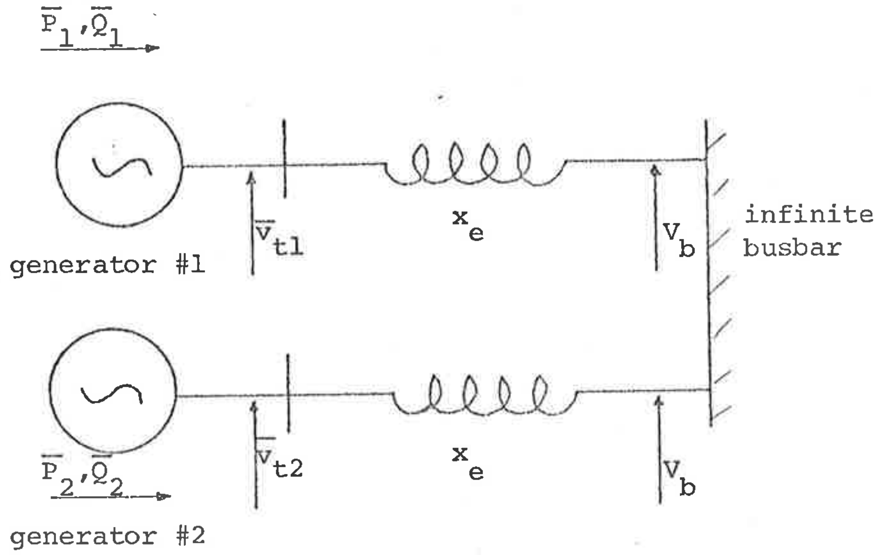

(b) Two single-machine infinite-bus systems

FIGURE 6.1 CONFIGURATIONS FOR THE COMPARISON OF INTERCONNECTED AND ISOLATED GENERATORS

(a) generators #1 and #2 are identical, with the machine parameters being those of row (2) in Table 3.2. To allow easy comparison with earlier results, the MVA base of the system is taken to be the rating of a single machine.

(b) for simplicity, the generators are adequately represented by third-order machine models.

(c) as in Chapters 2 and 3, all excitation controller time-constants are negligible, and that during transients the mechanical power inputs are constant.

(d) the generators in Figure 6.1(a) are connected to a common busbar by unit transformers represented by a series of reactances, x_t, equal to 0.15 p.u.

6.1.2 Changes in the system poles resulting from interaction

Consider the case when the generators are equally loaded such that $\overline{P}_1 = \overline{P}_2 = 0.8$ p.u., $\overline{Q}_1 = \overline{Q}_2 = 0.3$ p.u. and $\overline{v}_{t1} = \overline{v}_{t2} = 1$ p.u. Suppose the controllers provide only terminal voltage feedback with gain $f_v = 50$. When the tie-line reactance, x_{e1} in Figure 6.1(a) is zero, the two-machine infinite bus (TMIB) system is equivalent to two non-interacting SMIB systems, each with poles at $s = -0.64 \pm j\ 8.73$ and $s = -3.70$. The choice of $x_e = x_t$ in Figure 6.1(b) makes the systems in Figures 6.1(a) and (b) identical.

Suppose that the value of x_{el} is set to 0.05 p.u. instead of zero; the generators in Figure 6.1(a) now interact and the system poles lie at

$$s = -0.64 \pm j\,8.73$$

$$s = -0.46 \pm j\,8.03$$

$$s = -5.12 \text{ and } s = -3.70$$

Three of the poles are the same as before, but the other three have changed. Since the generators are identical there is clearly no way that one set of poles can be attributed to one generator and a second different set to the other. Wilson [32] has applied eigenvector analysis to explain the behaviour of the various modes in multimachine dynamic performance. The application of eigenvectors to the analysis of power system dynamic behaviour is discussed in the following section.

6.2 A REVIEW OF EIGENVECTOR ANALYSIS AND ITS APPLICATION TO INVESTIGATION OF POWER SYSTEM BEHAVIOUR

6.2.1 Theory

Consider the n^{th} order system with m inputs and outputs described by the equations:

$$\dot{\underset{\sim}{x}} = A_o \underset{\sim}{x} + B\underset{\sim}{u} \tag{6.1}$$

$$\underset{\sim}{y} = C\underset{\sim}{x} \tag{6.2}$$

where $\underset{\sim}{x}$, $\underset{\sim}{y}$ and $\underset{\sim}{u}$ are the state vector, output vector and control vector respectively. A, B and C are the plant, control and output matrices.

Suppose feedback is applied such that the control signal is:

$$\underset{\sim}{u} = \underset{\sim}{u}_{ref} - F\underset{\sim}{y} \tag{6.3}$$

The behaviour of the closed-loop system is given by:

$$\dot{\underset{\sim}{x}} = (A_o - BFC)\ \underset{\sim}{x} + B\underset{\sim}{u}_{ref}$$

$$\text{i.e.}\quad \dot{\underset{\sim}{x}} = A\underset{\sim}{x} + B\underset{\sim}{u}_{ref} \tag{6.4}$$

Following Timothy and Bona [63], the time response of the states may be written in terms of the state transition matrix, $\Phi(t,\tau)$:

$$\underset{\sim}{x}(t) = \Phi(t,0)\underset{\sim}{x}(0) + \int_o^t \Phi(t,\tau)B\underset{\sim}{u}_{ref}(\tau)d\tau \tag{6.5}$$

Provided the system matrix A has distinct eigenvalues, the state transition matrix may be written in terms of these eigenvalues denoted $\lambda_1, \lambda_2, \ldots, \lambda_n$ and corresponding eigenvectors denoted $\underset{\sim}{u}_1, \underset{\sim}{u}_2, \ldots, \underset{\sim}{u}_n$.

$$\Phi(t,\tau) = T \begin{bmatrix} e^{\lambda_1(t-\tau)} & & & \\ & e^{\lambda_2(t-\tau)} & & \\ & & \ddots & \\ & & & e^{\lambda_n(t-\tau)} \end{bmatrix} T^{-1} \qquad (6.6)$$

where $T = [\underset{\sim}{u}_1, \underset{\sim}{u}_2, \ldots, \underset{\sim}{u}_n]$, a matrix of eigenvectors.

Suppose the rows of T^{-1} are denoted $\underset{\sim}{v}_1, \underset{\sim}{v}_2, \ldots, \underset{\sim}{v}_n$, then:

$$\Phi(t,\tau) = [\underset{\sim}{u}_1,\underset{\sim}{u}_2,\ldots,\underset{\sim}{u}_n]\mathrm{diag}(e^{\lambda_i(t-\tau)})[\underset{\sim}{v}_1,\underset{\sim}{v}_2,\ldots,\underset{\sim}{v}_n]^t$$

and equation (6.5) may be written as:

$$\underset{\sim}{x}(t) = \sum_{i=1}^{n} \underset{\sim}{v}_i^t \underset{\sim}{x}(0)\underset{\sim}{u}_i e^{\lambda_i t} + \int_o^t \sum_{i=1}^{n} \underset{\sim}{v}_i^t B \underset{\sim}{u}_{ref}(\tau)\underset{\sim}{u}_i e^{\lambda_i(t-\tau)} d\tau \quad (6.7)$$

The disturbances used to test the behaviour of a multi-machine power system are usually either:

(a) A non-equilibrium state for the system at time zero. The response, called the "natural response", is:

$$\underset{\sim}{x}(t) = \sum_{i=1}^{n} \underset{\sim}{v}_i^t \underset{\sim}{x}(0)\underset{\sim}{u}_i e^{\lambda_i t} \qquad (6.8)$$

or

(b) A step-input applied to the system at time zero with the system in equilibrium. The so-called "forced response" is:

$$\underset{\sim}{x}(t) = \sum_{i=1}^{n} \underset{\sim}{v}_i^t B\underset{\sim}{u}_{ref}\underset{\sim}{u}_i \int_o^t e^{\lambda_i(t-\tau)} d\tau$$

$$= \sum_{i=1}^{n} \frac{\underset{\sim}{v}_i^t B\underset{\sim}{u}_{ref}}{\lambda_i} \underset{\sim}{u}_i (e^{\lambda_i t} - 1) \qquad (6.9)$$

In either case the system response is the sum of modes corresponding to the eigenvalues. Each eigenvalue fully describes the time dependence of its component of the response. It is important to notice that:

(a) The extent to which a mode affects each state of the system, relative to the other states, is fully described by the corresponding eigenvector, u_i, irrespective of the disturbance which excites the response.

(b) The terms $\underset{\sim}{v}_i^t \underset{\sim}{x}(0)$ and $(\underset{\sim}{v}_i^t B\underset{\sim}{u}_{ref})/\lambda_i$ are <u>scalars</u> which determine to what extent a disturbance excites a given mode.

(c) Any eigenvector corresponding to a given eigenvalue may be multiplied by a real or complex scalar. The expression for the system response is unaffected because an increase in the scale of $\underset{\sim}{u}_i$ is accompanied by a corresponding decrease in $\underset{\sim}{v}_i$.

6.2.2 An example

Suppose the states for the sixth-order, two-machine infinite-bus system of section 6.1.2 are chosen to be the deviations in rotor angles, rotor speeds and the voltages proportional to field flux linkages, that is $\underset{\sim}{x} = (\Delta v'_{q1}, \Delta\delta_1, \Delta\omega_{s1}, \Delta v'_{q2}, \Delta\delta_2, \Delta\omega_{s2})^t$. When the system is perturbed by a 1 p.u. error in $\Delta\delta_1$ at time zero, the response is:

$$\begin{bmatrix}\Delta v'_{q1}\\ \Delta\delta_1\\ \Delta\omega_{s1}\\ \Delta v'_{q2}\\ \Delta\delta_2\\ \Delta\omega_{s2}\end{bmatrix} = \begin{bmatrix}.0230\\ -.0176\\ .0002\\ .0230\\ -.0176\\ .0002\end{bmatrix} e^{-5.12t} + \begin{bmatrix}.0219\\ -.0195\\ .0002\\ -.0219\\ .0195\\ -.0002\end{bmatrix} e^{-3.70t} + \begin{bmatrix}.0297\angle 112^\circ\\ .2602\angle -3^\circ\\ .0060\angle 91^\circ\\ .0297\angle -68^\circ\\ .2602\angle 177^\circ\\ .0060\angle -89^\circ\end{bmatrix} e^{-0.64t+j8.73t}$$

$$+ \begin{bmatrix}.0297\angle -112^\circ\\ .2602\angle 3^\circ\\ .0060\angle -91^\circ\\ .0297\angle 68^\circ\\ .2602\angle -177^\circ\\ .0060\angle 89^\circ\end{bmatrix} e^{-0.64t-j8.73t} + \begin{bmatrix}.0221\angle 121^\circ\\ .2590\angle -2^\circ\\ .0055\angle 91^\circ\\ .0221\angle 121^\circ\\ .2590\angle -2^\circ\\ .0055\angle 91^\circ\end{bmatrix} e^{-0.46t+j8.03t} + \begin{bmatrix}.0221\angle -121^\circ\\ .2590\angle 2^\circ\\ .0055\angle -91^\circ\\ .0221\angle -121^\circ\\ .2590\angle 2^\circ\\ .0055\angle -91^\circ\end{bmatrix} e^{-0.46t-j8.03t}$$

where $v\angle\alpha$ denotes a complex number with magnitude v and angle α which equals $v(\cos\alpha + j\sin\alpha)$.

When the system is perturbed by a 1 p.u. error in $\Delta v'_{q2}$ at time zero the response is:

$$\begin{bmatrix}\Delta v'_{q1}\\ \Delta\delta_1\\ \Delta\omega_{s1}\\ \Delta v'_{q2}\\ \Delta\delta_2\\ \Delta\omega_{s2}\end{bmatrix} = \begin{bmatrix}.5362\\ -.4095\\ .0056\\ .5362\\ -.4095\\ .0056\end{bmatrix} e^{-5.12t} + \begin{bmatrix}-.5406\\ .4811\\ -.0047\\ .5406\\ -.4811\\ .0047\end{bmatrix} e^{-3.70t} + \begin{bmatrix}.0291\angle -46^\circ\\ .2549\angle -161^\circ\\ .0059\angle -66^\circ\\ .0291\angle 134^\circ\\ .2549\angle 19^\circ\\ .0059\angle 114^\circ\end{bmatrix} e^{-0.64t+j8.73t}$$

$$+ \begin{bmatrix}.0291\angle 46^\circ\\ .2549\angle 161^\circ\\ .0059\angle 66^\circ\\ .0291\angle -134^\circ\\ .2549\angle -19^\circ\\ .0059\angle -114^\circ\end{bmatrix} e^{-0.64t-j8.73t} + \begin{bmatrix}.0202\angle 153^\circ\\ .2367\angle 30^\circ\\ .0051\angle 123^\circ\\ .0202\angle 153^\circ\\ .2367\angle 30^\circ\\ .0051\angle 123^\circ\end{bmatrix} e^{-0.46t+j8.03t} + \begin{bmatrix}.0202\angle -153^\circ\\ .2367\angle -30^\circ\\ .0051\angle -123^\circ\\ .0202\angle -153^\circ\\ .2367\angle -30^\circ\\ .0051\angle -123^\circ\end{bmatrix} e^{-0.46t-j8.03t}$$

(i) Consider the coefficients for the mode corresponding to the eigenvalue at $s = -5.12$; although the amplitude of this mode is much greater when the second disturbance is applied, the relative amplitudes of the perturbations to the states are invariant, because they are components of eigenvectors (i.e. .0230:-.0176:.0002:... = .5362:-.4095:.0056...).

(ii) Although the amplitudes of the modes corresponding to the real poles are greatly increased for the second disturbance, the amplitudes of the other modes are not greatly affected - the relative amplitudes of the modes depend on the disturbance applied.

(iii) The effect of a complex pair of poles is to produce a single mode of double amplitude. For example, in the latter case -

$$\begin{aligned}\Delta v'_{q1} &= 0.5362e^{-5.12t} - 0.5406e^{-3.70t} + 0.0291\angle{-46°}\,e^{-0.64t+j8.73t} \\ &\quad + 0.0291\angle{+46°}\,e^{-0.64t-j8.73t} + 0.0202\angle{+153°}\,e^{-0.46t+j8.03t} \\ &\quad + 0.0202\angle{-153°}\,e^{-0.46t-j8.03t} \\ &= 0.5362e^{-5.12t} - 0.5406e^{-3.70t} + 2(0.0291e^{-0.64t}\cos(8.73t-46°)) \\ &\quad + 2(0.0202e^{-0.46t}\cos(8.03t+153°))\end{aligned}$$

(iv) In order to assess the effect of various modes on different machines it is useful to compare the coefficients for like physical quantities. For example, in the latter case -

$$\Delta\omega_{s1} = 0.0056e^{-5.12t} - 0.0047e^{-3.70t} + 0.0118e^{-0.64t}\cos(8.73t - 66^\circ)$$
$$+ 0.102e^{-0.46t}\cos(8.03t + 123^\circ)$$

$$\Delta\omega_{s2} = 0.0056e^{-5.12t} + 0.0047e^{-3.70t} + 0.0118e^{-0.64t}\cos(8.73t + 114^\circ)$$
$$+ 0.102e^{-0.46t}\cos(8.03t + 123^\circ)$$

The generators swing in phase for the 8.03 rad/s mode of oscillation but antiphase for the 8.73 rad/s mode. Wilson pointed out that this type of information may be deduced by inspection of the $\Delta\omega_1$ and $\Delta\omega_2$ coefficients of the eigenvectors for these modes.

6.3 THE APPLICATION OF SMIB POLE-PLACEMENT CONTROLLER DESIGNS TO A TWO-MACHINE INFINITE-BUS SYSTEM

6.3.1 Equal loads

Table 6.1 shows the effect of changing x_{e1} on the poles of the TMIB system described in section 6.1. Inspection of the components of the eigenvectors reveals that, irrespective of the value of x_{e1}, the symmetry of this special case with identical generators means that each mode perturbs both generators equally. The generators oscillate in phase for some modes which are referred to below as "group" modes, and antiphase for others which are referred to as "inter-machine" modes. The system behaviour is most clearly described in terms of these inter-machine modes and group modes rather than in terms of modes due to individual generators. As the coupling to the infinite-bus becomes weaker the damping of the group mode deteriorates.

In designing an excitation system by SMIB pole-placement one of the important parameters to be specified is the value for the equivalent tie-line reactance, x_e, which is required for the feedback gain calculations (see equations (A3.7) - (A3.11) in Appendix 10.3). The eigenvalues for a SMIB system with the same terminal conditions as the generators in the TMIB system are listed in Table 6.2 for various values of x_e. Comparison of Tables 6.1 and 6.2 reveals that, for each value of x_{e1}, the eigenvalues of the TMIB system are the same as those for an SMIB system with $x_e = x_t$ plus those for an SMIB system with $x_e = x_t + 2x_{e1}$. This result

eigen value no.	eigenvalue	eigenvector component corresponding to speed of generator no. 1	eigenvector component corresponding to speed of generator no. 2	type of mode
1,2	$-0.64 \pm j8.73$	1.0	-1.0	intermc
3	-3.70	1.0	-1.0	intermc
4,5	$-0.46 \pm j8.03$	1.0	1.0	group
6	-5.12	1.0	1.0	group
Case 1 : $x_{e1} = 0.05$				
1,2	$-0.64 \pm j8.73$	1.0	-1.0	intermc
3	-3.70	1.0	-1.0	intermc
4,5	$-0.16 \pm j7.08$	1.0	1.0	group
6	-7.00	1.0	1.0	group
Case 2 : $x_{e1} = 0.15$				
1,2	$-0.64 \pm j8.73$	1.0	-1.0	intermc
3	-3.70	1.0	-1.0	intermc
4,5	$+0.28 \pm j5.32$	1.0	1.0	group
6	-9.40	1.0	1.0	group
Case 3 : $x_{e1} = 0.45$				

Operating Conditions: $\overline{P}_1 = \overline{P}_2 = 0.8$, $\overline{Q}_1 = \overline{Q}_2 = 0.3$, $\overline{v}_{t1} = \overline{v}_{t2} = 1$ p.u., voltage feedback only ($f_v = 50$ for both generators).

TABLE 6.1 EIGENANALYSIS OF THE TMIB SYSTEM IN FIGURE 6.1(a)

x_e	eigenvalues	comment
0.15	$-0.64 \pm j8.73, -3.70$	$x_e = x_t$; cf. intermc mode in Table 6.1
0.2	$-0.55 \pm j8.35, -4.46$	
0.25	$-0.46 \pm j8.03, -5.12$	cf. group mode in case 1 of Table 6.1
0.3	$-0.38 \pm j7.75, -5.70$	design value of x_e
0.4	$-0.22 \pm j7.29, -6.62$	
0.45	$-0.16 \pm j7.08, -7.00$	cf. group mode in case 2 of Table 6.1
0.5	$-0.10 \pm j6.89, -7.34$	
0.6	$0.00 \pm j6.55, -7.90$	
1.05	$+0.28 \pm j5.31, -9.41$	cf. group mode in case 3 of Table 6.1

Operating conditions: $\overline{P} = 0.8$, $\overline{Q} = 0.3$, $\overline{v}_t = 1$ p.u., $f_v = 50$ (only voltage feedback)

TABLE 6.2 EIGENVALUES FOR ONE SMIB HALF OF FIGURE 6.1(b) suggests that a value of x_e such that $x_t \leqslant x_e \leqslant x_t + 2x_{e1}$ should be used in the application of SMIB pole-placement to design the controllers for the TMIB system. A value of 0.3 p.u. is used for x_e in this thesis for applying SMIB pole-placement to multi-machine systems. (This choice is arrived at by taking the mean of x_t and $x_t + 2x_{e1}$ with a value of 0.15 p.u. for x_t and a nominal value of 0.15 p.u. for x_{e1}.)

Although it is concluded in Chapter 5 that the PP/4/AG/Ff$_v$/B control strategy is the most effective of the pole-placement strategies, the present system does not include exciter time-constants so the PP/3/AG/Ff$_v$ strategy is employed. Table 6.3 shows the eigenvalues of the TMIB system for several values of x_{e1}, when the generators are equipped with controllers designed by SMIB pole-placement assuming $x_e = 0.3$. The eigenvalues of an SMIB system with the same controller are listed in Table 6.4 for various values of x_e. As in the case with no subsidiary feedback, the symmetry of the system means that the intermachine mode does not depend on the value of x_{e1}. The damping of the group mode is dependent on the value of x_{e1} and deteriorates as it becomes large, however, the system does have good damping for a wide range of values of x_{e1}.

6.3.2 Unequal loads

In order to further investigate interaction in multi-machine systems and the suitability of SMIB pole-placement controller designs, consider the case when the generators of

eigen value no.	eigenvalue	eigenvector component corresponding to speed of generator 1	eigenvector component corresponding to speed of generator 2	type of mode
1,2	$-4.86 \pm j9.36$	1.0	-1.0	intermc
3	-2.55	1.0	-1.0	intermc
4,5	$-4.16 \pm j8.12$	1.0	1.0	group
6	-3.98	1.0	1.0	group

Case 1 : $x_{e1} = 0.05$

1,2	$-4.86 \pm j9.36$	1.0	-1.0	intermc
3	-2.55	1.0	-1.0	intermc
4,5	$-2.81 \pm j6.66$	1.0	1.0	group
6	-6.72	1.0	1.0	group

Case 2 : $x_{e1} = 0.15$

1,2	$-4.87 \pm j9.36$	1.0	-1.0	intermc
3	-2.55	1.0	-1.0	intermc
4,5	$-1.15 \pm j5.01$	1.0	1.0	group
6	-10.09	1.0	1.0	group

Case 3 : $x_{e1} = 0.45$

Loading: $\bar{P}_1 = \bar{P}_2 = 0.8$, $\bar{Q}_1 = \bar{Q}_2 = 0.3$, $\bar{v}_{t1} = \bar{v}_{t2} = 1.0$ p.u.

Controllers: $f_v = 50$, $f_s = 885$, $f_p = -16.1$ for both generators

(PP/3/AG/Ff_v design using $x_e = 0.3$ p.u.)

TABLE 6.3 EIGENANALYSIS OF THE TMIB SYSTEM IN FIGURE 6.1(a)

x_e	eigenvalues	comments
0.15	$-4.87 \pm j9.36, -2.55$	$x_e = x_t$; cf. intermc mode in Table 6.3
0.2	$-4.52 \pm j8.69, -3.26$	
0.25	$-4.16 \pm j8.12, -3.99$	cf. group mode in case 1 of Table 6.3
0.3	$-3.80 \pm j7.63, -4.72$	PP/3/AG/Ff_v controller designed for $x_e = 0.3$
0.4	$-3.11 \pm j6.92, -6.12$	
0.45	$-2.81 \pm j6.66, -6.72$	cf. group mode in case 2 of Table 6.3
0.5	$-2.55 \pm j6.45, -7.25$	
0.6	$-2.13 \pm j6.11, -8.10$	
1.05	$-1.15 \pm j5.00, -10.1$	cf. group mode in case 3 of Table 6.3

Operating conditions: $\bar{P} = 0.8$, $\bar{Q} = 0.3$, $\bar{v}_t = 1.0$, $f_v = 50$, $f_s = 885$, $f_p = -16.1$

TABLE 6.4 EIGENVALUES FROM ONE SMIB HALF OF FIGURE 6.1(b) the TMIB system have identical parameters but are at different loading conditions. Table 6.5 lists the eigenvalues for such a case, before the application of subsidiary feedback signals. In contrast to the case in the previous section, the modes have differing effects on the two generators. Furthermore, when the electrical coupling to the infinite bus is strong, each oscillatory mode tends to be associated with a particular generator. However, as the coupling becomes weaker, the behaviour more closely resembles that of intermachine and group modes as in the previous section.

The eigenvalues of two SMIB systems with generators having identical terminal conditions to those of the TMIB system are listed in Table 6.6. Unlike the symmetrical case, comparison of Tables 6.5 and 6.6 yields no simple relation between the poles of the SMIB systems and those of the TMIB system.

Table 6.7 shows the eigenvalues of the TMIB system when controllers employing the PP/3/AG/Ff$_v$ strategy are applied to the generators (using $x_e = 0.3$ in the gain calculations, as in section 6.3.1). The SMIB pole-placement designed controllers again provide heavy damping for a wide range of x_{e1}. For comparison, Table 6.8 lists the eigenvalues which result when these controllers are applied to the two SMIB systems in Figure 6.1(b).

Comparison of the eigenvector components in Tables 6.5 and 6.7 shows that in addition to improving the damping of

eigen value no.	eigenvalue	eigenvectors components corresp.to speed of generator 1	eigenvectors components corresp.to speed of generator 2	comments
1,2	$-0.62\pm j8.58$	1.0	$0.066\angle 169^\circ$	gen.1
3,4	$-0.47\pm j5.66$	$0.087\angle 6^\circ$	1.0	gen.2
5	-6.04	$0.072\angle 0^\circ$	1.0	gen.2
6	-4.06	1.0	$0.37\angle 180^\circ$	gen.1
				tendency towards modes associated with individual generators

Case 1 : $x_{e1} = 0.05$

eigen value no.	eigenvalue	eigenvectors components corresp.to speed of generator 1	eigenvectors components corresp.to speed of generator 2	comments
1,2	$-0.53\pm j8.17$	1.0	$0.18\angle 168^\circ$	intermediate case between individual and group behaviour
3,4	$-0.37\pm j5.47$	$0.21\angle 9^\circ$	1.0	
5	-7.84	1.0	$0.76\angle 0^\circ$	
6	-4.17	1.0	$0.52\angle 180^\circ$	

Case 2 : $x_{e1} = 0.15$

eigen value no.	eigenvalue	eigenvectors components corresp.to speed of generator 1	eigenvectors components corresp.to speed of generator 2	comments
1,2	$-0.39\pm j7.33$	1.0	$0.43\angle 168^\circ$	intermc
3,4	$-0.21\pm j4.69$	$0.48\angle 11^\circ$	1.0	group
5	-10.05	1.0	$0.48\angle 0^\circ$	group
6	-4.17	1.0	$0.66\angle 180^\circ$	intermc
				tendency towards group and intermc mode behaviour

Case 3 : $x_{e1} = 0.45$

Loading: $\bar{P}_1 = 0.8$, $\bar{Q}_1 = 0.3$, $\bar{P}_2 = 0.2$, $\bar{Q}_2 = 0.0$, $\bar{v}_{t1} = 1.045$, $\bar{v}_{t2} = 1.008$ p.u.
Controllers: voltage feedback only ($f_v = 50$)

TABLE 6.5 EIGENANALYSIS OF THE TMIB SYSTEM IN FIGURE 6.1(a)

x_e	eigenvalues of generator 1	eigenvalues of generator 2	comments
0.15	$-0.68\pm j8.92$ -3.70	$-0.51\pm j5.81$ -4.91	$x_e = x_t$
0.25	$-0.53\pm j8.22$ -5.11	$-0.43\pm j5.54$ -6.48	cf. values for case 1 in Table 6.5
0.45	$-0.24\pm j7.27$ -7.00	$-0.33\pm j5.18$ -8.35	cf. values for case 2 in Table 6.5
1.05	$+0.19\pm j5.52$ -9.42	$-0.23\pm j4.52$ -10.57	cf. values for case 3 in Table 6.5

Loading: $\bar{P}_1 = 0.8$, $\bar{Q}_1 = 0.3$, $\bar{P}_2 = 0.2$, $\bar{Q}_2 = 0.0$, $\bar{v}_{t1} = 1.045$, $\bar{v}_{t2} = 1.008$ p.u.
Controllers: voltage feedback only ($f_v = 50$)

TABLE 6.6 EIGENVALUES FROM SMIB SYSTEMS IN FIGURE 6.1(b)

eigen value no.	eigenvalue	eigenvector component corresp.to speed of generator 1	eigenvector component corresp.to speed of generator 2	comments
1,2 3,4 5 6	$-4.56\pm j9.01$ $-2.79\pm j6.90$ -4.01 -2.58	1.0 $0.32\angle -35°$ 1.0 1.0	$0.15\angle 166°$ 1.0 0.70 -0.80	gen.1 } oscillatory modes can be assigned to individual generators gen.2?

Case 1 : $x_{e1} = 0.05$

1,2 3,4 5 6	$-4.03\pm j8.74$ $-2.26\pm j5.95$ -6.73 -2.61	1.0 $0.68\angle 16°$ 1.0 1.0	$0.35\angle 179°$ 1.0 0.51 -0.78	intermediate case between individual and group behaviour

Case 2 : $x_{e1} = 0.15$

1,2 3,4 5 6	$-3.51\pm j8.41$ $-1.39\pm j4.72$ -9.99 -2.47	1.0 $0.99\angle 41°$ 1.0 1.0	$0.62\angle 170°$ 1.0 0.31 -0.90	intermc group group intermc } tendency to group and intermc mode behaviour

Case 3 : $x_{e1} = 0.45$

Loads: Generator 1, $\bar{P}_1 = 0.8$ p.u., $\bar{Q}_1 = 0.3$ p.u., $\bar{V}_{t1} = 1.045$ p.u.
Generator 2, $\bar{P}_2 = 0.2$ p.u., $\bar{Q}_2 = 0.0$ p.u., $\bar{V}_{t2} = 1.008$ p.u.
PP/3/AG/Ff$_v$ controllers designed using $x_e = 0.3$ p.u.
Generator 1, $f_v = 50$, $f_s = 885$, $f_p = -16.1$
Generator 2, $f_v = 50$, $f_s = 1409$, $f_p = -11.0$

TABLE 6.7 EIGENANALYSIS OF THE TMIB SYSTEM IN FIGURE 6.1(a)

x_e	eigenvalues of generator 1	eigenvalues of generator 2	comments
0.15	$-4.94\pm j9.53$ -2.58	$-2.86\pm j7.52$ -2.58	$x_e = x_t$
0.25	$-4.25\pm j8.29$ -4.01	$-2.67\pm j6.52$ -4.03	cf. case 1 of Table 6.7
0.45	$-2.92\pm j6.83$ -6.72	$-2.00\pm j5.46$ -6.65	cf. case 2 of Table 6.7
1.05	$-1.26\pm j5.18$ -10.1	$-1.17\pm j4.42$ -10.4	cf. case 3 of Table 6.7

Loads: Generator 1, $\bar{P}_1 = 0.8$ p.u., $\bar{Q}_1 = 0.3$ p.u., $\bar{V}_{t1} = 1.045$ p.u.
Generator 2, $\bar{P}_2 = 0.2$ p.u., $\bar{Q}_2 = 0.0$ p.u., $\bar{V}_{t2} = 1.008$ p.u.
PP/3/AG/Ff$_v$ controllers designed using $x_e = 0.3$ p.u.
Generator 1, $f_v = 50$, $f_s = 885$, $f_p = -16.1$
Generator 2, $f_v = 50$, $f_s = 1409$, $f_p = -11.0$

TABLE 6.8 EIGENVALUES FROM SMIB SYSTEMS IN FIGURE 6.1(b) the system, the introduction of the subsidiary feedbacks appears to increase the interaction between the generators and make each mode less clearly identified with a particular machine. However, although the components of the eigenvector do give a useful measure of the extent to which the states of a system are affected by a given mode of oscillation, it is necessary to consider the relative amplitudes and phases of all modes in order to assess the overall behaviour of the system; it is possible for the effect of one mode to be largely cancelled by that of other modes in the response. The question of interaction between generators is discussed further in the next chapter.

In summary, this chapter demonstrates that for a simple TMIB system, as the electrical coupling between generators becomes significant in comparison to the coupling to the "infinite-bus", the poles of the system become more closely identified with intermachine and group modes of oscillation than with the behaviour of individual generators. Eigenvector analysis allows the effect of a mode on the system to be determined. For the two loading conditions considered, controllers designed by the PP/3/AG/Ff_v pole-placement strategy based on a SMIB model provide adequate damping for a wide range of tie-line reactance, x_{e1}. The effectiveness of pole-placement strategies in multi-machine power systems is investigated more fully in Chapter 8 using more accurate generator and controller models.

CHAPTER 7

THE ANALYSIS OF MULTIMACHINE POWER SYSTEM DYNAMIC BEHAVIOUR USING THE INVERSE NYQUIST ARRAY

7.1 INTERACTION BETWEEN GENERATORS

In the previous chapter the term "interaction" is used loosely to mean that the behaviour of a generator is affected by the presence of other nearby generators. The neglect of these generators during controller design with a SMIB model results in errors in performance (i.e. pole-placement). In dealing with the design of multivariable feedback control systems "interaction" is generally used in two somewhat different senses meaning either:

(a) an input or disturbance perturbs output quantities other than those desired, or

(b) the performance of one feedback loop is dependent on the gains in other loops.

Interaction in the second sense prevents the successive application of single input - single output (s.i.s.o.) design methods from being a viable design technique for multivariable systems (MacFarlane [35]). A number of design techniques have been proposed in which the interaction is first made insignificant, allowing the subsequent application of s.i.s.o. methods. For example, Nolan [81] applied one such method based on state feedback, devised by Falb and Wolovich [82], to simplify the design of a speed governor and excitation controller for an SMIB system. This chapter considers an alternative method developed by Rosenbrock [36], based on the inverse Nyquist array (INA), and discusses how it may be adapted to provide useful information concerning the behaviour of a multimachine power system.

The INA displays information about interaction in sense (a) with the inputs being sinusoidally excited. The theory developed by Rosenbrock allows conclusions to be drawn concerning interaction in sense (b); such information is useful in excitation controller design.

When considering the performance of generators in a power system, it is also desirable that interaction in sense (a) be minimised so that disturbances at any one generator (e.g. a change in voltage set point) result in negligible transients at other generators in the system. An aim of the investigation into the application of the INA to the analysis of power system dynamic behaviour is to determine what information concerning these transients may be obtained from the sinusoidal steady-state information in the INA. "Interaction" in the remainder of this thesis refers to the undesirable transients arising from step-like disturbances. Useful results relevant to this investigation are:

(a) Bumby [39] showed that making the generators of a TMIB system non-interacting for small amplitude input signals improves transient stability. In the event of a major fault near the terminals of one generator, the non-interacting controller reduces the amplitude of the disturbance to the other generator eliminating the possibility of instability on the second swing.

(b) Muttik [40] demonstrated that adjusting subsidiary feedback gains for closed-loop diagonal dominance (see section 7.2.2) reduces interaction between generators following changes in voltage set-point.

(c) Daly [80] proposed an integral measure for the degree of diagonal dominance in an INA. He showed that it is related to interaction in the time domain via the responses at outputs 1,2,3,...,i-1,i+1,...,m following an impulse at input i.

The results of the previous chapter suggest that eigenvector analysis might be useful in assessing interaction. However, shortcomings of this method are that the results only hold for a single gain setting and the effects of gain changes are not evident. Furthermore, unless the system is of low-order, the response is the sum of several modes so that its shape cannot be comprehended without detailed calculation.

In this thesis INA analysis is primarily considered as a simple way of finding modifications necessary to tune controllers designed by SMIB pole-placement for use in multimachine power systems. It is useful because it indicates the effect of interaction (sense (b)) on performance. A secondary aim of the investigations is to find what information can be deduced from the INA concerning interaction (sense (a)) between generators.

7.2 THEORY FOR THE ANALYSIS OF MULTIVARIABLE SYSTEMS USING THE INVERSE NYQUIST ARRAY

7.2.1 A relationship between open- and closed-loop systems

Consider the multivariable system shown in Figure 7.1. In the absence of feedback, the response of the system is described by a transfer function matrix, $Q(s)$, with elements $q_{ij}(s)$ which are functions of the Laplace operator (s) describing the behaviour of output i following an impulse at input j. The following theory is largely taken from Rosenbrock's book and is based on the properties of the inverse of $Q(s)$, denoted $\hat{Q}(s)$, having elements $\hat{q}_{ij}(s)$. For the existence of an inverse it is necessary that $Q(s)$ be square, that is, the number of inputs must equal the number of outputs; this number is denoted m.

Suppose the i^{th} output is fed back to the i^{th} input with a gain f_i, as shown in Figure 7.1, and that the resulting closed-loop transfer-function matrix is denoted $H(s)$. There is a simple relationship between the elements of the inverse of $H(s)$, $\hat{H}(s)$, and the inverse of $\hat{Q}(s)$, namely:

$$\hat{h}_{ii}(s) = f_i + \hat{q}_{ii}(s) \qquad i=1,2,\ldots,m$$

$$\hat{h}_{ij}(s) = \hat{q}_{ij}(s) \qquad j=1,2,\ldots,i-1,i+1,\ldots,m$$

$$i=1,2,\ldots,m \qquad (7.1)$$

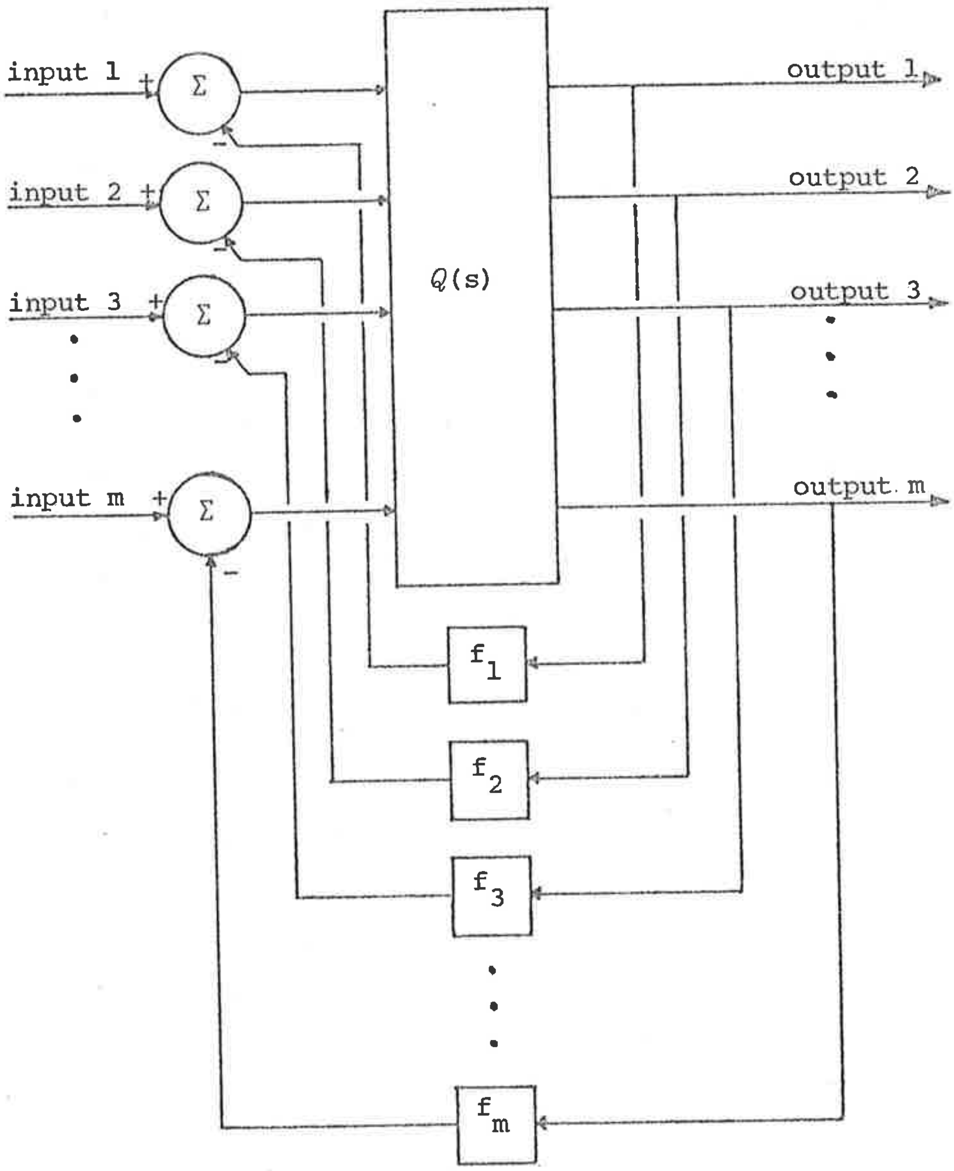

FIGURE 7.1 AN m-INPUT m-OUTPUT MULTIVARIABLE CONTROL SYSTEM

7.2.2 Diagonal dominance and a test for stability

If at some value of s, say s_o, the elements of $\hat{Q}(s_o)$ obey the relation

$$|\hat{q}_{ii}(s_o)| > \sum_{\substack{j=1 \\ j\neq i}}^{m} |\hat{q}_{ij}(s_o)|, \qquad i=1,2,\ldots,m \tag{7.2}$$

then $\hat{Q}$ is termed row diagonally dominant for $s = s_o$. Similarly if the relation

$$|\hat{q}_{ii}(s_o)| > \sum_{\substack{j=1 \\ j\neq i}}^{m} |\hat{q}_{ji}(s_o)|, \qquad i=1,2,\ldots,m \tag{7.3}$$

is true then $\hat{Q}$ is termed column diagonally dominant for $s = s_o$. If either or both of the relations hold, then $\hat{Q}$ is simply termed diagonally dominant.

There is a simple graphical test to reveal the values of s at which the open-loop system is row (or column) diagonally dominant. The method is to draw the m Nyquist plots for the $\hat{q}_{ii}(s)$ and then for each value of s to draw circles of radius

$$\sum_{\substack{j=1 \\ j\neq i}}^{m} |\hat{q}_{ij}(s)| \qquad \left(\text{or} \quad \sum_{\substack{j=1 \\ j=i}}^{m} |\hat{q}_{ji}(s)|\right)$$

with centres $\hat{q}_{ii}(s)$. If the origin of each of the m plots lies outside the band formed by the envelope of the circles (called the Gershgorin band), the open-loop system is diagonally dominant.

If both $\hat{Q}(s)$ and $\hat{H}(s)$ are diagonally dominant for all values of s on a Nyquist contour enclosing the right-half s-plane, the difference between the number of poles in the right-half s-plane for the two systems is equal to the difference in the total number of encirclements of the origin by the $\hat{q}_{ii}(s)$ and the $\hat{h}_{ii}(s)$. If the number of right-half s-plane poles is known for the open-loop system, then this analysis reveals whether the closed-loop system is stable. (The number of encirclements of the origin of the i^{th} plot by $\hat{h}_{ii}(s)$ is easily determined, being equal to the number of encirclements of $(-f_i,0)$ by $\hat{q}_{ii}(s)$).

In applying the above theory to practical problems, crossings of the Gershgorin band by a critical point moving from (0,0) to $(-f_i,0)$ rather than changes in the number of encirclements are usually employed to determine changes in the number of right-half plane poles. Rosenbrock (p. 153 of [36]) proves that provided the Gershgorin bands do not enclose the real axis at a suitably high frequency, the change in the number of poles may be determined in this manner.

7.2.3 Ostrowski's theorem and the prediction of closed-loop performance

The elements of $\hat{H}(s)$ do not relate to physically measurable quantities in the closed-loop system. Suppose $h_{ii}(s)$ is the transfer function between the i^{th} input and the i^{th} output for the closed-loop system. Ostrowski's theorem may be applied to show that the inverse of $h_{ii}(s)$, denoted $h_{ii}^{-1}(s)$ always lies inside the Gershgorin band about $\hat{h}_{ii}(s)$ whenever the system is closed-loop diagonally dominant. If, in addition, the gains in all feedback loops except the i^{th} are known, then $h_{ii}^{-1}(s)$ lies inside a narrower band called the Ostrowski band.

The radius of the i^{th} Ostrowski band at a frequency $s = s_o$ is equal to

$$r_i(s_o) \times \max_{\substack{k=1,2,\ldots,m \\ k \neq i}} \left\{ \frac{r_k(s_o)}{f_k + \hat{q}_{kk}(s_o)} \right\} \quad ,$$

where $r_k(s_o)$, $\hat{q}_{kk}(s_o)$ and f_k are the radius of the k^{th} Gershgorin band, the value of the k^{th} diagonal element of the INA and the feedback gain specified for the k^{th} loop.

The methods which are available to predict the transient response of a single-input single-output system from an inverse Nyquist frequency response plot (e.g. M circles) may be applied to the multivariable case via the Ostrowski bands. For systems of higher than second order these methods are not exact but do allow estimates of the damping and frequency of oscillation to be made (page 72 of [36]).

7.2.4 Rosenbrock's approach

The method proposed by Rosenbrock for the design of controllers for multivariable systems has two distinct stages. First a precontroller matrix $K(s)$ is devised, which makes the resulting $\hat{Q}(s)$ matrix diagonally dominant with narrow Gershgorin bands over a suitable range of frequencies. At this point the system consists of m input-output pairs

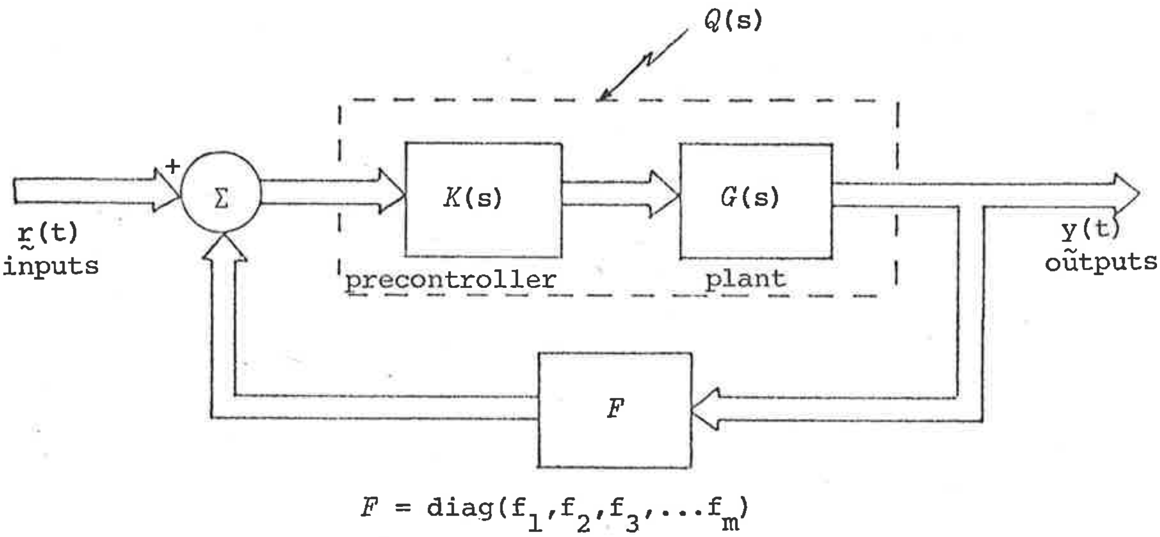

FIGURE 7.2 MULTIVARIABLE CONTROL SCHEME USED BY ROSENBROCK

which are almost non-interacting. The second stage is the design of m s.i.s.o. feedback control systems using the Ostrowski bands.

This method has been applied to the design of coordinated governor and excitation controllers for a SMIB system by Huseyin [64] and Ahson [38]. A major problem in extending this method to multimachine power systems is that diagonal dominance is achieved by the introduction of off-diagonal terms in the $K(s)$ matrix; to implement such a controller would usually involve the telemetry of signals between generators, which is undesirable for reasons of reliability and cost. Bumby [39] showed that for a TMIB system similar to that in Figure 6.1(a), making the generators non-interacting improves transient stability. However, the method he used involves frequency dependent cross feedback between the generators; although feedback between generators in the same power station might be acceptable, large scale telemetry between generators in different geographical locations is undesirable.

7.3 A MODIFIED APPROACH TO THE USE OF THE INVERSE NYQUIST ARRAY

7.3.1 Philosophy

In this thesis, the inverse Nyquist array is used to analyse the performance of excitation controllers which are initially designed by SMIB pole-placement. It is demonstrated in Chapter 8 and Appendix 10.5 that when these controllers are applied to a multimachine system diagonal dominance can be achieved by suitable adjustment of local feedback gains. Therefore, useful results may be obtained using the theory in section 7.2.

(i) Choice of inputs

This thesis deals solely with the design of excitation control systems; it is assumed that the generator is equipped with a conventional mechanical-hydraulic speed governor which has a relatively slow speed of response. In calculating the inverse Nyquist array, the governor loop is considered as part of the plant and each generator is considered to have one input acting through the excitation system. With advent of electro-hydraulic governing best performance will result from coordinated governor and excitation controller designs. Turbogenerators so equipped will need to be represented as having two inputs in future studies.

(ii) Dealing with several feedback signals

It is generally desirable to view the effect of adjusting each of several local feedback gains. However, at any given time, in order to satisfy the requirement for equal numbers of inputs and outputs it is necessary to choose only one of the signals fed back to the exciter as the output. The other feedback loops must be considered to be part of the "plant", that is, the "open loop" transfer function, $Q(s)$, for the system is calculated with these loops closed with specified fixed values of feedback gain. Provided diagonal dominance is achieved, the position of the critical point in the INA clearly indicates the effect of varying the feedback gain for the chosen output of each generator. It is proposed that several Nyquist arrays using different sets of variables as outputs be plotted in order to show the effect of changing various local feedback gains.

(iii) Choice of generators

It is not necessary for the INA to include an output for every generator. If the controller gains for a certain generator in the system are specified and its performance is not of immediate interest, it may be treated as part of the "plant"; the resulting INA will have less off-diagonal terms and hence diagonal dominance may be more easily achieved. The limiting case is that of the s.i.s.o. inverse Nyquist plot where there are no off-diagonal elements to be considered.

Information about the behaviour of a generator having no subsidiary feedback loops may be obtained by postulating a "fictitious" loop and maintaining the gain at zero; the position of the Gershgorin band with respect to the origin gives some measure of the likely damping and frequency of oscillation when this machine is disturbed. The behaviour of a generator with a controller whose gains cannot be changed may be investigated in a similar way with the position of the critical point being predetermined by the specified gain.

(iv) Assessing the extent of interaction

It is demonstrated that usually diagonal dominance can be achieved through the careful selection of local feedback gains. However, the fact that cross signals between the generators are to be avoided, severely restricts the operations which are available to reduce the width of the Gershgorin bands. In contrast to Rosenbrock's method where the bands are narrow once the precompensator is applied, the Gershgorin bands are usually quite wide in the current application, thus restricting the accuracy of predicting closed-loop performance.

The width of the Gershgorin bands for the generators should provide some information about interaction in the multimachine power system. It should be noted that unlike $q_{ij}(s)$, the magnitude of $\hat{q}_{ij}(s)$ at a given frequency does not directly relate to the steady-state sinusoidal interaction between loops i and j. For example, when the feedback gain for some loop is changed, the off-diagonal elements of $\hat{Q}$ are not affected but in general all elements of Q are altered.

7.3.2 Preliminary tests using a simple TMIB system

The feasibility of applying the INA to power system analysis in the manner described in section 7.3.1 was investigated using the simple TMIB system of section 6.1.1.

A digital computer program was written to calculate the transfer function matrix for this system and to plot the INA. (The algorithms employed to perform these calculations are discussed in section 7.4 and Appendix 10.6.) An analogue computer model of the system was constructed so that the time domain behaviour of the generators could be easily observed. The relation between the time responses and the positions of the critical points relative to the Gershgorin bands was examined. An example of this type of analysis was the basis for a paper [40] by the author.

The example used INA analysis to investigate the effect of various settings for the speed and power feedback gains of two unequally loaded generators in a TMIB system. (For details see Appendix 10.5.) The INA for the terminal voltage, shaft speed and electrical power feedback loops were calculated for the TMIB system at several other loading conditions in addition to that in this example. The effects of various values of tie-line reactance (x_{el}) and of dissimilar inertia constants (H) for the generators were investigated. In each case it was found that:

(i) By adjusting the values of local feedback gain it is possible to achieve closed-loop diagonal dominance for the speed and power INA. Cross feedback between generators is therefore unnecessary. This result is most important because it means that the INA can be used to assess the effect of gain changes for systems similar to those in present practice which employ only local feedback signals. Inspection of the INA provides useful information on the effect of gain changes on the damping and frequency of rotor oscillations.

(ii) In general, diagonal dominance for the terminal voltage INA cannot be obtained without unrealistically high voltage gains (say, 1000 or more) which would cause limiting of the field voltage for minor disturbances.

(iii) It is proved in Appendix 10.7 that altering the speed and power feedback gains for generators in a multimachine power system does not affect the width of the Gershgorin bands in either the speed or power INA. However, the results of the preliminary study clearly show that placing the critical point away from the Gershgorin band significantly reduces the interaction between generators. Comparison of Figure 4(a) and (b) of Appendix 10.5 demonstrates that minimising interaction does not necessarily improve performance.

(iv) Provided the guidelines of section 3.2 are followed in designing controllers by SMIB pole-placement, the resulting designs generally produce closed-loop diagonal dominance for the speed and power INA. Hence they are a convenient starting point for the multimachine controller design problem.

The value of ω_1 (f_v) which is used to design the pole-placement controller of Appendix 10.5 was deliberately chosen to be too high, resulting in an excessively high speed feedback gain balanced by a destabilising power feedback gain. Although the performance with the simple SMIB model is excellent, the use of this controller in the TMIB system leads to a poorly damped high frequency intermachine mode of oscillation. The INA (Figure 2 of the paper) clearly indicates the changes in feedback gain required to improve its performance.

The results of this preliminary investigation demonstrate that the inverse Nyquist array provides valuable insight for the application of controllers to a simple TMIB system. The use of the INA is investigated further in Chapter 8 where it is applied to a more extensive power system with detailed generator and controller models. The remainder of this chapter describes the methods used to calculate the INA for the examples in Appendix 10.5 and Chapter 8.

7.4 INA COMPUTATION FOR A MULTIMACHINE POWER SYSTEM

Digital computer programmes to analyse the behaviour of multimachine power systems were written using FORTRAN IV. Only a brief description of the methods is given because all the algorithms are adequately described in the literature cited. An Electrical Engineering Departmental report presenting annotated listings of the programmes and instructions for their use with the University of Adelaide CYBER 173 computer is being prepared. The computation proceeds in several distinct stages:

(i) Loadflow

The admittances between the generator and load buses of the system are specified together with trial values for the real and reactive power inputs for all buses except the slack bus. The voltage at the slack bus is specified and a method such as the Gauss-Seidel iterative method (Stagg [65], Elgerd [66]) is used to calculate the resulting voltage at each bus. If the bus voltages are not acceptable, new loads are chosen and the calculation repeated. When an acceptable solution is found, the loads are replaced by equivalent values of shunt admittance and a reduced nodal admittance matrix describing the interconnections between the generator buses is calculated.

(ii) Formation of a state space model

Equations describing the small-signal performance of the generators and their controllers (for example see section 10.4.3) are put in the form:

$$\Delta\dot{\underset{\sim}{x}} = A_o \Delta\underset{\sim}{x} + A_t \Delta\underset{\sim}{z} + B\Delta\underset{\sim}{u}$$

$$\Delta\underset{\sim}{y} = C_o \Delta\underset{\sim}{x} + C_t \Delta\underset{\sim}{z}$$

where $\Delta\underset{\sim}{x}$ is the vector of state variables chosen for the system; $\Delta\underset{\sim}{z}$ is a vector of the direct and quadrature axis components of terminal voltage and terminal current; $\Delta\underset{\sim}{u}$ is a vector of controller inputs and $\Delta\underset{\sim}{y}$ is a vector of system outputs.

In order to form the usual state-space equations of the system, the $\Delta\underset{\sim}{z}$ terms must be eliminated and expressed in terms of $\Delta\underset{\sim}{x}$. A matrix equation of form $L\Delta\underset{\sim}{z} = R\Delta\underset{\sim}{x}$ may be formed by combining equations relating the terminal voltage of each generator to its states (e.g. equations (A4-41) to (A4-46) of Appendix 10.4) with a relation between the terminal voltages and currents derived by Undrill [26]. The equations for the system may thus be written

$$\Delta\dot{\underset{\sim}{x}} = A_1 \Delta\underset{\sim}{x} + B\Delta\underset{\sim}{u}$$

$$\Delta\underset{\sim}{y} = C_1 \Delta\underset{\sim}{x}$$

where $A_1 = A_o + L^{-1}RA_t$ and $C_1 = C_o + L^{-1}RC_t$.

The eigenvalues of matrix A_1 describe the modes of dynamic performance of the system in the absence of excitation control.

(iii) Specification of feedback gain

Excitation control is applied to the system by specifying an input, $\Delta\underset{\sim}{u} = \Delta\underset{\sim}{u}_{ref} - F\Delta\underset{\sim}{y}$ so that the system equations are:

$$\Delta\dot{\underset{\sim}{x}} = A\Delta\underset{\sim}{x} - B\Delta\underset{\sim}{u}_{ref}$$

$$\Delta\underset{\sim}{y} = C_1\Delta\underset{\sim}{x}$$

where $A = A_1 - BFC_1$.

The entries in the matrix F specify the gains for the signals fed back to the excitation systems. The eigenvalues of matrix A describe the dynamic behaviour of the closed-loop system. Once the feedback gains are specified, the programmes calculate these eigenvalues and the corresponding eigenvectors using subroutines from the EISPACK library [67]. Comparison of eigenvector components corresponding to different generators allows the determination of which machines are significantly affected by any given mode in the response (see section 6.2). The programmes are designed for interactive use so that the gains may be repeatedly modified and the resulting effects on the eigenanalysis noted.

(iv) Calculation of the INA

Several methods of finding the inverse Nyquist array from the state space model of the system are possible (see Appendix 10.6). The steps in the most successful method employed are:

(a) Calculate the coefficients of the transfer function matrix for the system using an algorithm by Daly [75].

(b) Evaluate the transfer function matrix at a number of points in the frequency range of interest.

(c) Invert the matrix of complex numbers at each point to find the values for the chosen inverse transfer function matrix. The radii of the row and column based Gershgorin bands are calculated by summing the magnitudes of off diagonal elements.

The transfer function matrix in steps (a) and (b) need not be square so that the number of inputs and outputs does not have to be equal. Prior to step (c), the generators in the INA and their chosen outputs must be specified (see section 7.3.1).

The conceptual position of the feedback loops for INA calculation as discussed in section 7.3.1 is shown in Figure 1 of Appendix 10.5; the origin in the INA corresponds to zero feedback gain for the chosen output. The plant or "A" matrix for the system in this "open-loop" case depends on the set of outputs chosen. In the programmes which have been written, the INA is calculated for the *closed-loop* system because this requires only the storage of matrices A, B_1 and C_1 on the completion of step (iii) irrespective of which INA are to be plotted. Equation (7.1) shows that the only change resulting from the use of the closed-loop system is a translation such that the origin corresponds to the specified feedback gain. Displacement of the critical point from the origin corresponds to changing the gain from the specified value. The new arrangement of feedback loops is shown in Figure 7.3.

(v) Plotting the INA

The INA is used most conveniently and effectively when displayed via an interactive graphics facility. Because such equipment has not been available, the simplest way to produce the required graphs has been to employ a set of subroutines which plot graphs by printing characters over a page of lineprinter output [68]. One problem with this off-line method of output is that the scale for the graphs must be specified in the input data. The procedure used is initially to employ a small scale so that a large portion of the complex plane is shown and the overall form of the INA is evident. Revised scale factors are then chosen and the programme re-run so that the parts of the INA of particular interest may be examined more closely. Although this method of use is somewhat cumbersome and time-consuming, it has demonstrated the potential advantages of this type of analysis, especially when interactive graphics becomes available.

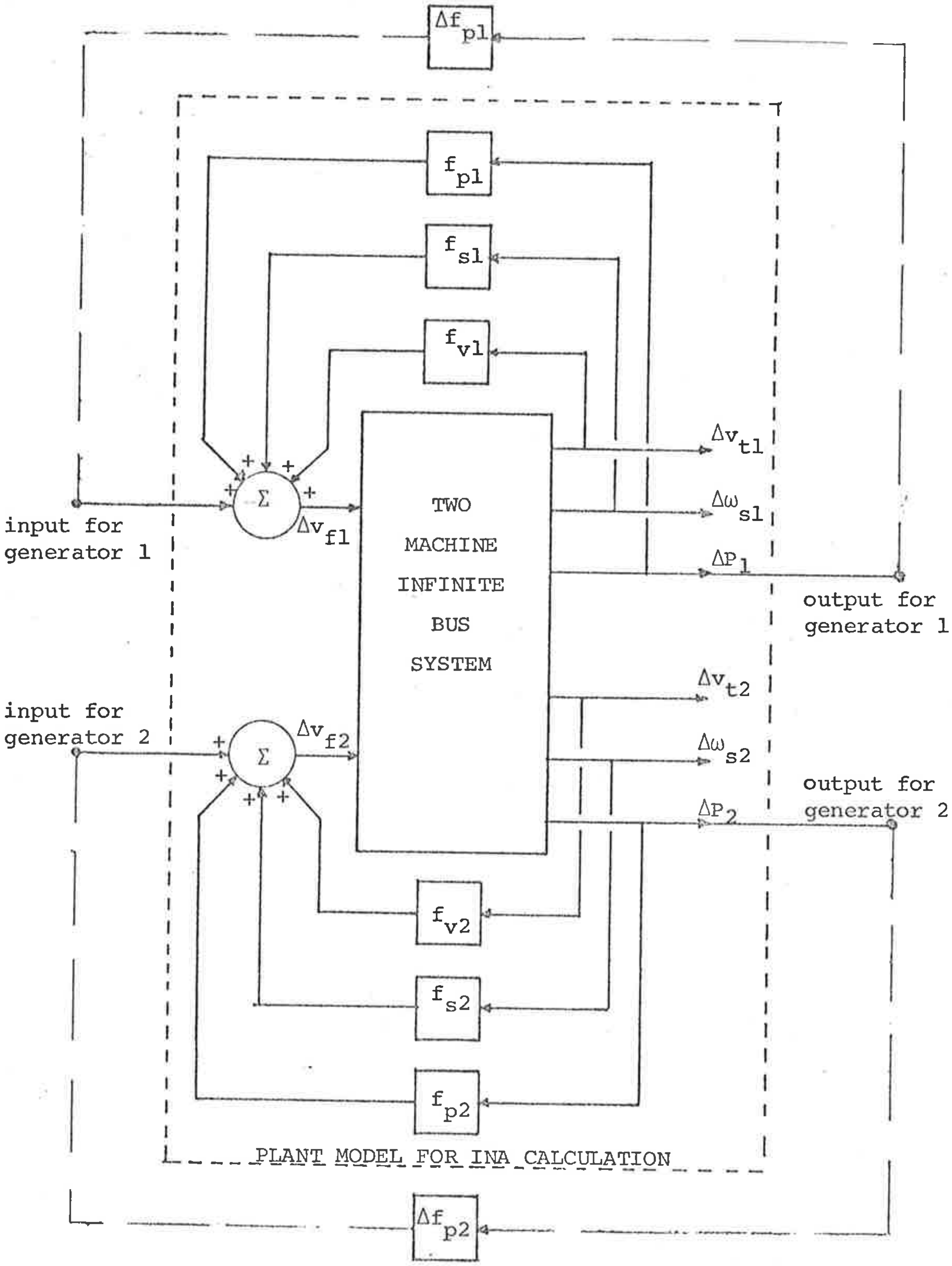

FIGURE 7.3 CALCULATION OF THE INA FOR THE POWER FEEDBACK LOOPS OF A CLOSED-LOOP TMIB SYSTEM

CHAPTER 8

INVESTIGATION OF THE SMALL-SIGNAL BEHAVIOUR OF A THREE-MACHINE INFINITE-BUS SYSTEM

8.1 PRELIMINARY REMARKS

This chapter investigates the behaviour of a three-machine power system under four different loading and network conditions to determine whether:

(a) Pole-placement strategies, based on a simple SMIB model, provide reasonable dynamic performance when the generators and their controllers are modelled more accurately and connected in a multimachine power system with several transmission lines and shunt loads. The performance of the PP/4/FG/B fixed-gain strategy is compared with that of the PP/4/AG/Ff$_v$/B adjustable-gain strategy.

(b) The inverse Nyquist array provides useful information in assessing and modifying the performance of controllers applied to a high-order model of a multimachine power system.

(c) The omission of the q-axis transient time-constant (T'_{qo}) significantly affects the dynamic behaviour of generators in a multimachine system.

The steady-state loading conditions for the examples are chosen to cover a wide range of feasible operating points.

Different values for line reactances are chosen for the transmission system model in each of the four examples, in order to ensure that the conclusions of this study do not depend on the choice of reactance values.

The system which is studied is shown in Figure 8.1. It is assumed that controllers are to be designed for the generators denoted units #1, #2 and #3 which supply three load bases numbered 5, 6 and 7. The shunt loads and the line reactances connecting these buses are considered to form an equivalent network representing an extensive transmission and distribution system. A generator at bus 1 represents a large power system electrically distant from the three generators; it is assigned a large inertia and modelled by a constant voltage behind a transient reactance.

Interaction between generators is to be investigated, therefore the system is chosen such that units #2 and #3 are closely coupled electrically, being connected to the same high-voltage busbar with the reactances between buses 3, 4 and 5 representing unit transformers. Craven [69] showed that closely-coupled generators should be modelled accurately, therefore sixth-order generator models are used to represent units #2 and #3. The generator at bus 2 is not electrically close to other units so it is represented by a fourth-order model which neglects the effect of the amortisseur windings. For convenience it is assumed that the three generators are identical and described by the data in column BB of Table 5.1.

In order to avoid the numerical instability problems

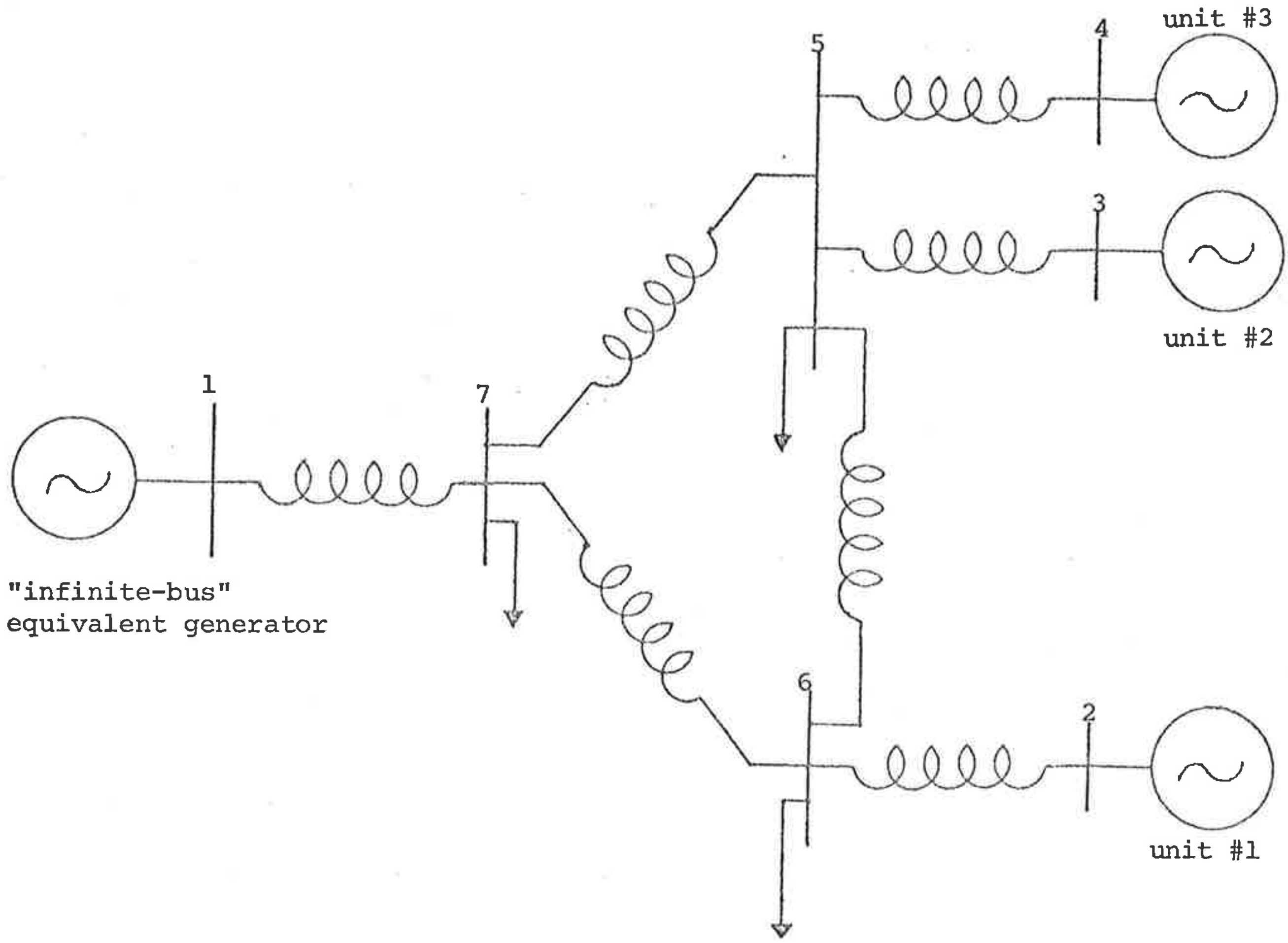

FIGURE 8.1 A THREE-MACHINE INFINITE-BUS POWER SYSTEM

described in Appendix 10.6, it is necessary to use as low order generator and controller models as possible. In order to illustrate that governor effects may be included during INA analysis, units #2 and #3 are provided with simple, first-order governor models. All excitation systems are represented by simple first-order models similar to that used in Chapter 5. The power feedback loops for units #2 and #3 include a washout filter, but for simplicity, the effect of the washout is neglected for unit #1.

8.2 EXAMPLE 1: OPERATION AT LAGGING POWER-FACTOR

It is concluded in Chapter 5 that, for the SMIB case, an adjustable-gain controller offers significant improvement in dynamic performance at low lagging power factor loading. In order to investigate whether this conclusion holds in a multimachine case in which the SMIB model is not valid, such a load is set for unit #1. The shunt loads are chosen to promote interaction between this generator and other units (generators #2 and #3 supply part of the load at bus 6, close to unit #1). Figure 8.2 shows the loading conditions and line reactances for this example.

8.2.1 Comparison of performance with fixed- and adjustable-gain controllers

(a) Fixed-gain design

Consider the case when units #1, #2 and #3 are equipped with the same fixed-gain controller designed by PP/4/FG/B pole-placement for a design load of $\overline{P} = 0.9$, $\overline{Q} = 0.1$ p.u. Suppose the value of SMIB tieline reactance, x_e, chosen for the calculation of feedback gain is 0.3 p.u. (see section 6.3.1); at the design load, the feedback gains $f_v = 100$, $f_s = 478$, $f_p = -49.1$, $f_F = -0.65$ place the poles of the fourth-order SMIB design model at $s = -3.68 \pm j7.56$, -5.0 and -21.2.

Row 1 of Table 8.1 lists the eigenvalues corresponding to the larger amplitude modes of oscillation in the multimachine power system at the lagging power-factor

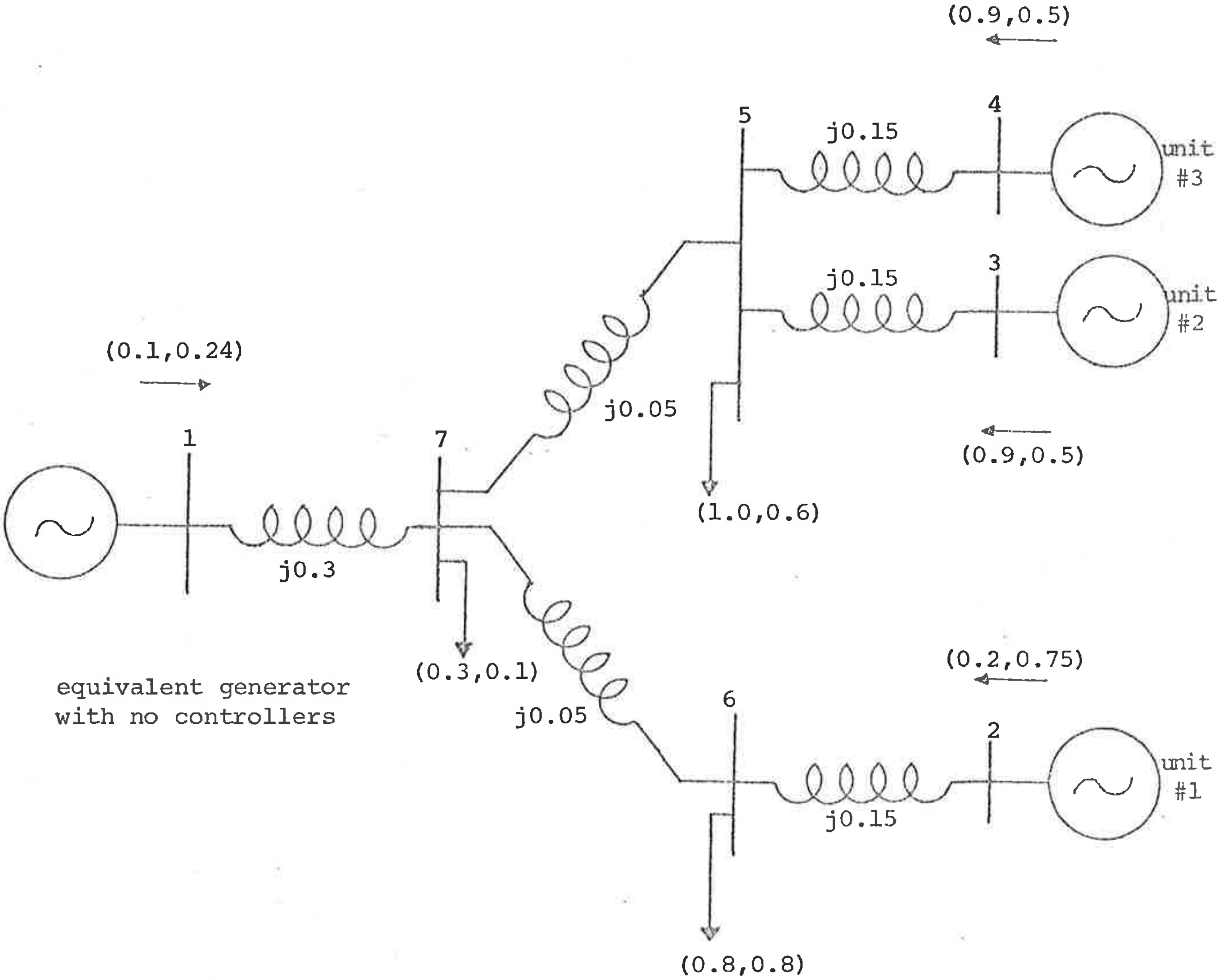

Bus	Voltage (p.u.)	Angle (deg.)
1	1.00	0
2	1.03	-2.0
3	1.00	9.2
4	1.00	9.2
5	0.93	0.8
6	0.92	-3.9
7	0.93	-1.9

Figures in brackets indicate real and reactive power flow.

Generator data as in column BB of Table 5.

FIGURE 8.2 LOAD AND NETWORK FOR SECTION 8.2
(Example 1 : Lagging p.f.)

Row	Gain Settings	f_v	f_s	f_p	f_F	Unit #
1	PP/4/FG/B fixed-gain	100	478	- 49.1	-0.65	1
	controllers for all	100	478	- 49.1	-0.65	2
	units	100	478	- 49.1	-0.65	3
2	nominal gain settings	100	6100	-213	-0.67	1
	PP/4/AG/Ff$_v$/B	100	1060	- 60.8	-0.70	2
	controllers	100	1060	- 60.8	-0.70	3
3	nominal gains	100	6100	-213	-0.67	1
	except f_s high	100	4400	- 60.8	-0.70	2
	for #2	100	1060	- 60.8	-0.70	3
4	nominal gains	100	6100	-213	-0.67	1
	except f_s low	100	-2000	- 60.8	-0.70	2
	for #2	100	1060	- 60.8	-0.70	3
5	nominal gains	100	6100	-163	-0.67	1
	except f_p low	100	1060	- 60.8	-0.70	2
	for #1	100	1060	- 60.8	-0.70	3
6	nominal gains	100	6100	-263	-0.67	1
	except f_p high	100	1060	- 60.8	-0.70	2
	for #1	100	1060	- 60.8	-0.70	3
7	nominal gains	100	6100	-213	-0.67	1
	except f_p low	100	1060	- 10.8	-0.70	2
	for #2	100	1060	- 60.8	-0.70	3
8	nominal gains	100	6100	-213	-0.67	1
	except f_p high	100	1060	-110.8	-0.70	2
	for #2	100	1060	- 60.8	-0.70	3
9	nominal gains	100	6100	-213	-0.67	1
	except f_p high	100	1060	-110.8	-0.70	2
	for #2 and #3	100	1060	-110.8	-0.70	3

Rows continued on page below to show corresponding modes.

Row	MODE A S_{1A}	MODE A S_{2A}	MODE A S_{3A}	MODE B S_{1B}	MODE B S_{2B}	MODE B S_{3B}	MODE C S_{1C}	MODE C S_{2C}	MODE C S_{3C}
1	$-1.08 \pm j5.54$			$-1.58 \pm j9.97$			$-4.33 \pm j12.50$		
	$1.24\angle 173$	$1.37\angle 162$	$1.37\angle 162$	$1.72\angle 39$	$.907\angle -145$	$.907\angle -145$	$0\angle -31$	$0\angle 161$	$0\angle -19$
2	$-2.44 \pm j4.88$			$-2.46 \pm j12.90$			$-4.54 \pm j13.58$		
	$.737\angle 152$	$1.36\angle 168$	$1.36\angle 168$	$.910\angle 38$	$.938\angle 152$	$.938\angle 152$	$0\angle -64$	$0\angle 168$	$0\angle -12$
3	$-3.30 \pm j4.73$			$-1.45 \pm j14.56$			$-3.16 \pm j13.60$		
	$1.11\angle 165$	$0.992\angle 172$	$2.54\angle 175$	$0.388\angle -31$	$0.975\angle 123$	$0.474\angle 27$	$0.687\angle 64$	$0.624\angle -61$	$1.62\angle 168$
4	$-0.58 \pm j4.71$			$-2.94 \pm j13.00$			$-7.59 \pm j12.65$		
	$0.193\angle 130$	$0.777\angle 155$	$0.249\angle 160$	$0.932\angle 28$	$0.435\angle 111$	$1.42\angle 155$	$1.11\angle -5$	$2.68\angle 127$	$2.45\angle -71$
5	$-2.45 \pm j5.09$			$-1.96 \pm j12.46$			$-4.54 \pm j13.58$		
	$0.684\angle 162$	$1.34\angle 168$	$1.34\angle 168$	$1.07\angle 49$	$0.848\angle 161$	$0.848\angle 161$	$0\angle -51$	$0\angle 3$	$0\angle -177$
6	$-2.47 \pm j4.66$			$-2.91 \pm j13.29$			$-4.54 \pm j13.58$		
	$0.816\angle -143$	$1.42\angle 169$	$1.42\angle 169$	$0.769\angle 39$	$0.986\angle 147$	$0.986\angle 147$	$0\angle 150$	$0\angle 66$	$0\angle -114$
7	$-2.89 \pm j5.08$			$-0.87 \pm j11.28$			$-3.36 \pm j13.19$		
	$1.12\angle 155$	$1.53\angle 178$	$2.21\angle 164$	$0.213\angle 92$	$0.557\angle -166$	$0.085\angle 131$	$0.548\angle 18$	$0.419\angle -8$	$1.33\angle 149$
8	$-2.12 \pm j4.57$			$-2.83 \pm j13.20$			$-6.49 \pm j16.78$		
	$0.462\angle 161$	$1.06\angle 169$	$0.827\angle -177$	$0.917\angle 35$	$0.381\angle 167$	$1.42\angle 150$	$0.300\angle -116$	$1.18\angle 55$	$0.535\angle -126$
9	$-1.92 \pm j4.44$			$-4.07 \pm j14.52$			$-6.79 \pm j18.21$		
	$0.362\angle 159$	$0.777\angle 173$	$0.777\angle 173$	$1.62\angle -9$	$1.46\angle 132$	$1.46\angle 132$	$0\angle -155$	$0\angle 57$	$0\angle 123$

NOTE (1) The value of S_{iA} indicates the amplitude and phase of oscillations in the speed of generator i, due to mode A, excited by an error in the initial value of field voltage for generator #1.

(2) For system data see Figure 8.2.

TABLE 8.1 EIGENVALUES AND EIGENVECTOR COMPONENTS FOR SECTION 8.3 (Example 1: Lagging p.f.)

loading conditions with the above gains set in the controllers. The damping is inferior to that of the design model. Analysis of the eigenvector components corresponding to the generator speeds, as described in section 6.2, reveals that none of the modes can be attributed to a single generator:

(i) Mode A corresponds to a complex pair of poles at $s = -1.08 \pm j5.54$. The eigenvector components show that the oscillations in speed for units #1, #2 and #3 due to this mode are of similar amplitude and phase, therefore the generators swing together against the remote system. This group mode of oscillation is evident in Figure 8.3(a) which shows the response of the system following a step change in voltage set-point at unit #1.

(ii) Mode B corresponds to higher frequency oscillations associated with the poles at $s = -1.58 \pm 9.97$. Comparison of the phase angles of the eigenvector components indicates that unit #1 swings antiphase to units #2 and #3. The magnitudes show that for this mode, the amplitude of the oscillations in speed for unit #1 are almost double the amplitudes for units #2 and #3. The effect of this mode may be discerned in Figure 8.3(a).

(iii) Mode C is a well-damped higher frequency mode of oscillation associated with the poles at $s = -4.33 \pm j12.50$. The magnitudes of the eigenvector components show that this mode is not excited by an initial error in field voltage for unit #1. Further analysis, not shown, reveals that when the mode is excited, for example by a similar disturbance at unit

DATA FOR FIGURE 8.3

Disturbances applied

(a),(b),(e),(f): Step change in voltage set-point of unit #1.

(c): Perturbation to shaft speed for unit #1.

(d): Perturbation to shaft speed for unit #2.

System data

Example 1: Lagging p.f. (see Figure 8.2).

Feedback gains

(a): PP/4/FG/B for #1, #2 and #3

($f_v = 100$, $f_s = 478$, $f_p = -49.1$, $f_F = -0.65$)

(b),(c),(d): PP/4/AG/f_v/B

unit #1 — $f_v = 100$, $f_s = 6100$, $f_p = -213$, $f_F = -0.67$

units #2, #3 — $f_v = 100$, $f_s = 1060$, $f_p = -60.8$, $f_F = -0.70$

(e): as for (b) but $f_s = 4400$ instead of 1060 for unit #2.

(f): as for (b) but $f_s = -2000$ instead of 1060 for unit #2.

NOTE: Graphs show speed deviations in rad/s and are *not* drawn to the same scale.

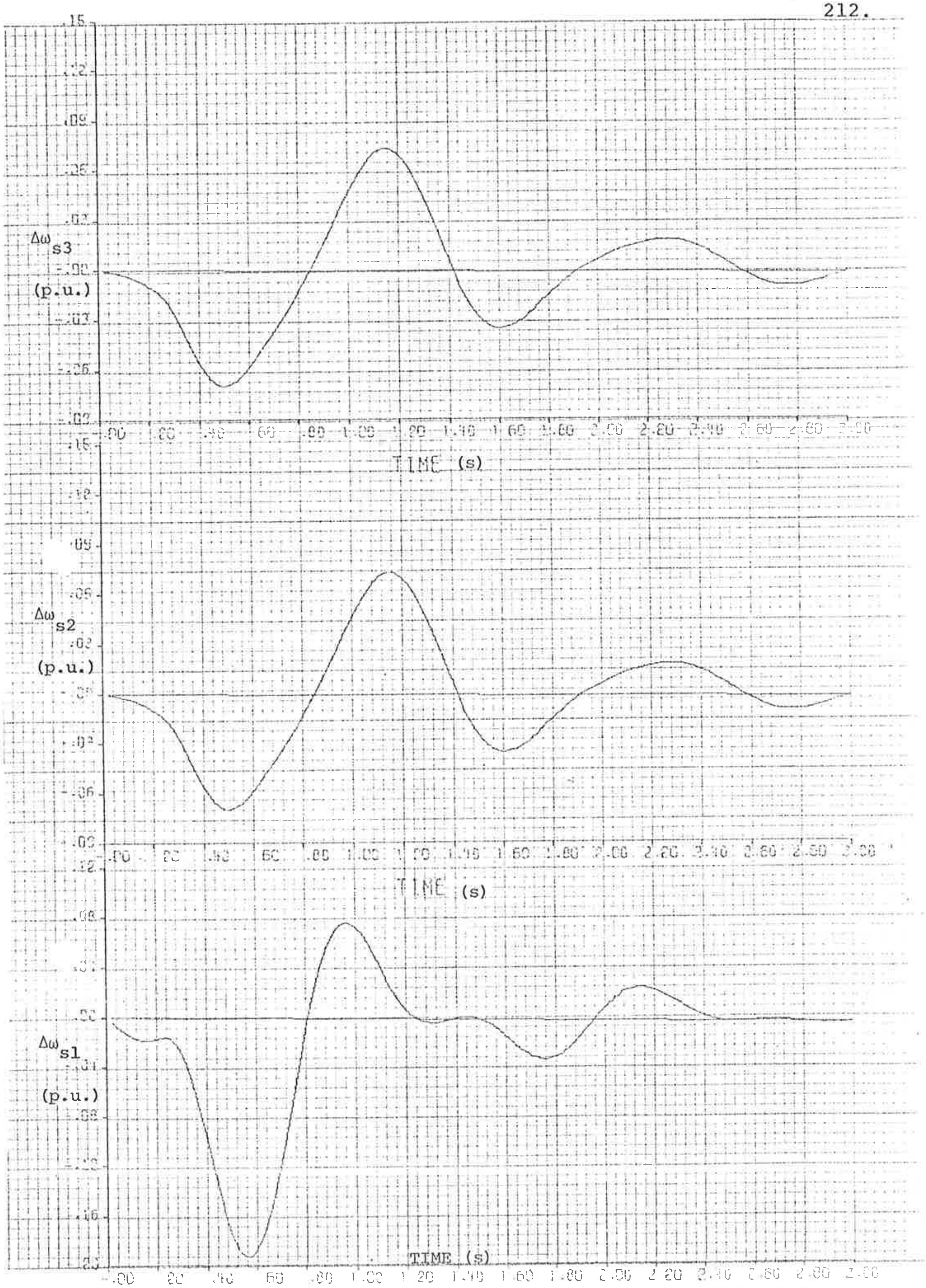

FIGURE 8.3(a) RESPONSE OF SYSTEM AT LAGGING p.f. TO A STEP IN V_{ref1}
(PP/4/FG/B gains)

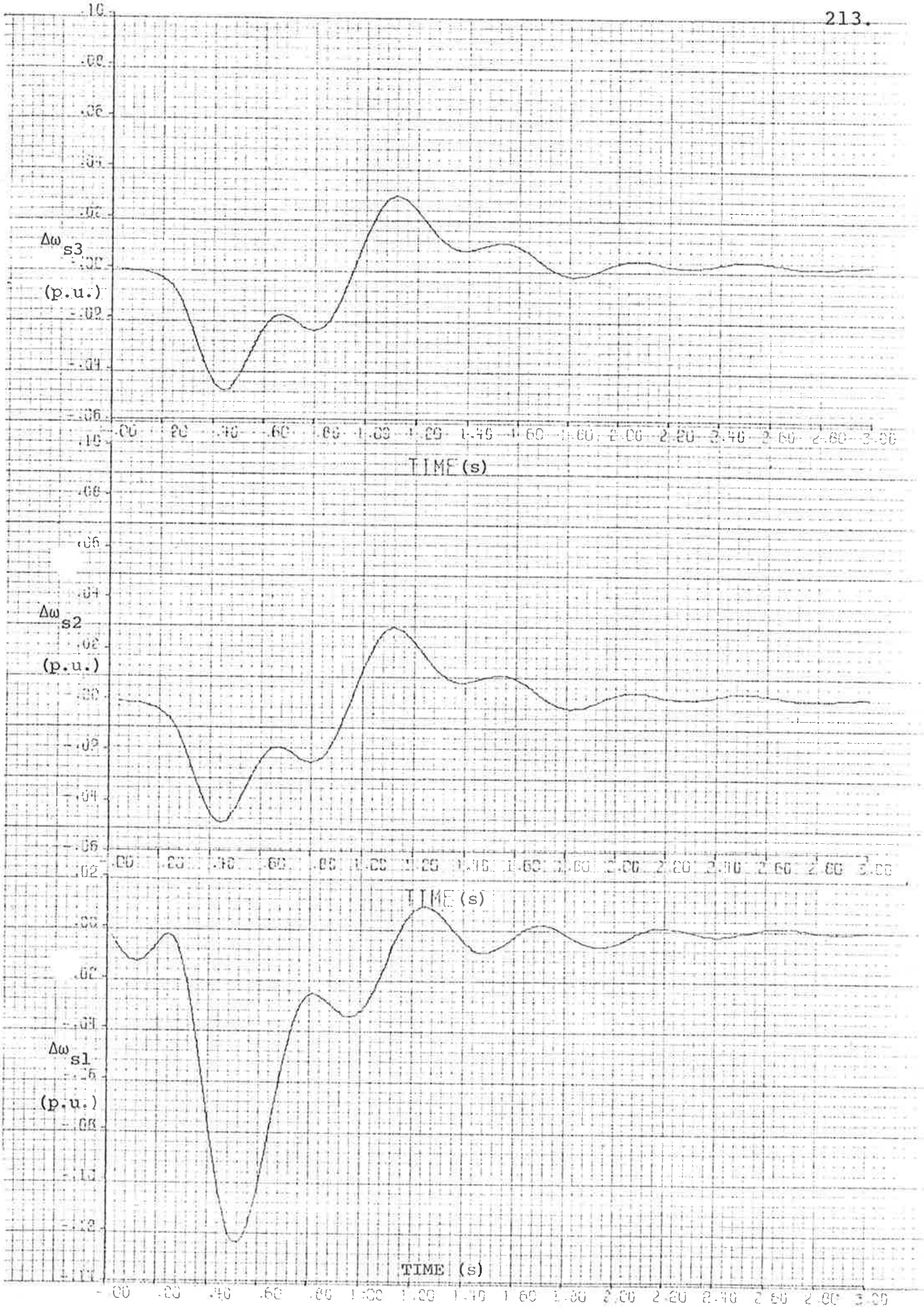

FIGURE 8.3(b) RESPONSE OF SYSTEM AT LAGGING p.f. TO A STEP IN V_{refl}

($PP/4/AG/Ff_V/B$ gains)

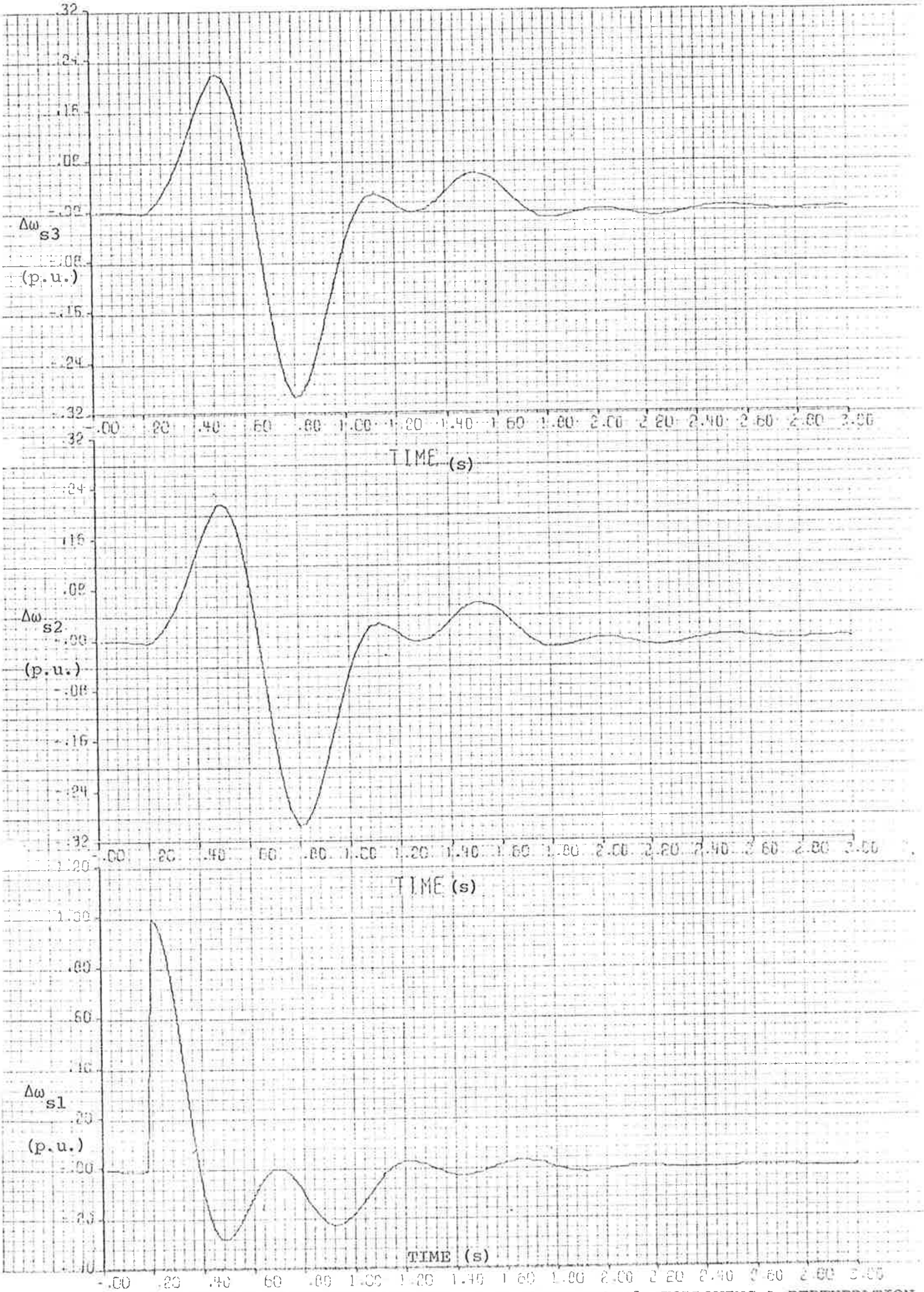

FIGURE 8.3(c) RESPONSE OF SYSTEM AT LAGGING p.f. FOLLOWING A PERTURBATION TO ω_{s1} (PP/4/AG/Ff$_V$/B gains)

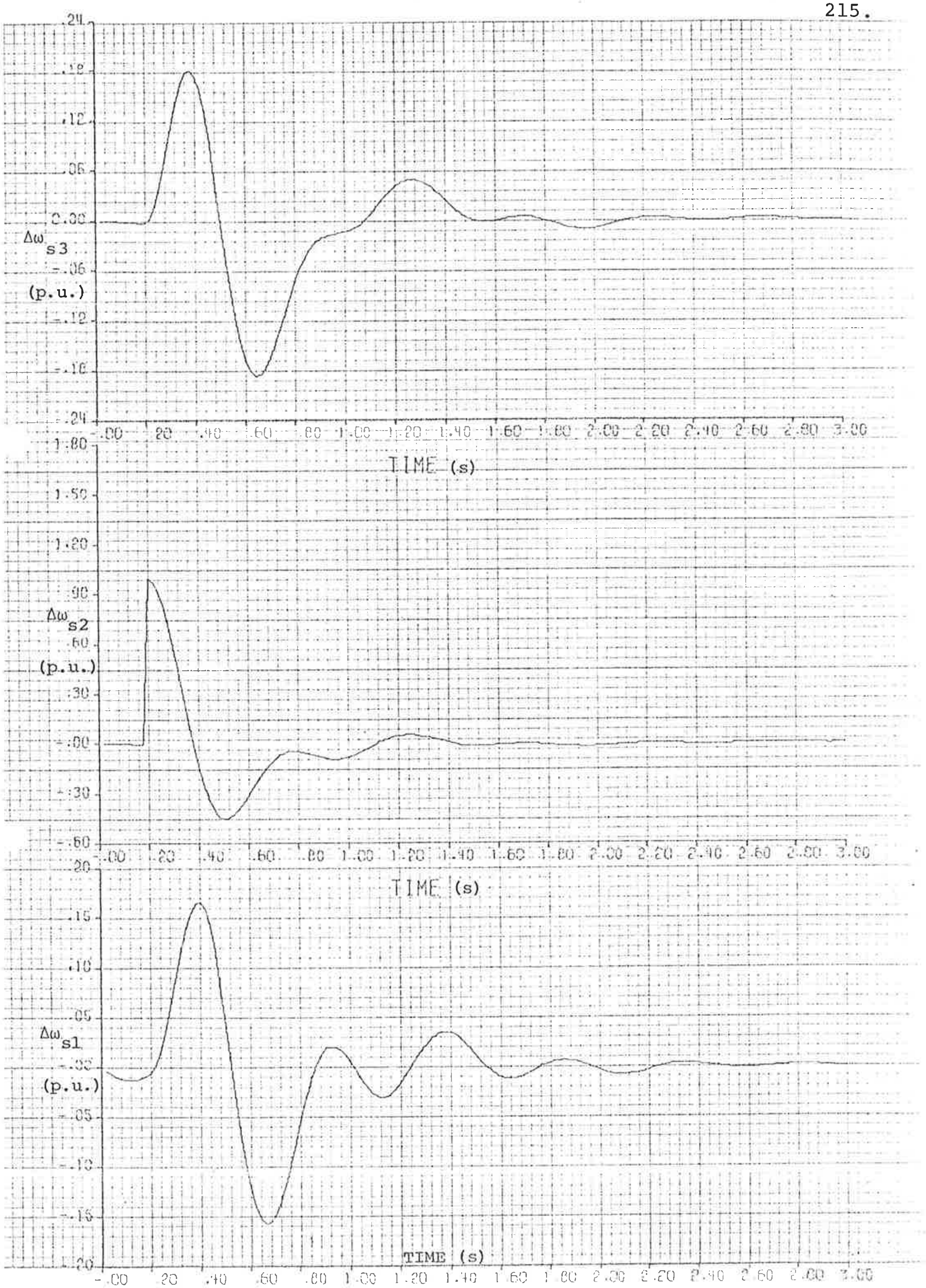

FIGURE 8.3(d) RESPONSE OF SYSTEM AT LAGGING p.f. FOLLOWING A PERTURBATION TO ω_{s2}

(PP/4/AG/Ff$_v$/B gains)

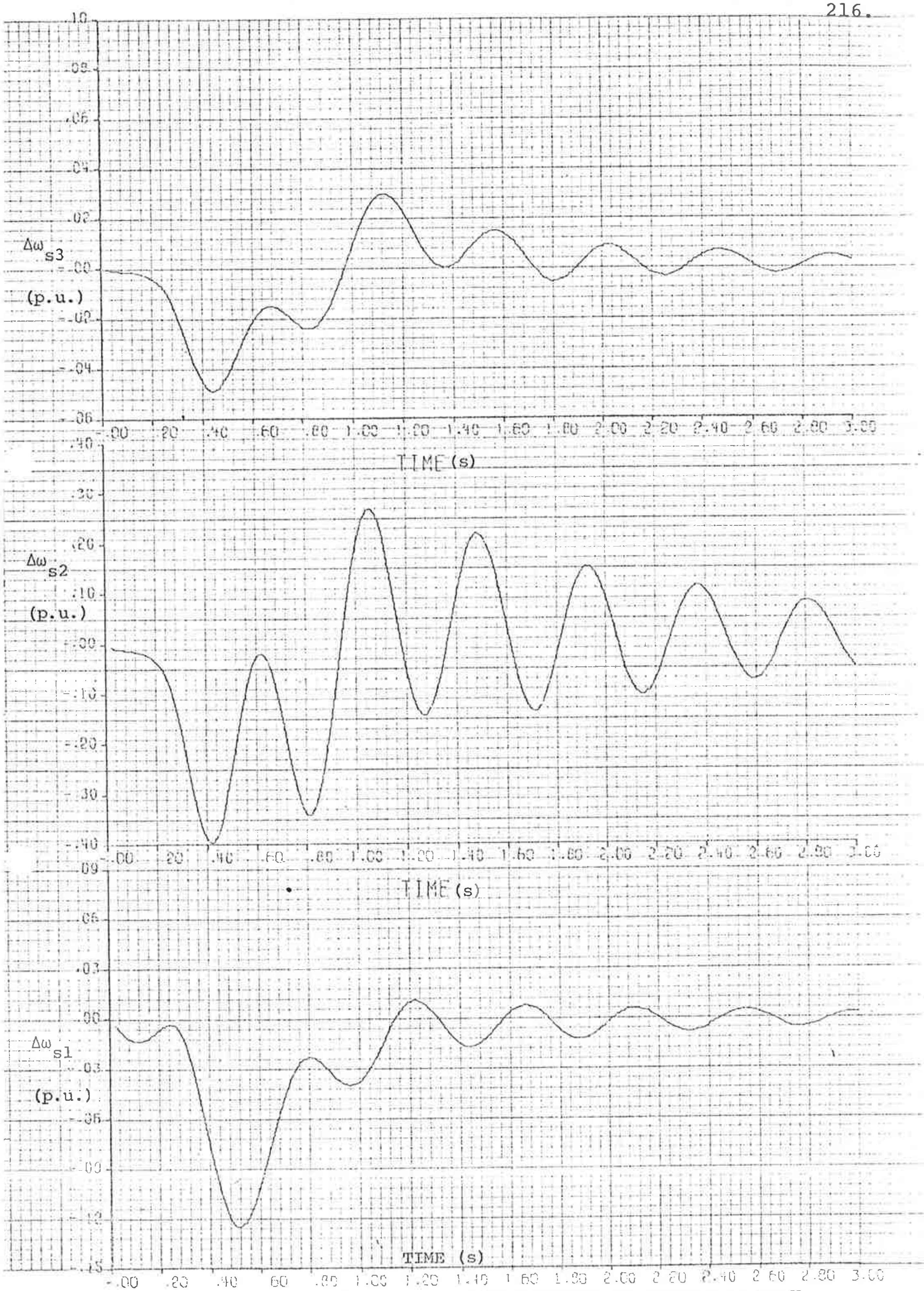

FIGURE 8.3(e) RESPONSE OF SYSTEM AT LAGGING p.f. TO A STEP IN V_{refl}

($PP/4/AG/Ff_v/B$ gains with f_s increased for unit #2)

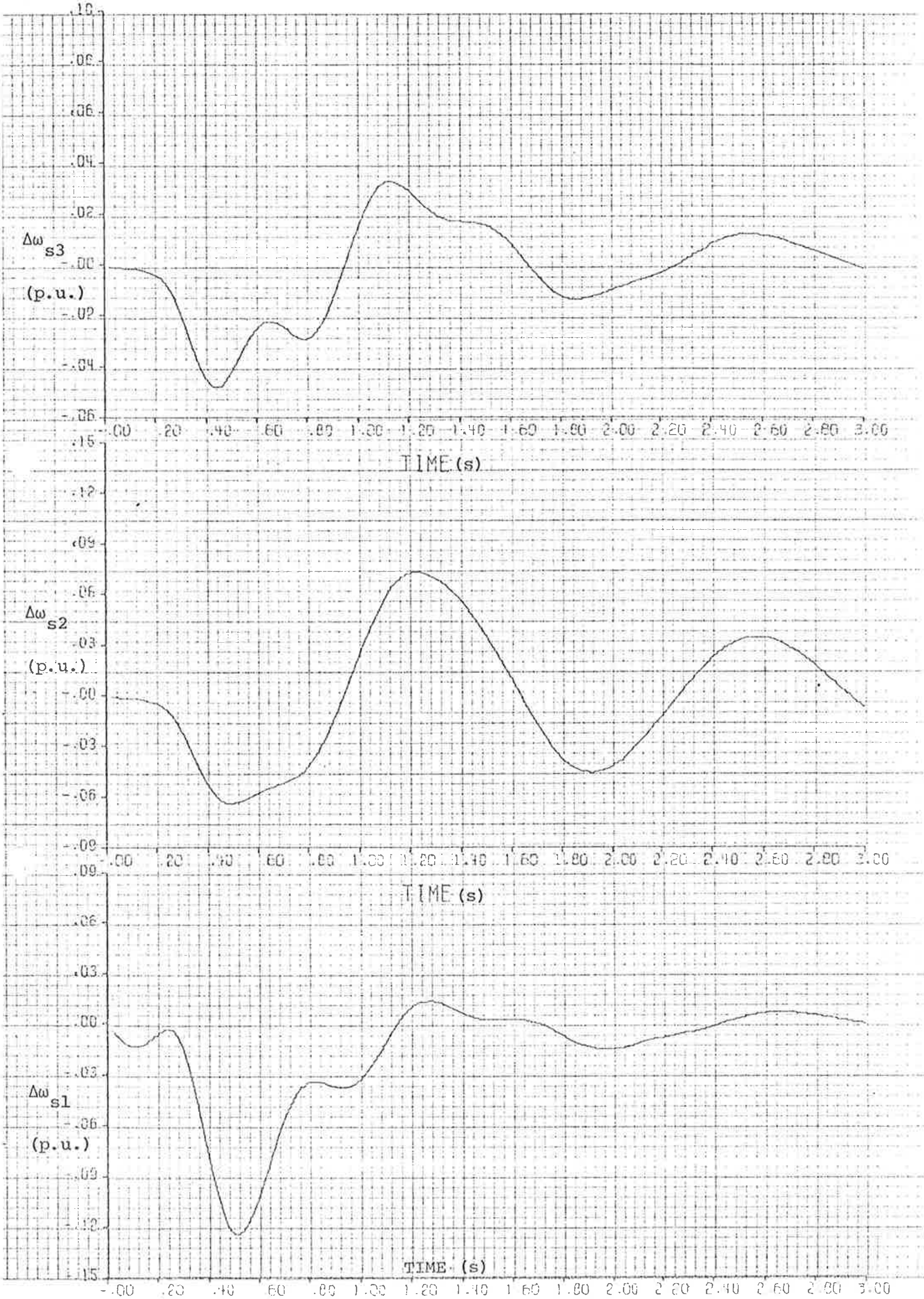

FIGURE 8.3(f) RESPONSE OF SYSTEM AT LAGGING p.f. TO A STEP IN V_{refl}

($PP/4/AG/Ff_V/B$ gains with f_s reduced for unit #2)

#2, unit #1 remains largely unaffected while unit #2 swings against unit #3.

(b) Adjustable-gains

Consider the case when an adjustable-gain regulator using the PP/4/AG/Ff_v/B control strategy is applied to each generator, with f_v being specified to remain at 100. Suppose a value of 0.3 p.u. for x_e is used for the calculation of feedback gains, as for the fixed-gain case. When the voltage, real and reactive load at the generator terminals (shown in Figure 8.2), are used in the evaluation of the feedback gain expressions of section 4.2, the resulting values of gain are:

unit #1	$f_v = 100$,	$f_s = 1056$,	$f_p = -60.8$,	$f_F = -0.70$
unit #2	$f_v = 100$,	$f_s = 6100$,	$f_p = -213$,	$f_F = -0.67$
unit #3	$f_v = 100$,	$f_s = 6100$,	$f_p = -213$,	$f_F = -0.67$

These gains are treated as the nominal values of gain for this example. Comparison of the resulting eigenvalues in row 2 of Table 8.1 with the fixed-gain eigenvalues in row 1, indicates that the adjustable-gain strategy results in a significant improvement in damping. This improvement is also seen from a comparison of the time response in Figure 8.3(b) with that in Figure 8.3(b).

8.2.2 Eigenvector analysis

The eigenvector analysis of the system with the adjustable-gain controllers is examined at length, in order to demonstrate the difficulties involved in fully assessing the behaviour of a high-order system by applying eigenvector analysis. Table 8.2 lists all the modes in the system response together with their amplitudes and phases for two different disturbances. The responses following these disturbances are plotted in Figures 8.3(c) and (d). The early part of the response is determined not only by the oscillatory modes shown in row 2 of Table 8.1 and rows 1, 2 and 3 of Table 8.2 but also by quickly decaying modes of high amplitude. When the disturbance is applied at unit #1 such modes are evident in rows 5, 13, 16 and 18 of Table 8.2, and when the disturbance is at unit #2 the amplitudes of the modes in rows 5, 14 and 15 are significant. It is difficult to visualise the early part of the response because there are many modes with different amplitudes and phases.

However, later in the response, after the decay of the heavily damped modes, eigenvector analysis provides insight into the behaviour of the system, especially if there are only one or two poorly damped modes. Therefore, for most cases considered in this chapter, only the eigenvalues and eigenvectors for the dominant modes of rotor oscillations are listed. For example, although the eigenvectors are weighted for different disturbances, the data in row 2 of Table 8.1 is used to describe the same operating condition as the whole of Table 8.2. A procedure similar to that adopted in part (a) of section 8.2.1 is recommended for the interpretation of the eigen-analysis. The steps in this procedure are:

		eigenvector components weighted for non-zero speed at time-zero for unit # 1			eigenvector components weighted for non-zero speed at time-zero for unit # 2		
mode	eigenvalue	ω_{s1}	ω_{s2}	ω_{s3}	ω_{s1}	ω_{s2}	ω_{s3}
1	$-2.44 \pm j\,4.88$	$5.22\angle{-17}$	$9.62\angle{-1}$	$9.62\angle{-1}$	$2.58\angle{16}$	$4.76\angle{32}$	$4.76\angle{32}$
2	$-2.46 \pm j12.90$	$4.92\angle{-28}$	$5.08\angle{86}$	$5.08\angle{86}$	$2.08\angle{177}$	$2.14\angle{-69}$	$2.14\angle{-69}$
3	$-4.54 \pm j13.58$	$0.00\angle{168}$	$0.00\angle{40}$	$0.00\angle{-140}$	$0.00\angle{83}$	$5.04\angle{-44}$	$5.04\angle{136}$
4	$-0.63 \pm j\,0.16$	$0.00\angle{120}$	$0.00\angle{49}$	$0.00\angle{-131}$	$0.00\angle{-45}$	$0.38\angle{-116}$	$0.38\angle{64}$
5	$-12.14 \pm j11.00$	$5.16\angle{-109}$	$6.28\angle{143}$	$6.28\angle{143}$	$0.12\angle{2}$	$0.14\angle{-105}$	$0.14\angle{-105}$
6	-0.115	0.02	0.02	0.02	0.00	0.00	0.00
7	-0.604	0.00	-0.01	-0.01	0.04	0.18	0.18
8	-0.883	0.03	0.21	0.21	-0.04	-0.32	-0.32
9	-1.00	0.00	0.00	0.00	0.00	0.00	0.00
10	-1.08	-0.26	-0.13	-0.13	-0.04	-0.02	-0.02
11	-1.52	-0.14	-0.15	-0.15	-0.03	-0.03	-0.03
12	-1.81	0.00	0.00	0.00	0.00	-0.01	0.01
13	-3.91	-5.25	2.09	2.09	0.10	-0.04	-0.04
14	-6.18	0.00	0.00	0.00	0.00	-7.98	7.98
15	-8.66	0.00	0.00	0.00	0.00	9.55	-9.55
16	-11.1	5.60	-6.60	-6.60	-0.40	0.47	0.47
17	-17.8	0.00	0.00	0.00	0.00	0.06	-0.06
18	-20.2	2.34	-0.22	-0.22	-0.17	0.02	0.02
19	-42.4	-0.01	0.03	0.03	0.01	-0.03	-0.03
20	-42.7	0.00	0.00	0.00	0.00	-0.06	0.06

Feedback gains:

unit #1 $\quad f_v = 100,\ f_s = 6100,\ f_p = -213,\ f_F = -0.67$

units #2 and #3 $\quad f_v = 100,\ f_s = 1060,\ f_p = -60.8,\ f_F = -0.70$

System data: See Figure 8.2.

Interpretation:

Suppose the system at time-zero has all its states at their equilibrium values except that the speed of unit #1 is perturbed by 10 p.u.; the subsequent time response for speed of unit #1 may be read from the first column as:

$$5.22e^{-2.44t}\cos(4.88t - 17^\circ) + 4.92e^{-2.46t}\cos(12.9t - 28^\circ) + 5.16e^{-12.14t}$$
$$\cos(11t - 109^\circ) + 0.02e^{-0.115t} + 0.03e^{-0.883t} + \ldots$$

TABLE 8.2 EIGENVECTOR ANALYSIS FOR THE THREE MACHINE SYSTEM AT LAGGING P.F. WITH NOMINALLY ADJUSTED GAINS

(i) By inspection of the eigenvalues, find the mode with the lightest damping - the effects of this mode on the response are the most protracted provided it has a significant amplitude relative to other modes.

(ii) The inspection of the eigenvector components for this mode indicates the relative effect this mode has on various generators; the relative amplitudes of oscillation and which generators swing in phase may be determined.

(iii) Repeat steps (i) and (ii) for the modes in order of increasing damping; comparison of the real parts of the eigenvalues and of the damping ratios for the modes indicates the relative effect each should have on the response.

(iv) Provided the eigenvectors have been weighted according to the extent to which they are excited by a test disturbance, comparison of the components of different eigenvectors corresponding to any given state reveals the resulting effect of the various modes on that state. The relative importance of the modes depends on the disturbance applied.

As an example, consider row 2 of Table 8.1. The eigenvalues for modes A and B have similar real parts smaller than that for mode C. The damping ratio for mode B is smaller than that for mode A, therefore it should be more evident in the response. The eigenvector components for mode B indicate that it affects the generators to a similar extent and that unit #1 swings approximately 120° out of phase with units #2 and #3. The effect of this mode is evident in the responses in Figures 8.3 (b), (c) and (d). The eigenvector components for mode A indicate that the generators swing in phase for this mode and that its amplitude is greater for units #2 and #3. The presence of this mode can be detected in Figures 8.3 (b), (c) and (d). The eigenvalue for mode C has a large real part, therefore its amplitude decays rapidly. However, the damping ratio is moderate because the frequency of oscillation is high so that its effect might be evident early in the response. The eigenvector components reveal that this mode is not excited by the disturbance at unit #1.

8.2.3 Inverse Nyquist array analysis of shaft-speed feedback gain settings

In this section the settings of the shaft-speed feedback gains are examined in order to determine whether any improvement in dynamic performance might result by changing their values from those calculated above using the PP/4/AG/Ff$_v$/B strategy.

(i) Calculation of a three-loop INA

Figure 8.4 shows the inverse Nyquist array which is derived when the system operates at the lagging p.f. loading condition specified in Figure 8.2 and the deviations in shaft-speed of generators #1, #2 and #3 are chosen as output variables. The nominal feedback gains used are those calculated using the PP/4/AG/Ff$_v$/B SMIB pole-placement strategy. As discussed in section 7.4, each origin of the INA corresponds to the nominal value of speed gain for a

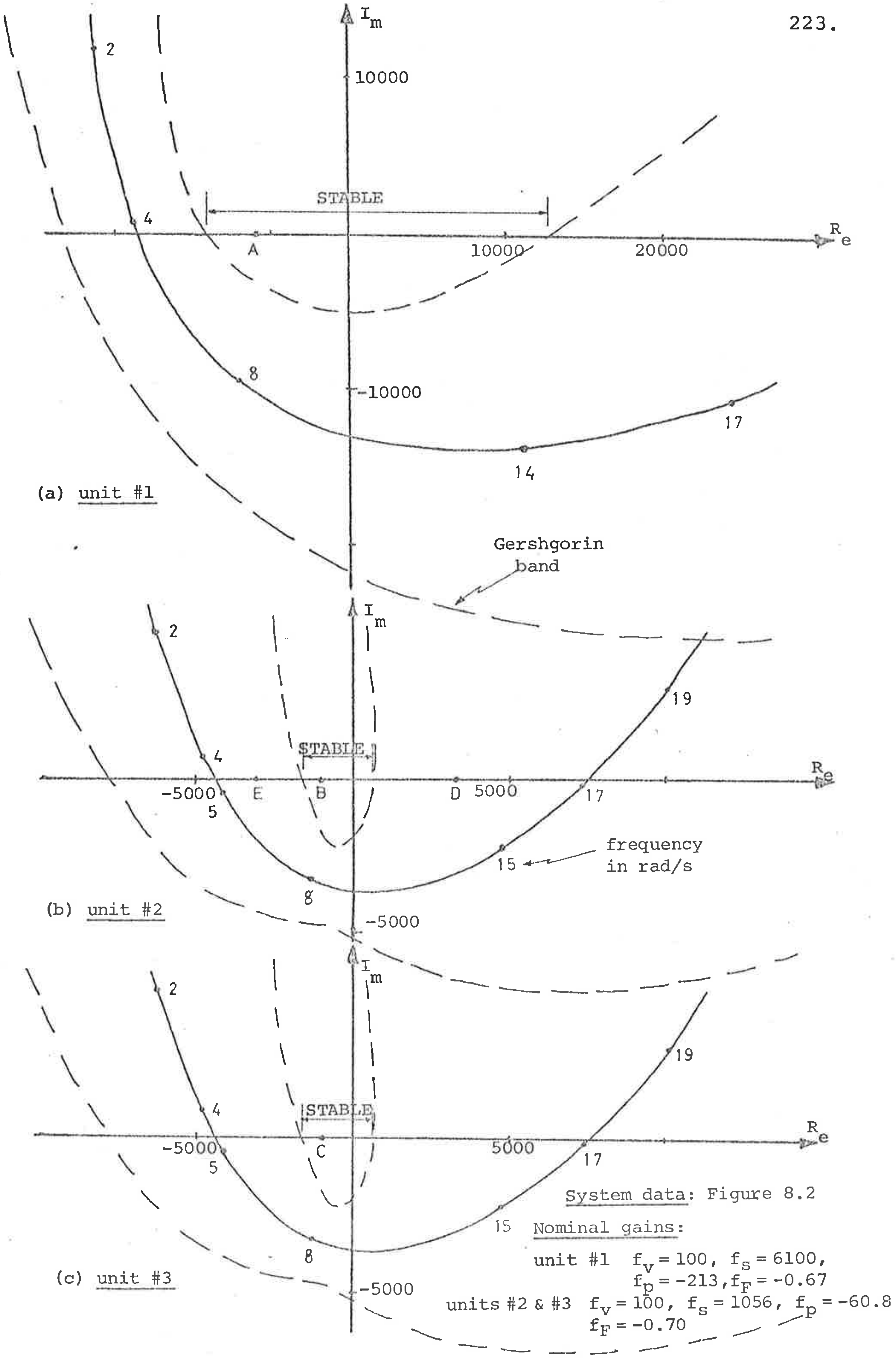

FIGURE 8.4 INA FOR THREE SPEED FEEDBACK LOOPS IN THE POWER SYSTEM AT LAGGING P.F.

particular unit. If this gain is changed the critical point moves from the origin to a point on the real axis corresponding to the change in gain. Because the origin for every loop of the INA lies outside the Gershgorin band, the system is diagonal dominant for the nominal gain settings and hence INA theory may be applied to analyse the effects of gain changes on stability.

(ii) Integrity

The points A, B and C in Figure 8.4 correspond to zero speed-gains for generators #1, #2 and #3 respectively. These points and the origins of the INA lie outside the Gershgorin bands and in addition, the number of Nyquist-type encirclements by the Gershgorin bands does not change when the critical points are moved from the origins to these points (A, B and C); therefore, as discussed in section 7.2.2, it is concluded that the system will remain stable if speed feedback is removed from any one or all of the generators. This means that the system has high integrity with respect to the possible failure of speed transducers. Provided the speed feedback gains for the generators are set such that all critical points in Figure 8.4 lie outside the Gershgorin bands and in the region marked "STABLE", this integrity will be maintained.

(iii) Calculation of a two-loop INA

In the three-loop INA shown in Figure 8.4 the Gershgorin bands for generators #2 and #3 are very wide. In addition, the distance from the range of stable critical points to the locus is approximately the same as the radius of the Gershgorin band, which means that the Ostrowski bands will not be much narrower than the Gershgorin bands. Wide Ostrowski bands imply that it is not possible to make accurate predictions about the position of the locus h_{ii}^{-1} (see section 7.2.3).

If the speed-gain for generator #1 is held at a fixed value, then, as discussed in point (iii) of section 7.3.1, it is possible to treat the speed loop for this generator as part of the "plant" and to calculate an INA with only the shaft speeds of generators #2 and #3 as output variables. Figure 8.5 shows the INA which results. For comparison the loci and Gershgorin bands for the three-loop case are superimposed on those for this two-loop case. The fact that the loci are not coincident for the two- and three-loop INA demonstrates the fact that unlike the single-input single-output case, the values along the i^{th} locus are *not* the inverse of the values of the i^{th} diagonal element of the transfer function matrix; the locus of h_{ii}^{-1} may lie anywhere inside the Ostrowski band.

The Gershgorin bands in the two-loop INA allow the prediction that, provided the gain for generator #1 remains at the nominal value, the system will remain stable when the gains for units #2 and #3 are set in the enlarged region marked "STABLE" in Figure 8.5.

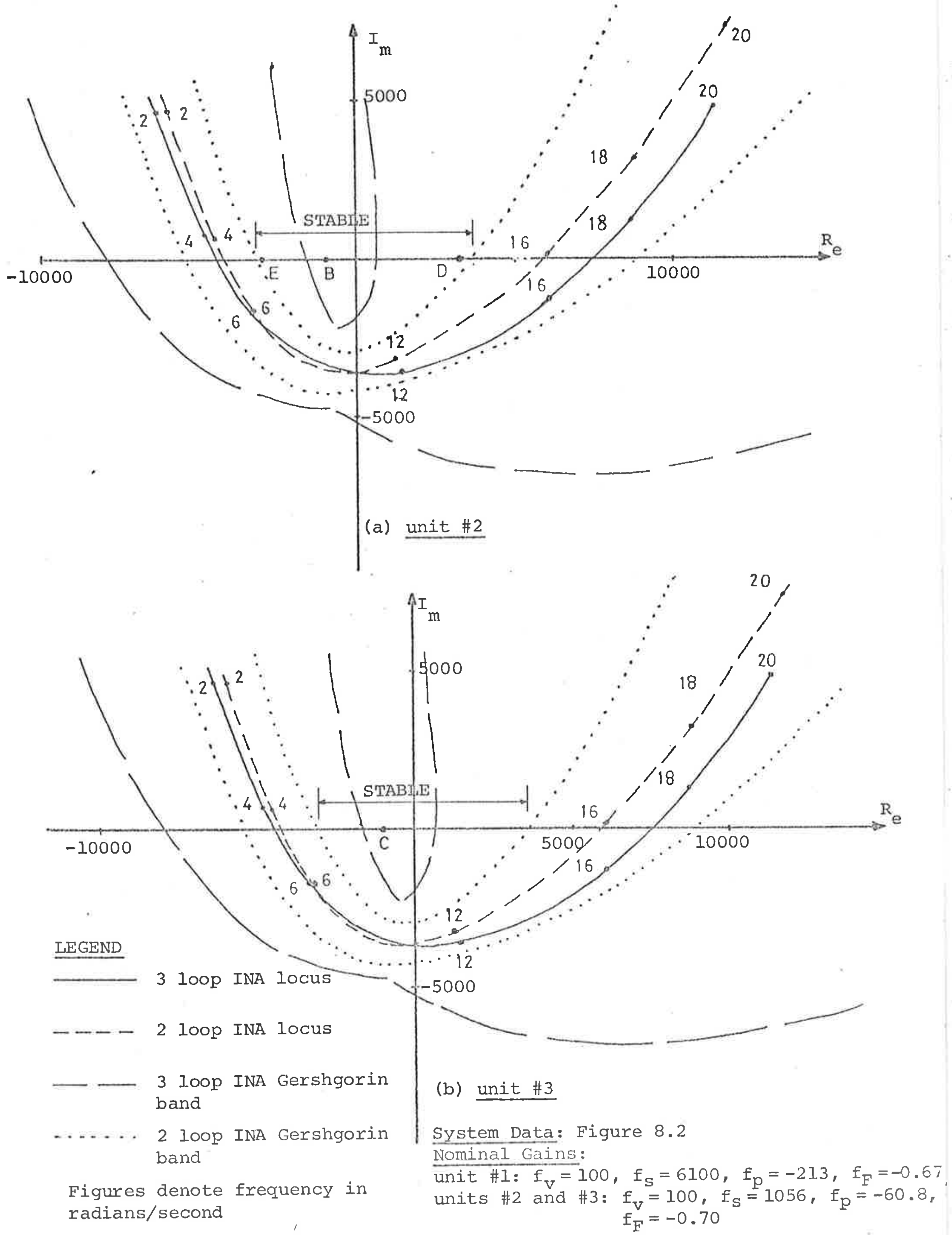

FIGURE 8.5 INA FOR TWO SPEED FEEDBACK LOOPS IN THE POWER SYSTEM AT LAGGING P.F.

(iv) Damping Performance

The damping for a single-input single-output system may be estimated from the inverse Nyquist plot by using M circles. In a similar fashion, in the inverse Nyquist array, the distance from the i^{th} critical point to the locus of h_{ii}^{-1} is related to the damping in that loop. However, the exact position of the h_{ii}^{-1} locus is not usually known but, provided the system is diagonal dominant, it lies inside an Ostrowski band centred on the $\hat{q}_{ii}$ locus. Therefore, an estimate of the effect of a gain change on damping may be made by considering the resultant change to the distance between the critical point and the $\hat{q}_{ii}$ locus plotted in the INA. This is illustrated by the following example:

Suppose the speed-gain for generator #2 is increased so that the critical point lies at point D in Figures 8.4(b) and 8.5(a). Because the distance from the critical point to the part of the locus corresponding to higher frequencies is reduced significantly, the damping at higher frequencies should deteriorate. The system remains stable because the point D lies outside the Ostrowski band in Figure 8.5(a) and the number of Nyquist-type encirclements does not change. The eigenvalues for the system under these conditions are shown in row 3 of Table 8.1 from which it is evident that the damping for modes B and C is smaller than for the nominal case shown in row 2. The deterioration in damping is observed in comparing Figures 8.3(b) and 8.3(e) which show the responses following a step in voltage set-point for unit #1.

Although the distance from the critical point to the higher frequency part of the locus is reduced when the speed gain is increased, the distance to the lower frequency region is increased so that damping at these frequencies should be improved. The values for mode A in rows 2 and 3 of Table 8.1 show that this does happen.

Suppose that, instead of the speed-gain for generator #2 being increased, the value is reduced so that the critical point in Figure 8.4(b) lies at E. In this case the distance to the lower frequency part of the locus is reduced and the distance to the higher frequency region increased. The system remains stable because point E lies outside the Gershgorin band in Figure 8.5 and the number of encirclements does not change from the nominal case. Row 4 of Table 8.1 shows the eigenvalues for this case and Figure 8.3(f) the time response. It is seen clearly that, as expected, the low frequency damping deteriorates and the higher frequency damping improves.

The origin for each of the speed feedback loops shown in Figure 8.4 lies roughly equidistant from the lower and higher frequency parts of the loci. This shows that the nominal gains, calculated by the PP/4/AG/Ff$_v$/B strategy provide a good compromise between damping at low and at high frequencies.

(v) Reducing the interaction between generators

As discussed in point (iv) of section 7.3.1, the extent of the interaction between the loops of a system for sinusoidal inputs is related to the ratio of the width of the Gershgorin band at the input frequency to the distance from the corresponding part of the locus to the critical point. It is shown in Appendix 10.7 that changing the speed and power feedback gains for generators does not affect the width of the Gershgorin bands in the speed and power INA's. Therefore, in order to reduce interaction by adjusting these gains, it is necessary to ensure the distance from the critical point to the locus is as large as possible. It is shown above that this distance is related to damping, therefore damping and interaction are closely related.

It is evident from Figure 8.4 that, as with the damping performance, there must be a compromise between the interaction at low frequencies and that at higher frequencies. Suppose the critical point is again moved from the origin to the point D in the INA, Figure 8.4(b). Evaluation of the closed-loop transfer function matrix, $H(s)$, at various frequencies reveals that it tends towards a diagonal matrix at frequencies such as $\omega = 5$ rad/s; the ratio of the width of the Gershgorin band to the distance from the critical point is reduced at these frequencies. However, at higher frequencies, such as $\omega = 15$ rad/s the off-diagonal elements of $H(j\omega)$ become more significant than before in comparison to the diagonal elements; for these frequencies the distance from the critical point to the locus is smaller, hence the ratio of the Gershgorin band radius to this distance is larger. The eigenvector analysis in row 3 of Table 8.1 and the time responses in Figure 8.3(e) show that when a step disturbance is applied at unit #1, the amplitude of the poorly-damped, high frequency oscillation is greater at unit #2 than at the perturbed generator after the initial transients have died away.

The Gershgorin band gives some guidance as to the gain settings which reduce interaction for step inputs. Provided the critical point is placed outside the band, the radius of the Gershgorin band is less than the distance to the critical point at all frequencies. The origin corresponding to the nominal gains in this example lies in such a position in each loop. It is clear that the interaction for sinusoidal inputs at any given frequency cannot be significantly reduced in this case by adjusting the speed-gains, without increasing the interaction at other frequencies.

8.2.4 Inverse Nyquist array analysis of electrical power feedback gain settings

(i) Calculation of two- and three-loop INA

Figure 8.6 shows two inverse Nyquist arrays calculated for the 3 generator power system of Figure 8.2 at the lagging power-factor operating conditions, using nominal gain settings derived from the PP/4/AG/Ff$_v$/B control strategy. For the one case shown in Figure 8.6 the output variables are taken to be the electrical power outputs of units #1, #2 and #3. In the other case, only the electrical power outputs of units #2 and #3 are used, with the power feedback loop of unit #1 being considered as part of the "plant" and having the nominal feedback gain.

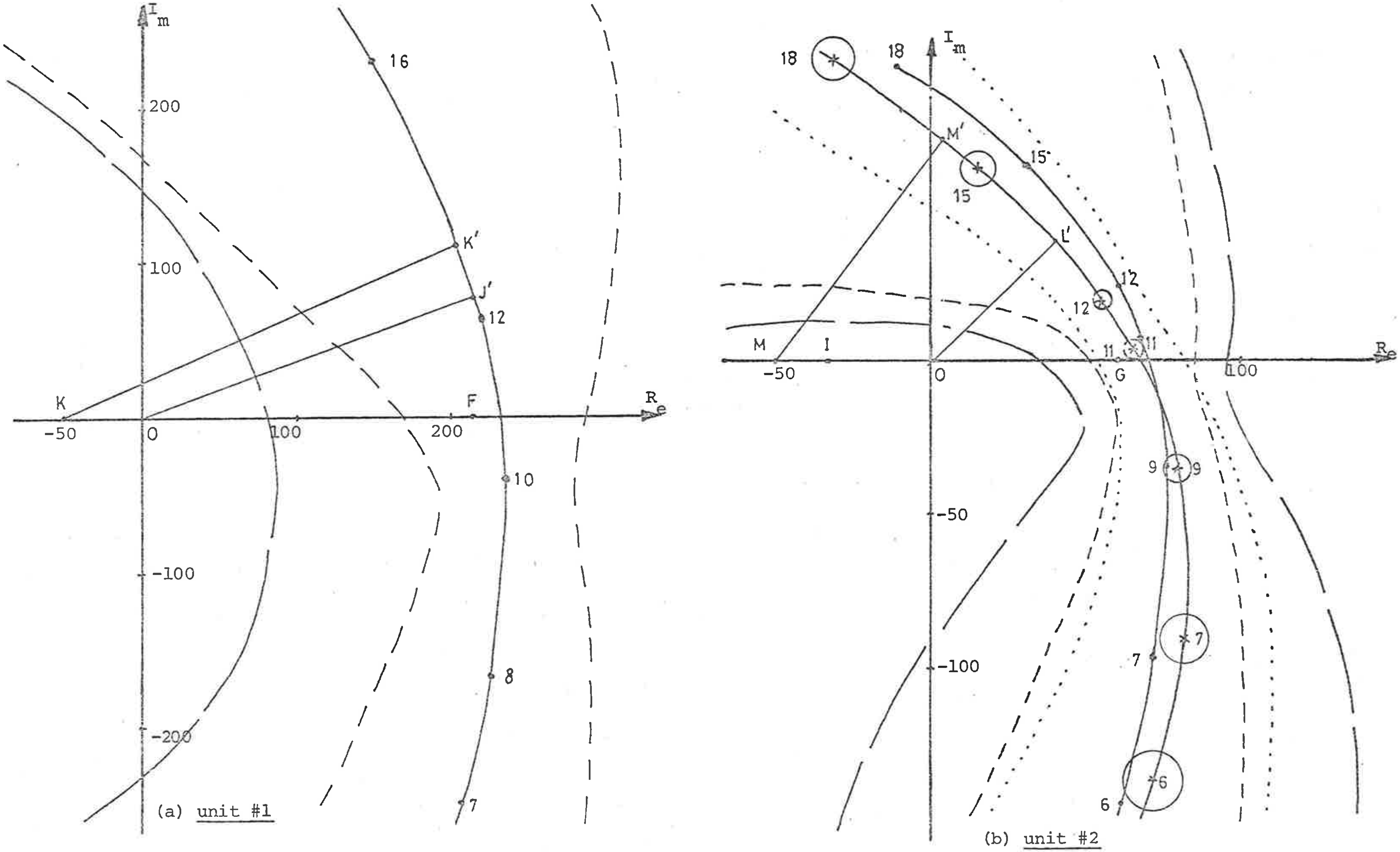

FIGURE 8.6 INVERSE NYQUIST ARRAYS FOR TWO AND THREE POWER FEEDBACK LOOPS IN THE POWER SYSTEM AT LAGGING P.F. (Figure continued on next page)

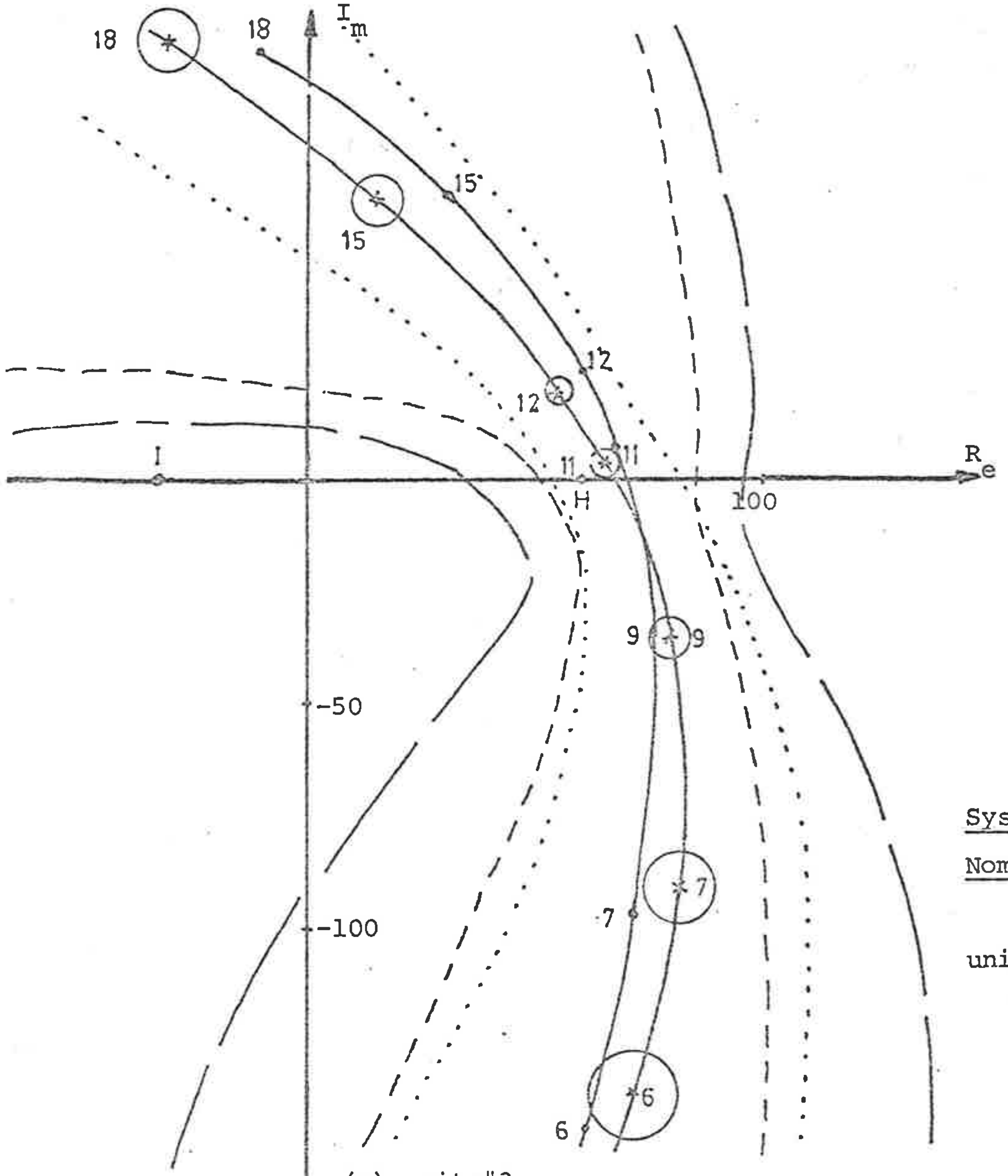

LEGEND

locus of 3 loop INA (frequency marked in rad/s)

locus of 2 loop INA (frequency marked in rad/s)

Ostrowski band for 3 loop INA with nominal gain settings

Gershgorin band for 3 loop INA

Gershgorin band for 2 loop INA

Circles indicate the width of the Ostrowski band for the 2 loop INA with nominal gain settings.

System Data: Figure 8.2

Nominal Gain:

unit #1 $f_v = 100$, $f_s = 6100$, $f_p = -213$, $f_F = -0.67$

units #2 and #3 $f_v = 100$, $f_s = 1056$, $f_p = -60.8$, $f_F = -0.70$

(c) unit #3

FIGURE 8.6 INVERSE NYQUIST ARRAYS FOR TWO AND THREE POWER FEEDBACK LOOPS IN THE POWER SYSTEM AT LAGGING P.F. (continued from previous page)

The Gershgorin bands for both the two- and the three-loop INA are quite wide so, in order to improve the accuracy of locating the h_{ii}^{-1} for the closed-loop system, the Ostrowski bands are drawn for each case. In calculating the band for a given loop it is assumed that the gains in all other loops are fixed at their nominal values (i.e. critical points at the origin).

(ii) Integrity

The points F, G and H in Figure 8.6 correspond to the critical points with zero power feedback for units #1, #2 and #3 respectively. These points lie inside the Gershgorin and Ostrowski bands for the three-loop INA so the INA cannot be used to predict whether the system will be stable in the event of a power feedback loop being open-circuited. However, the points G and H do lie outside the Ostrowski band of the two-loop INA. Thus it may be deduced that provided the power feedback loop on unit #1 is closed with the nominal feedback gain and one of the power feedback loops for generators #2 or #3 is operating with the nominal value of gain, stability will be retained when the remaining loop is open-circuit. These conclusions have been checked by eigenvalue analysis.

Eigenvalue analysis further reveals that if the nominal values of power feedback gain are used for units #2 and #3, the open-circuiting of the power feedback loop for generator #1 gives rise to instability because a complex pair of poles then lies at $s = +0.14 \pm j10.94$. Inspection of the three-loop INA shows that if the power gains for units #2 and #3 is increased from -60.8 to approximately -250, the radius of the Ostrowski band for unit #1 in Figure 8.6(a) is reduced such that it does not include the point F; hence the number of poles in the right half s-plane will not change in the event of the failure of the power feedback on unit #1. Trial and error computation of eigenvalues shows that a smaller increase in gain will suffice because the system will retain stability provided the critical points for units #2 and #3 lie to the left of the point I. Such an increase in the magnitude of the feedback gain for these units may be used to ensure that the failure of any one power feedback loop does not result in instability.

(iii) Damping performance

Figure 8.6 indicates that heavier damping than that resulting from the nominal gain settings is possible with increased amounts of negative power feedback. This is because the distances of closest approach between the loci and the critical points increase as the critical points are moved towards the left. The improvement in damping is accompanied by an increase in oscillation frequency.

For example, suppose the electrical power feedback gain for generator #1 is changed by -50, from -213 to -263, so that the critical point moved from the origin to point K in Figure 8.6(a). The lines OJ' and KK' have been drawn from the critical points to the point of closest approach. The points J' and K' correspond to 12.3 and 13.0 rad/s and the ratio KK'/OJ' is 1.22. Eigenvalue analysis in rows 2 and 6 of Table 8.1 shows that the actual damped frequencies of oscillation are 12.9 and 13.3 rad/s and that the damping ratio increases by a factor 1.14. Thus, even though the Ostrowski band is wide so that h_{ii}^{-1} may be some distance from $\hat{h}_{ii}$, the INA allows quick estimates of the change in oscillation frequency and damping ratio to be made.

As a further example, suppose that the electric power feedback gain for generator #2 is changed from -60.8 to -110.8, corresponding to a change in critical point from the origin to the point M in Figure 8.6(b). Using the two-loop INA for accuracy, the points of closest approach are L' and M' corresponding to 13.3 and 15.8 rad/s and the ratio MM'/OL' is 1.61. Eigenvalue analysis in rows 2 and 8 of Table 8.1 shows that the dominant mode for this machine shifts from 12.5 to 16.8 rad/s and the damping ratio increases by a factor of 1.89. Despite the fact that there are two modes of oscillation with similar frequencies associated with this generator, the INA allows quick insight into the effect of gain changes.

Although the nominal gains give strong damping, it is shown above that integrity is improved if the gains for units #2 and #3 is increased. The above analysis suggests that this will result in improved damping but an increase in the oscillation frequency of the generators. This is confirmed by eigenvalue analysis in row 9 of Table 8.1 and the comparison of the time responses in Figure 8.7(a) and (b).

DATA FOR FIGURE 8.7

Disturbances applied

Step change in voltage set-point for unit #1.

System data

Example 1: Lagging p.f. (see Figure 8.2).

For (d), q-axis transient time-constant omitted from all generator models.

Feedback gains

(a) and (d): PP/4/AG/Ff_v/B controllers for all units.

unit #1 $f_v = 100$, $f_s = 6100$, $f_p = -213$, $f_F = -0.67$

units #2, #3 $f_v = 100$, $f_s = 1060$, $f_p = -60.8$, $f_F = -0.70$

(b): As for (a) except f_p increased from -60.8 to -110.8 for units #2 and #3.

(c): As for (a) except f_p increased from -60.8 to -110.8 for unit #2.

NOTE: Graphs show electrical power output in p.u. and are *not* drawn to the same scale.

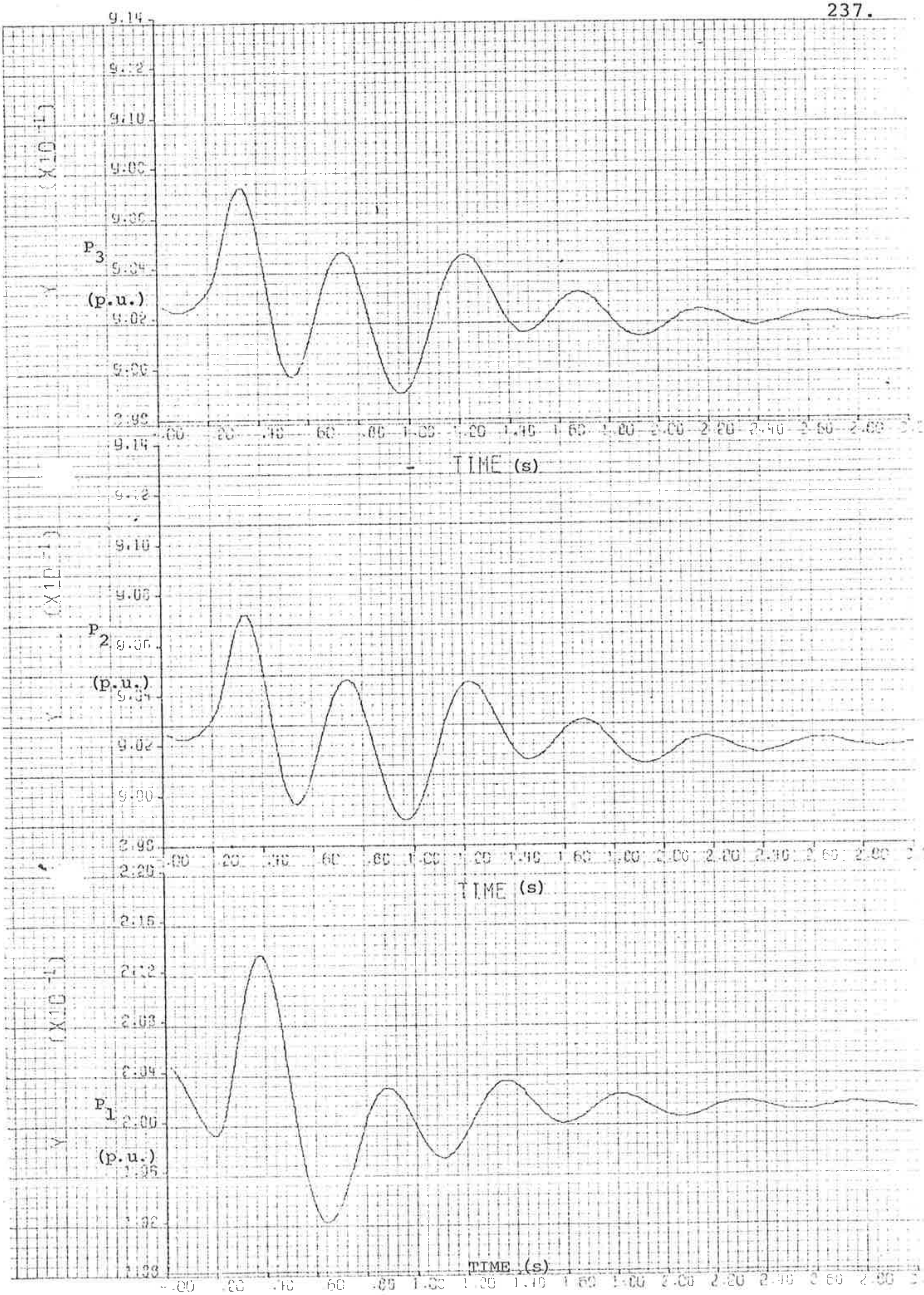

FIGURE 8.7 RESPONSE OF SYSTEM AT LAGGING p.f. TO A STEP IN V_{refl}
($PP/4/AG/Ff_V/B$ gains)

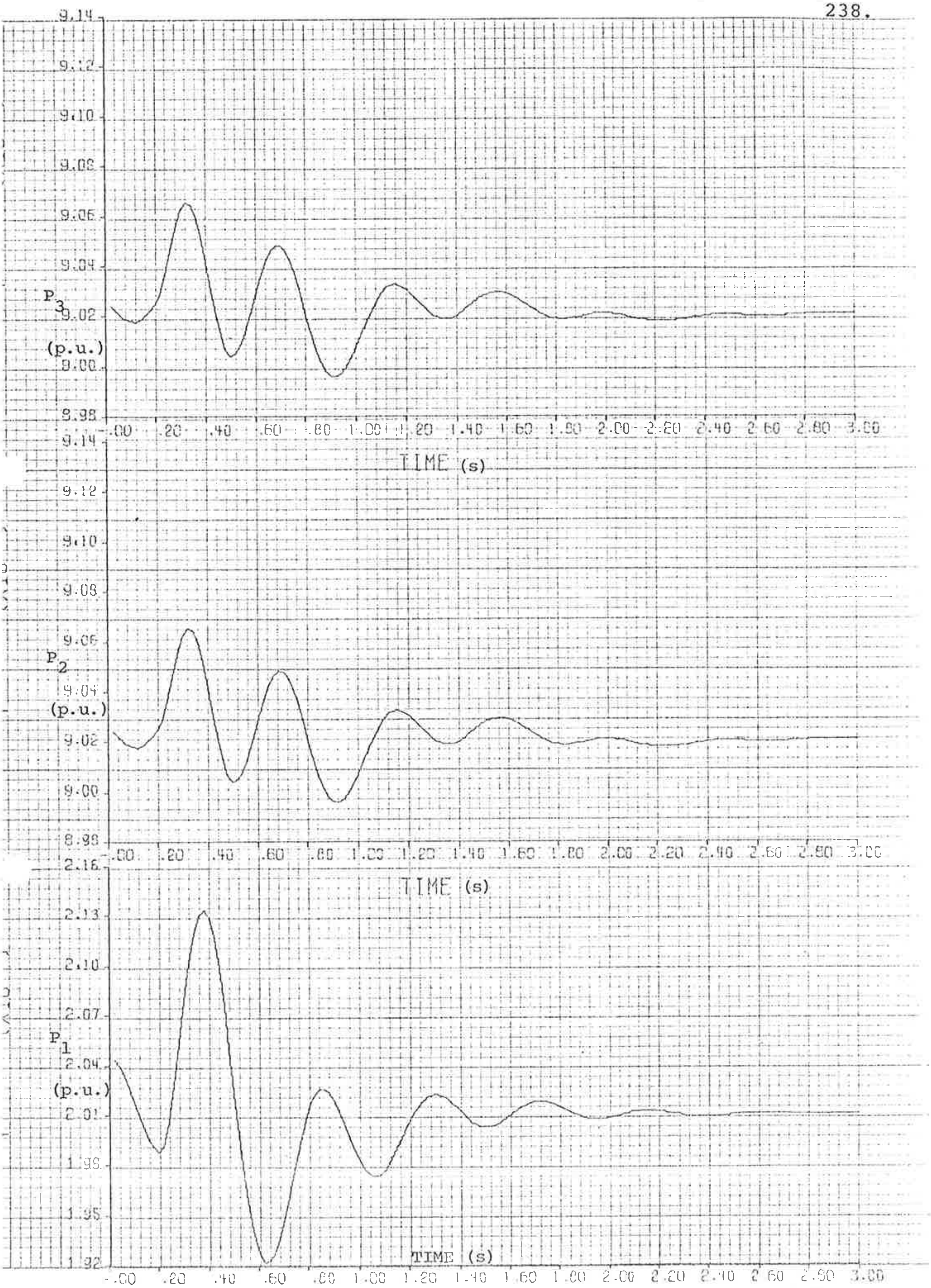

FIGURE 8.7(b) RESPONSE OF SYSTEM AT LAGGING p.f. TO A STEP IN V_{refl}
($PP/4/AG/Ff_v/B$ gains with f_p increased for units #2 and #3)

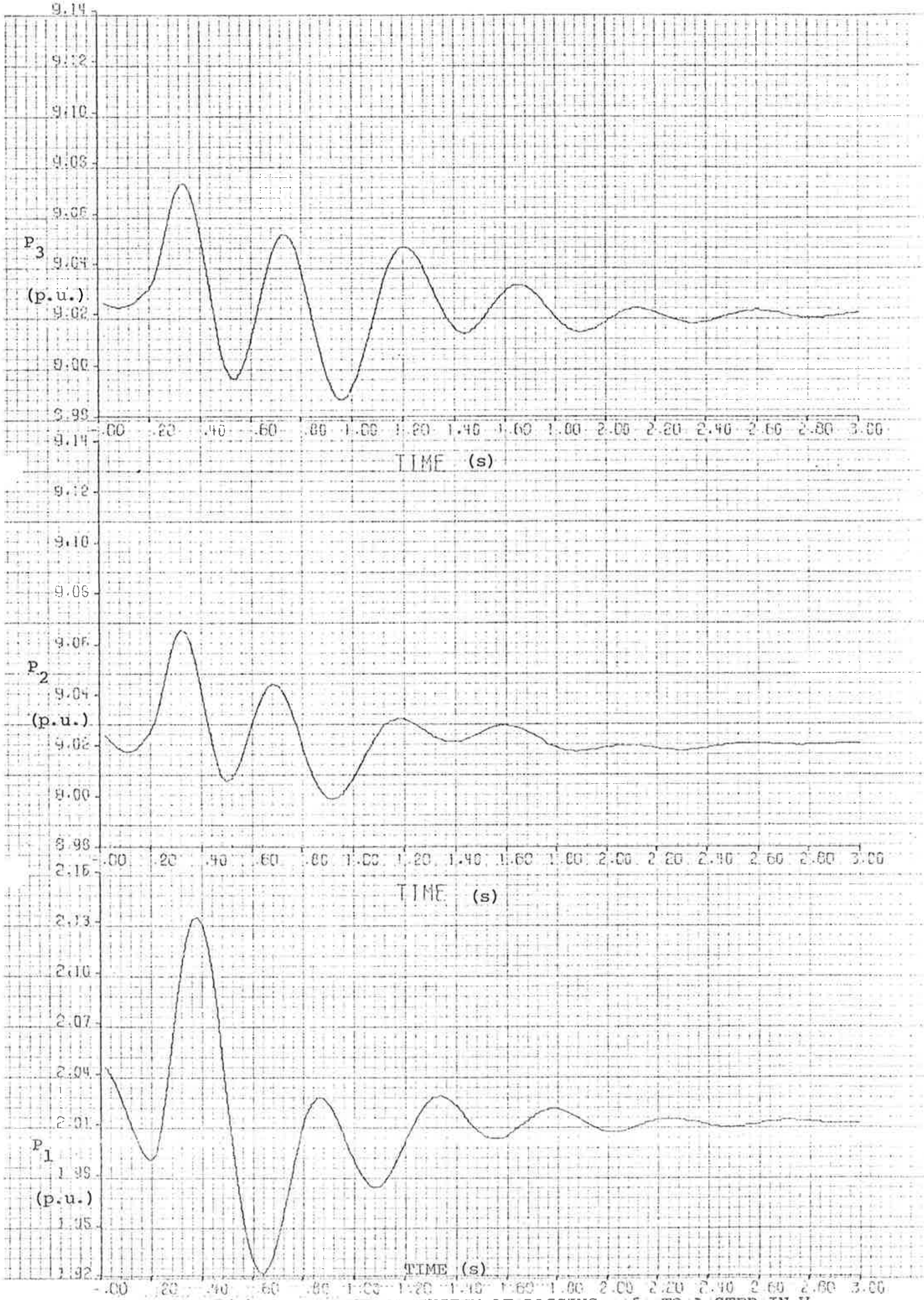

FIGURE 8.7(c) RESPONSE OF SYSTEM AT LAGGING p.f. TO A STEP IN V_{refl}
($PP/4/AG/Ff_v/B$ gains with I_p increased for unit #2)

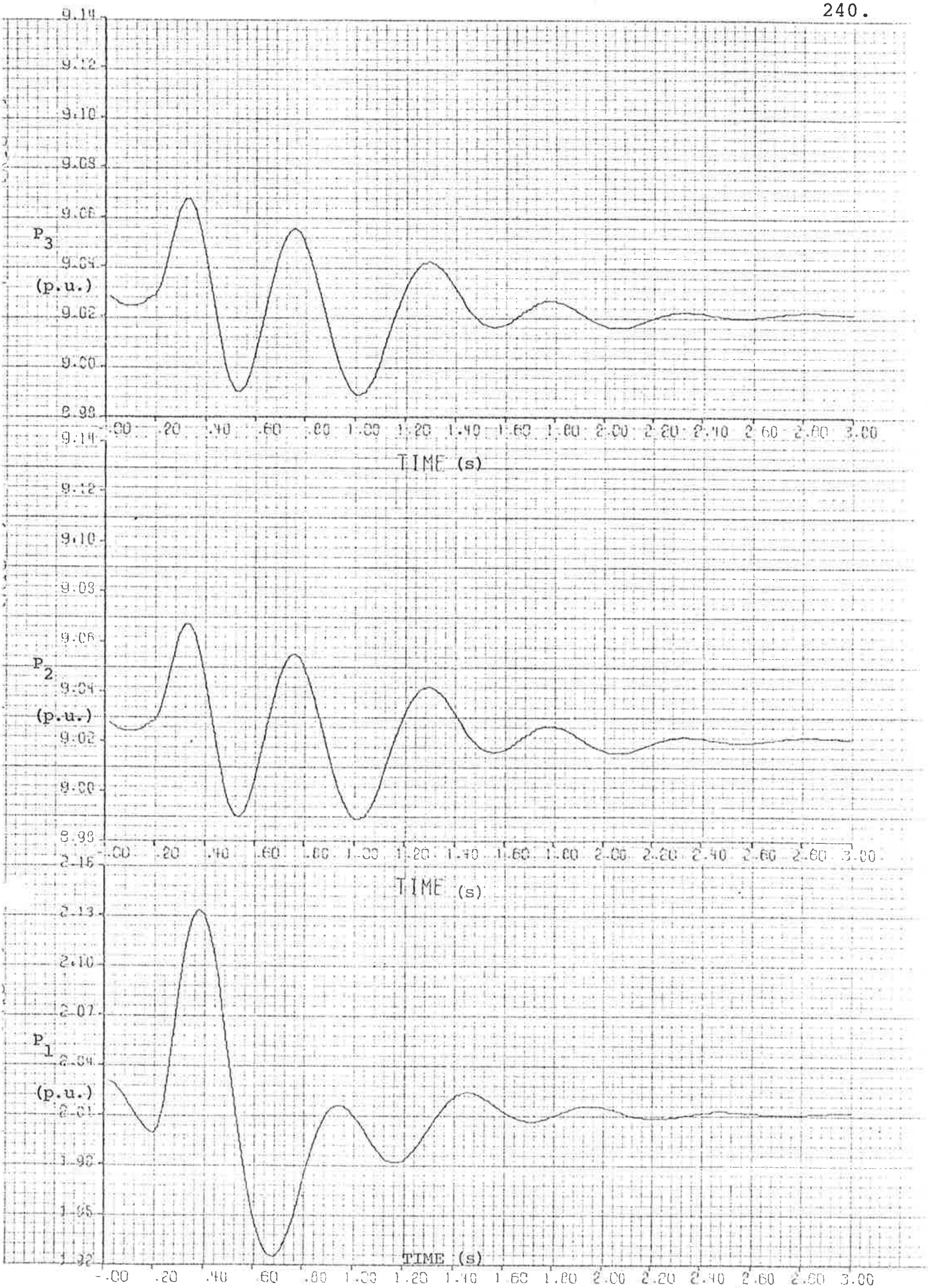

FIGURE 8.7(d) RESPONSE OF SYSTEM AT LAGGING p.f. TO A STEP IN V_{refl}
(PP/4/AG/Ff_v/B gains, T'_{qo} omitted from generator models)

(iv) Reducing interaction between generators

It may be deduced from Figure 8.6 that interaction between the power loops of the generators can be reduced to some extent by increasing the power feedback gains. However, consider changing the position of the critical point in Figure 8.6(a). The Gershgorin bands are very wide, having a radius of at least 150 units. In order to reduce significantly the ratio of the radius of the Gershgorin band to the distance from the locus to the critical point at any frequency, a large increase in power feedback gain is necessary. However, the nominal power feedback gain for unit #1 is already high (-213) so that such an increase is impractical because any minor disturbance will cause undesirable perturbations to the terminal voltage (Quazza [1]).

Alternatively, consider increasing the power feedback gain for unit #2. As the critical point moves towards the left in Figure 8.6(b), the frequency at which the locus is closest to the critical point rises, and the distance of closest approach increases. As shown above this corresponds to an increase in frequency of the dominant mode of oscillation and an improvement in the damping. The increase in the distance between the critical point and the locus is accompanied by an increased Gershgorin band radius at the oscillation frequency so that the ratio $\frac{r_i(\omega)}{f_i + q_{ii}(\omega)}$ is not reduced significantly at this frequency. However, at lower frequencies the distance from the critical point to the locus is increased so this ratio is reduced and interaction should be lessened. Comparison of Figure 8.7(a) and (c) shows that generator #2 is slightly less affected by a disturbance at unit #1 when the power gain on unit #2 is increased. Reduced interaction is also evident in Figure 8.7(c) from a comparison of the responses of units #2 and #3, which are identical except for the modified gain for unit #2.

8.2.5 The effect of omitting T'_{qo} from the generator models

The eigenvalue analysis in Table 8.3 shows that the effect of omitting the quadrature-axis transient time-constant from the generator models at the lagging p.f. loading condition is to remove 3 real eigenvalues and to introduce some error in the damping and frequency of the oscillatory modes.

Comparison of time responses such as those in Figure 8.7(a) and (d) shows that, as might be expected, for lagging p.f. operation, the overall behaviour of the multimachine system is not significantly affected by this omission. This result is consistent with those of section 5.2.2 for lagging p.f. SMIB operation.

T'_{qo} included	T'_{qo} omitted
-0.115	-0.115
-0.604	-0.589
-0.628 ± j0.156	-0.715 ± j0.074
-0.88	-
-1.08	-1.05
-1.52	-
-1.81	-
-2.44 ± j4.88	-2.41 ± j4.64
-2.46 ± j12.90	-3.13 ± j11.64
-4.54 ± j13.58	-4.91 ± j12.46
-3.91	-3.47
-6.18	-6.16
-8.66	-8.55
-11.05	-13.24
-12.1 ± j11.00	-12.0 ± j11.08
-17.8	-13.2
-20.2	-42.0
-42.4	-43.2
-42.7	-46.1

TABLE 8.3 EFFECT OF OMITTING T'_{qo} ON THE EIGENVALUES AT LAGGING POWER-FACTOR

8.3 EXAMPLE 2: OPERATION AT LEADING POWER-FACTOR

In order to investigate the suitability of the pole-placement designs for leading p.f. operation in a multimachine power system, bus loads and generator outputs as shown in Figure 8.8 are applied. The capacitive shunt loads result from the inclusion of line-charging effects for lightly-loaded transmission lines or cables. In this example the loads for the closely-coupled generators, units #2 and #3, are quite different, unlike those in the previous case.

8.3.1 Comparison of performance with fixed-gain and adjustable-gain controllers

Rows 1 and 2 of Table 8.4 list the dominant oscillatory modes which result when PP/4/FG/B and PP/4/AG/Ff_v/B control strategies are applied to the generators. The overall damping performance for the two strategies is similar, the adjustable-gain controller displaying better damping for the low frequency modes but poorer damping for a high frequency mode. These trends are also evident from a comparison of Figures 8.9(a) and (b) showing the time responses of the system following a step in voltage set-point for unit #2. It may be noted that associated with unit #1, which has a significantly leading power-factor load, there is a lower frequency mode similar to that determining the leading p.f. stability limit for the SMIB cases considered in Chapter 5. For a SMIB system, the adjustable-gain strategy only becomes superior to a fixed gain design at extremely high reactive

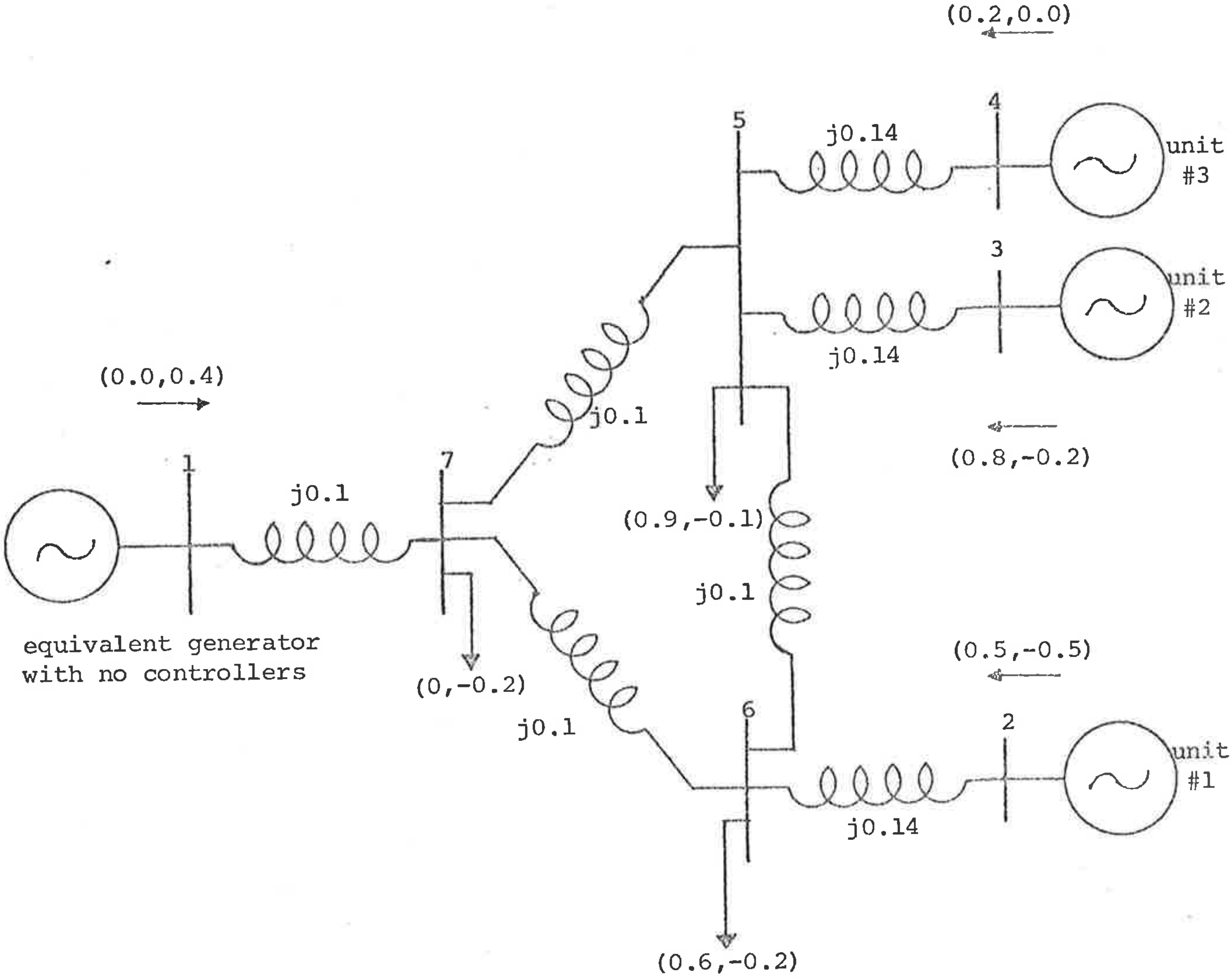

Bus	Voltage (p.u.)	Angle (deg.)
1	1.1	0.0
2	0.96	4.0
3	1.00	6.5
4	1.04	1.7
5	1.04	0.2
6	1.03	-0.2
7	1.06	0.0

Figures in brackets indicate real and reactive power flow.

Generator data for units #1, #2 and #3 is identical (column BB of Table 5.1).

FIGURE 8.8 LOADS AND NETWORK FOR SECTION 8.3
(Example 2 : Leading p.f.)

Row	Gain Settings	f_v	f_s	f_p	$f_{F'}$	Unit #
1	PP/4/FG/B fixed gains, all units	100	478	-49.1	-0.65	1
	(f_v=100, f_s=478, f_p=-49.1, f_F=-0.65)	100	478	-49.1	-0.65	2
	PP/4/FG/B design at(P,Q)=(0.9, 0.1)	100	478	-49.1	-0.65	3
2	nominal PP/4/AG/Ff_v/B gain settings	100	8.4	-43.3	-0.40	1
	(see NOTE (1) for values)	100	114	-43.1	-0.58	2
		100	1840	-52.8	-0.43	3
3	nominal gains except f_s for	100	8.4	-43.3	-0.40	1
	unit #2 decreased	100	-356	-43.1	-0.58	2
		100	1840	-52.8	-0.43	3
4	nominal gains except f_s for	100	8.4	-43.3	-0.40	1
	unit #2 decreased further	100	-1466	-43.1	-0.58	2
		100	1840	-52.8	-0.43	3
5	nominal gains except f_s for	100	8.4	-43.3	-0.40	1
	unit #2 increased	100	1694	-43.1	-0.58	2
		100	1840	-52.8	-0.43	3
6	nominal gains except zero	100	8.4	0	-0.40	1
	f_p for unit #1	100	114	-43.1	-0.58	2
		100	1840	-52.8	-0.43	3
7	nominal gains except zero	100	8.4	-43.3	-0.40	1
	f_p for unit #2	100	114	0	-0.58	2
		100	1840	-52.8	-0.43	3
8	nominal gains except zero	100	8.4	-43.3	-0.40	1
	f_p for unit #2 increased	100	114	-58.9	-0.58	2
		100	1840	-52.8	-0.43	3
9	nominal gains with T'_{qo} omitted	100	8.4	-43.3	-0.40	1
	from all m/c models	100	114	-43.1	-0.58	2
		100	1840	-52.8	-0.43	3

Rows continued on page below to show corresponding modes.

Row	MODE A S_{1A}	S_{2A}	S_{3A}	MODE B S_{1B}	S_{2B}	S_{3B}	MODE C S_{1C}	S_{2C}	S_{3C}	MODE D S_{1D}	S_{2D}	S_{3D}
1	$-2.64 \pm j6.92$			$-4.86 \pm j10.67$			$-4.51 \pm j12.00$			$-1.26 \pm j1.07$		
	.239∠-11	.216∠-1	.174∠22	.320∠-63	.345∠92	.400∠-157	.042∠107	.169∠-138	.183∠47	.095∠116	.012∠175	.005∠173
2	$-2.76 \pm j6.15$			$-6.43 \pm j10.74$			$-3.14 \pm j12.50$			$-1.43 \pm j1.49$		
	.259∠-26	.231∠2	.091∠29	.148∠-106	.277∠94	.078∠-158	.009∠-87	.015∠-71	.064∠158	.168∠121	.018∠-165	.006∠-175
3	$-2.16 \pm j5.82$			$-8.23 \pm j11.30$			$-3.19 \pm j12.43$			$-1.43 \pm j1.48$		
	.147∠-13	.192∠2	.055∠34	.057∠179	.155∠39	.040∠176	.011∠-73	.013∠-60	.071∠170	.166∠120	.018∠-159	.006∠-176
4	$-0.80 \pm j5.00$			$-5.40 \pm j6.78$			$-3.24 \pm j12.36$			$-1.40 \pm j1.47$		
	.042∠24	.106∠6	.015∠47	.748∠-42	.197∠-170	.129∠3	.014∠-59	.009∠-49	.082∠-180	.165∠118	.019∠-143	.005∠178
5	$-3.92 \pm j6.50$			$-3.74 \pm j11.85$			$-2.44 \pm j13.24$			$-1.44 \pm j1.51$		
	.600∠-31	.162∠16	.158∠31	.052∠-27	.064∠147	.143∠-152	.002∠100	.038∠-155	.042∠77	.173∠121	.015∠177	.007∠-176
6	$+0.26 \pm j7.43$			$-4.10 \pm j7.18$			$-3.23 \pm j12.42$			$-1.49 \pm j1.18$		
	.528∠10	.101∠-44	.080∠-2	.077∠-95	.218∠164	.074∠-141	.004∠148	.014∠-120	.048∠95	.026∠-90	.003∠-27	.001∠-37
7	$-4.03 \pm j7.00$			$-0.53 \pm j9.12$			$-3.19 \pm j12.15$			$-1.46 \pm j1.46$		
	.694∠.34	.201∠61	.168∠37	.025∠137	.128∠-117	.036∠-157	.016∠-16	.011∠-105	.085∠-151	.170∠121	.026∠-166	.006∠-168
8	$2.66 \pm j5.57$			$-7.43 \pm j13.89$			$-3.31 \pm j12.47$			$-1.43 \pm j1.49$		
	.198∠6	.191∠13	.066∠55	.018∠-113	.075∠83	.028∠-123	.017∠-82	.016∠-32	.096∠167	.168∠121	.016∠-165	.006∠-177
9	$-1.89 \pm j5.75$			$-6.19 \pm j10.43$			$-3.83 \pm j10.48$			-		
	.319∠-2	.199∠20	.105∠39	.196∠-100	.350∠90	.084∠-114	.066∠-159	.122∠-92	.120∠143	-	-	-

NOTES: (1) For system data, see Figure 8.8.

(2) Eigenvector components weighted to show response following an arbitrary 1 p.u. initial speed error at unit #1.

TABLE 8.4 EIGENVALUES AND EIGENVECTOR COMPONENTS FOR SECTION 8.3 (Example 2: Leading p.f.)

DATA FOR FIGURE 8.9

System data

Example 2: Leading p.f. (see Figure 8.8).

For (f) q-axis transient time-constant (T'_{qo}) omitted from generator models.

Disturbance applied

Step change in voltage set-point for unit #2.

Feedback gains

(a): PP/4/FG/B fixed gains - $f_v = 100$, $f_s = 478$, $f_p = -49.1$, $f_F = -0.65$ for all units.

(b) and (f): PP/4/AG/Ff_v/B adjustable gains:

unit #1 $f_v = 100$, $f_s = 8.4$, $f_p = =43.3$, $f_F = -0.40$

unit #2 $f_v = 100$, $f_s = 114$, $f_p = -43.1$, $f_F = -0.58$

unit #3 $f_v = 100$, $f_s = 1840$, $f_p = -52.8$, $f_F = -0.43$

(c): As for (b) except f_s reduced to -256 for unit #2.

(d): As for (b) except f_s reduced to -1476 for unit #2.

(e): As for (b) except f_s reduced to 1694 for unit #2.

NOTE: Graphs show speed deviation in rad/s and are *not* drawn to the same scale.

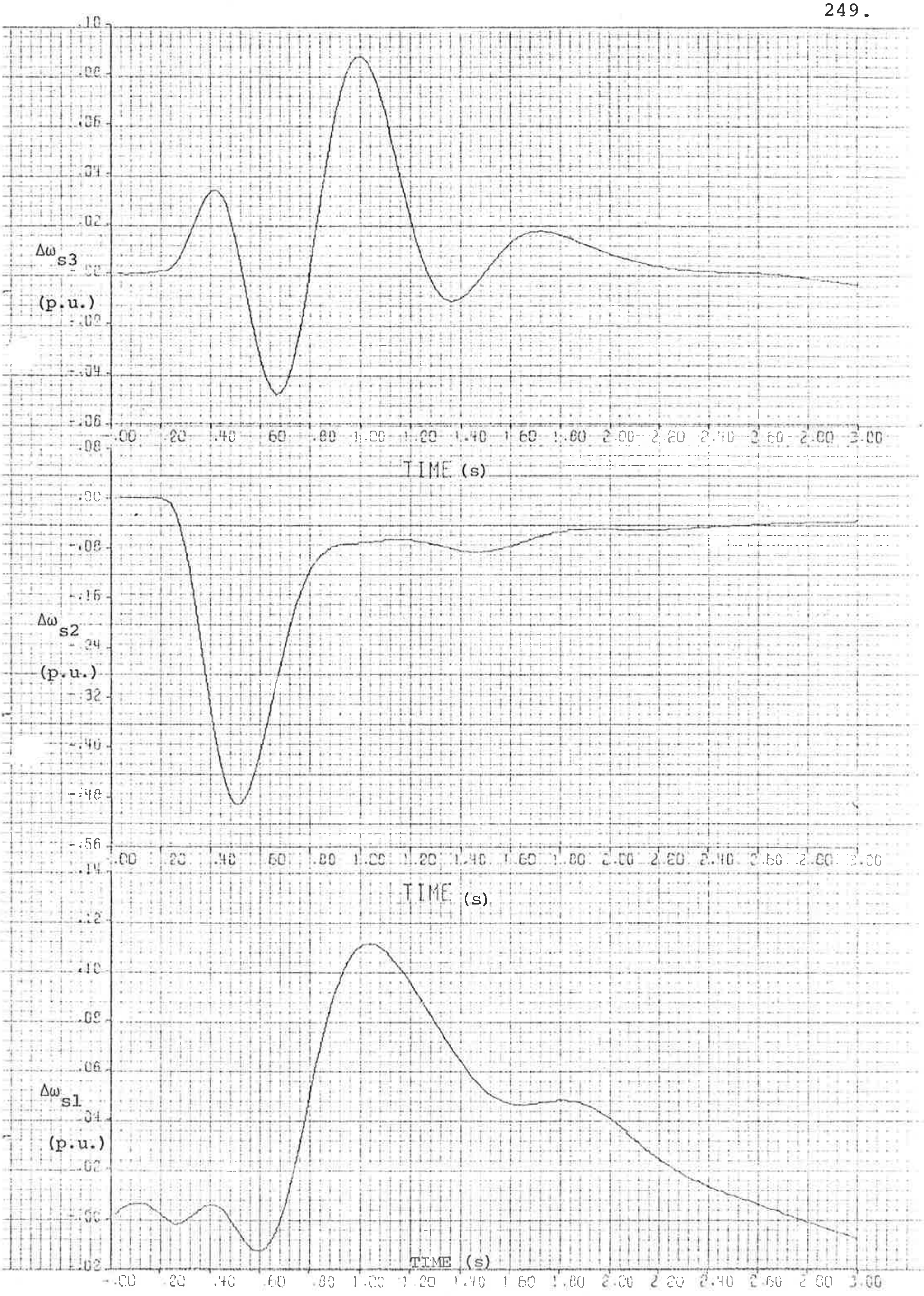

FIGURE 8.9(a) RESPONSE OF SYSTEM AT LEADING p.f. TO A STEP IN V_{ref2} (PP/4/FG/B gains)

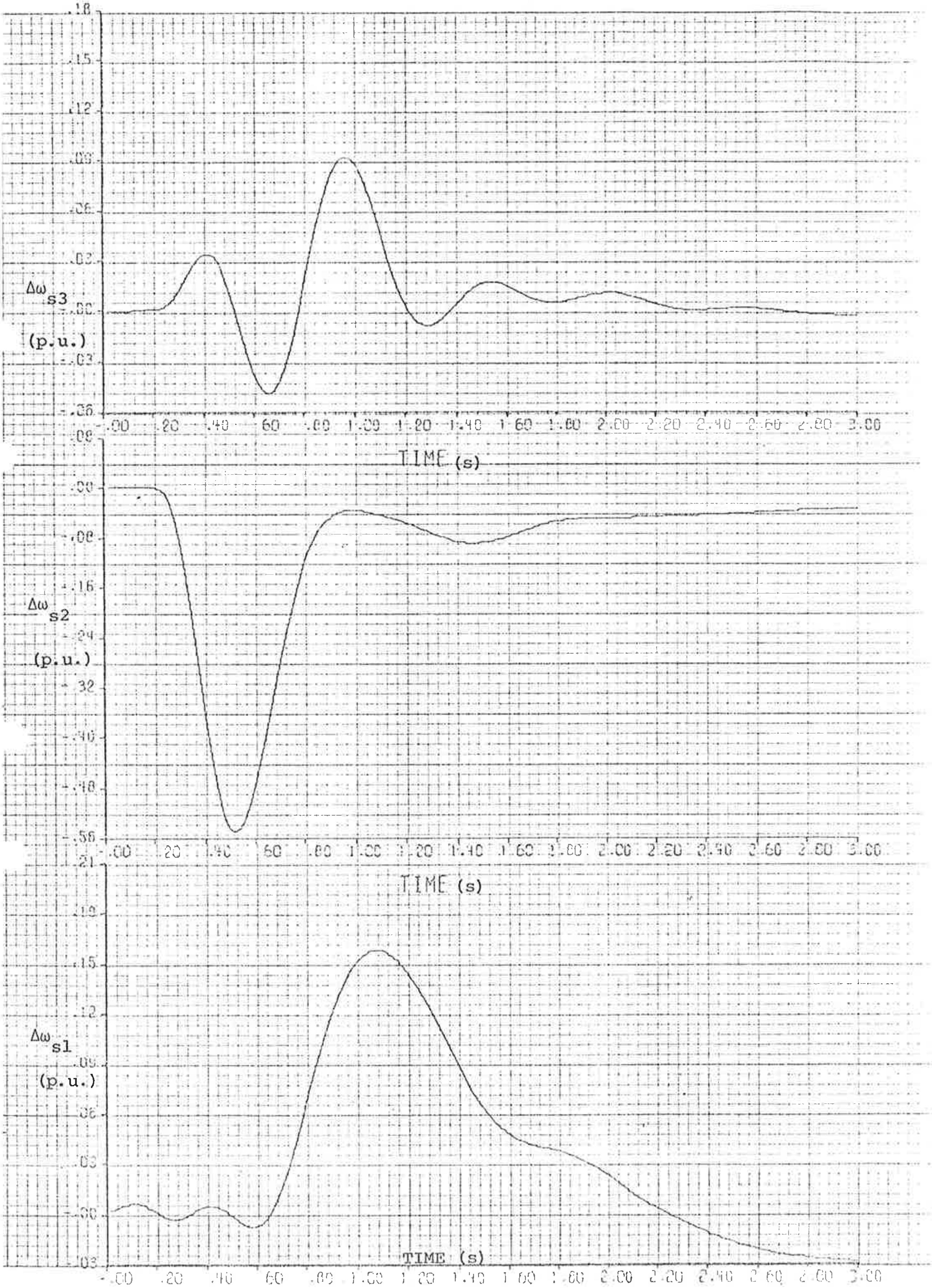

FIGURE 8.9(b) RESPONSE OF SYSTEM AT LEADING p.f. TO A STEP IN V_{ref2}
($PP/4/AG/Ff_V/B$ gains)

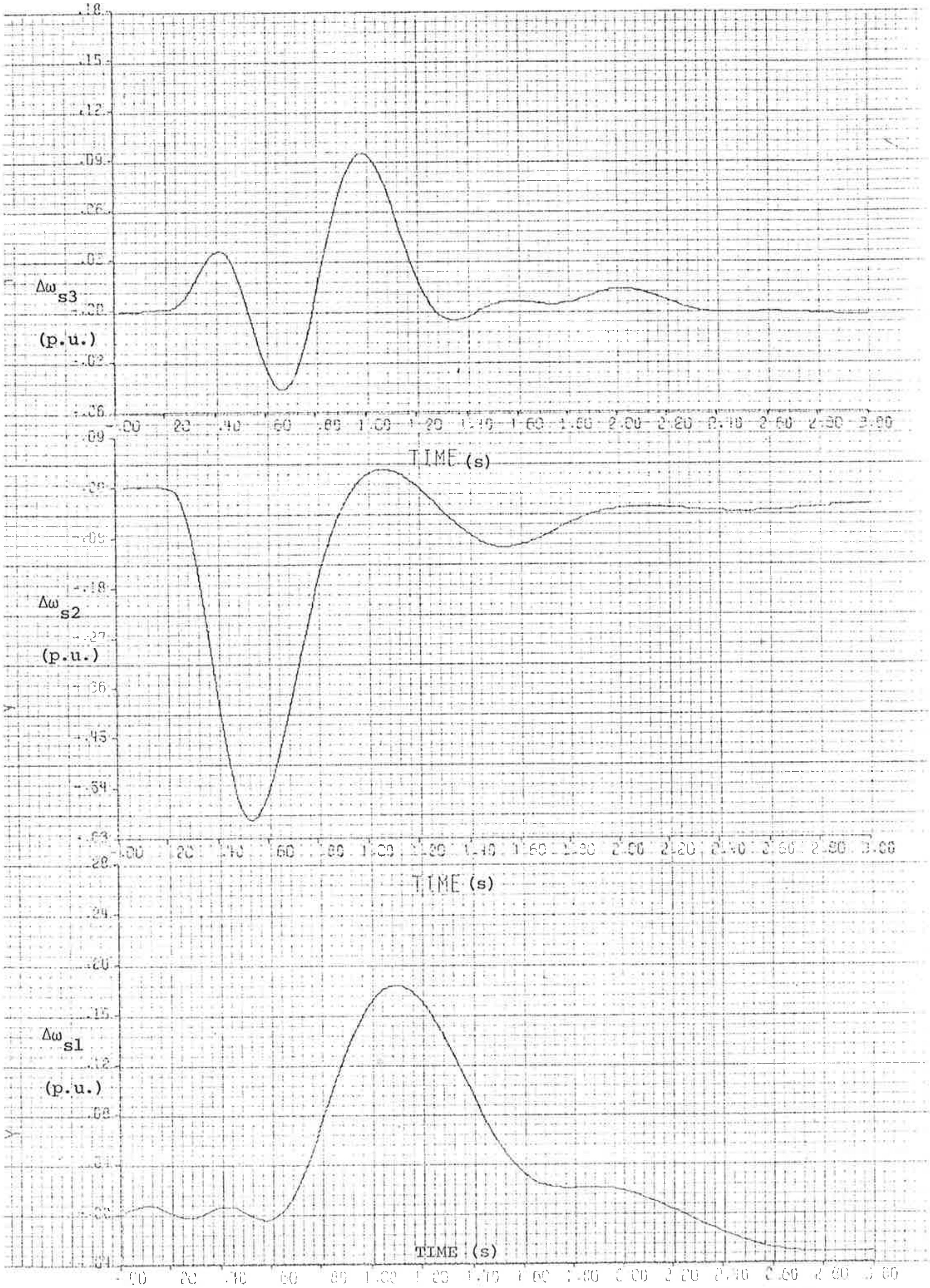

FIGURE 8.9(c) RESPONSE OF SYSTEM AT LEADING p.f. TO A STEP IN V_{ref2}

($PP/4/AG/Ff_V/B$ gains with f_s reduced for unit #2)

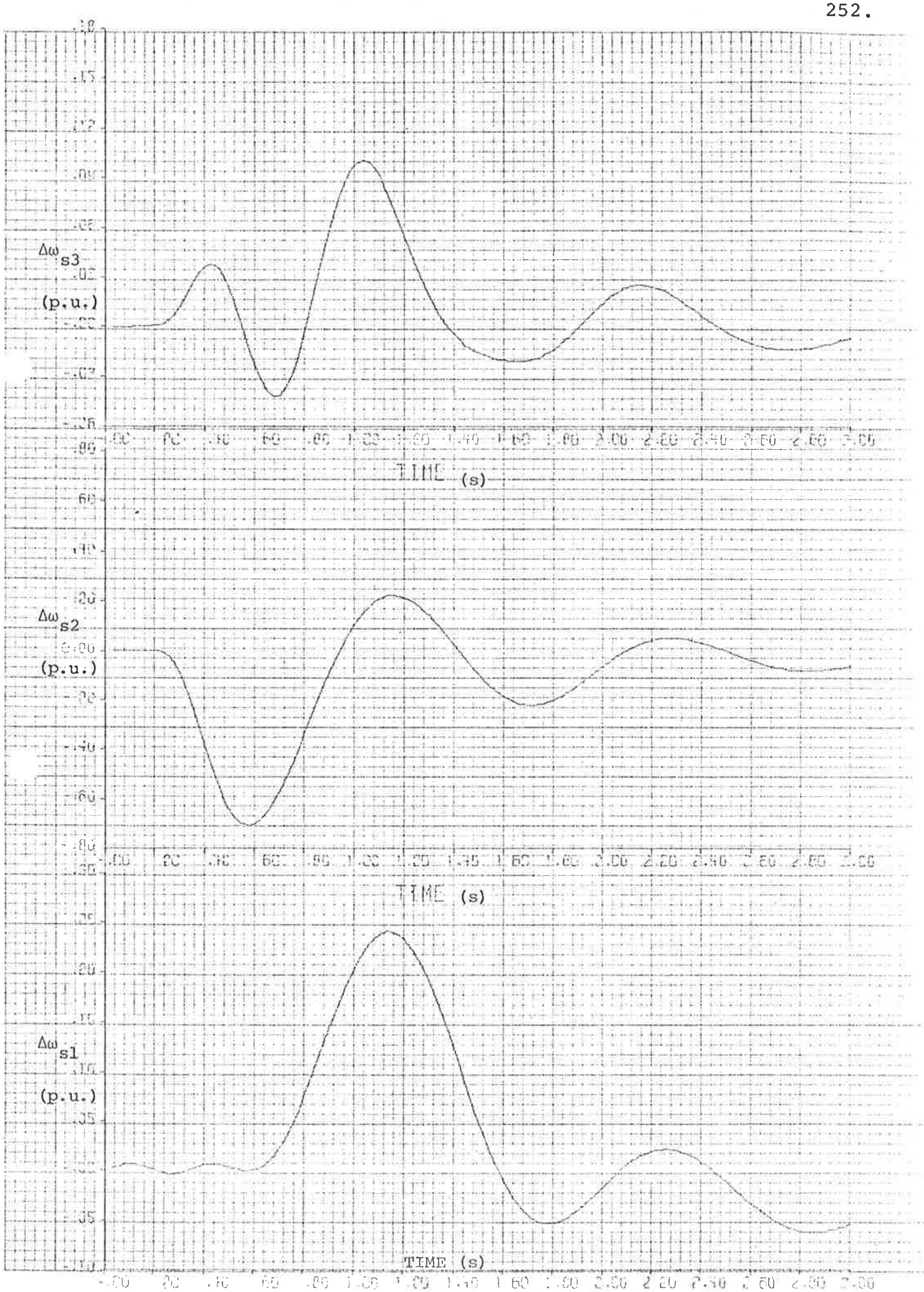

FIGURE 8.9(d) RESPONSE OF SYSTEM AT LEADING p.f. TO A STEP IN V_{ref2}
PP/4/AG/Ff_V/B gains with f_S reduced for unit #2)

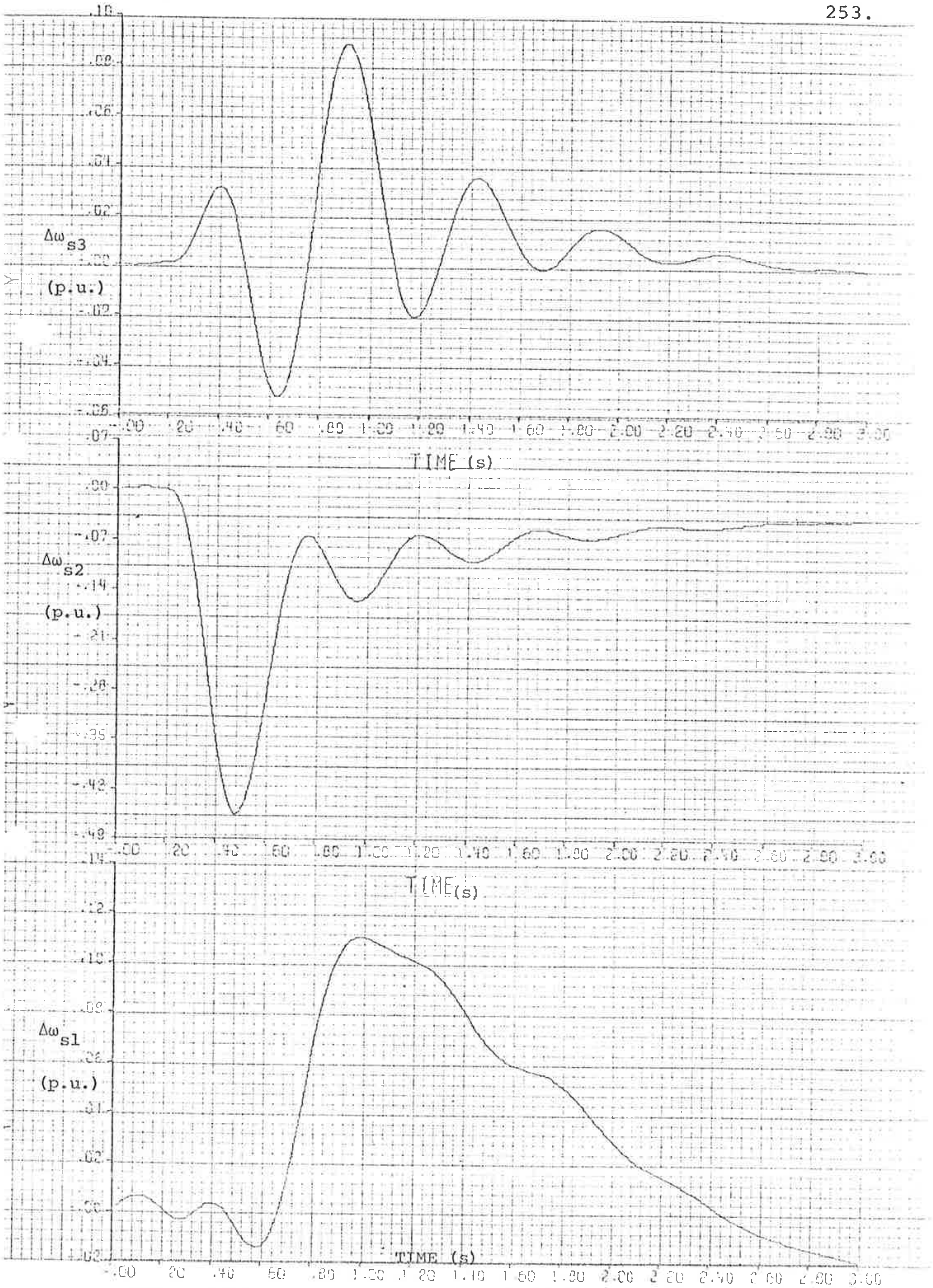

FIGURE 8.9(e) RESPONSE OF SYSTEM AT LEADING p.f. TO A STEP IN V_{ref2}

($PP/4/AG/Ff_V/B$ gains with f_s increased for unit #2)

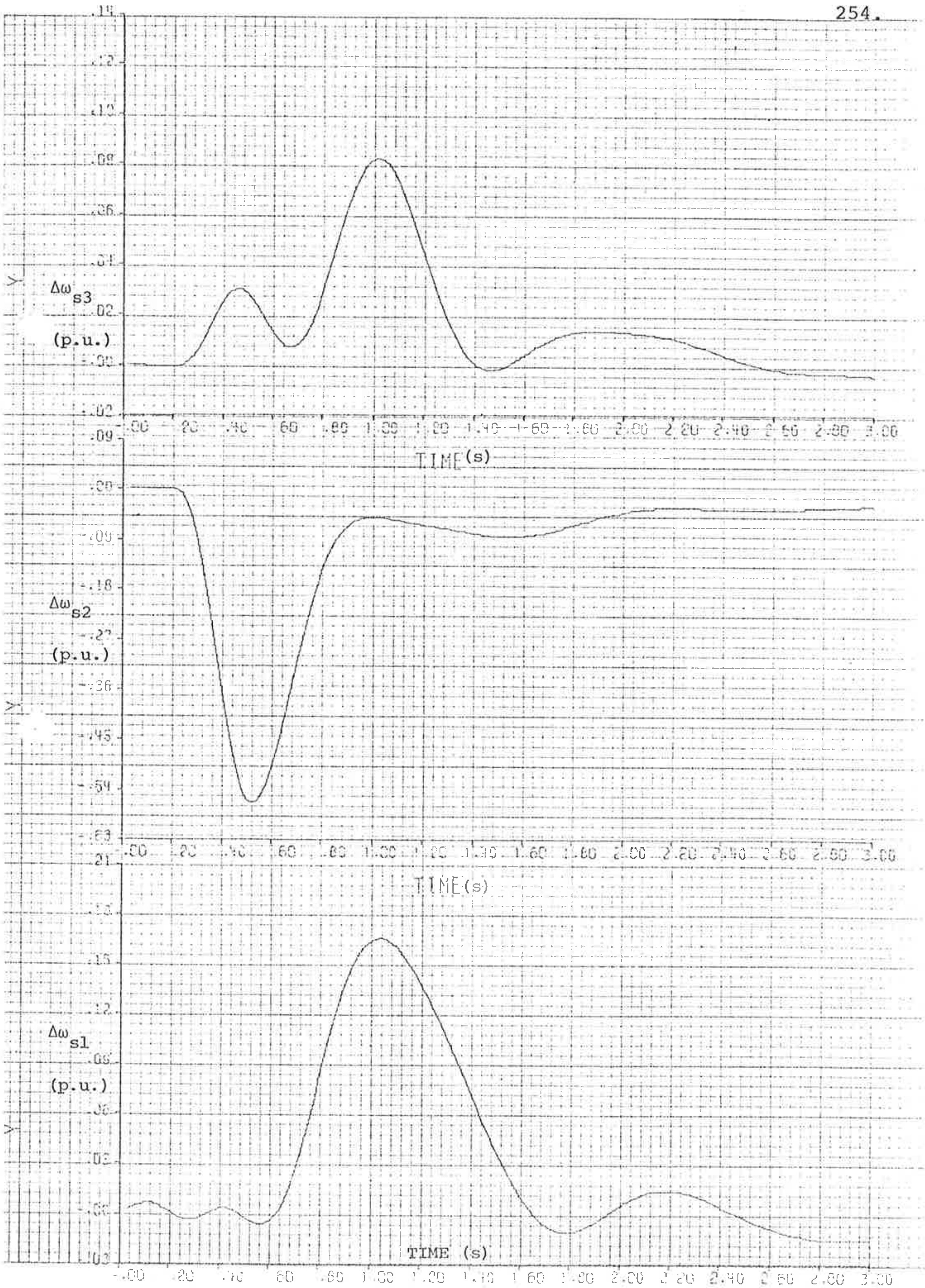

FIGURE 8.9(f) RESPONSE OF SYSTEM AT LEADING p.f. TO A STEP IN V_{ref2}
(PP/4/AG/Ff_V/B gains, T'_{qo} omitted from generator models)

load; the results in the present example suggest that this is also the case with the multimachine system under consideration.

8.3.2 Inverse Nyquist array analysis of feedback gain settings

(a) The speed feedback loops

An INA having the shaft speeds of units #1, #2 and #3 as output variables is plotted in Figure 8.10:

(i) The nominal gain settings correspond to the use of the PP/4/AG/Ff$_v$/B strategy for each unit and produce closed-loop diagonal dominance because the origin of each INA lies outside its respective Gershgorin band.

(ii) The points marked A in Figures 8.10(a), (b) and (c) correspond to open speed feedback loops for units #1, #2 and #3 respectively. Because the system is stable at the nominal operating point and the critical points do not cross the Gershgorin bands if moved from the origin to the "open-loop" positions, it may be deduced that the system remains stable when any or all of the speed feedback loops are open-circuited.

(iii) In order to investigate whether performance can be improved by changing the settings for the speed feedback gains, consider moving the critical point for unit #2 to the point B in Figure 8.10(b). As discussed in section 8.2.3, this will improve damping and reduce interaction at higher frequencies but cause a deterioration at lower frequencies;

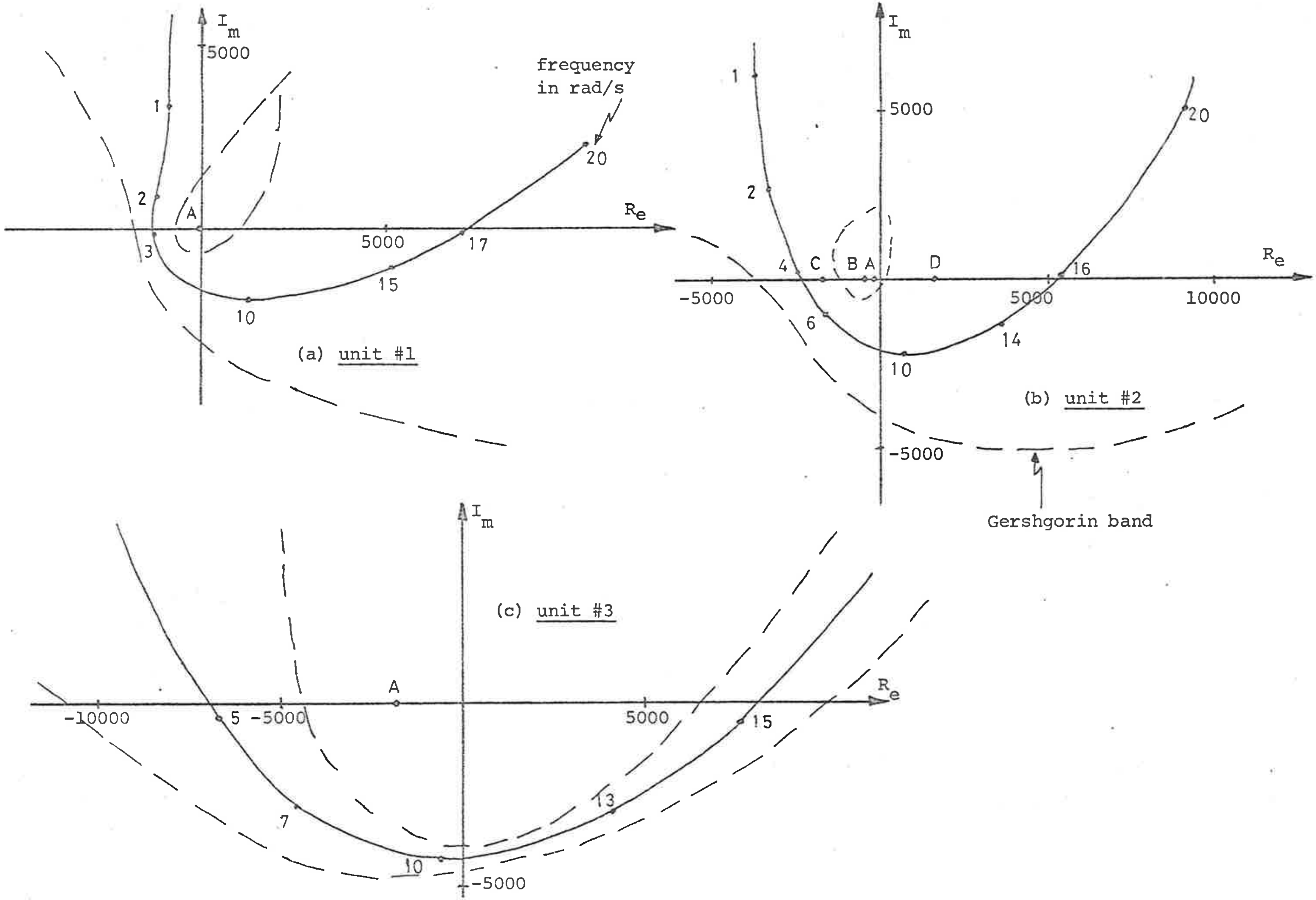

FIGURE 8.10 INA FOR SPEED FEEDBACK LOOPS WITH SYSTEM UNDER LEADING p.f. LOAD
(PP/4/AF/Ff_v/B controllers using x_e = 0.3 p.u. for gain calculations)

these trends are evident in Figure 8.9(c) and also in a comparison of rows 2 and 3 of Table 8.4. There is only a slight difference between the performance with the nominal (PP/4/AG/Ff$_v$/B) gains and that with the critical point shifted to B where it lies in the centre of the "STABLE" region. Row 4 of Table 8.4 and Figure 8.9(d) show the performance which results when the Gershgorin bands are ignored and the critical point in Figure 8.10(b) is moved further to the point C; the performance is clearly inferior to that obtained by setting the gains for diagonal dominance. The performance which results from increasing the speed-gain for unit #2 so that the critical point in Figure 8.10(b) lies at D, inside the Gershgorin band, is shown by Figure 8.9(e) and row 5 of Table 8.4; it is evident that the damping at higher frequencies is poorer than for the gain settings giving diagonal dominance. These results illustrate the fact that performance cannot be improved by simply changing the speed-gains of the generators from the values calculated by PP/4/AG/Ff$_v$/B pole-placement.

(b) <u>The power feedback loops</u>

An INA having the perturbations in electrical power output for units #1, #2 and #3 as the output variables is plotted in Figure 8.11.

(i) The nominal gain settings correspond to the use of the PP/4/AG/Ff$_v$ strategy and result in closed-loop diagonal dominance.

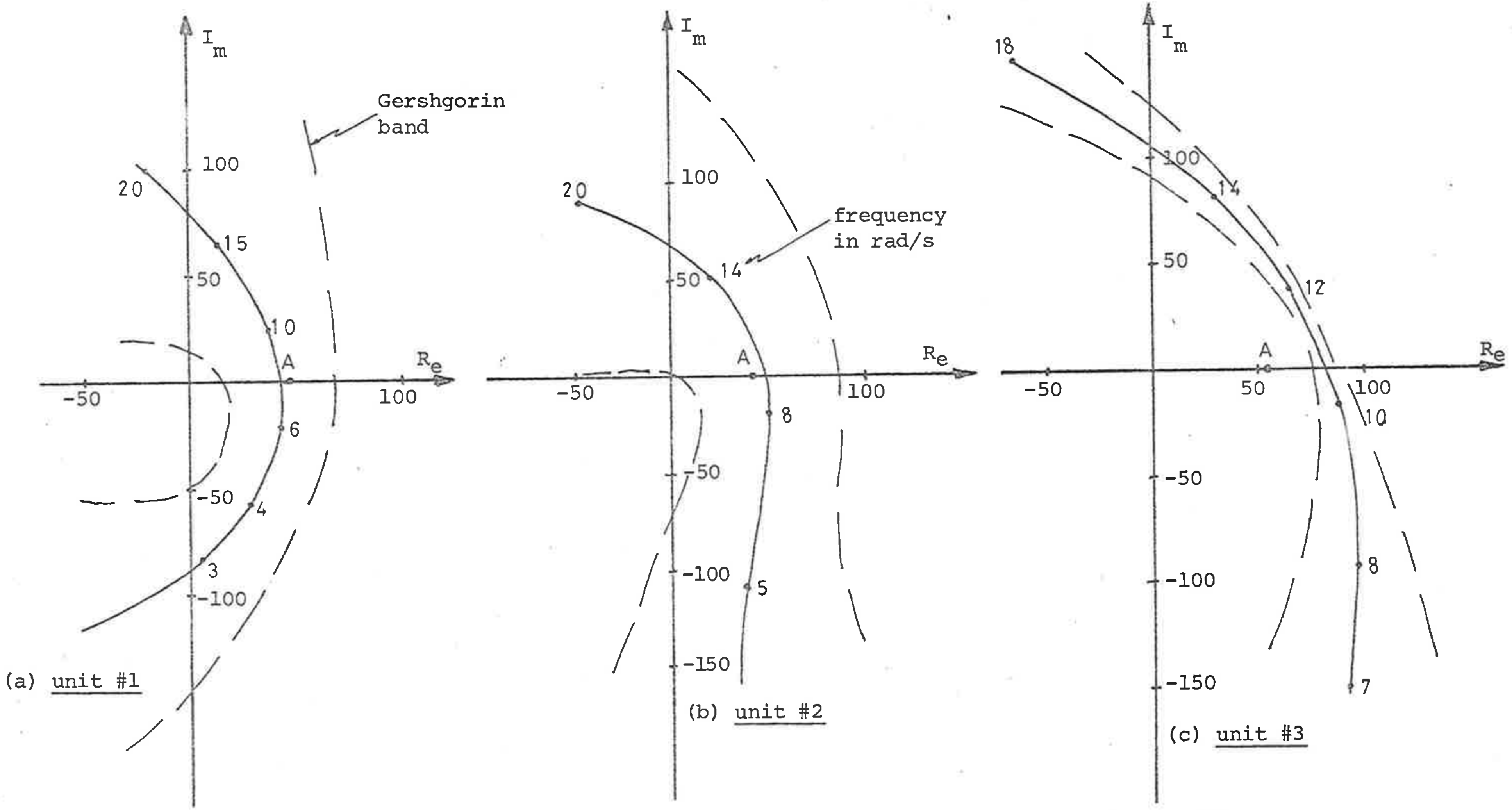

FIGURE 8.11 INA FOR POWER FEEDBACK LOOPS WITH SYSTEM UNDER LEADING p.f. LOAD
(PP/4/AG/Ff_V/B controllers using x_e = 0.3 p.u. for gain calculations)

(ii) The points marked A in Figures 8.11(a), (b) and (c) correspond to zero feedback gain for units #1, #2 and #3. It may be deduced that stability is retained in the event of a transducer failure for unit #3. No information concerning such failures for units #1 and #2 can be deduced because the open-loop values are so close to the locus that they will always lie inside the Ostrowski bands unless these are narrowed by unrealistically high gains. Eigenvalue analysis reveals that stability is lost on opening the power feedback loop for unit #1 but retained for unit #2 (see rows 6 and 7 of Table 8.4).

(iii) The damping for any one of the generators may be improved by increasing its power feedback gain so that the critical point moves to the left from the origin, thus increasing the distance between the locus and the critical point. An increase in the oscillation frequency will also result from such a change because the point of closest approach occurs at a higher frequency (for example, see mode B in row 8 of Table 8.4). Interaction between the power feedback loops cannot be reduced significantly by adjustment of power feedback gain because the Gershgorin band for unit #2 lies close to the negative real-axis.

8.3.3 The effect of omitting T'_{qo} from the generator models

In the SMIB studies in Chapter 5 it is found that for low, leading power-factor loads the omission of T'_{qo}, the q-axis transient time-constant arising from the behaviour of the flux linkages deep in the q-axis rotor iron, leads to the absence of an important low-frequency mode of oscillation. Table 8.5 shows that the same effect results from the neglect of T'_{qo} for the leading p.f. multimachine example: The omission of T'_{qo} for units #2 and #3 which are at relatively high p.f. results in the neglect of two real-poles and errors in the damping and frequency of the oscillatory modes. However, the omission of T'_{qo} for unit #1, which is operating at a considerably lower p.f. will not only cause errors in the frequencies of oscillatory modes but also the disappearance of the 1.5 rad/s mode.

The effect of omitting T'_{qo} on the time response may be seen by comparing Figures 8.9(b) and (f). The change in behaviour for this case is small but more significant than for the corresponding change in the lagging power-factor example (compare the latter figures with Figures 8.7(a) and (d)). The increased change is also evident in a comparison of the values in Tables 8.3 and 8.5.

full model	T'_{qo} omitted for units #2 and #3	T'_{qo} omitted for unit #1 only	T'_{qo} omitted for units #1, #2 and #3
-0.106	-0.106	-0.106	-0.106
-0.488 ± j.154	0.585, -0.966	-0.488 ± j.154	-0.587, -0.94
-0.656 ± j.120	-0.613 ± j0.202	-0.652 ± j0.122	-0.613 ± j0.20
-1.433 ± j1.485	-1.492 ± j1.472	-3.016, -	-3.107, -
-1.695	-	-1.726	-
-1.845	-	-1.844	-
-2.755 ± j6.145	-2.623 ± j5.660	-2.028 ± j6.006	-1.892 ± j5.751
-3.138 ± j12.501	-3.888 ± j10.441	-3.036 ± j12.518	-3.828 ± j10.48
-5.65	-5.374	-5.866	-5.525
-6.43 ± j10.736	6.218 ± j10.472	-6.375 ± j10.745	-6.190 ± j10.43
-7.747 ± j7.079	-7.417 ± j6.866	-8.296 ± j6.430	-7.853 ± j6.18
-9.042	-9.031	-8.757	-8.700
-14.346	-19.112	-14.508 ± j1.892	-18.249
-16.060	-30.237		-29.913
-17.770	-41.665	-17.830	-41.660
-38.564	-41.844 ± j2.077	-38.612	-41.821 ± j2.33
-40.269		-40.272	

System data: See Figure 8.8.

Controller gains: $PP/4/AG/Ff_v/B$ "nominal" gains.

TABLE 8.5 EFFECT OF OMITTING T'_{qo} FROM GENERATOR MODELS ON THE EIGENVALUES AT A LEADING POWER-FACTOR LOAD

8.4 EXAMPLE 3: OPERATION WITH HEAVY LOADS

In order to investigate the behaviour of a multimachine system at a "normal" operating condition, the loads are chosen such that the generator outputs are close to typical rated values, as shown in Figure 8.12.

8.4.1 Comparison of performance with fixed-gain and adjustable-gain controllers

For the SMIB case, the dynamic performance with the PP/4/AG/Ff_v/B adjustable-gain control strategy is little different from that with the PP/4/FG/B fixed-gain strategy for operating points in the normal operating region near rated load. This is not surprising since the fixed-gain controller is designed at such an operating point. Comparison of both the eigenvalues in rows 1 and 2 in Table 8.6 and of the time responses in Figures 8.13(a) and (b) shows that there is also little difference in performance in this multimachine example.

Inspection of the eigenvalues and the time responses reveals that there is a poorly damped oscillatory mode with a frequency of approximately 0.75 Hz. Consideration of the time responses or the eigenvector components in Table 8.6 shows that this is a group mode with units #1, #2 and #3 swinging in phase and that unit #1 is the most heavily affected generator. This behaviour resembles that of the two machine infinite bus system in section 6.3 when the tieline reactance x_{e1} is high. It should be noted that an equivalent SMIB tieline reactance (x_e) equal to 0.3 p.u. is

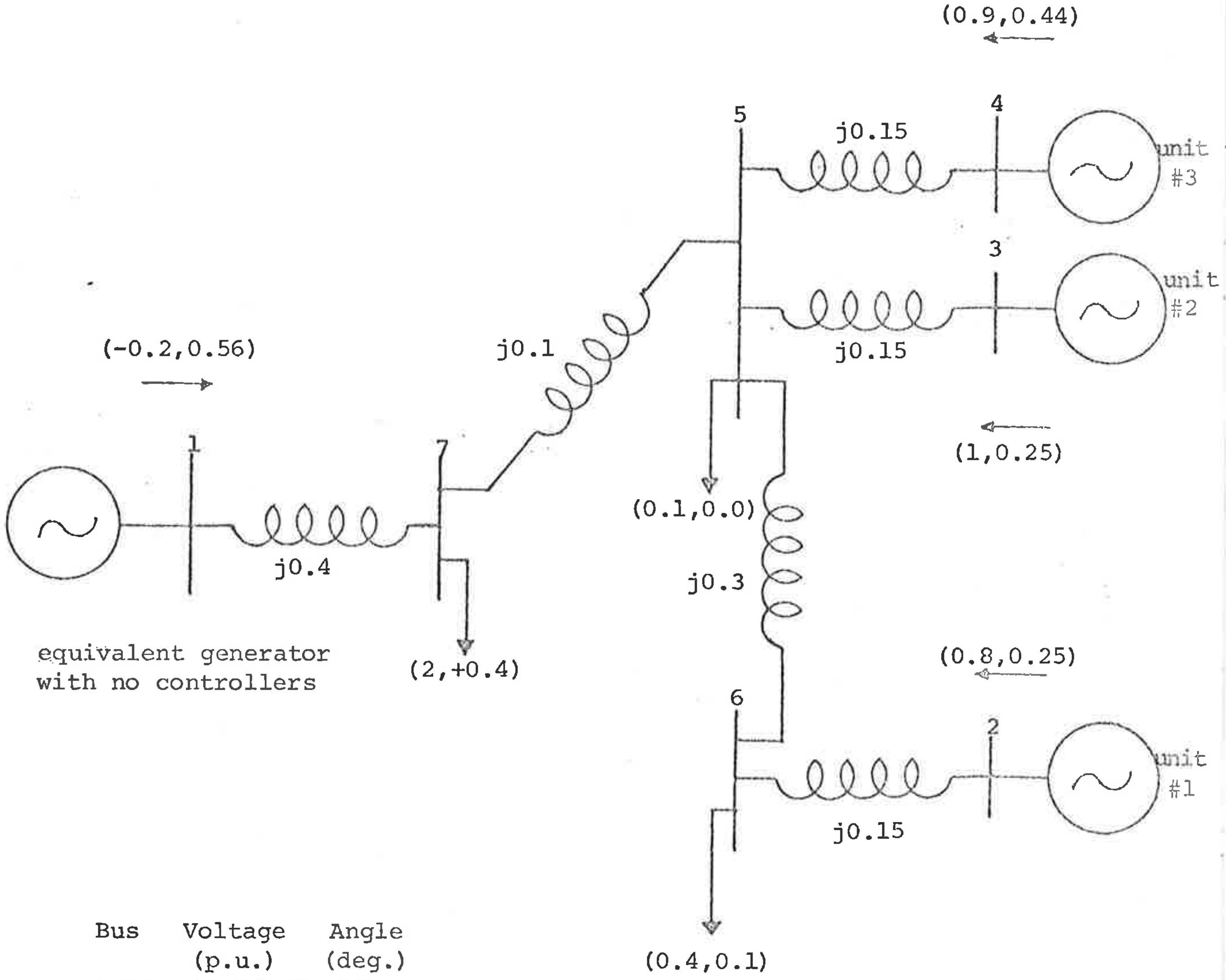

Bus	Voltage (p.u.)	Angle (deg.)
1	1.19	0.0
2	1.06	29.0
3	1.05	24.2
4	1.08	23.2
5	1.02	16.2
6	1.03	22.7
7	1.01	3.8

Figures in brackets indicate real and reactive power flow.

Generator data for units #1, #2 and #3 is given by column BB of Table 5.1.

FIGURE 8.12 LOAD AND NETWORK DATA FOR SECTION 8.4
(Example 3 : Heavy load)

row no.	case	f_v	f_s	f_p	f_F	unit #
1	PP/4/FG/B fixed-gains	100	478	-49.1	-0.65	1
		100	478	-49.1	-0.65	2
		100	478	-49.1	-0.65	3
2	PP/4/AG/Ff_v/B adjustable-gains (nominal gains)	100	462	-50.1	-0.67	1
		100	514	-52.5	-0.71	2
		100	672	-57.2	-0.73	3
3	gains modified on the basis of INA analysis	100	3720	-100	-0.67	1
		100	514	-52.5	-0.71	2
		100	672	-69.5	-0.73	3
4	gains further modified using INA analysis	100	5390	-100	-0.67	1
		100	514	-52.5	-0.71	2
		100	1537	-69.5	-0.73	3
5	PP/4/AG/Ff_v/B nominal gains (no T'_{qo} in generator models	100	462	-50.1	-0.67	1
		100	514	-52.5	-0.71	2
		100	672	-57.2	-0.73	3

Rows continued on page below to show corresponding modes.

row no.	Mode A S_{1A}	Mode A S_{2A}	Mode A S_{3A}	Mode B S_{1B}	Mode B S_{2B}	Mode B S_{3B}	Mode C S_{1C}	Mode C S_{2C}	Mode C S_{3C}
1	$-0.52 \pm j4.63$			$-3.72 \pm j8.66$			$-4.62 \pm j13.67$		
	$.199\angle{-4}$	$.137\angle{8}$	$.134\angle{7}$	$.328\angle{158}$	$.251\angle{-19}$	$.229\angle{-10}$	$.007\angle{93}$	$.228\angle{137}$	$.266\angle{-40}$
2	$-0.57 \pm j4.59$			$-3.96 \pm j8.58$			$-4.86 \pm j13.97$		
	$.206\angle{-4}$	$.141\angle{7}$	$.133\angle{5}$	$.355\angle{154}$	$.284\angle{-19}$	$.239\angle{-11}$	$.011\angle{109}$	$.215\angle{132}$	$.276\angle{-42}$
3	$-1.52 \pm j4.87$			$-6.60 \pm j12.95$			$-5.96 \pm j14.83$		
	$.143\angle{-17}$	$.255\angle{19}$	$.219\angle{24}$	$.165\angle{149}$	$.103\angle{-105}$	$.167\angle{-34}$	$.052\angle{7}$	$.221\angle{119}$	$.191\angle{-84}$
4	$-1.94 \pm j5.05$			$-4.97 \pm j14.29$			$-6.22 \pm j14.78$		
	$.100\angle{-12}$	$.278\angle{19}$	$.180\angle{27}$	$.201\angle{131}$	$.208\angle{168}$	$.376\angle{-56}$	$.108\angle{-88}$	$.079\angle{58}$	$.027\angle{158}$
5	$-0.56 \pm j4.56$			$-4.32 \pm j7.50$			$-5.26 \pm j12.86$		
	$.205\angle{-4}$	$.133\angle{12}$	$.125\angle{10}$	$.474\angle{158}$	$.340\angle{-17}$	$.303\angle{-10}$	$.009\angle{122}$	$.208\angle{116}$	$.271\angle{-43}$

NOTES: (1) For system data, see Figure 8.12.

(2) Eigenvector components are weighted to show the response following an 1 p.u. initial speed error for unit #3.

TABLE 8.6 EIGENVALUES AND EIGENVECTOR COMPONENTS FOR SECTION 8.4 (Example 3: Heavy load)

DATA FOR FIGURE 8.13

System data

Example 3: Heavy load (see Figure 8.12).

In (d), q-axis transient time-constant (T'_{qo}) omitted from all generator models.

Disturbance applied

Step in voltage set-point for unit #3.

Feedback gains

(a): PP/4/FG/B fixed gains, $f_v = 100$, $f_s = 478$, $f_p = -49.1$, $f_F = -0.65$ for all units.

(b) and (d): PP/4/AG/Ff_v/B adjustable-gains

unit #1 $f_v = 100$, $f_s = 462$, $f_p = -50.1$, $f_F = -0.67$

unit #2 $f_v = 100$, $f_s = 514$, $f_p = -52.5$, $f_F = -0.71$

unit #3 $f_v = 100$, $f_s = 672$, $f_p = -57.2$, $f_F = -0.73$

(c): modified gains

unit #1 $f_v = 100$, $f_s = 1670$, $f_p = -100$, $f_F = -0.67$

unit #2 $f_v = 100$, $f_s = 514$, $f_p = -69.5$, $f_F = -0.71$

unit #3 $f_v = 100$, $f_s = 672$, $f_p = -57.2$, $f_F = -0.73$

NOTE: The graphs show electrical power outputs in p.u. and are *not* plotted to the same scale.

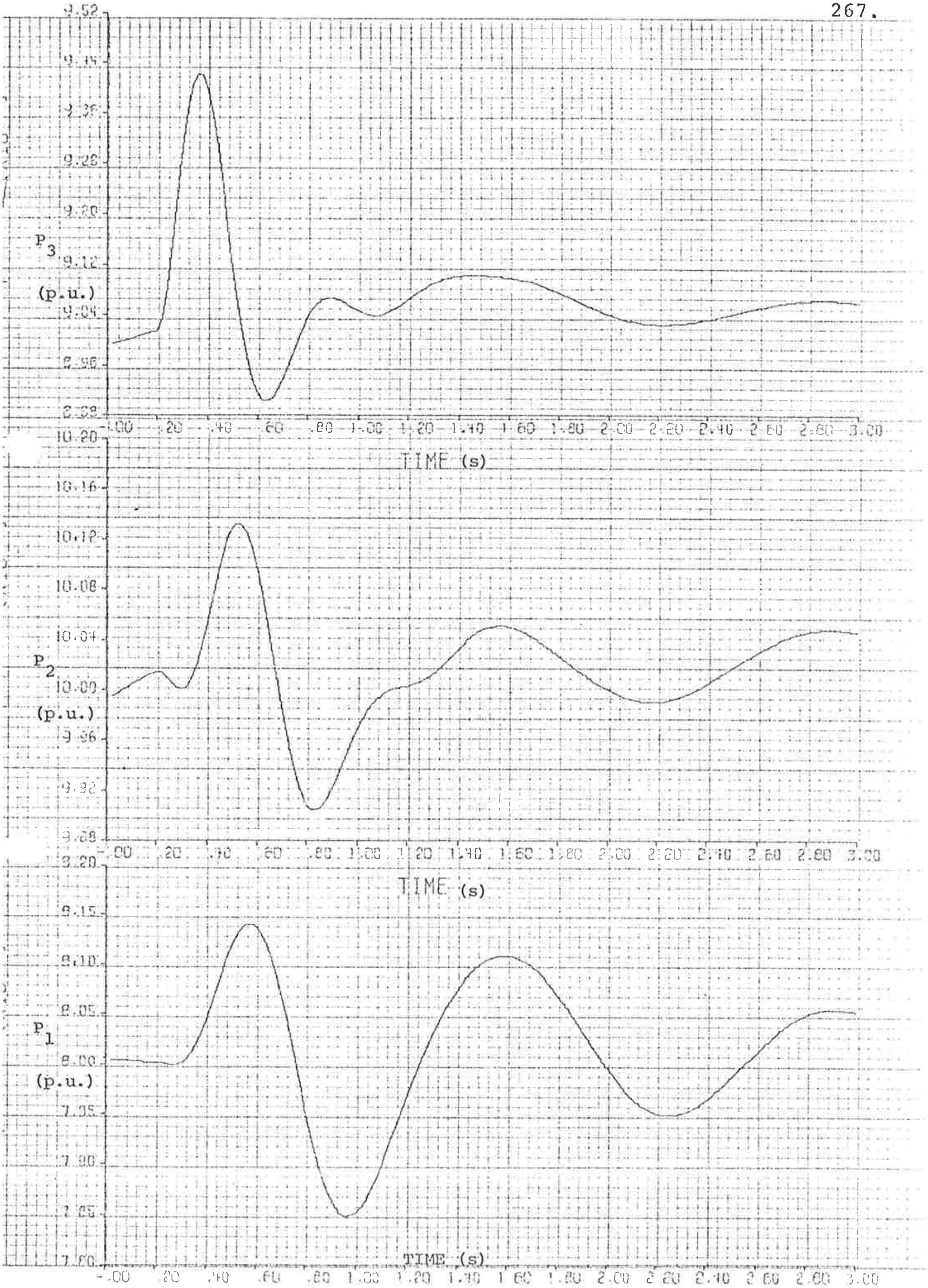

FIGURE 8.13(a) RESPONSE OF SYSTEM UNDER HEAVY LOAD TO A STEP IN V_{ref3}
(PP/4/FG/B gains)

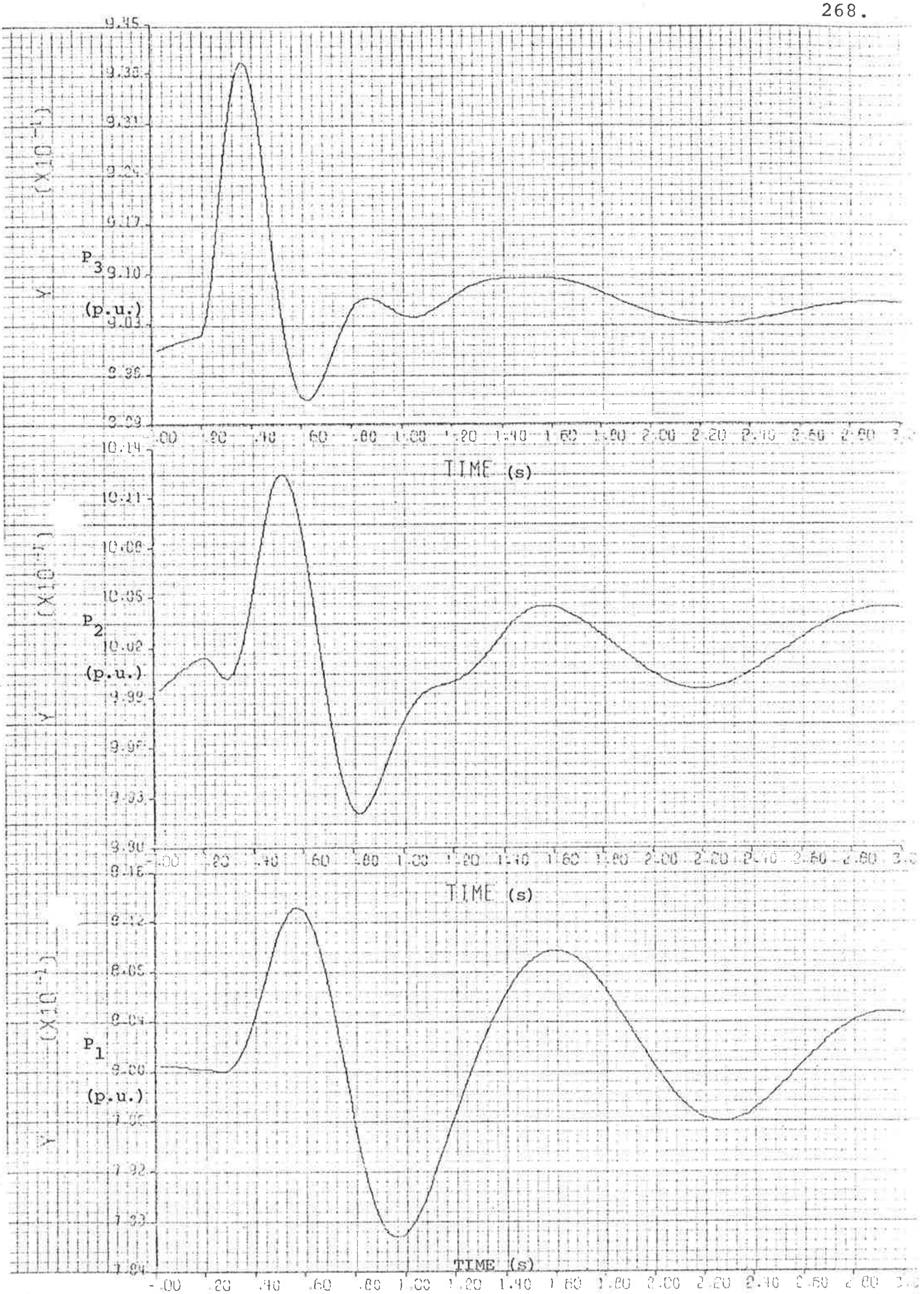

FIGURE 8.13(b) RESPONSE OF SYSTEM UNDER HEAVY LOAD TO A STEP IN V_{ref3}
($PP/4/AG/Ff_V/B$ gains)

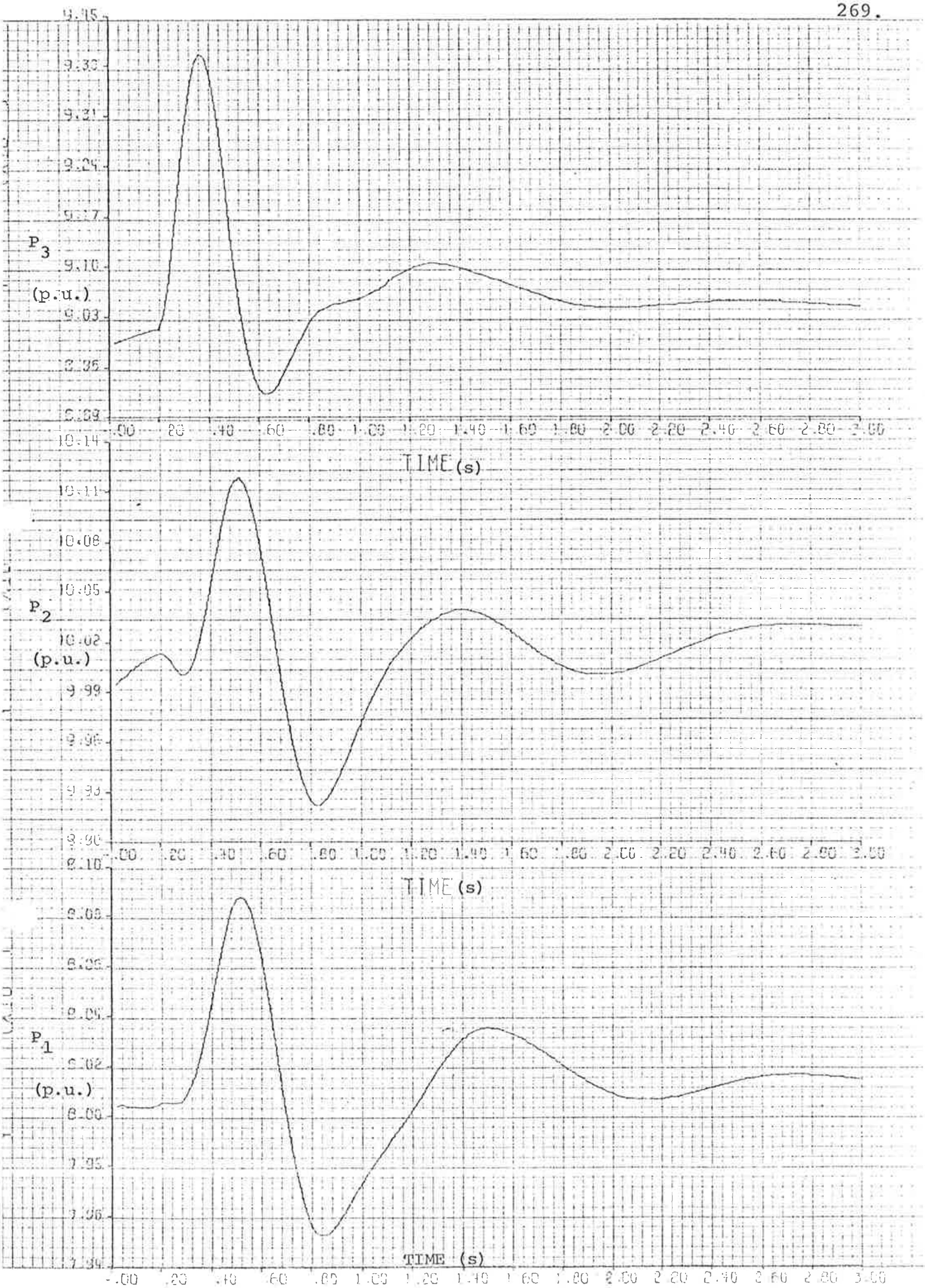

FIGURE 8.13(c) RESPONSE OF SYSTEM UNDER HEAVY LOAD TO A STEP IN V_{ref3}
(gains modified as described in section 8.4.2)

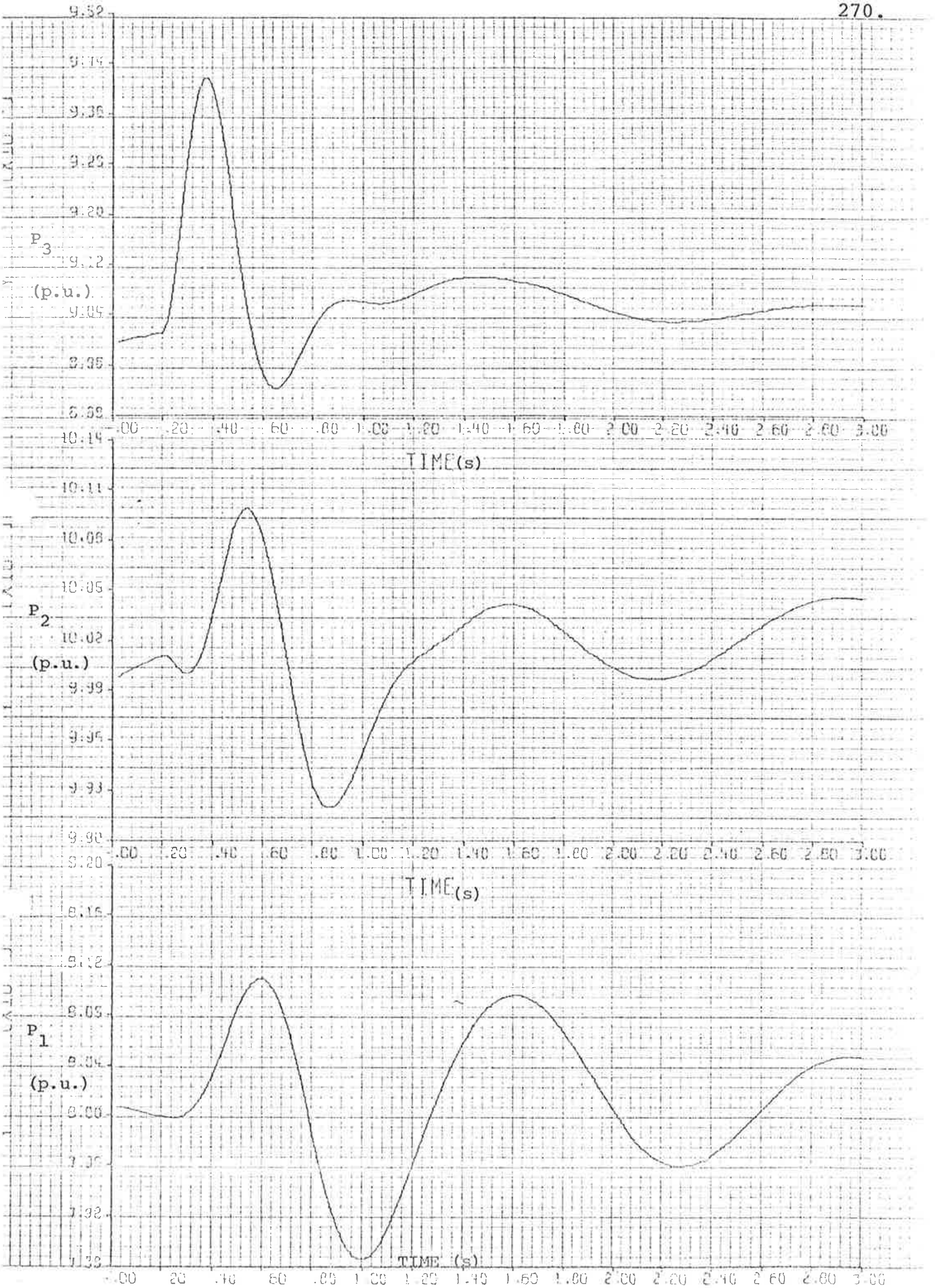

FIGURE 8.13(d) RESPONSE OF SYSTEM UNDER HEAVY LOAD TO A STEP IN V_{ref3}

($PP/4/AG/Ff_v/B$ gains, T'_{qo} omitted from generator models) used in calculating the feedback gains for units #1, #2 and #3; this is considerably less than the sum of the reactances of the lines connecting unit #1 to the main load centre at bus 7. One way to improve the performance of the multimachine system is to redesign the controller for unit #1 using a higher value for x_e in the feedback gain calculations (see section 8.6). An alternative approach, which is adopted below, is to determine the necessary modifications to the feedback gains by analysing the corresponding inverse Nyquist arrays.

8.4.2 INA analysis of feedback gain settings

Inverse Nyquist arrays for the feedback of electrical power and of shaft speed are plotted in Figures 8.14 and 8.15 for the multimachine system with PP/4/AG/Ff_v/B controllers. In both cases there are critical points inside the Gershgorin bands so that the system is not diagonally dominant.

Consider first the power loop INA in Figure 8.14; increasing the power feedback gains for units #1 and #2 so that the critical points in Figures 8.14(a) and (b) lie at A and B respectively, achieves diagonal dominance. In addition damping should be improved because the distance between the locus and critical point is increased.

Both row and column based Gershgorin bands are shown for the speed loop INA in Figure 8.15; neither row nor column diagonal dominance can be achieved by changing speed feedback gains alone. However, it is evident that the critical point

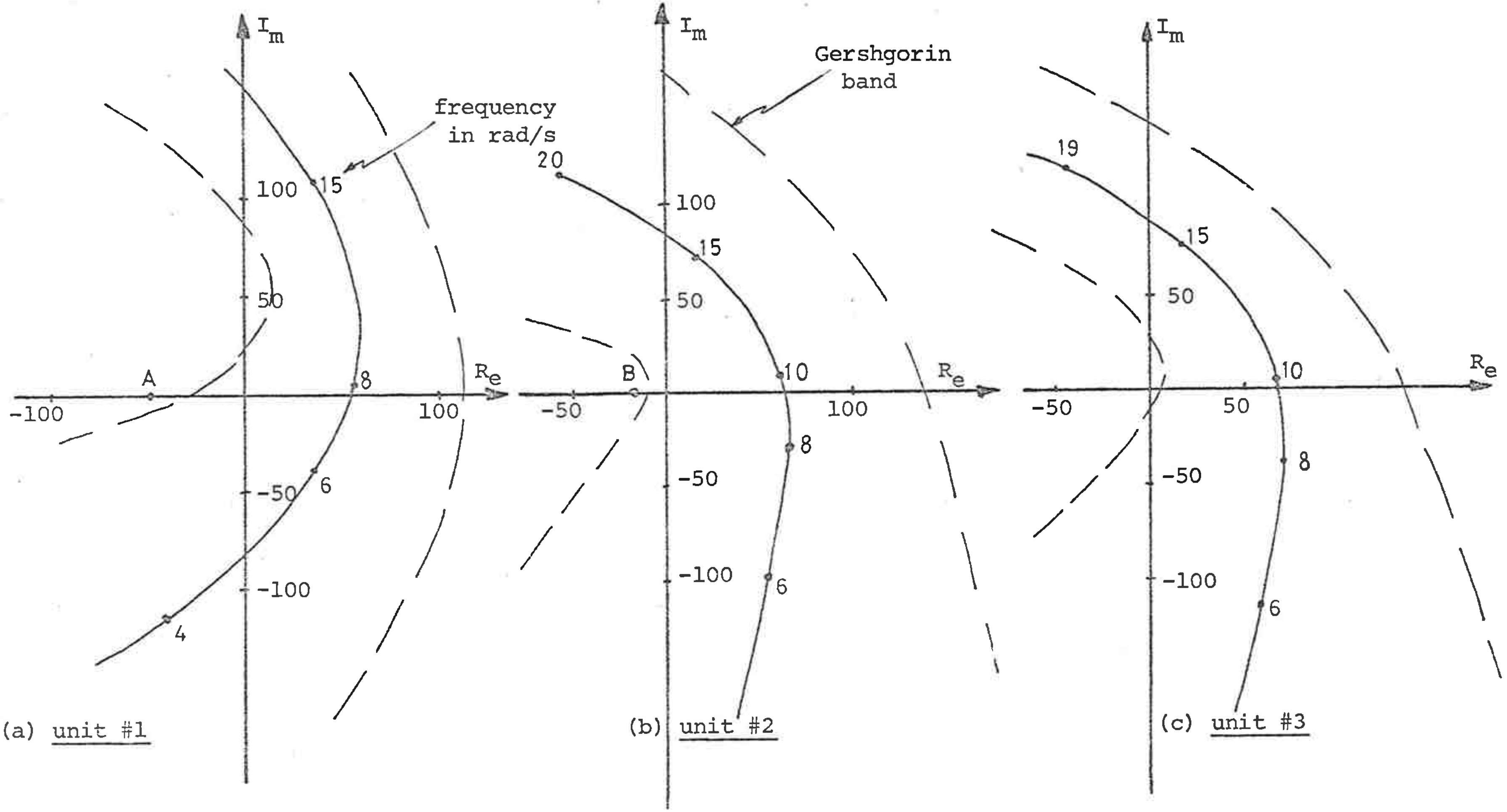

FIGURE 8.14 INA FOR POWER FEEDBACK LOOPS WITH SYSTEM UNDER HEAVY LOAD
($PP/4/AG/Ff_V/B$ controllers using x_e = 0.3 p.u. for gain calculations)

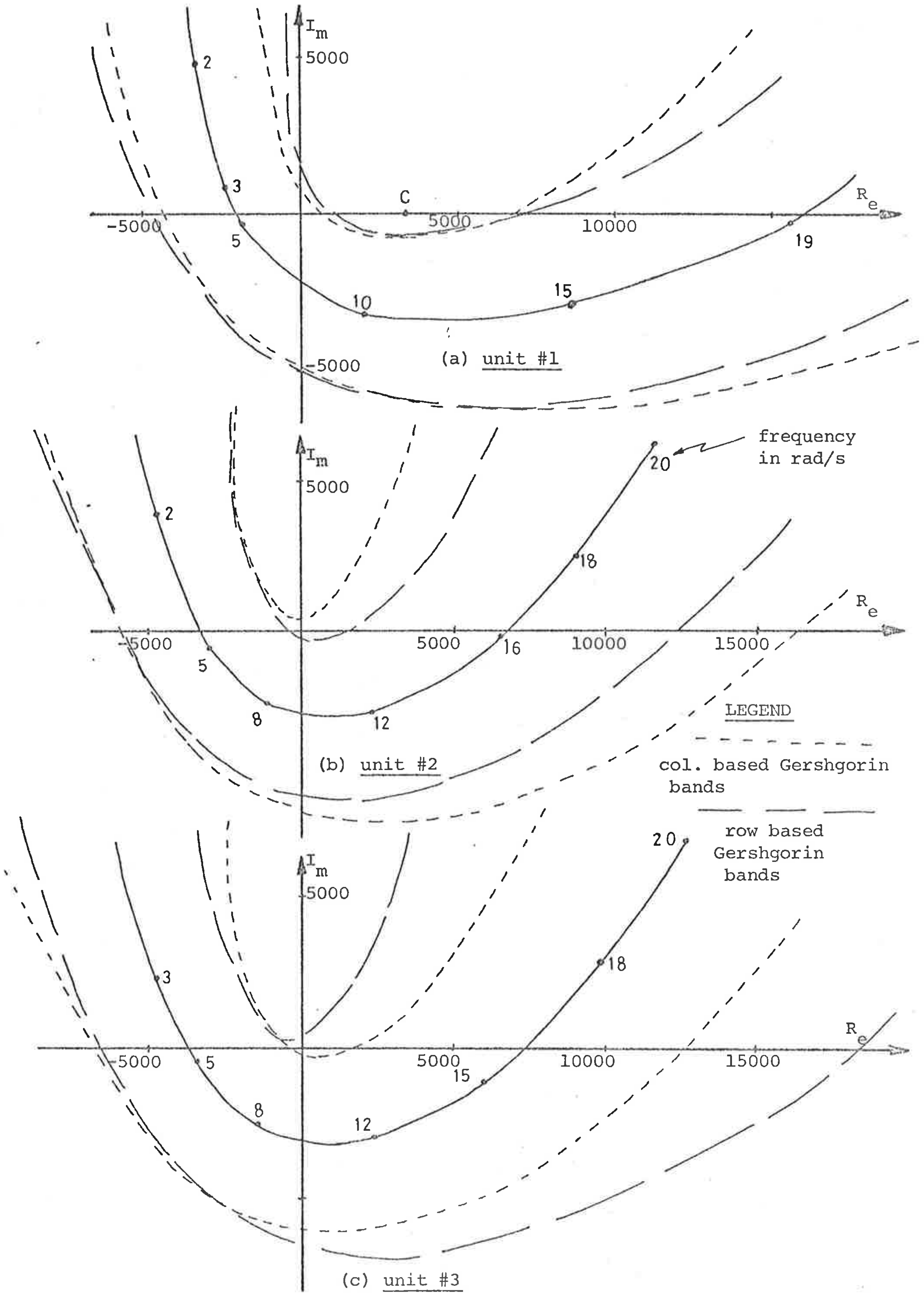

FIGURE 8.15 INA FOR SPEED LOOPS WITH SYSTEM UNDER HEAVY LOAD
(PP/4/AG/Ff$_v$/B controllers using x_e = 0.3 p.u. for gain calculations)

for unit #1 lies close to the part of the locus corresponding to the 4.6 rad/s mode and that an increase in speed gain for unit #1 will move the critical point away from the locus and thus improve the damping. Figures 8.16 and 8.17 show the INA's which result when the feedback gains are modified so that the critical points in Figures 8.14(a), 8.14(b) and 8.15(a) lie at A, B and C respectively.

Comparison of the new INA's with the previous ones shows that:

(i) The radius of each Gershgorin band at any given frequency is the same for either set of gains (see proof in Appendix 10.7).

(ii) The loci for unit #3 are the same in each case because the gains for this unit are not altered (compare Figure 8.14(c) with 8.16(c) and Figure 8.15(c) with 8.17(c)).

(iii) The modifying of the power feedback gain for unit #2 causes a translation of the locus in the power INA (Figures 8.14(b) and 8.16(b)) but a change of shape in the speed INA (Figures 8.15(b) and 8.17(b)).

(iv) Because both the speed and power feedback gains for unit #1 are altered, the corresponding speed and power loci are both translated and changed in shape. However, note (i) still applies.

The system with the modified gains is diagonally dominant for both the speed and power INA's. It may be noted that the speed INA in Figure 8.17 is column diagonally dominant but not row diagonally dominant (see section 8.5.2).

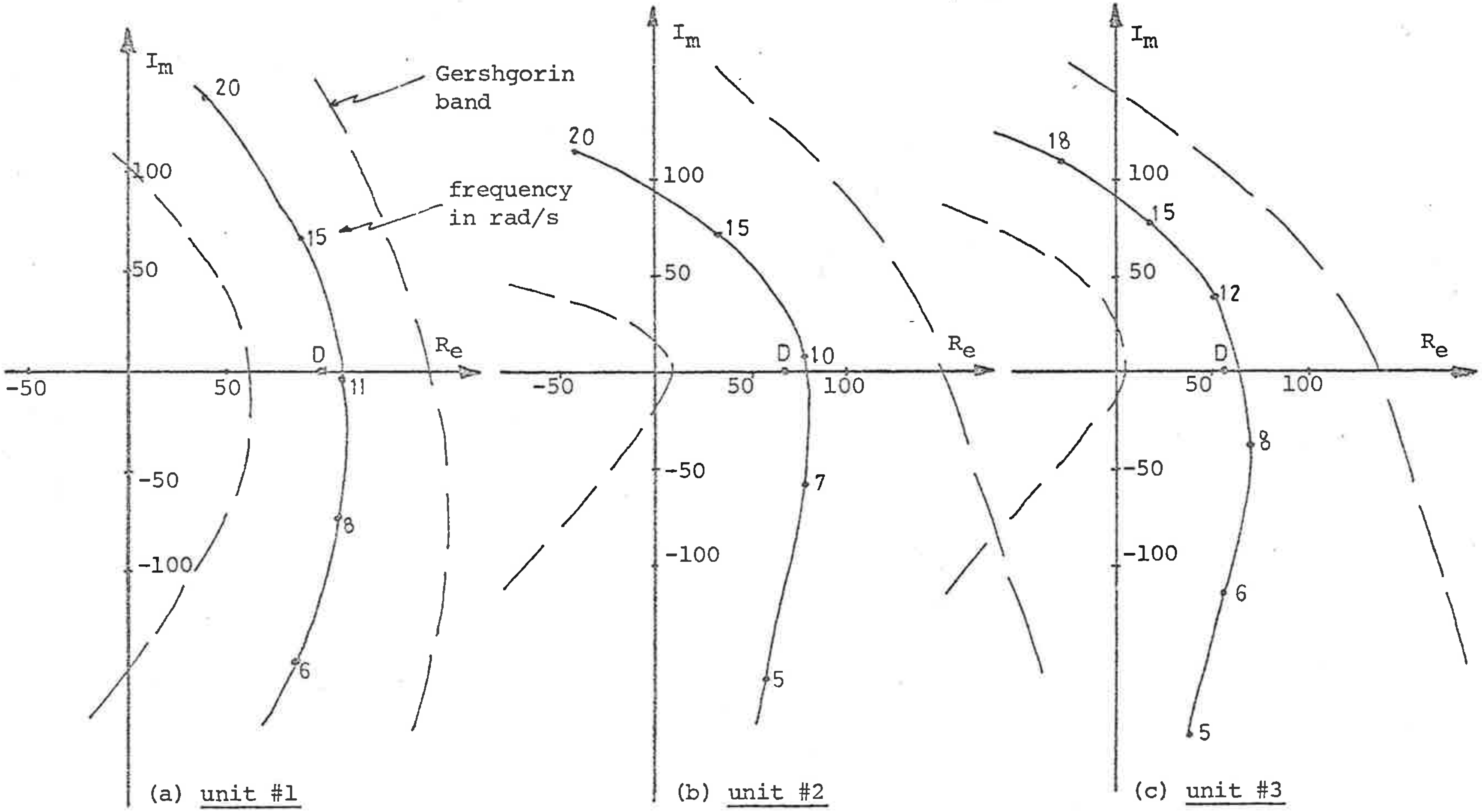

FIGURE 8.16 INA FOR POWER FEEDBACK LOOPS WITH SYSTEM UNDER HEAVY LOAD
(Controller gains modified as described in section 8.4.2)

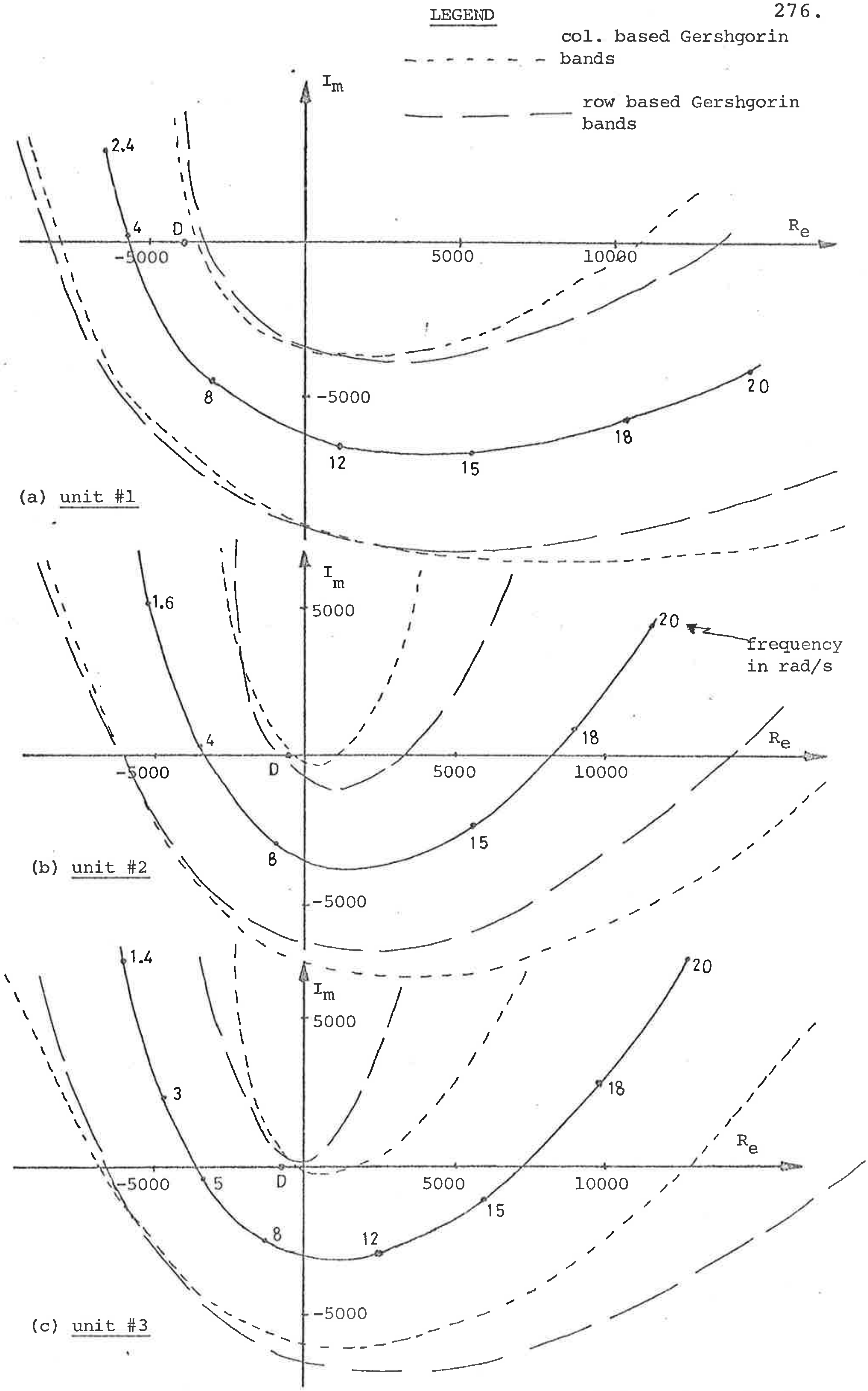

FIGURE 8.17 INA FOR SPEED FEEDBACK LOOPS WITH SYSTEM UNDER HEAVY LOAD
(Controller gains modified as described in section 8.4.2)

Comparison of the eigenvalues in rows 2 and 3 of Table 8.6 shows that the damping is considerably improved with these gains. This improvement is also evident in Figures 8.13(b) and (c).

The INA in Figures 8.16 and 8.17 provide no information concerning stability in the event of transducer failure. In Figure 8.16 the points corresponding to zero feedback gain are marked D; these lie inside the Gershgorin bands and so close to the loci that they also lie inside the Ostrowski band unless unrealistically high gains are used. In Figure 8.17 these points are also inside the Gershgorin bands - in this case the Ostrowski band radius cannot be made significantly smaller than the Gershgorin band for frequencies of interest because the critical points for units #2 and #3 lie close to the Gershgorin band. If integrity information is required this must be obtained using eigenvalue analysis.

The INA in Figures 8.16 and 8.17 do provide useful information because it may be deduced that:

(i) Damping at low frequencies may be improved further if necessary by increasing the speed feedback gains for units #1 and #3 (see row 4 of Table 8.6).

(ii) Interaction may be reduced and damping improved by the increasing of the power feedback gains for units #2 and #3.

8.4.3 The effect of omitting T'_{qo} from the generator models

Comparison of the eigenvalues in rows 2 and 5 of Table 8.5 and of the time responses in Figures 8.13(b) and (d) shows that when the system operates as shown in Figure 8.12 with PP/4/AG/Ff$_v$/B controllers, the neglect of T'_{qo} has a negligible effect on performance. This result is consistent with the SMIB cases in which δ is close to 90° (section 5.2.2).

8.5 EXAMPLE 4: OPERATION WITH LIGHT LOADS

In this section the generator loads are chosen so that they are in the "normal" operating region but somewhat smaller than those of the previous section (see Figure 8.18 for details of the network and loads).

8.5.1 Comparison of performance with fixed-gain and adjustable-gain controllers

Comparison of the eigenvalues in rows 1 and 2 of Table 8.7 or of the time responses in Figures 8.19(a) and (b) shows that there is no significant difference in the performance with the PP/4/FG/B and PP/4/AG/Ff_v/B control strategies. Again, this result is consistent with the behaviour of the SMIB system for near unity p.f. loads.

It is evident from the time responses and eigenvectors that there is a lightly-damped low frequency group mode of oscillation similar to that in section 8.3. It should be noted that in contrast to the previous case units #2 and #3 are distant from the load centre and most affected by this mode; the performance could be improved by redesigning the controllers for these units using a higher value of x_e (see section 8.6). The alternative method of inspecting the inverse Nyquist array to assess the gain changes required for improved performance is used.

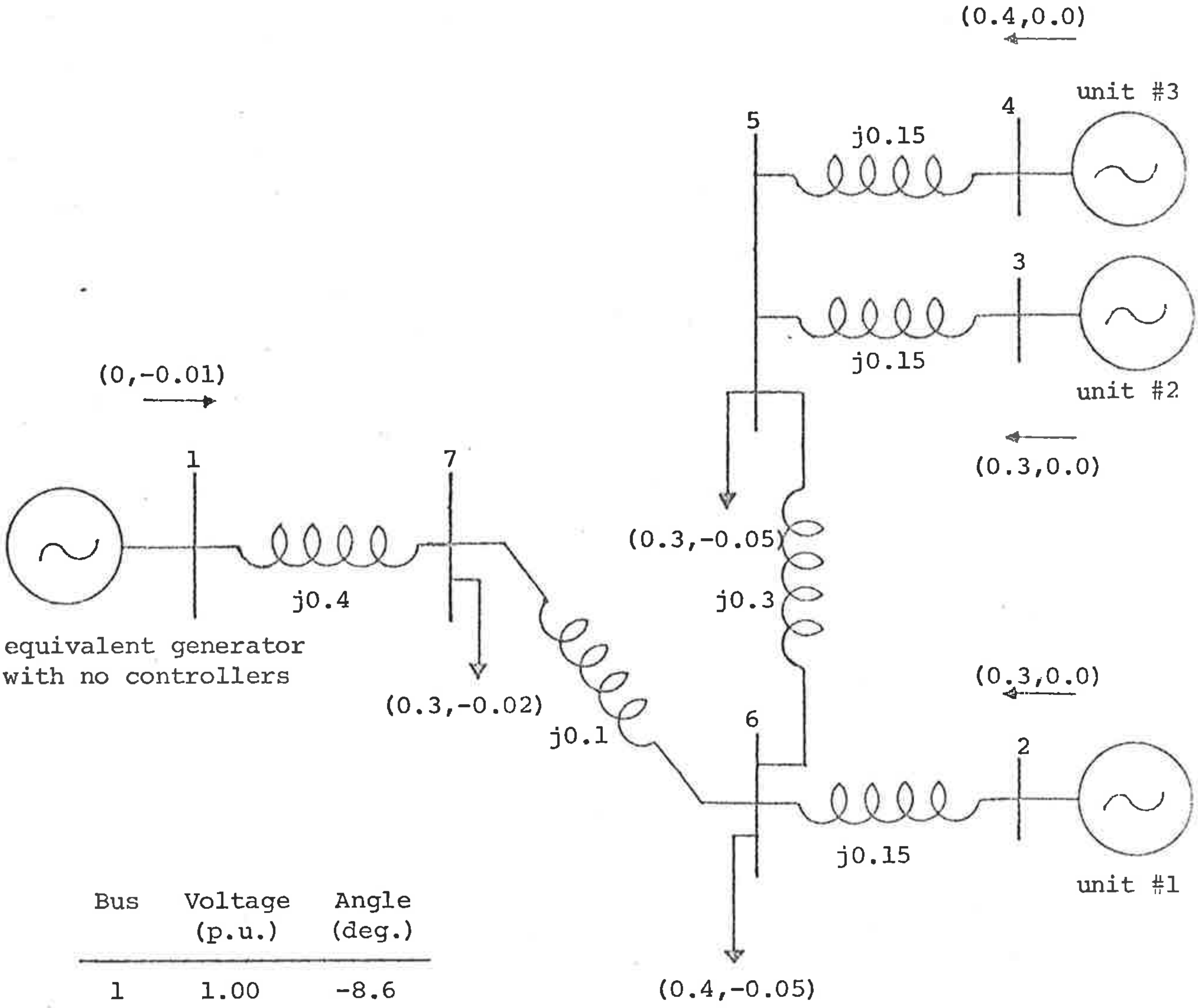

Bus	Voltage (p.u.)	Angle (deg.)
1	1.00	-8.6
2	1.00	-4.3
3	1.00	2.6
4	1.00	3.4
5	1.00	0.0
6	1.00	-6.9
7	1.00	-8.6

Figures in brackets indicate real and reactive power flow.

Generator data is identical for units #1, #2 and #3 (column BB of Table 5.1).

FIGURE 8.18 LOAD AND NETWORK DATA FOR SECTION 8.5
(Example 4 : Light load)

row no.	case	f_v	f_s	f_p	f_F	unit #
1	PP/4/FG/B fixed-gain controller on each unit	100	478	-49.1	-0.65	1
		100	478	-49.1	-0.65	2
		100	478	-49.1	-0.65	3
2	PP/4/AG/Ff_v/B adjustable-gains for each unit ("nominal" case)	100	901	-39.1	-0.43	1
		100	897	-38.9	-0.43	2
		100	500	-36.8	-0.46	3
3	modified gains chosen by INA analysis	100	4470	-67.5	-0.43	1
		100	897	-53.1	-0.43	2
		100	500	-51.4	-0.46	3
4	gains further modified by INA analysis	100	4470	-67.5	-0.43	1
		100	897	-53.1	-0.43	2
		100	2320	-51.4	-0.46	3
5	PP/4/AG/Ff_v/B gains (no T'_{qo} in generator models)	100	901	-39.1	-0.43	1
		100	897	-38.9	-0.43	2
		100	500	-36.8	-0.46	3

Rows continued on page below to show corresponding modes.

row no.	MODE A s_{1A}	MODE A s_{2A}	MODE A s_{3A}	MODE B s_{1B}	MODE B s_{2B}	MODE B s_{3B}	MODE C s_{1C}	MODE C s_{2C}	MODE C s_{3C}
1	$-0.88 \pm j4.95$			$-2.99 \pm j8.23$			$-4.88 \pm j11.98$		
	$.180\angle 3$	$.201\angle 7$	$.203\angle 6$	$.252\angle 167$	$.119\angle -23$	$.112\angle -28$	$.004\angle -104$	$.269\angle -38$	$.263\angle 138$
2	$-1.01 \pm j5.14$			$-2.79 \pm j9.05$			$-3.80 \pm j12.07$		
	$.176\angle 4$	$.200\angle 7$	$.225\angle 6$	$.209\angle 161$	$.088\angle -27$	$.096\angle -37$	$.014\angle 131$	$.284\angle -33$	$.245\angle 145$
3	$-1.32 \pm j5.22$			$-3.68 \pm j12.64$			$-4.98 \pm j13.19$		
	$.090\angle -5$	$.256\angle 9$	$.295\angle 6$	$.098\angle 162$	$.022\angle -87$	$.024\angle -44$	$.028\angle 43$	$.238\angle -50$	$.212\angle 129$
4	$1.78 \pm j5.36$			$-3.62 \pm j12.89$			$-3.84 \pm j13.47$		
	$.126\angle 1$	$.376\angle 10$	$.273\angle 14$	$.269\angle 102$	$.156\angle -159$	$.120\angle -42$	$.017\angle -106$	$.310\angle -12$	$.298\angle 143$
5	$-1.17 \pm j4.68$			$-3.45 \pm j7.07$			$-4.22 \pm j9.90$		
	$.202\angle 5$	$.190\angle 17$	$.219\angle 16$	$.326\angle 155$	$.166\angle -39$	$.182\angle -49$	$.020\angle -155$	$.320\angle -39$	$.293\angle 124$

NOTES: (1) For system data see Figure 8.18.

(2) Eigenvectors are weighted to show the response following an initial speed error for unit #2.

TABLE 8.7 EIGENVALUES AND EIGENVECTOR COMPONENTS FOR SECTION 8.5 (Example 4: Light load)

DATA FOR FIGURE 8.19

System data

Example 4: Light load (see Figure 8.18).

For (d), q-axis transient time-constant (T'_{qo}) omitted from generator models.

Disturbance applied

Step in voltage set-point for unit #2.

Feedback gains

(a): PP/4/FG/B fixed-gains - $f_v = 100$, $f_s = 478$, $f_p = -49.1$, $f_F = -0.65$ for all units.

(b) and (d): PP/4/AG/Ff_v/B adjustable-gains

unit #1 $f_v = 100$, $f_s = 901$, $f_p = -39.1$, $f_F = -0.43$

unit #2 $f_v = 100$, $f_s = 897$, $f_p = -38.9$, $f_F = -0.43$

unit #3 $f_v = 100$, $f_s = 500$, $f_p = -36.8$, $f_F = -0.46$

(c): modified gains

unit #1 $f_v = 100$, $f_s = 4470$, $f_p = -67.5$, $f_F = -0.43$

unit #2 $f_v = 100$, $f_s = 897$, $f_p = -53.1$, $f_F = -0.43$

unit #3 $f_v = 100$, $f_s = 500$, $f_p = -51.4$, $f_F = -0.46$

NOTE: Graphs show electrical power outputs in p.u. and are *not* drawn to the same scale.

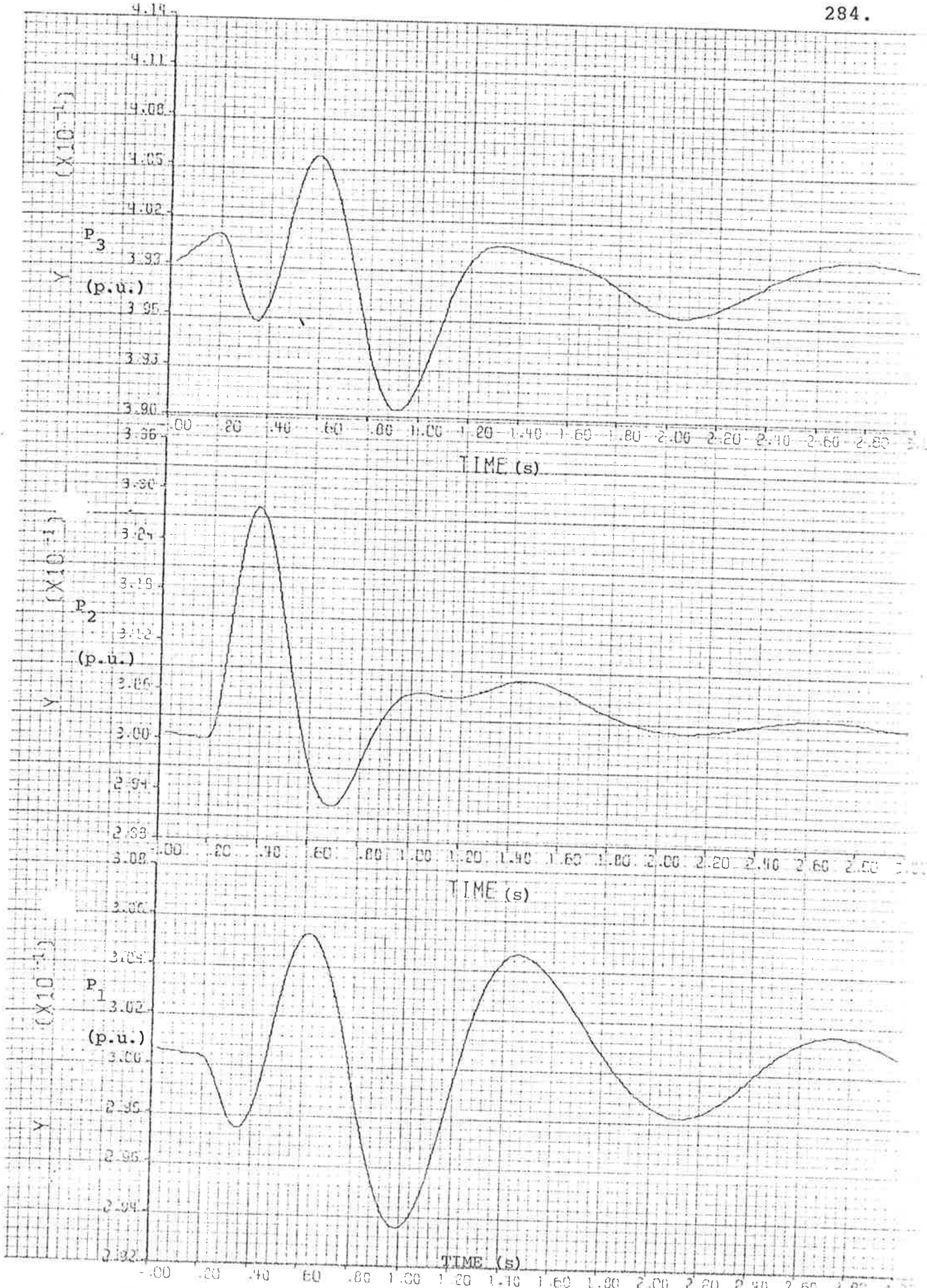

FIGURE 8.19(a) RESPONSE OF SYSTEM UNDER LIGHT LOAD TO A STEP IN V_{ref2}

(PP/4/FG/B gains)

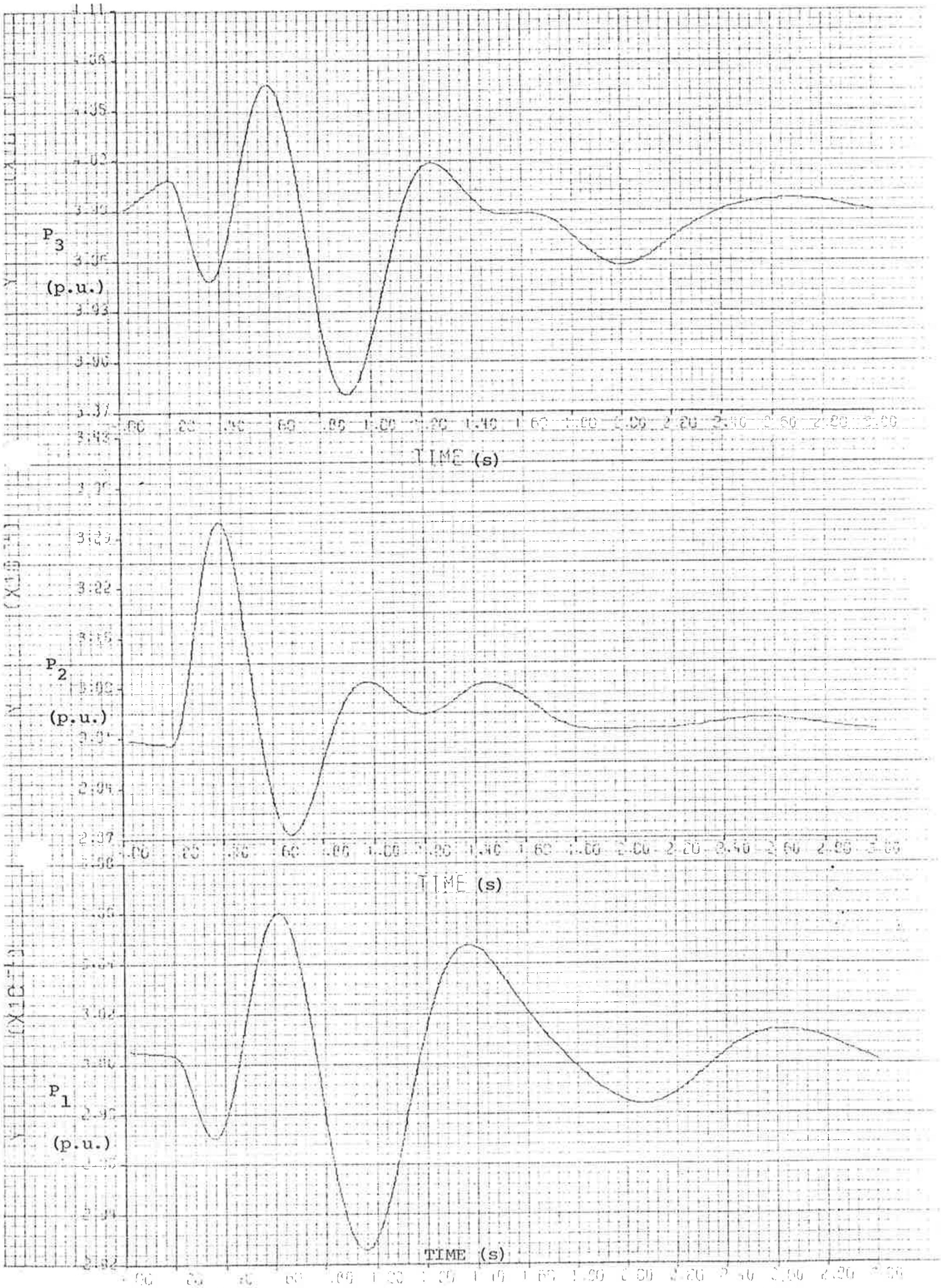

FIGURE 8.19(b) RESPONSE OF SYSTEM UNDER LIGHT LOAD TO A STEP IN V_{ref2}

($PP/4/AG/Ff_V/B$ gains)

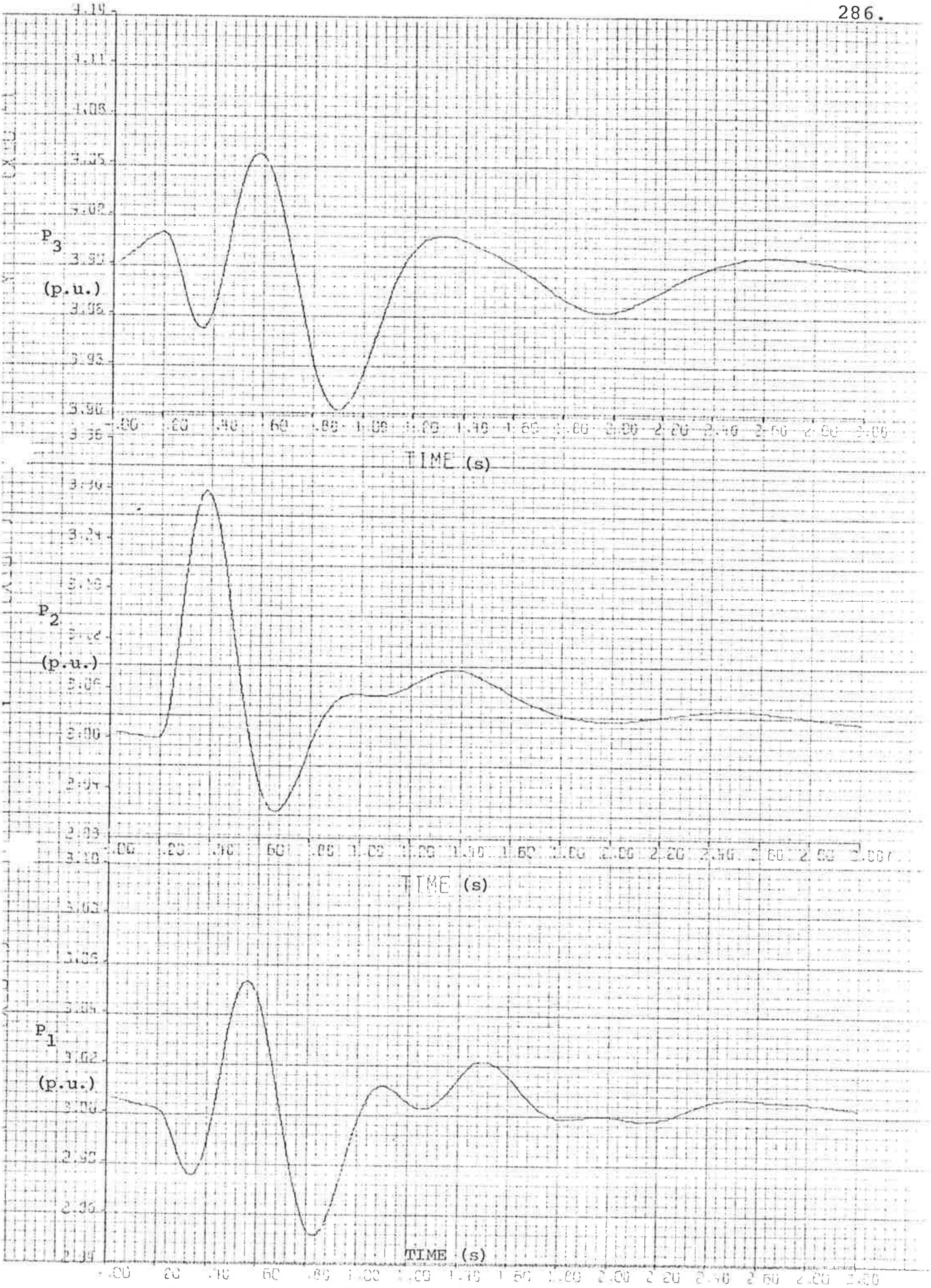

FIGURE 8.19(c) RESPONSE OF SYSTEM UNDER LIGHT LOAD TO A STEP IN V_{ref2}
(gains modified as described in section 8.5.2)

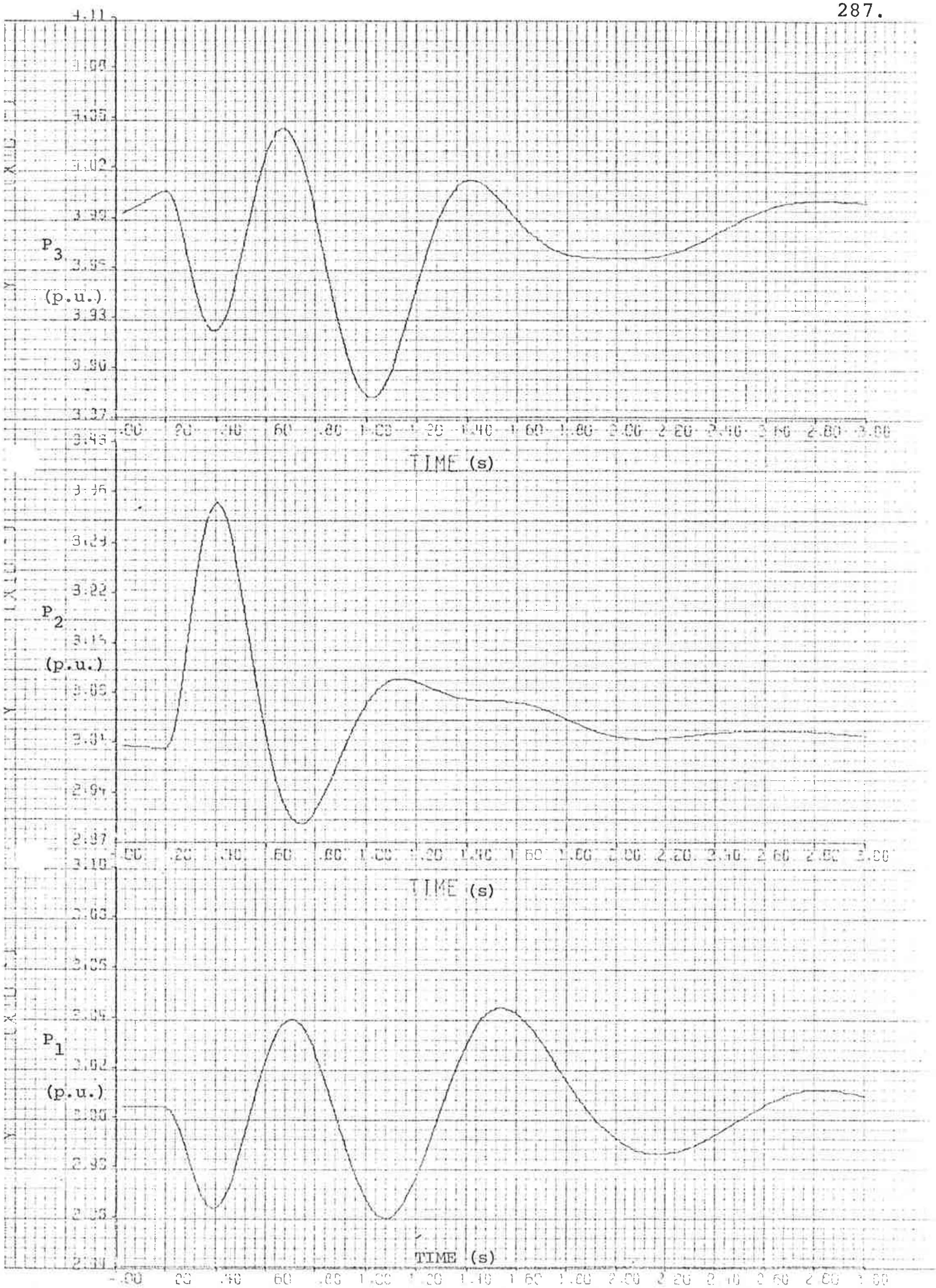

FIGURE 8.19(d) RESPONSE OF SYSTEM UNDER LIGHT LOAD TO A STEP IN V_{ref2}
(PP/4/AG/Ff_V/B gains, T'_{qo}, omitted from generator models)

8.5.2 INA analysis of feedback gain settings

The inverse Nyquist arrays for the electrical power and shaft speed feedback loops are plotted in Figures 8.20 and 8.21 for the multimachine system at light load with PP/4/AG/Ff_v/B controllers. Although the power loop INA in Figure 8.20 is not diagonally dominant, it is not evident that there is poor performance due to a lightly damped oscillatory mode. In order to achieve diagonal dominance the power feedback gain for unit #1 is increased so that the critical point in Figure 8.20(a) lies at A. Suppose the gains for units #2 and #3 are also increased so that the critical points lie at B and C respectively; the damping should improve because each critical point is more distant from the locus.

The INA for the speed loops is shown in Figure 8.21. The Gershgorin bands calculated from the rows and the columns are both drawn in this diagram; in most of the examples presented previously, either row-based bands only or column-based bands only are indicated for simplicity. The position of the critical points near the low frequency part of the locus in Figures 8.21(a) and (c) suggests that the damping at such frequencies may be poor. The speed feedback gain for unit #1 is increased so that the critical point in Figure 8.21(a) lies at D.

The inverse Nyquist arrays with the modified gains are plotted in Figures 8.22 and 8.23. The corresponding eigenvalues are listed in row 3 of Table 8.7 and it may be

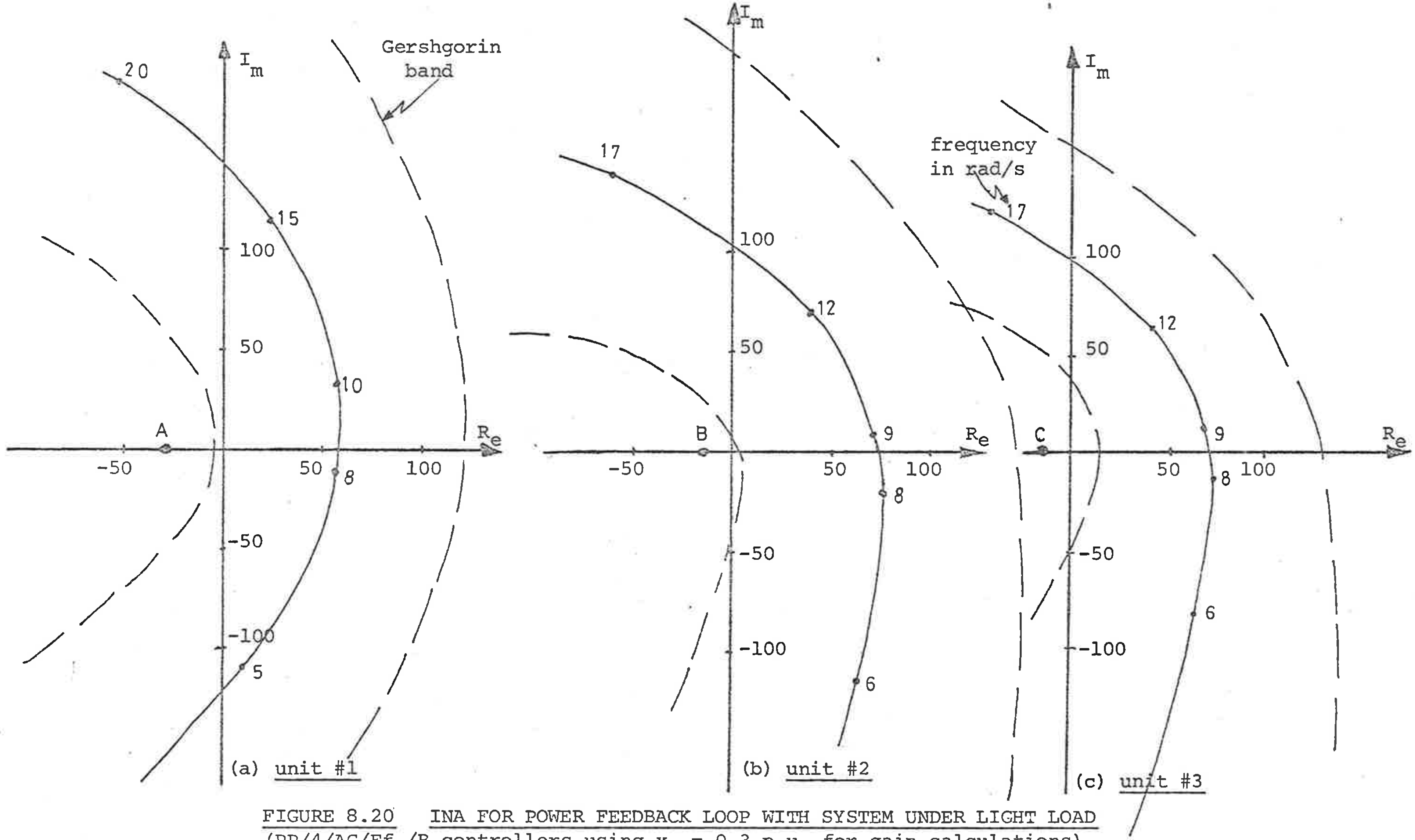

FIGURE 8.20 INA FOR POWER FEEDBACK LOOP WITH SYSTEM UNDER LIGHT LOAD
(PP/4/AG/Ff$_v$/B controllers using x_e = 0.3 p.u. for gain calculations)

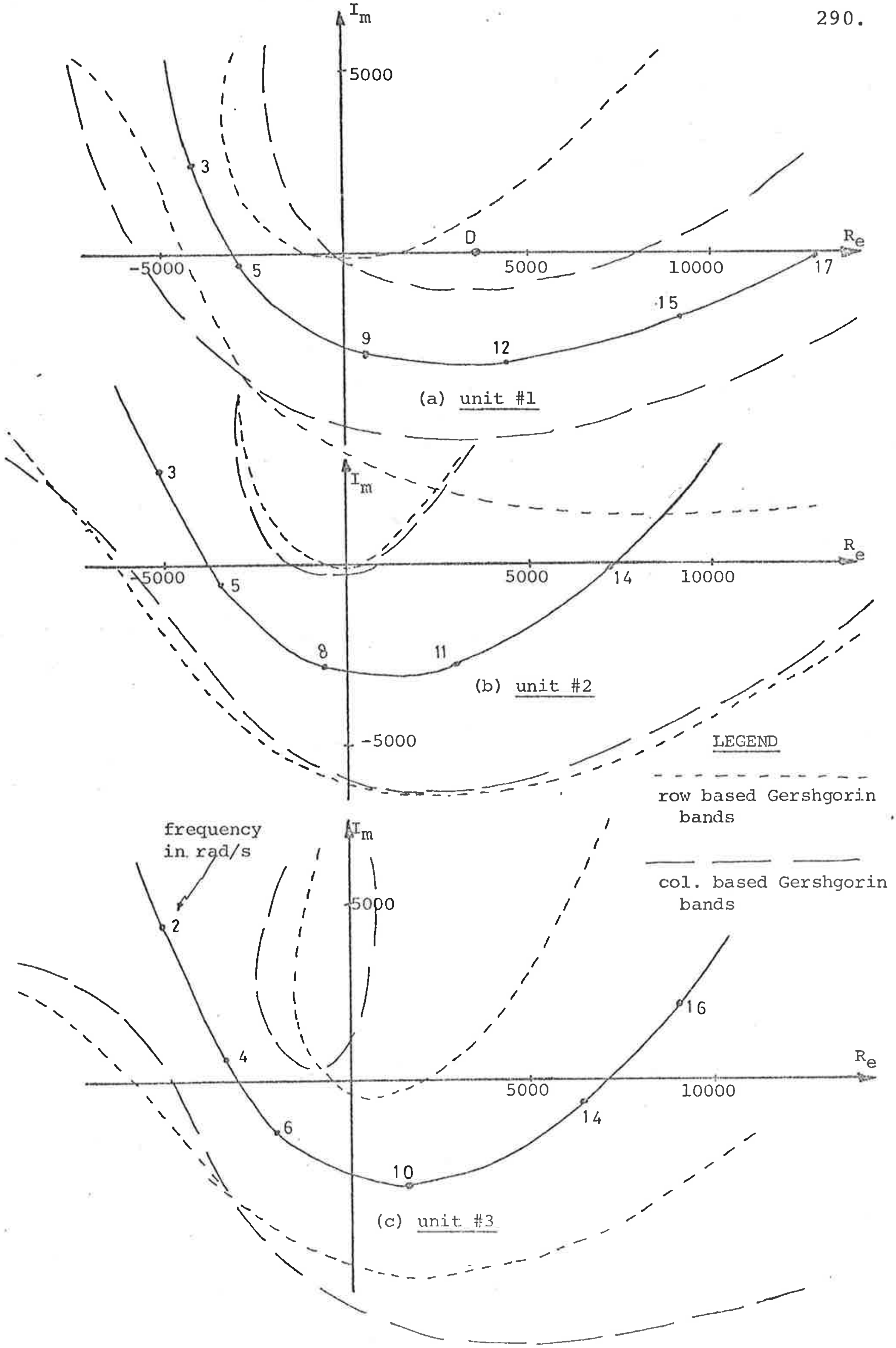

FIGURE 8.21 INA FOR SPEED FEEDBACK LOOP WITH SYSTEM UNDER LIGHT LOAD
(PP/4/AG/Ff_v/B controllers using x_e = 0.3 p.u. for gain calculations)

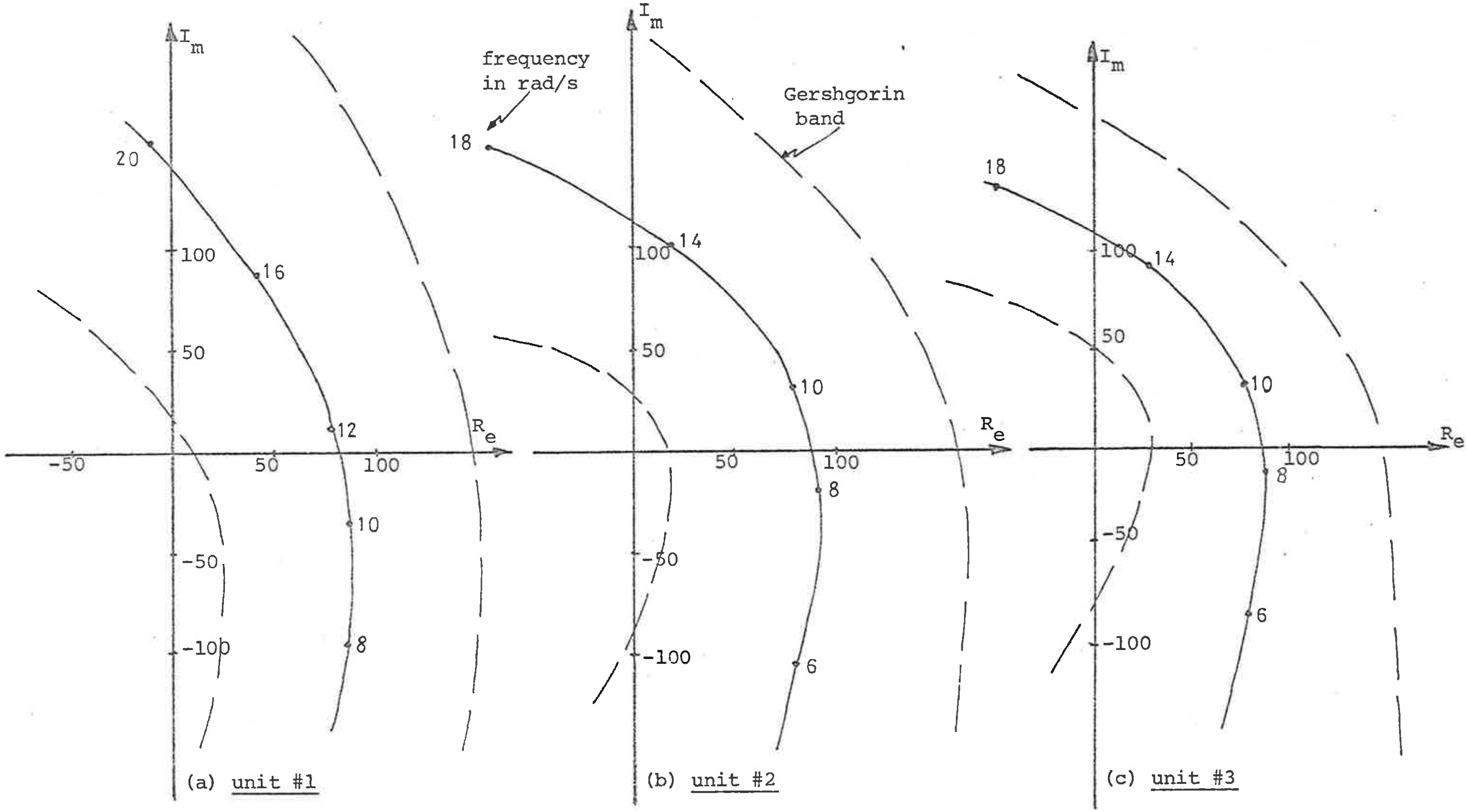

FIGURE 8.22 INA FOR POWER FEEDBACK LOOPS WITH SYSTEM UNDER LIGHT LOAD
(Controller gains modified as described in section 8.5.2)

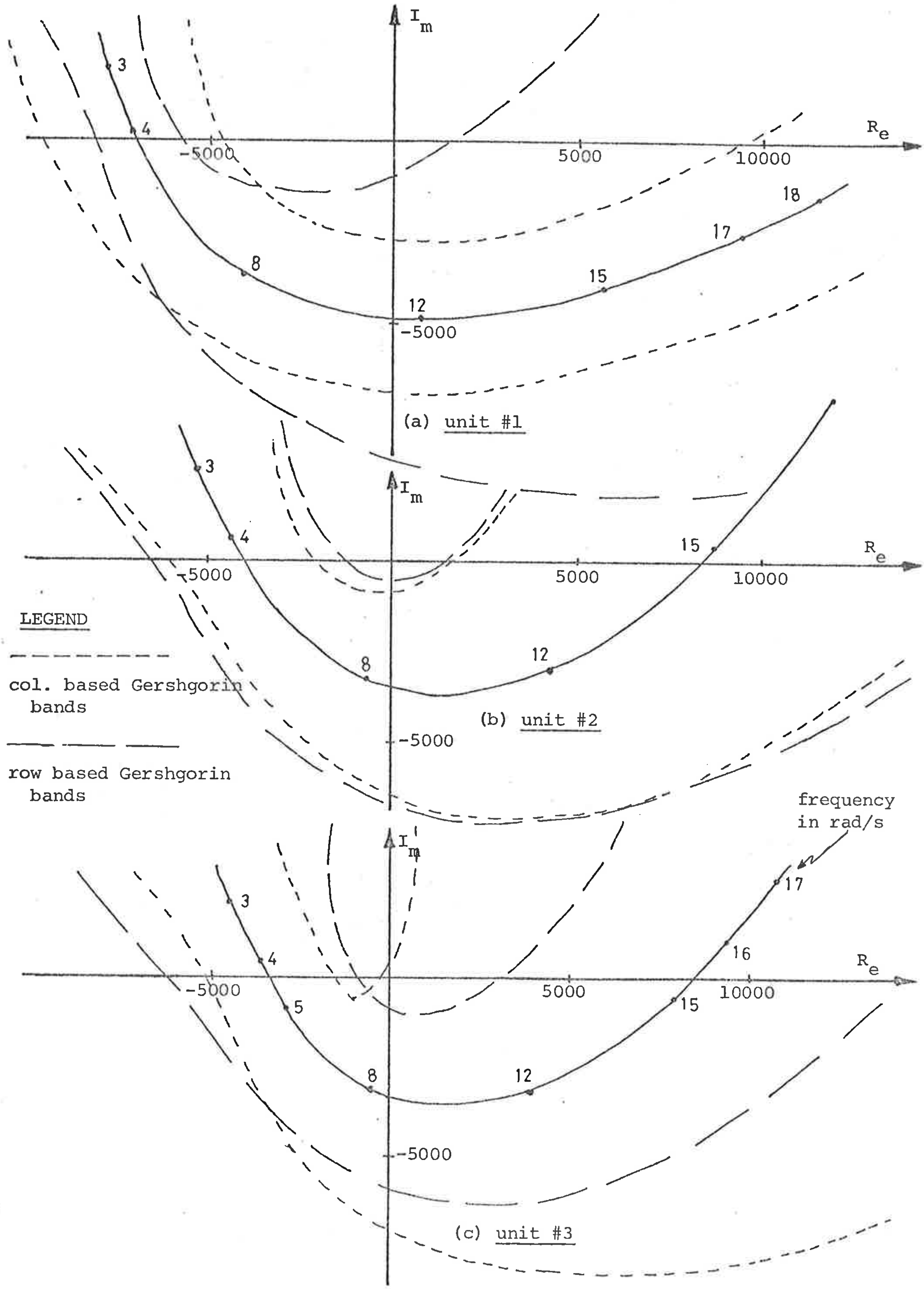

FIGURE 8.23 INA FOR SPEED FEEDBACK LOOPS WITH SYSTEM UNDER LIGHT LOAD
(Controller gains modified as described in section 8.5.2)

seen that damping has been improved. Comparison of the time responses in Figures 8.19(b) and (c) shows that in addition to this improvement in damping, interaction is slightly reduced because the amplitudes of the perturbations to the power outputs of units #1 and #3 are reduced when unit #2 is disturbed.

It may be noted in Figure 8.17 that the speed INA is column diagonally dominant but not row diagonally dominant. The row based Gershgorin bands suggest that the speed gains for units #1 and #3 should be increased to place the critical points in the centre of the "STABLE" region between the bands. On the other hand such a movement places the critical points deeper into the column based Gershgorin bands. The reason behind the conflicting indications is that the column-based bands are related to the columns of the transfer function matrix and hence convey the effect a given input has on all other loops, but the row-based bands are related to the rows and therefore convey the effect that inputs from other loops have on a given output. Because the interaction between generators is not reciprocal (Moussa [24]), the gain setting which minimises the disturbance to other loops need not be the same as that which minimises the effect from other loops.

If the performance with the modified gain values is not adequate, the INA in Figures 8.22 and 8.23 allows insight into modifications which may further improve performance. For example, suppose the damping at low frequencies is to be increased. Because the critical point in Figure 8.23(c) is fairly close to the locus at these frequencies, an increase in speed feedback gain for unit #3 moves the critical point from the origin to the point E, increasing the distance of closest approach and hence improving the damping (see row 4 of Table 8.7).

8.5.3 The effect of omitting T'_{qo} from the generator models

The effect of neglecting T'_{qo} may be observed by comparing Figures 8.19(b) and (d) or the eigenvalues in rows 2 and 5 of Table 8.7; the magnitude of error introduced appears to be about the same as that in section 8.3 at the leading power-factor operating point. The increased error relative to the heavy load case in section 8.4 is consistent with the results of the SMIB case where the effect of the T'_{qo} time-constant is related to $\cos\delta$ (see section 5.2.2).

8.6 REVISED POLE-PLACEMENT DESIGNS

8.6.1 Preamble

The pole-placement designs using the PP/4/AG/Ff$_v$/B strategy provide suitable performance in the first two examples (sections 8.2 and 8.3), but require modification in the latter cases (sections 8.4 and 8.5) because there is a poorly damped mode of oscillation. The explanation for this difference in behaviour lies in the fact that the gains are calculated using a value of 0.3 p.u. for the tieline reactance (x_e) in the SMIB design model; this value of x_e is suitable to represent the transformer reactance plus the low network reactances in the first examples. In the later examples the network reactances are higher and result in poor damping for a group mode of oscillation, similar to that found in section 6.3. The changes to the feedback gain settings necessary for improved performance are found above by INA analysis. This section demonstrates that performance can also be improved in these cases by redesigning the controllers with a higher value of x_e.

8.6.2 Revised design for operation with heavy loads

A PP/4/FG/B fixed-gain controller is designed as in section 8.2.1 by assuming a design load of $\overline{P} = 0.9$ p.u. and $\overline{Q} = 0.1$ p.u. with $\overline{v}_t = 1$ p.u. However, the design value of x_e is increased from 0.3 p.u. to 0.5 p.u. The eigenvalues in row 4 of Table 8.8 show the dominant modes of oscillation when this controller is applied to units #1, #2 and #3 and the network reactances and loads are those of Figure 8.12. Comparison with row 1 reveals that increasing the design value of x_e from 0.3 p.u. to 0.5 p.u. produces a significant improvement in damping of the low frequency mode. This improvement is also evident in a comparison of the time responses in Figures 8.13(a) and 8.24(a).

The eigenvalues in row 5 of Table 8.8 and the time response in Figure 8.24(b) show the performance of the system when PP/4/AG/Ff_v/B adjustable-gain controllers designed using x_e = 0.5 p.u. are applied to units #1, #2 and #3. Comparison with row 4 of Table 8.8 and Figure 8.24(a) shows that, as in section 8.4, for this operating point the fixed- and adjustable-gain controllers have comparable performance.

Comparison of the eigenvalues in rows 4 and 5 of Table 8.8 with those in row 3 shows that the performance of the SMIB pole-placement designs using the revised value of x_e (0.5 p.u.) approaches that which is obtained by modifying the previous (x_e = 0.3 p.u.) gains on the basis of INA analysis.

Figure 8.25 shows the INA for the electrical power feedback loops of units #1, #2 and #3 when the revised PP/4/AG/Ff_v/B controllers are applied to the system. A modification is necessary to the gain setting for unit #2 in order to move the critical point in Figure 8.25(b) to the left and obtain diagonal dominance; the change in gain required is smaller than that required for the case with the pole-placement gains calculated using x_e = 0.3 p.u. (see Figure 8.14).

row no.	case	f_v	f_s	f_p	f_F	unit #
1	PP/4/FG/B gains	100	478	-49.1	-0.65	1
	calculated using	100	478	-49.1	-0.65	2
	x_e = 0.3	100	478	-49.1	-0.65	3
2	PP/4/AG/Ff_v/B gains	100	462	-50.1	-0.67	1
	calculated using	100	514	-52.5	-0.71	2
	x_e = 0.3	100	572	-57.2	-0.73	3
3	modified gains	100	5390	-100.0	-0.67	1
	(using INA analysis)	100	514	-69.5	-0.71	2
	section 8.4	100	1537	-57.2	-0.73	3
4	PP/4/FG/B gains	100	1722	-64.2	-0.72	1
	calculated using	100	1722	-64.2	-0.72	2
	x_e = 0.5	100	1722	-64.2	-0.72	3
5	PP/4/AG/Ff_v/B	100	1675	-61.8	-0.72	1
	calculated using	100	1872	-66.6	-0.76	2
	x_e = 0.5	100	2063	-68.2	-0.76	3
6	modified gain	100	1675	-61.8	-0.72	1
	using INA analysis	100	1872	-84.1	-0.76	2
	(section 8.6)	100	2063	-68.2	-0.76	3

Rows continued on page below to show corresponding modes.

row no.	MODE A S_{1A}	S_{2A}	S_{3A}	MODE B S_{1B}	S_{2B}	S_{3B}	MODE C S_{1C}	S_{2C}	S_{3C}
1	$-0.52 \pm j4.63$			$-3.72 \pm j8.66$			$-4.62 \pm j13.67$		
	$.199\angle{-4}$	$.137\angle{8}$	$.134\angle{7}$	$.328\angle{158}$	$.251\angle{-19}$	$.229\angle{-10}$	$.007\angle{93}$	$.228\angle{137}$	$.266\angle{-40}$
2	$-0.57 \pm j4.59$			$-3.96 \pm j8.58$			$-4.86 \pm j13.97$		
	$.206\angle{-4}$	$.141\angle{7}$	$.133\angle{5}$	$.355\angle{154}$	$.284\angle{-19}$	$.239\angle{-11}$	$.011\angle{109}$	$.215\angle{132}$	$.276\angle{-42}$
3	$-1.94 \pm j5.05$			$-4.97 \pm j12.49$			$-6.22 \pm j14.78$		
	$.100\angle{-12}$	$.278\angle{19}$	$.180\angle{27}$	$.201\angle{131}$	$.208\angle{168}$	$.376\angle{-56}$	$.108\angle{-88}$	$.079\angle{58}$	$.027\angle{158}$
4	$-1.80 \pm j4.73$			$-4.57 \pm j11.74$			$-4.15 \pm j15.35$		
	$.263\angle{4}$	$.188\angle{19}$	$.184\angle{20}$	$.210\angle{108}$	$.207\angle{-71}$	$.230\angle{-58}$	$.004\angle{66}$	$.189\angle{137}$	$.220\angle{-41}$
5	$-1.90 \pm j4.74$			$-4.44 \pm j11.93$			$-4.09 \pm j15.54$		
	$.275\angle{5}$	$.190\angle{16}$	$.179\angle{17}$	$.193\angle{107}$	$.207\angle{-70}$	$.217\angle{-57}$	$.006\angle{77}$	$.186\angle{137}$	$.229\angle{-42}$
6	$-1.85 \pm j4.66$			$-4.97 \pm j12.71$			$-4.96 \pm j16.29$		
	$.250\angle{7}$	$.184\angle{16}$	$.165\angle{20}$	$.189\angle{98}$	$.205\angle{-89}$	$.313\angle{-45}$	$.016\angle{-28}$	$.177\angle{127}$	$.150\angle{-68}$

NOTES: (1) The first three rows of this table are identical to rows 1, 2 and 4 of Table 8.6.

(2) For system data, see Figure 8.12.

(3) Eigenvectors are weighted to show the response following a 1 p.u. initial error in shaft speed for unit #3.

TABLE 8.8 EIGENVALUES AND EIGENVECTOR COMPONENTS FOR SYSTEM AT HEAVY LOAD

DATA FOR FIGURE 8.24

System data

Example 3: Heavy load (see Figure 8.12).

Disturbance applied

Step in voltage set-point for unit #3.

Feedback gains

(a): PP/4/FG/B fixed gains (based on x_e = 0.5 p.u. in SMIB design model)

$f_v = 100$, $f_s = 1722$, $f_p = -64.2$, $f_F = -0.72$

(b): PP/4/AG/Ff_v/B adjustable-gains (based on x_e = 0.5 p.u. in SMIB design model)

unit #1 $f_v = 100$, $f_s = 1675$, $f_p = -61.8$, $f_F = -0.72$

unit #2 $f_v = 100$, $f_s = 1872$, $f_p = -66.6$, $f_F = -0.76$

unit #3 $f_v = 100$, $f_s = 2063$, $f_p = -68.2$, $f_F = -0.76$

(c): As for (b) except $f_p = -84.1$ for unit #2.

NOTE: The graphs show electrical power outputs in p.u. and are *not* plotted to the same scale.

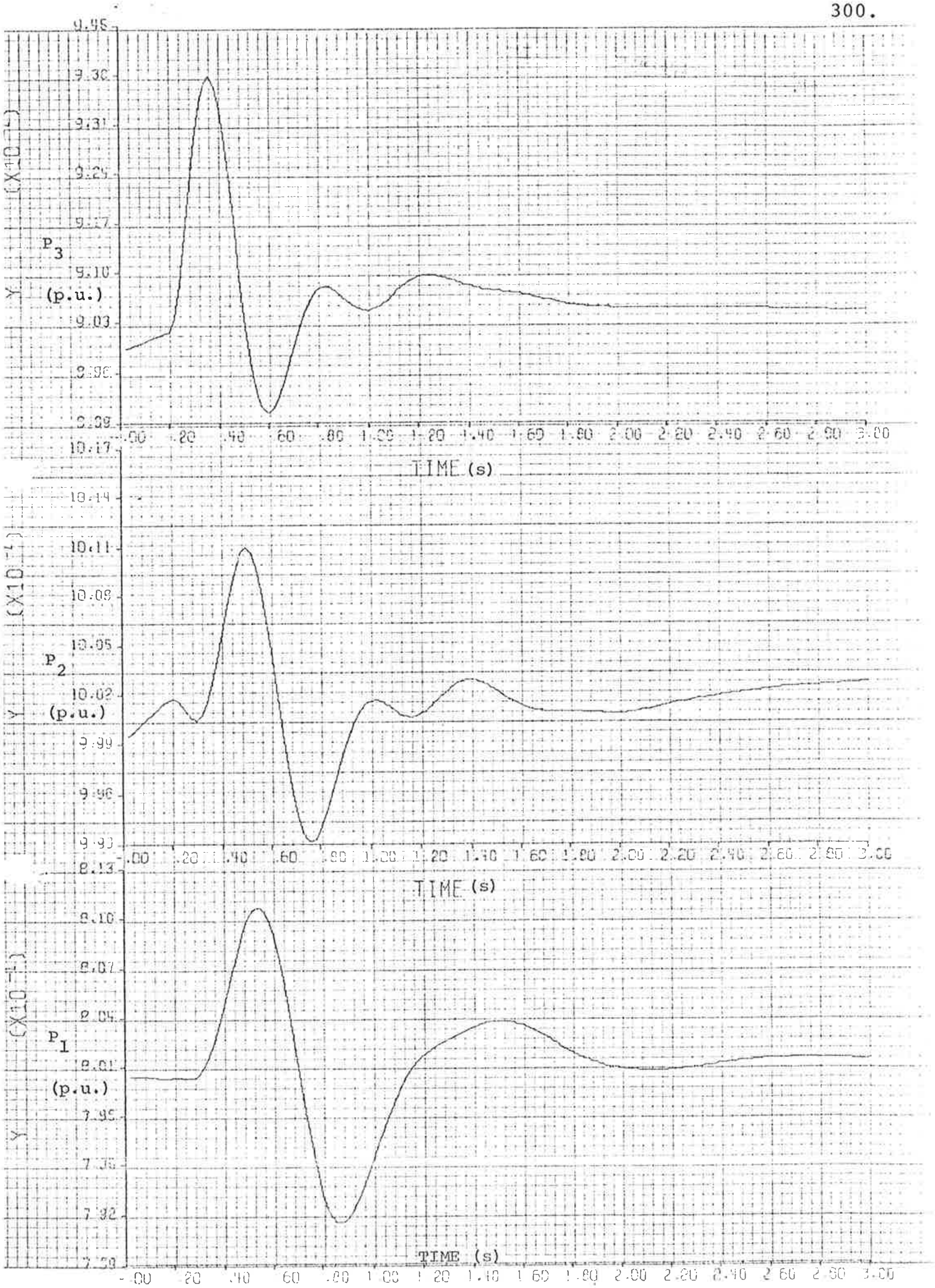

FIGURE 8.24(a) RESPONSE OF SYSTEM UNDER HEAVY LOAD TO A STEP IN V_{ref3}
(PP/4/FG/B gains calculated using x_e = 0.5 p.u.)

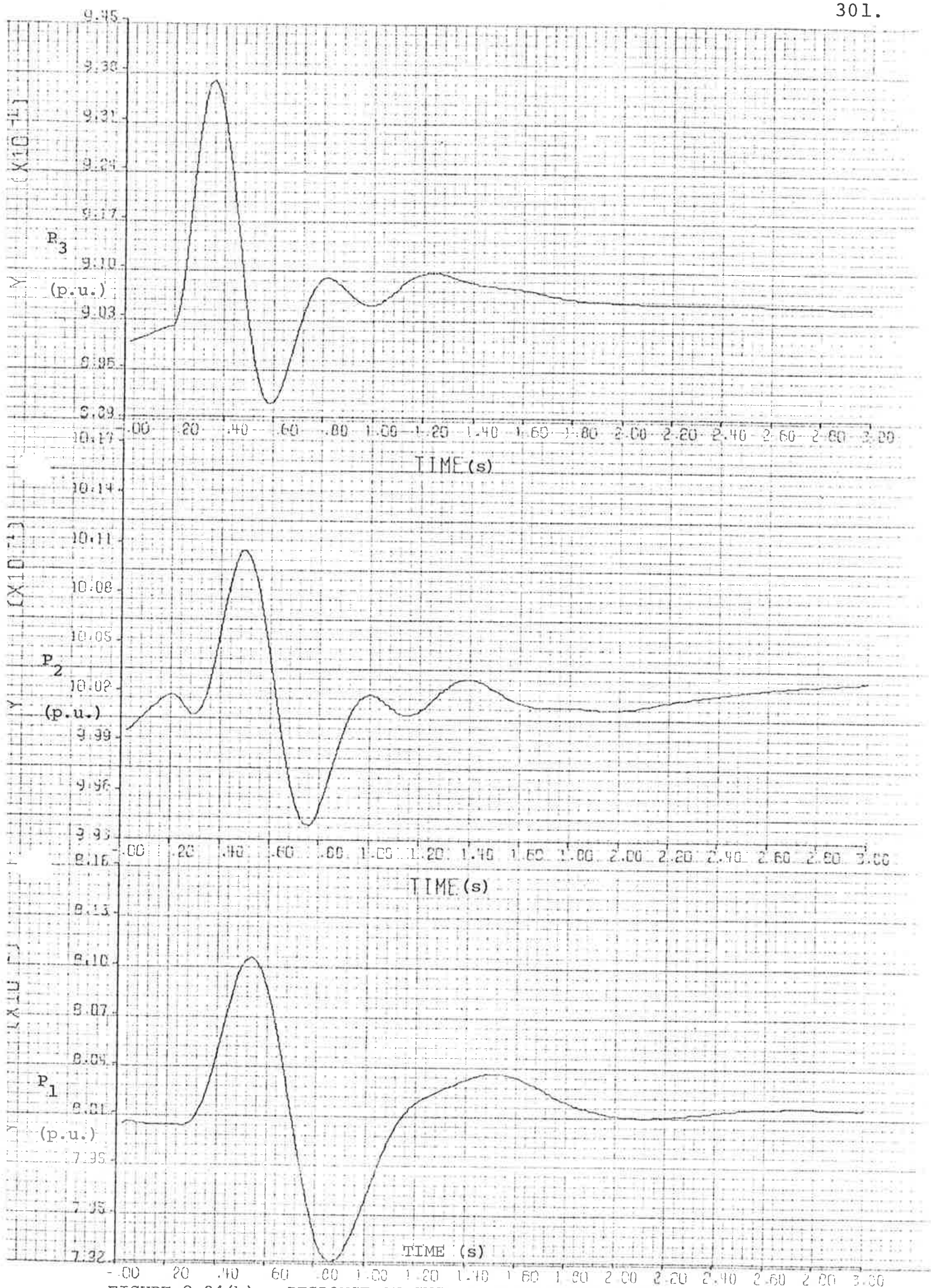

FIGURE 8.24(b) RESPONSE OF SYSTEM UNDER HEAVY LOAD TO A STEP IN V_{ref3}

(PP/4/AG/Ff_V/B gains calculated using x_e = 0.5 p.u.)

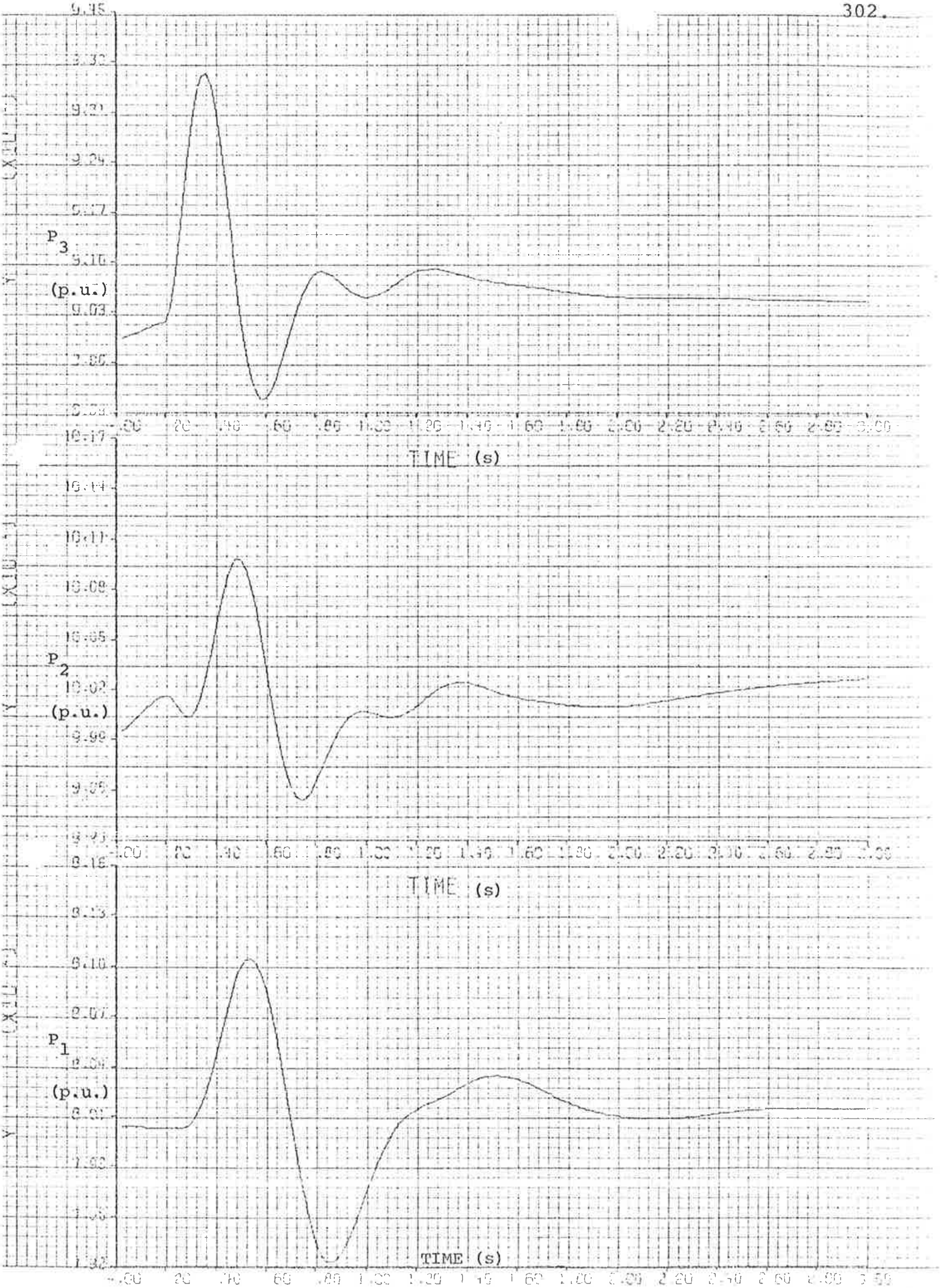

FIGURE 8.24(c) RESPONSE OF SYSTEM UNDER HEAVY LOAD TO A STEP IN V_{ref3}
($PP/4/AG/Ff_V/B$ gains calculated using x_e = 0.5 p.u. with f_p increased for unit #3)

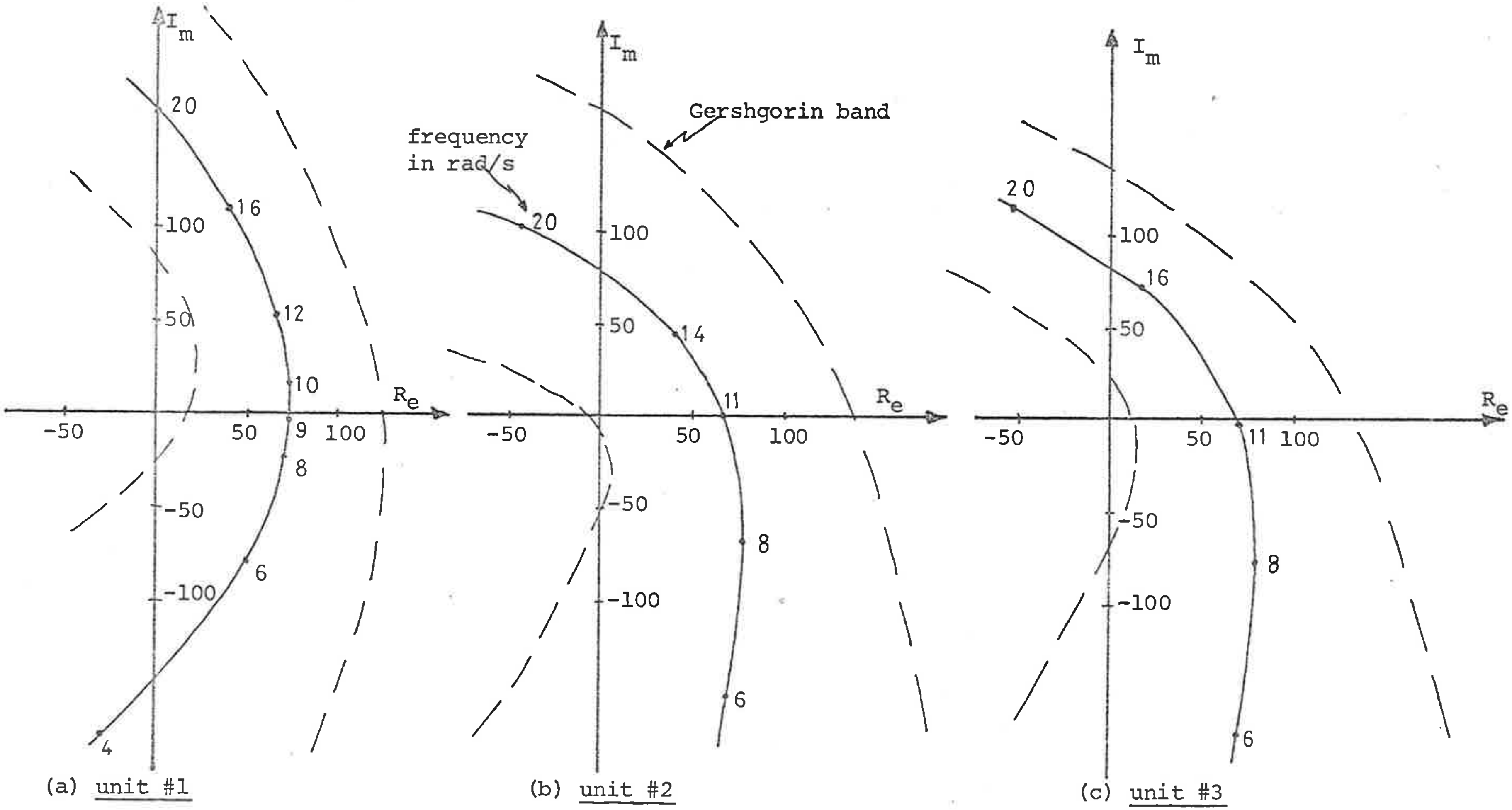

FIGURE 8.25 INA FOR POWER FEEDBACK LOOPS WITH SYSTEM UNDER HEAVY LOAD
(PP/4/AG/Ff_v/B controllers using x_e = 0.5 p.u. in gain calculations)

The INA for the shaft-speed feedback loops of the generators with the PP/4/AG/Ff$_v$/B controllers (x_e = 0.5 p.u. design) is plotted in Figure 8.26. The critical points for units #2 and #3 lie inside the higher frequency part of the Gershgorin band; inspection of the time response in Figure 8.24(b) reveals a corresponding mode of oscillation involving these units, whose damping could be improved (mode C in row 5 of Table 8.8). One way to achieve diagonal dominance is to decrease the speed feedback gain for unit #2 such that the critical point in Figure 8.26(b) moves to the left and column diagonal dominance results. Another method is to reduce the speed feedback gain for unit #3 so that the critical point in Figure 8.26(c) moves to the left and row diagonal dominance results. Both of these methods reduce the damping at lower frequencies because the critical point is moved towards this part of the locus. A superior method is to increase the power feedback gain for either or both of these generators so that the locus moves away from the critical point (compare Figure 8.15(b) and 8.17(b)).

The eigenvalues in row 6 of Table 8.8 describe the behaviour of the system when the magnitude of the power feedback gain for unit #2 is increased such that diagonal dominance is obtained with the critical point in Figure 8.25(b) lying at A. Comparison with the eigenvalues in row 5 shows that damping is improved at higher frequencies but deteriorates slightly at low frequency. Comparison of the corresponding time responses in Figures 8.24(b) and (c) reveals that overall performance is similar but the amplitude

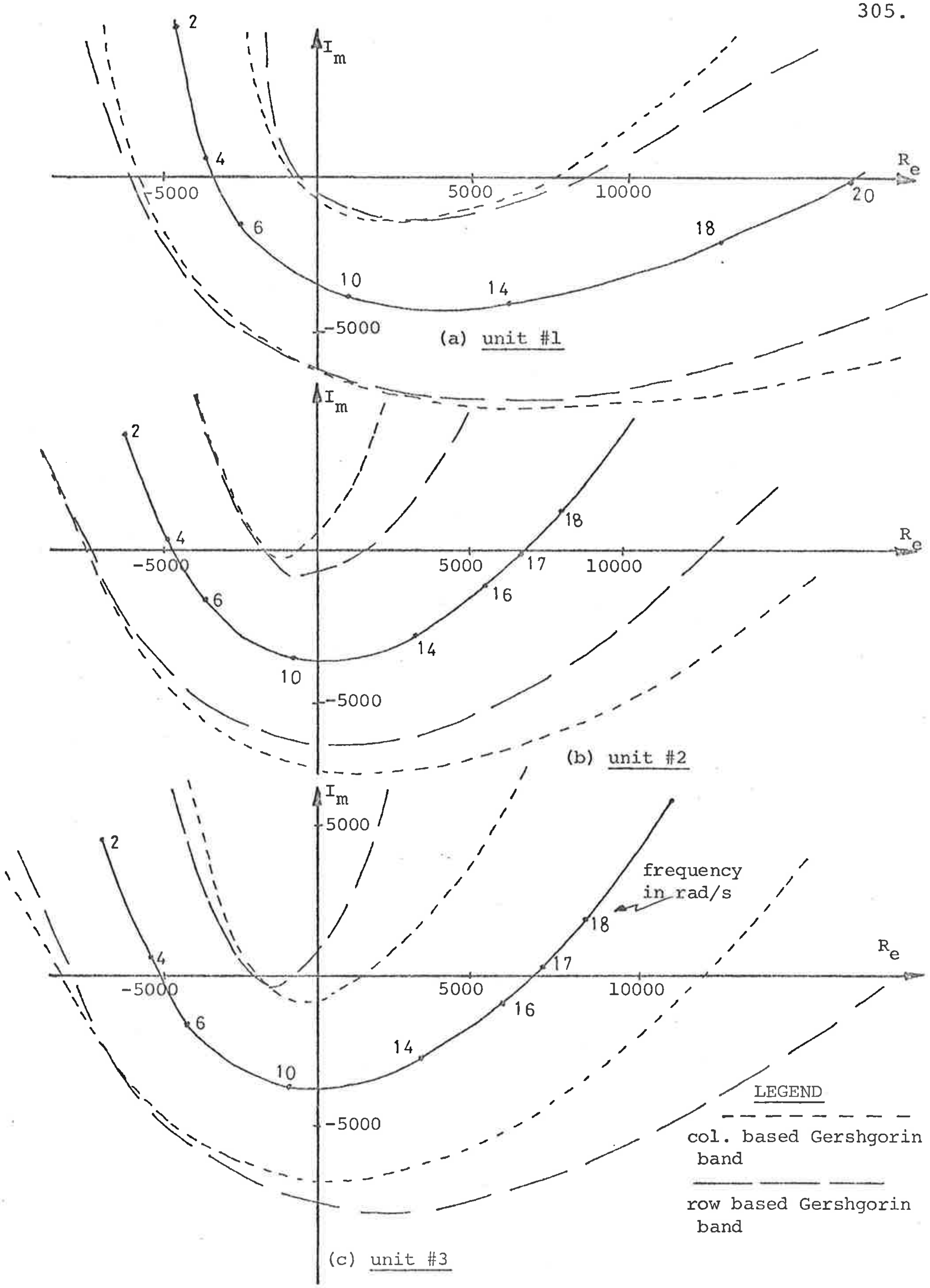

FIGURE 8.26 INA FOR SPEED FEEDBACK LOOPS WITH SYSTEM UNDER HEAVY LOAD
(PP/4/AG/Ff$_v$/B controllers using x_e = 0.5 p.u. in gain calculations)

of the disturbance to unit #2 is slightly reduced when the gains are set for diagonal dominance.

8.6.3 Revised designs for operation with light loads

Row 4 of Table 8.9 lists the eigenvalues of the system at light load (Figure 8.18) with the PP/4/FG/B fixed-gain controllers which are designed using a value of 0.5 p.u. for x_e in section 8.6.2. Comparison with row 1 which lists the eigenvalues with the previous fixed-gain design based on $x_e = 0.3$ p.u. shows that the damping is considerably improved. This improvement may be seen also in a comparison of the time responses in Figures 8.19(a) and 8.27(a).

The eigenvalues which result when adjustable-gain controllers, using a design value of 0.5 p.u. for x_e in the PP/4/AG/Ff$_v$/B strategy, are applied to units #1, #2 and #3 are listed in row 5 of Table 8.9. Comparison with row 2 reveals that the higher specified design value of x_e results in improved damping for the group mode of oscillation (mode A) but poorer damping for intermachine modes. Comparison of the time responses in Figures 8.19(b) and 8.27(b) shows that overall performance is improved.

In most instances, the performances of the fixed- and adjustable-gain strategies are comparable for normal loading conditions. However, in this case the performance with adjustable-gain controllers is inferior to that with fixed-gain controllers (compare rows 4 and 5 of Table 8.9 and the time responses in Figures 8.27(a) and (b)).

row no.	case	f_v	f_s	f_p	f_F	unit #
1	PP/4/FG/B gains with x_e = 0.3 p.u.	100	478	-49.1	-0.65	1
		100	478	-49.1	-0.65	2
		100	478	-49.1	-0.65	3
2	PP/4/AG/Ff$_v$/B gains with x_e = 0.3 p.u.	100	901	-39.1	-0.43	1
		100	897	-38.9	-0.43	2
		100	500	-36.8	-0.46	3
3	modified gains using INA analysis (see 8.5)	100	4470	-67.5	-0.43	1
		100	897	-53.1	-0.43	2
		100	2320	-51.4	-0.46	3
4	PP/4/FG/B gains based on x_e = 0.5	100	1722	-64.2	-0.72	1
		100	1722	-64.2	-0.72	2
		100	1722	-64.2	-0.72	3
5	PP/4/AG/Ff$_v$/B gains calculated using x_e = 0.5 p.u.	100	1827	-43.8	-0.50	1
		100	1827	-43.8	-0.50	2
		100	1359	-44.0	-0.53	3
6	modified gains using INA analysis (section 8.6)	100	1827	-58.8	-0.50	1
		100	1827	-73.8	-0.50	2
		100	1359	-44.0	-0.53	3

Rows continued on page below to show corresponding modes.

row no.	MODE A			MODE B			MODE C		
	S_{1A}	S_{2A}	S_{3A}	S_{1B}	S_{2B}	S_{3B}	S_{1C}	S_{2C}	S_{3C}
1	$-0.88 \pm j4.95$			$-2.99 \pm j8.23$			$-4.88 \pm j11.98$		
	.180∠3	.201∠7	.203∠6	.252∠167	.119∠-23	.112∠-28	.004∠-104	.269∠-38	.263∠138
2	$-1.01 \pm j5.14$			$-2.79 \pm j9.05$			$-3.80 \pm j12.07$		
	.176∠4	.200∠7	.225∠6	.209∠161	.088∠-27	.096∠-37	.014∠131	.284∠-33	.245∠145
3	$-1.78 \pm j5.36$			$-3.62 \pm j12.89$			$-3.84 \pm j13.47$		
	.126∠1	.376∠10	.273∠14	.269∠102	.156∠-159	.120∠-42	.017∠-106	.310∠-12	.298∠143
4	$-1.71 \pm j5.13$			$-3.67 \pm j9.85$			$-4.41 \pm j13.48$		
	.218∠9	.253∠13	.252∠11	.264∠150	.141∠-41	.112∠-49	.004∠-74	.220∠-38	.215∠139
5	$-1.68 \pm j5.37$			$-2.73 \pm j10.27$			$-3.23 \pm j12.93$		
	.205∠9	.239∠11	.269∠8	.199∠157	.090∠-33	.085∠-45	.010∠103	.252∠-33	.223∠148
6	$-1.67 \pm j5.11$			$-3.82 \pm j10.44$			$-4.31 \pm j13.83$		
	.220∠6	.264∠8	.284∠14	.258∠108	.109∠-103	.154∠-80	.061∠165	.305∠-39	.187∠118

NOTES: (1) The first three rows of this table are identical to rows 1,2 and 4 of Table 8.7.

(2) For system data, see Figure 8.18.

(3) Eigenvectors are weighted to show the response following a 1 p.u. initial error in the shaft speed for unit #2.

TABLE 8.9 EIGENVALUES AND EIGENVECTOR COMPONENTS FOR SYSTEM AT LIGHT LOAD

DATA FOR FIGURE 8.27

System data

Example 4: Light load (see Figure 8.18).

Disturbance applied

Step in voltage set-point for unit #2.

Feedback gains

(a): PP/4/FG/B gains calculated using x_e = 0.5 p.u. in the SMIB design model.

$f_v = 100$, $f_s = 1722$, $f_p = -64.2$, $f_F = -0.72$

(b): PP/4/AG/Ff_v/B gains calculated using x_e = 0.5 p.u. in the SMIB design model.

unit #1 $f_v = 100$, $f_s = 1827$, $f_p = -43.8$, $f_F = -0.50$

unit #2 $f_v = 100$, $f_s = 1827$, $f_p = -43.8$, $f_F = -0.50$

unit #3 $f_v = 100$, $f_s = 1359$, $f_p = -44.0$, $f_F = -0.53$

(c): As for (b) except f_p for units #1 and #2 increased to -58.8 and -73.8 respectively.

NOTE: Graphs show electrical power outputs in p.u. and are *not* drawn to the same scale.

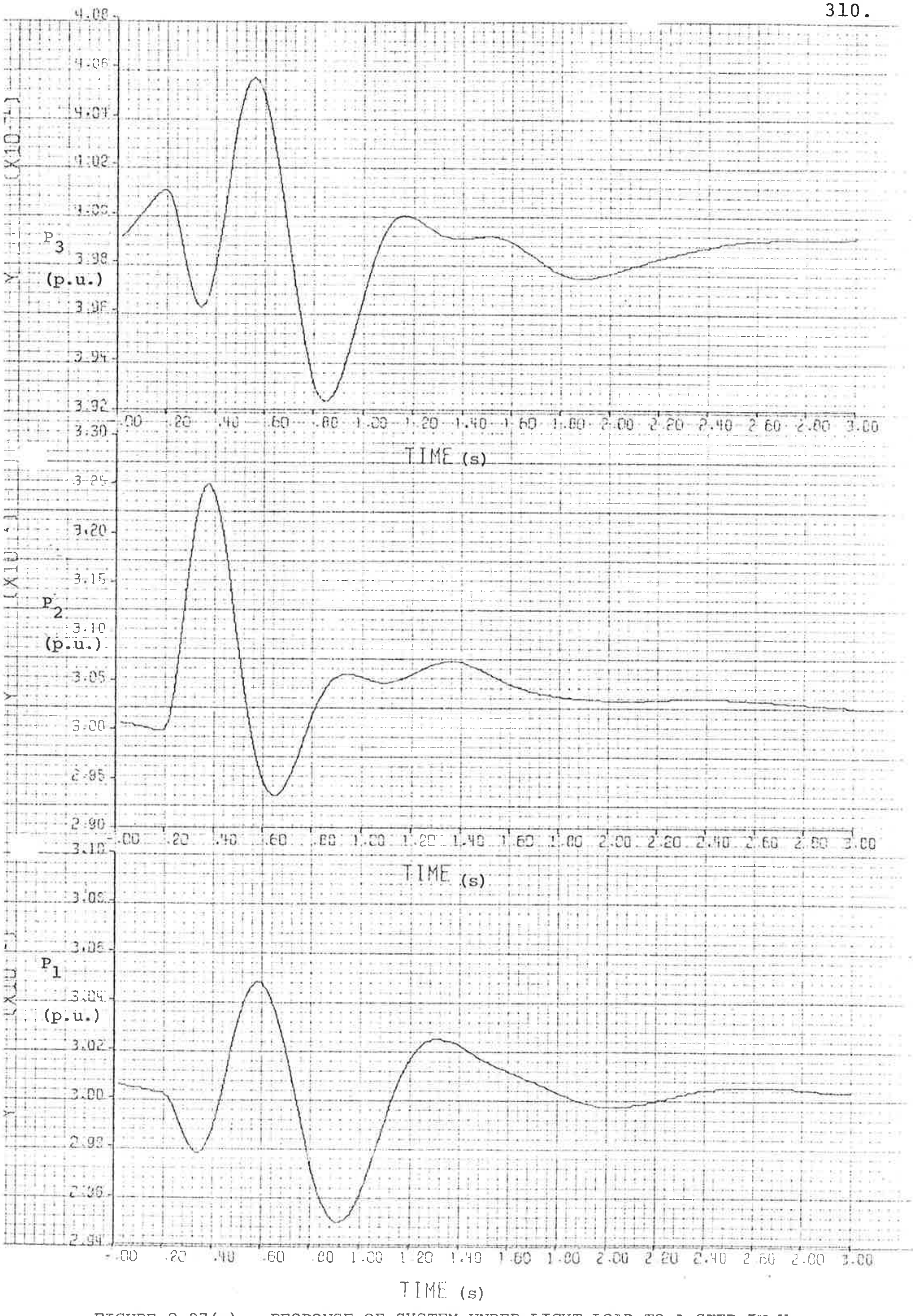

FIGURE 8.27(a) RESPONSE OF SYSTEM UNDER LIGHT LOAD TO A STEP IN V_{ref2}
(PP/4/FG/B GAINS CALCULATED USING x_e = 0.5 p.u.)

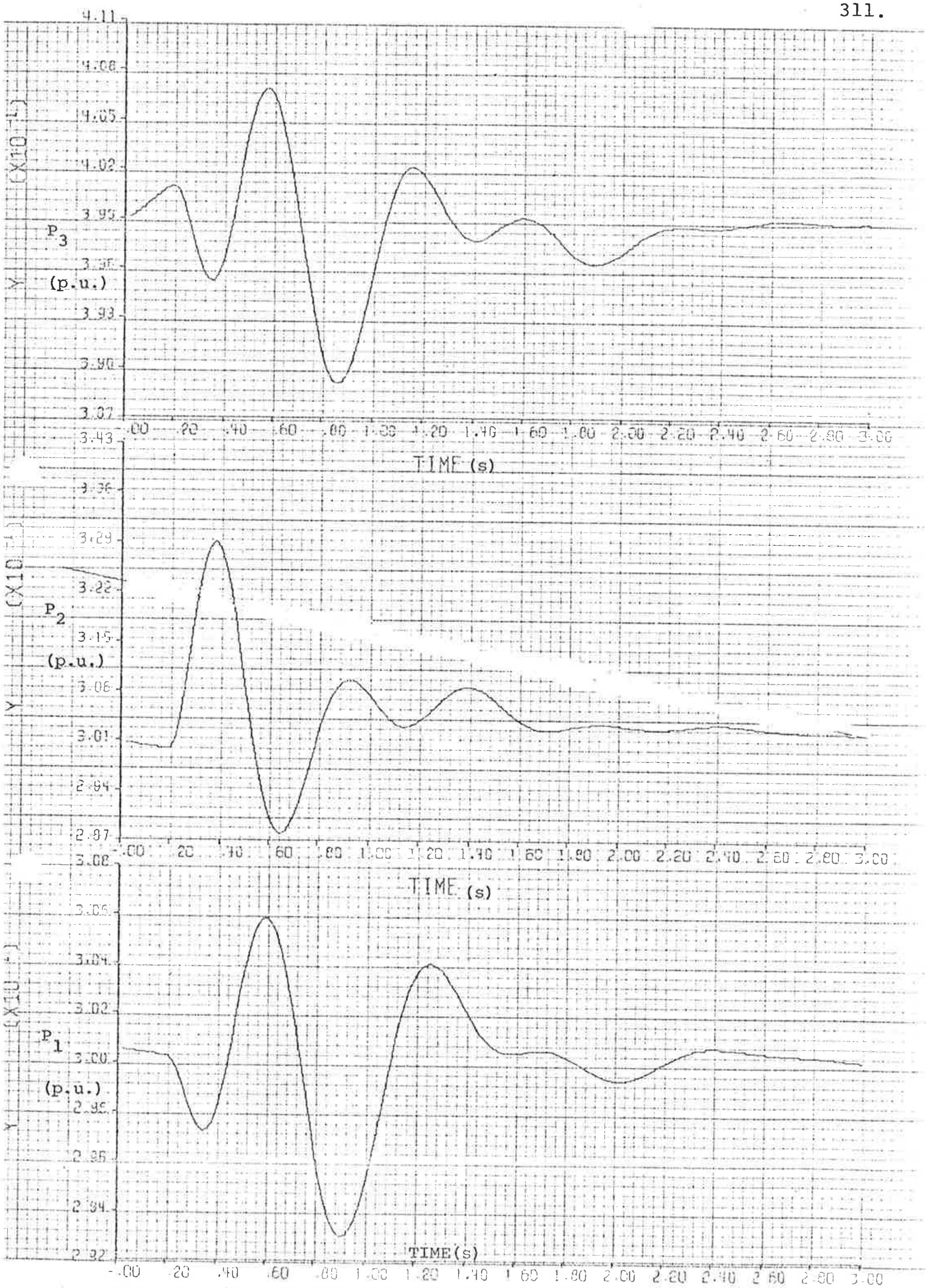

FIGURE 8.27(b) RESPONSE OF SYSTEM UNDER LIGHT LOAD TO A STEP IN V_{ref2}

($PP/4/AG/Ff_V/B$ gains calculated using $x_e = 0.5$ p.u.)

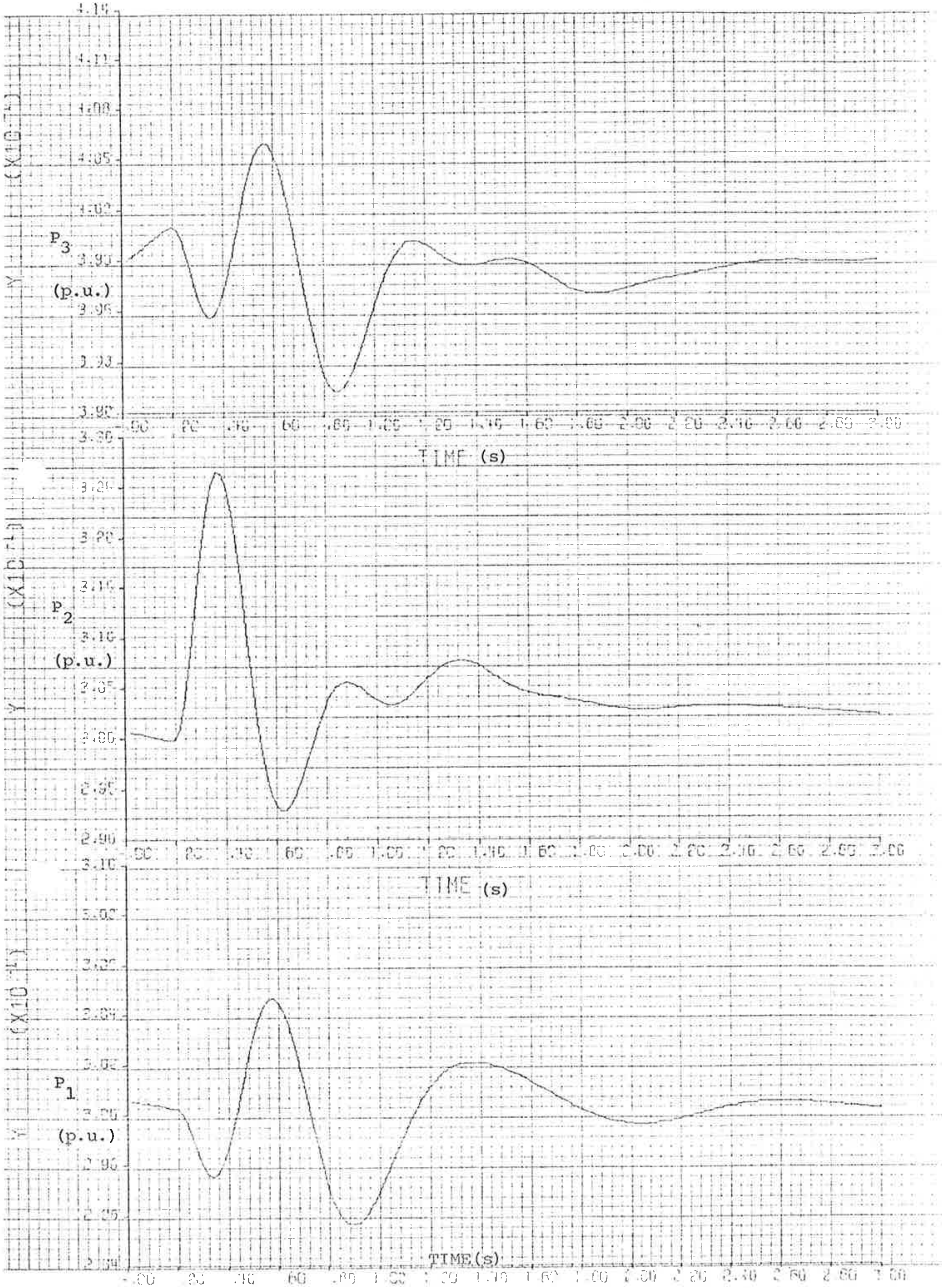

FIGURE 8.27(c) RESPONSE OF SYSTEM UNDER LIGHT LOAD TO A STEP IN V_{ref2}
(PP/4/AF/Ff$_V$/B gains calculated using x_e = 0.5 p.u. with f_p increased for units #1 and #2)

The inverse Nyquist arrays for the power and speed feedback loops of the generators with the revised adjustable-gain controllers are plotted in Figures 8.28 and 8.29. A small increase in the power feedback gains for units #1 and #2 is necessary to move the critical points in Figures 8.28(a) and (b) to the left to achieve diagonal dominance for the power loops. An increase in power feedback also produces (row) diagonal dominance for the speed loops because it causes the locus and Gershgorin band in Figure 8.19(b) to move downwards. The eigenvalues for the system when the critical points in Figures 8.28(a) and (b) are shifted to the points B and C are listed in row 6 of Table 8.9. The corresponding time response is shown in Figure 8.27(c). Comparison with the eigenvalues in row 5 and the time response in Figure 8.27(b) reveals that setting the gains for diagonal dominance improves damping and reduces interaction. (The amplitudes of the perturbations to units #1 and #2 are smaller in Figure 8.27(c) than in 8.27(b)).

The examples in this section demonstrate that:

(a) the success of the SMIB pole-placement design method for controllers in a multimachine power system depends on the value chosen for the equivalent tieline reactance (x_e), and

(b) INA analysis provides insight into the changes in gain settings which improve performance, irrespective of the choice of x_e in the initial pole-placement design.

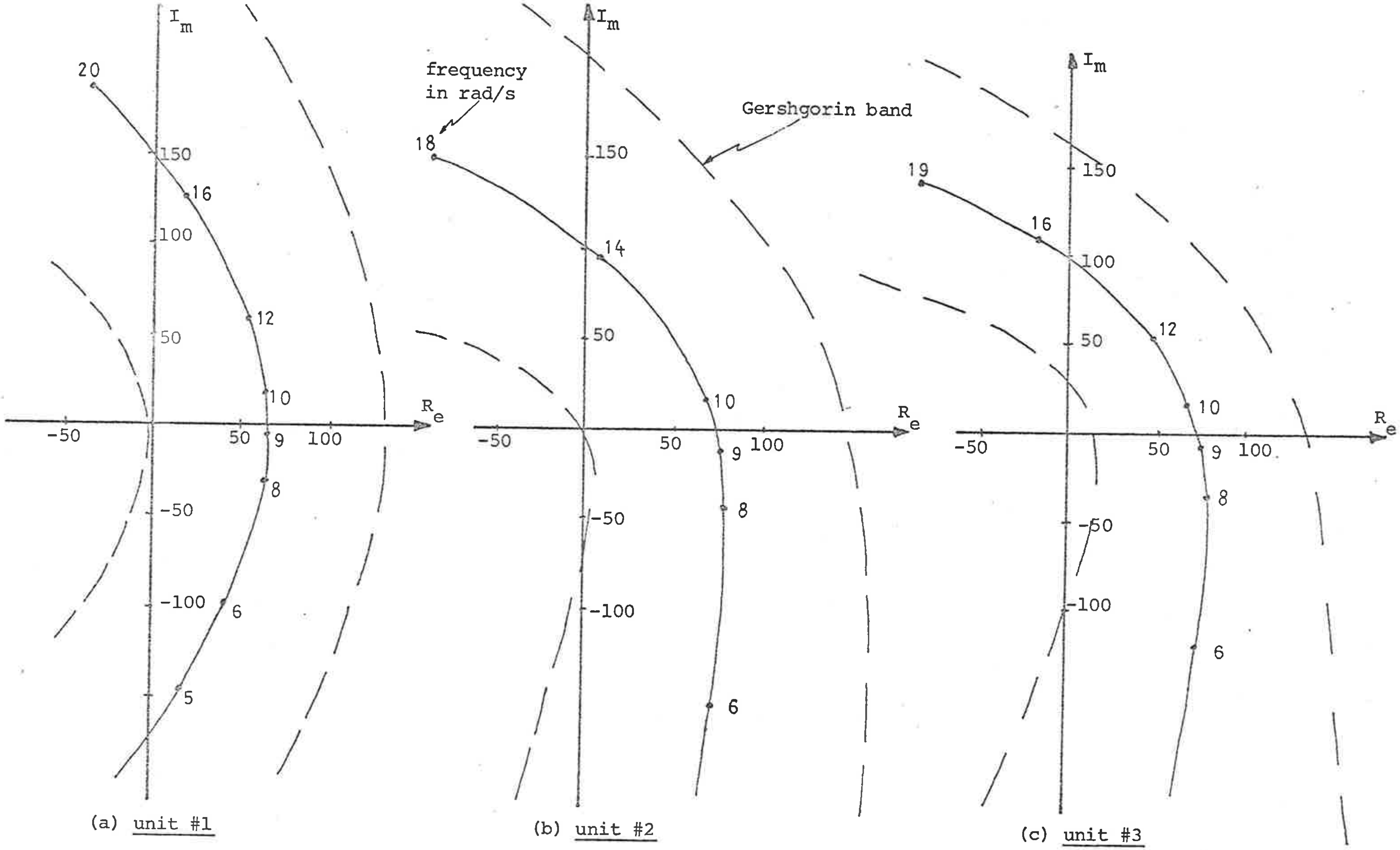

FIGURE 8.28 INA FOR POWER FEEDBACK LOOPS WITH SYSTEM UNDER LIGHT LOAD
(PP/4/AG/Ff$_V$/B controllers using x_e = 0.5 p.u. in gain calculations)

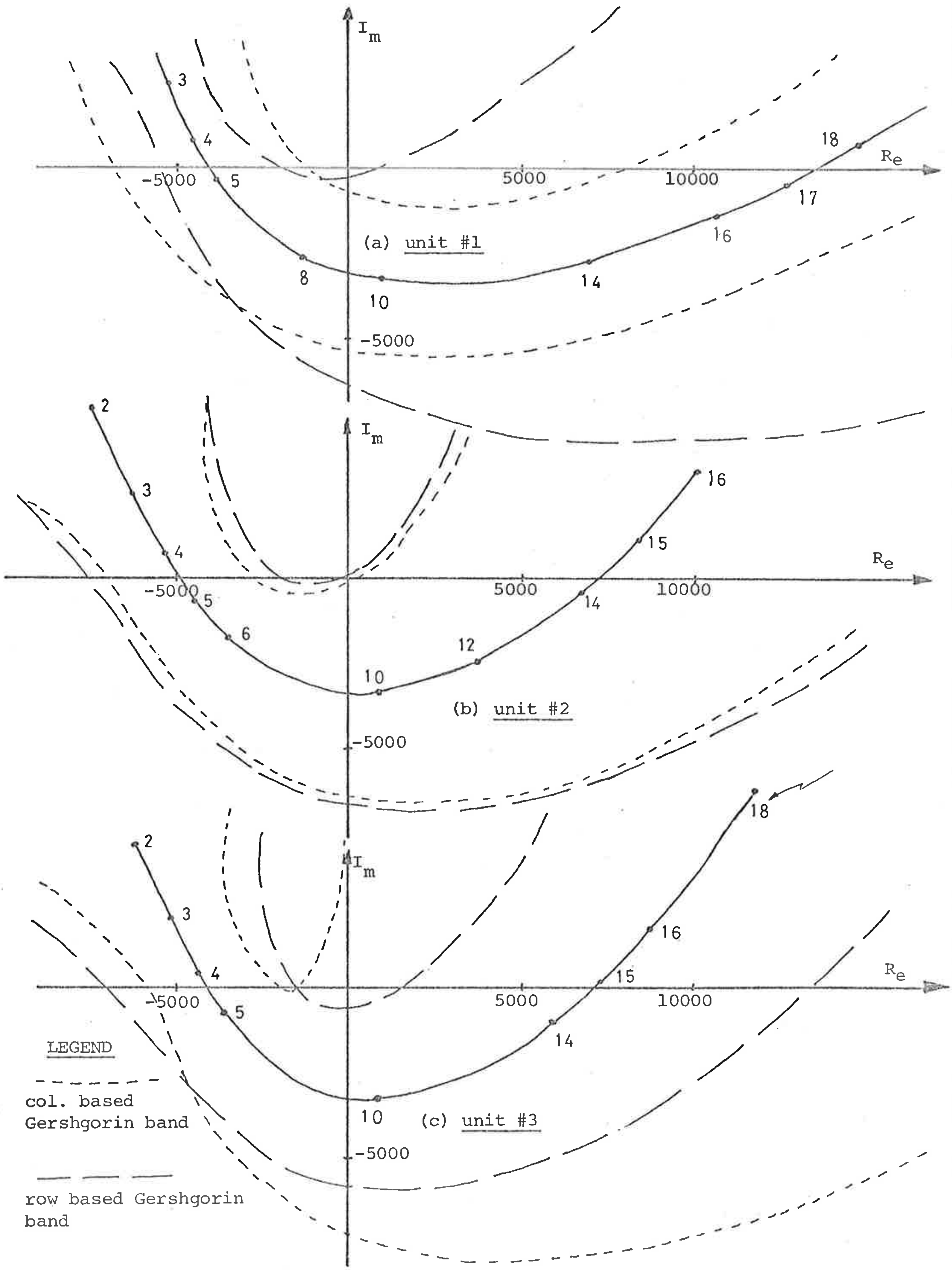

FIGURE 8.29 INA FOR SPEED FEEDBACK LOOPS WITH SYSTEM UNDER LIGHT LOAD
(PP/4/AG/Ff$_V$/B controllers using x_e = 0.5 p.u. in gain calculations)

CHAPTER 9

CONCLUSIONS AND RECOMMENDATIONS FOR FURTHER STUDY

9.1 CONCLUSIONS

9.1.1 The best pole-placement strategies

In Chapter 2, several strategies for setting the feedback gains of an excitation controller on the basis of pole-placement for a third-order single-machine infinite-bus (SMIB) model are devised. Further strategies are developed in a similar way in Chapter 4, based on a more accurate fourth-order SMIB model. The performance with the various control strategies (listed in Tables 2.2 and 4.1) is determined in Chapter 5, using a SMIB representation which incorporates a sixth-order generator model and includes controller time-constants. It is concluded that the PP/4/FG/B fixed-gain strategy and the PP/4/AG/Ff_v/B adjustable-gain strategy provide the best performance. This is not surprising because these strategies are based on the more accurate model of Chapter 4 and incorporate a priori knowledge of the effect of modelling simplifications on pole positions, as explained in section 5.3.2.

9.1.2 The necessity for adjustable-gain control

In Chapters 3 and 5, the small signal behaviour of the SMIB system with fixed- and adjustable-gain controllers is compared, for a wide range of normal and abnormal steady-state real and reactive power outputs. It is found that the performance of fixed-gain controllers designed for rated load deteriorates noticeably only under the following abnormal steady-state loading conditions:

(i) Near the leading p.f. stability limit

With the injection of fixed-gain subsidiary feedback signals into the excitation system, the leading p.f. stability limit lies well away from normal operating points. As this stability limit is approached the damping of electromechanical oscillations deteriorates. The adjustable-gain controllers proposed in this thesis extend the stability limit for real power outputs above about 0.4 p.u. Ideally an adjustable-gain strategy should allow stable operation at all loads. The reason for the failure of the pole-placement strategies to maintain stability at low leading power factors is the simplified representation of the q-axis of the rotor used in the design model.

(ii) At leading p.f. and low excitation

When a generator with a fixed-gain controller is operated at low real power output and with low field voltage, the real pole due to the field flux linkages moves close to the imaginary axis resulting in a slow exponential mode in the response. The adjustable-gain controllers move the real pole deeper into the left half s-plane at the expense of the damping of complex poles; the overall response is generally improved.

(iii) <u>At low lagging p.f.</u>

With a fixed-gain controller, the damping of electro-mechanical oscillations deteriorates as the power-factor is reduced for lagging p.f. loads. Adjustable-gain controllers offer increasingly superior performance under these conditions.

It is necessary to weigh the improvement in performance with an adjustable-gain controller against the cost and reliability of the hardware needed to implement the strategy. In the studies conducted in this thesis, the loading varies but the tieline reactance is constant. Although an adjustable-gain controller does offer improved performance under these conditions, the fixed-gain controller, designed by pole-placement for operation near rated load, provides adequate performance. These conclusions are similar to those expressed by D'Ans [84], who states, "A necessity for adaptive control exists only for extreme network situations or/and very large turbogenerators. For all other situations the existing static excitation system control with the additional signals from acceleration and slip are fully satisfactory."

Adjustable-gain control is advantageous in maintaining acceptable performance in cases such as those mentioned in Appendix 10.3 where the tieline reactance varies over a wide range. A practical case in which adaptive excitation control offers advantages has been reported recently (page 44 of [85]). Thus, it is possible that the pole-placement adjustable-gain control strategies which are developed in this thesis may be useful in a practical application.

9.1.3 The large signal performance of pole-placement controllers

The effectiveness of the pole-placement controllers in damping the large oscillations following a three-phase line-to-ground fault near the terminals of the generator in the SMIB system is examined in sections 3.4 and 5.4. It is demonstrated that these controllers provide heavy damping of electromechanical oscillations together with suitable terminal voltage recovery. The use of an adjustable-gain control strategy provides improvement in performance similar to that obtained under small-signal conditions.

The short critical-clearing-times for faults at operating points with large load angles indicate that transient stability is an important consideration under these conditions and that special provisions such as fast-valving or braking resistors are necessary to fully utilize the region of dynamic stability.

It is assumed that the process of gain adjustment with steady-state operating point is slow compared to generator rotor oscillations. However, even though the steady-state operating point is suddenly changed following the switching out of a faulted line, in the cases examined the prefault gains provide adequate damping whenever stability can be maintained on the first swing.

9.1.4 Generator modelling

The effects of various simplifying assumptions on the poles of the SMIB system are investigated in Chapter 5. In particular it is noted that neglect of the q-axis transient time-constant, as in most previous controller design studies, produces large errors near the leading p.f. stability limit. At normal operating points this omission produces small errors in the predicted damping and frequency of oscillations. Investigations in Chapter 8 indicate that the above results also hold for multimachine systems.

9.1.5 Operating point measurement errors

The sensitivities of the poles of the SMIB system with an adjustable-gain controller to errors in sensing operating point are examined in sections 3.3 and 5.3. The results indicate that care is necessary at low excitation levels to ensure that the deterioration in performance due to these errors is not excessive. However, Figures 3.13 and 3.14 show that at other loading conditions the problem is not severe; the sensitivities are less than 20 units which means that an 0.05 p.u. error in sensing the operating point variable produces less than $20 \times 0.05 = 1$ (s^{-1} or rad/s) shift in pole position.

9.1.6 The application of SMIB pole-placement controller designs to multimachine power systems

It is demonstrated that the excitation controllers for a multimachine power system can be designed in a way which utilises the large amount of information available concerning the single-machine infinite-bus system. Initial values of feedback gain are chosen by treating each generator as if it was in a SMIB system. The examples in Chapter 8 show that the PP/4/FG/B and PP/4/AG/Ff_v/B pole-placement control strategies result in moderate dynamic performance for the generators in a multimachine system. It is demonstrated that the design may be simply completed by employing eigen-analysis, Inverse Nyquist Array theory and the computation of step responses in a coordinated manner to determine modifications to the feedback gain settings which achieve acceptable performance.

9.1.7 Modes of dynamic behaviour in multimachine systems

Eigenvector analysis is applied in Chapter 6 to demonstrate that as the electrical coupling between generators is increased, the eigenvalues (poles) of a multimachine power system tend to be associated with group and intermachine modes of dynamic behaviour rather than with individual generators. It is shown that as network reactances are increased pole-placement controller designs based on a low tieline reactance result in poor damping for a group mode of oscillation; this information is used in section 8.6 where the damping of a lightly-damped low frequency group mode of oscillation is improved by increasing the value of tieline reactance in the SMIB design model.

9.1.8 Inverse Nyquist Array Analysis of power system dynamic behaviour

A method of applying Inverse Nyquist Array theory to the design of local controllers for multimachine power systems is developed in Chapter 7. The examples in Appendix 10.5 and Chapter 8 demonstrate that this method of using the INA provides useful engineering insight into the effect of gain changes for the electrical power and shaft-speed feedback loops. Information is gained concerning the range of feedback gains which result in stable performance; the effect of transducer failures on stability; and the damping at various oscillation frequencies for different gain settings.

It is demonstrated that the diagonal dominance needed to apply INA theory can be achieved without resorting to cross feedback between generators, therefore useful information can be obtained for the present-day system of local control. It is also shown that setting feedback gains for diagonal dominance tends to minimise the interaction between generators with the result that a disturbance to any generator has a reduced effect on other generators in the system.

9.2 POINTS REQUIRING FURTHER INVESTIGATION

9.2.1 Implementation of adjustable-gain control

It is demonstrated in Appendix 10.3 that the feedback gains for the adjustable-gain pole-placement control strategies can be calculated on-line provided the time-constants of the adaptation process are made comparable with or longer than the period of generator oscillations (e.g. 1 second). It will be necessary to perform tests to ensure that the adaptation process is stable and sufficiently fast to track the drift in steady-state operating point. Phung [50] has shown that this type of system can be implemented for a laboratory alternator.

9.2.2 Further large-signal tests

The pole-placement controllers are shown to be suitable for normal ("small-signal") operating conditions in a multimachine power system and following three-phase line-to-ground faults on the tieline of a SMIB system. The performance in the other possible operating circumstances needs to be checked. In particular, the rise in terminal voltage following full load rejection needs to be investigated with suitable governor and transmission line representation in the system model. Some authors find it necessary to disconnect stabilizing signals based on electrical power output during this type of fault. The suitability of controllers for generators in multimachine power systems designed by the methods proposed in this thesis following large magnitude disturbances needs to be verified.

9.2.3 Effects of modelling simplifications

Although the effects of a large number of modelling assumptions are determined in Chapter 5, those of the following major simplifications which are made throughout this thesis also need to be investigated. The simplifications are that:

(i) The effect of saturation on the generator parameters is neglected.

(ii) A grossly simplified model is used for the excitation system.

(iii) Stator transients and the effect of shaft speed variations on terminal voltage are neglected.

The effects of saturation may be significant because this was a major source of error in the Northfleet studies ([54], [58]). Ultimately the performance of any control strategy must be tested using prototype system such as a laboratory alternator or a model power system.

9.2.4 Analysis of interaction in multimachine systems

Although the INA is used to provide insight into the effect of feedback gain changes in the examples in Chapter 8, no serious attempt is made to reduce the interaction between generators. It is proposed that the process of iteratively adjusting local feedback gains for optimum performance employed in these examples should be a first step in designing controllers for a multimachine power system. Once the best possible performance with only local control has been achieved, the improvements possible by applying selected cross feedback signals may be investigated. The Gershgorin bands clearly indicate whether interaction affects the performance of a loop but give little guidance to its source. It is suggested that frequency response plots of the $q_{ij}(\omega)$ and $\hat{q}_{ij}(\omega)$ should be available to the designer to provide insight into the interaction between loops. If the INA is computed using method (a) of Appendix 10.6, the values for these plots are intermediate results which may be stored for future reference.

9.2.5 Application of INA analysis to practical power systems

In Chapter 8, the INA is applied to the analysis of a somewhat artificial system because the generators are identical and all have modern excitation systems with subsidiary feedback gains which may be adjusted at will. The usefulness of INA analysis should be investigated on a practical power system having generators with various ratings employing various types of excitation systems, including some with the longer time-constants characteristic of rotating exciters. It needs to be determined whether diagonal dominance or useful results can be obtained with the reduced flexibility in adjusting the excitation control. However, there are methods to improve diagonal dominance which are not employed in this thesis. Some methods such as the scaling of a row or column of the INA by a constant or the introduction of frequency dependent elements in the feedback loops do not involve signals between different generators.

In Chapter 8 the INA is used primarily to investigate modifications to the gains resulting from adjustable-gain control strategies. The INA method is also potentially useful in designing fixed-gain controllers for multimachine systems. A possible design procedure is:

(a) Find initial feedback gain values by considering each generator to be operating near rated load in a SMIB system.

(b) Calculate Inverse Nyquist Arrays for the multimachine power system with the initial values of gain at various operating conditions.

(c) The effect of feedback gain changes on performance at different loads can be simply assessed by considering the new position of the critical points in the INA's.

The feasibility and effectiveness of this design procedure needs to be investigated for practical power systems. The INA presents information concerning the stability and dynamic behaviour of detailed models of systems in a compact, quickly assessable form and hence its application to power system analysis should be further investigated.

APPENDIX 10.1

LINEARIZATION CONSTANTS

The linearization constants of the Reggiani's third-order SMIB model shown in Figure 2.1 may be expressed in terms of those of the commonly-used Heffron model (Heffron [42], DeMello and Concordia [23]). Let k_1, k_2, k_3, k_4, k_5 and k_6 be the constants used by Heffron, and K_1, K_1', K_2, K_3, K_3', K_4 and T be Reggiani's. It may be shown by block diagram manipulation that:

$$K_1 = k_1 - k_2k_3k_4 \tag{A1.1}$$

$$K_1' = k_1 \tag{A1.2}$$

$$K_2 = k_2k_3 \tag{A1.3}$$

$$K_3 = k_3k_4k_5 - k_5 \tag{A1.4}$$

$$K_3' = -k_5 \tag{A1.5}$$

$$K_4 = k_6k_3 \tag{A1.6}$$

$$T = k_3T'_{do} \tag{A1.7}$$

APPENDIX 10.2

VERIFICATION OF THE VALUES OF a_1 AND a_2 FOR THIRD-ORDER ITAE OPTIMUM RESPONSE

In order to minimise the ITAE for a third-order zero-position-error transfer function it is necessary to choose a_1 and a_2 equal to 1.75 and 2.15 respectively (see section 2.5.1). This appendix describes a test to ensure that these values also give the ITAE optimum response in terminal voltage for a SMIB system following a change in voltage set-point. The transfer function describing this response (listed in Figure 2.1) has zeroes whose positions vary with load and it is possible that different values of a_1 and a_2 might be required for optimum response at various loads.

The values of a_1 and a_2 which minimise the ITAE were determined using a Pacer 500 hybrid computer. The SMIB transfer function under study was modelled using the analogue part of the computer together with a circuit to calculate the ITAE following a step input. The digital part of the computer was programmed to adjust the potentiometers determining a_1 and a_2 to find the optimum setting using the "optimum gradient method" (Bekey [72]). To be reasonably sure that a global minimum was found, the computation was repeated with 9 different starting values of a_1 and a_2 for each case.

In order to test the optimization algorithm and to determine the accuracy of the computational procedure, a third-order zero-position-error system was modelled and the values of a_1 and a_2 for optimum response determined - the results were within 3% of those quoted by Graham.

The SMIB system was then substituted for the zero-position-error system and the power and speed gains were adjusted to minimise the ITAE. This calculation was repeated for a wide range of operating points ($\overline{P}$ ranging between 0.2 p.u. and 1 p.u. and $\overline{Q}$ ranging between -0.5 p.u. and +0.5 p.u.). The value of the ITAE with gains corresponding to $a_1 = 1.75$ and $a_2 = 2.15$ was compared with the global minimum - usually the difference was less than 1%, with the maximum difference being 5%. These errors are comparable with computational errors expected from this type of computer. It is thus concluded that the zeroes of the SMIB transfer function do not significantly affect the values of a_1 and a_2 for optimum response.

APPENDIX 10.3
REAL-TIME COMPUTATION OF FEEDBACK GAINS

10.3.1 PRELIMINARY REMARKS

One advantage of using pole-placement rather than optimal control theory for calculating the gains of an excitation controller is the considerably smaller amount of computation required (Seraji [12]). This appendix describes a simple test which was performed to ensure that the pole-placement gain calculations may be performed on-line.

An advantage of on-line calculation over the storage of pre-calculated values is that the value of x_e to be used in the gain calculations may be made an input parameter. Then, in the event of a large change in the effective tie-line reactance, say when one circuit of a double circuit transmission system is out of service, the regulator can be simply re-adjusted for optimum performance. Another possible application of the on-line computation capability is in a hierarchical control scheme proposed by Glavitsch [79], in which a central control computer transmits values of effective tie-line reactance to local generator controllers.

Most papers dealing with adjustable controller strategies propose only measurement of real and reactive power. In practically implementing such a strategy, Phung [50] found that it was necessary to store three different sets of pre-calculated gains to allow for different voltage levels in the SMIB system. An advantage of the method of on-line calculation of feedback gain proposed in this thesis is that a measurement of the terminal voltage is used which reduces the error between the existing terminal voltage and the value used in evaluating the feedback gain expressions; the sensitivity analysis in Chapter 3 shows that such errors cause degradation in performance at leading p.f. loads.

10.3.2 CALCULATION OF GAINS FROM TERMINAL MEASUREMENTS

In the expressions for the feedback gains required by each of the pole-placement strategies, the operating point of the generator is described by the K-constants K_1, K_1', K_2, K_3, K_3' and K_4. For the purpose of on-line calculation these must be expressed in terms of accessible variables and machine constants. It is assumed that measurements are made of the generator real and reactive power output and the terminal voltage. In practice the generator operating point is not constant and these values are continually changing. It is assumed that "pseudo-steady-state" values which do not change significantly during transients are derived from some low-pass filtering operation such as that described by Phung [50] - these values are denoted $\overline{P}$, $\overline{Q}$ and $\overline{v}_t$.

Reggiani [17] expressed the K-constants in terms of $\overline{P}$, $\overline{Q}$ and $\overline{v}_t$ plus the direct and quadrature axis components of $\overline{v}_t$, denoted v_{do} and v_{qo}. By manipulation of his equations

$$\bar{v}_t = \sqrt{v_{do}^{\;2} + v_{qo}^{\;2}} \tag{A3.1}$$

$$\bar{P} = v_{do} i_{do} + v_{qo} i_{qo} \tag{A3.2}$$

$$\bar{Q} = v_{qo} i_{do} - v_{do} i_{qo} \tag{A3.3}$$

$$v_{do} = x_q i_{qo} \tag{A3.4}$$

the d- and q-axis components of $\bar{v}_t$ may be expressed as:

$$v_{do} = \frac{\bar{P}}{\sqrt{\bar{P}^2 + \left(\frac{\bar{v}_t^{\,2}}{x_q} + \bar{Q}\right)^2}} \tag{A3.5}$$

$$v_{qo} = \frac{\bar{v}_t^{\,2}/x_q + \bar{Q}}{\sqrt{\bar{P}^2 + \left(\frac{\bar{v}_t^{\,2}}{x_q} + \bar{Q}\right)^2}} \tag{A3.6}$$

Substitution of these results into Reggiani's equations yields:

$$K_1' = \frac{x_q}{\left(1 + \frac{x_q}{x_e}\right)\bar{v}_t^{\,2}} \left[\left(\bar{Q} + \frac{\bar{v}_t^{\,2}}{x_q}\right)\left(\frac{\bar{v}_t^{\,2}}{x_e} - \bar{Q}\right) - \bar{P}^2 \right]$$

$$- (x_d' - x_q) \frac{(1 + x_q/x_e)\bar{v}_t^{\,2}}{(1 + x_d'/x_e)x_q^{\,2}} \cdot \frac{\bar{P}}{\bar{P}^2 + (\bar{Q} + \bar{v}_t^{\,2}/x_q)^2} \tag{A3.7}$$

$$K_2 = \frac{(1 + x_q/x_e)\bar{v}_t \bar{P}}{x_q(1 + x_d/x_e)\sqrt{\bar{P}^2 + (\bar{v}_t^{\,2}/x_q + \bar{Q})^2}} \tag{A3.8}$$

$$K_3' = \frac{x_q\overline{P}}{(1 + x_q/x_e)\overline{v}_t} + \frac{(x_d' - x_q)\overline{v}_t\overline{P}(\overline{Q} + \overline{v}_t^{\,2}/x_q)}{(1 + x_d'/x_e)x_q[\overline{P}^2 + (\overline{Q} + \overline{v}_t^{\,2}/x_q)^2]^{\frac{1}{2}}} \tag{A3.9}$$

$$K_4 = \frac{(\overline{Q} + \overline{v}_t^{\,2}/x_q)}{(1 + x_d/x_e)\sqrt{\overline{P}^2 + (\overline{v}_t^{\,2}/x_q + \overline{Q})^2}} \tag{A3.10}$$

The expressions for K_1 and K_3 are omitted for brevity because these are the same as those for K_1' and K_3' with x_d replacing x_d'. The term $K_1'K_4 + K_2K_3'$ appears in a number of gain expressions and may be expressed in a simpler form than combining the above equations in full.

$$K_1'K_4 + K_2K_3' = \frac{(\overline{v}_t^{\,2}/x_e - \overline{Q})\sqrt{\overline{P}^2 + (\overline{v}_t^{\,2}/x_q + \overline{Q})^2}}{(1 + x_d/x_e)(1 + x_q/x_e)\dfrac{\overline{v}_t^{\,2}}{x_q}} \tag{A3.11}$$

10.3.3 A TEST TO DETERMINE THE TIME REQUIRED FOR GAIN CALCULATIONS

In order to investigate the possibility of on-line calculation of feedback gains, such calculations were performed using an EAI Pacer 500 hybrid computer. A programme was written using the HOI language to:

(i) Convert the amplitudes of analogue signals corresponding to the values of $\overline{P}$, $\overline{Q}$ and $\overline{v}_t$ together with a set value of x_e into digital numbers.

(ii) Calculate the K-constants for the operating point using equations (A3.7) to (A3.10).

(iii) Calculate the feedback gains using equations (2.10)-(2.13) or (4.3)-(4.7), depending on the pole-placement strategy employed.

(iv) Set the coefficients of digitally controlled analogue multipliers to values corresponding to the computed gains.

A listing for the programme employing the PP/4/AG/Ff$_v$/B strategy is attached. The times for each part of the computation are shown. The overall time to revise the gains varies depending on the number of successive approximations required to find ω_1 - usually one pass is sufficient and the loop time is then 570 msec. (The calculations for the PP/3/AG/Ff$_v$ and PP/3/AG/FP strategies take 300 msec., requiring less time than for the PP/4/AG/Ff$_v$/B strategy because the equations are simpler and an explicit relationship is available for ω_1.)

The time constants of the filters used to derive $\overline{P}$, $\overline{Q}$ and $\overline{v}_t$ need to be longer than about 1 second because their outputs are supposed to be largely unaffected by generator transients, and generator rotor oscillation frequencies are generally of the order of 1 Hz. The updating of the gains by pole-placement twice a second, as is possible with HOI, should thus be adequate to track the variations in operating point described by $\overline{P}$, $\overline{Q}$ and $\overline{v}_t$. HOI is a high level language in which statements are decoded by an interpreter - a reduction in the time required to compute the gains will result from machine code programming and will allow the gains to be updated more frequently. It is concluded that on-line computation of adjustable feedback gains is feasible with the pole-placement strategies proposed in this thesis.

```
1.001     "HOI PROGRAM TO CALCULATE CFV34 FEEDBACK GAINS ":
1.002     "PREPARE COMPUTER FOR HYBRID OPERATION"
1.003     580, CONSOLE; , 1, USE;
1.100     "ENTER MACHINE DATA ":
1.101     XD, XDD, XQ←
1.102     TDO, D, H←
1.103     WO, FV, TEX←
1.104     A1, A2, A3, W1←

2.001     "GAIN CALCULATION LOOP "
2.002     "READ UPDATED P, Q, VT AND XE "
2.003     P=VAL(@AD00)
2.004     Q=VAL(@AD01)                                    28 ms
2.005     VT=VAL(@AD02)
2.006     XE=VAL(@AD03)
2.100     "CALCULATE COMMON TERMS "
2.101     DH=0.5*D/H
2.102     VT2=VT*VT
2.103     QQ=VT2/XQ+Q
2.104     QE=VT2/XE-Q
2.105     PQ2=P*P+QQ*QQ
2.106     PQ=PQ2**0.5                                     115 ms
2.107     CD=1.0+XD/XE
2.108     CQ=1.0+XQ/XE
2.109     CDD=1.0+XDD/XE
2.110     C1=XQ*(QQ*QE-P*P)/(VT2*CQ)
2.111     C2=XQ*P/(CQ*VT)
2.200     "CALCULATE K CONSTANTS "
2.201     K1=C1-(XD-XQ)*CQ*VT2*P*P/(CD*XQ*XQ*PQ2)
2.202     K1D=C1-(XDD-XQ)*CQ*VT2*P*P/(CDD*XQ*XQ*PQ2)
2.203     K2=CQ*VT*P/(XQ*CD*PQ)
2.204     K3=C2+(XD-XQ)*VT*P*QQ/(CD*XQ*PQ)               145 ms.
2.205     K3D=C2+(XDD-XQ)*VT*P*QQ/(CDD*XQ*PQ)
2.206     K4=QQ/(CD*PQ)
2.207     T=TDO*CDD/CD
2.208     KS=K1*K4+K2*K3
2.300     "CALCULATE UPDATED W1 BY NEWTON METHOD "
2.301     A=WO*A1*K1/(2.0*H*T)
2.302     B=(FV*WO*KS/TEX+K1*(D+2.0*H/T))/(2.0*H*T)
2.303     FW1=W1**4-A*W1-B                                105 ms
2.304     FW1*FW1<0.001? 2.307.                           per pass
2.305     W1=W1-FW1/(4.0*W1**3-A)
2.306     2.303.
2.307     "CALCULATE GAINS "
2.308     FF=1.0+TEX*(1.0/T+DH-A1*W1)
2.309     FP=TEX*(DH+T*(0.5*WO*K1D/H-A2*W1*W1))
2.310     FP=(FP+FV*K4+(1.0-FF)*(1.0+T*DH))/K2            145 ms
2.311     FS=TEX*(2.0*H*T*A3*W1**3-WO*K1)-D*(FV*K4-FP*K2)
2.312     FS=(FS+H*(FF-1.0)*(2.0*DH+WO*K1D*T/H))/K2
2.400     "SET DAM COEFFICIENTS TO NEW VALUES "
2.401     @DA00, FS*0.0001, SET;
2.402     @DA01, FP*0.01, SET;                            33 ms.
2.403     @DA02, FF*0.1, SET;
2.404     2.003.
```

NOTE: CFV34 is an earlier notation for the PP/4/AG/Ff_v/B strategy.

APPENDIX 10.4

POWER SYSTEM MODELS AND VERIFICATION OF COMPUTED RESULTS

10.4.1 A SIMPLE THIRD-ORDER NONLINEAR SMIB MODEL

In section 3.4 the following equations are used to model the SMIB system because for large amplitude rotor oscillations the power-load angle relation of the generator is nonlinear and the field voltage is limited so that linearized equations are no longer valid. The model is equivalent to Hammons' representation 2 [70], and those of Outhred [16] and Wilson [52].

$$pv'_q = \frac{(x_e - x'_d)v_f - (x_e + x_d)v'_q + (x_d - x'_d)V_b\cos\delta}{(x_e + x'_d)T'_{do}} \qquad \text{(A4.1)}$$

$$p\omega_s = \frac{P_m - P - D(\omega_s - 1)}{2H} \qquad \text{(A4.2)}$$

$$p\delta = 2\pi f_o(\omega_s - 1) \qquad \text{(A4.3)}$$

$$v_d = \frac{x_q V_b \sin\delta}{x_e + x_q} \qquad \text{(A4.4)}$$

$$v_q = \frac{x_e v'_q + x'_d V_b \cos\delta}{x_e + x'_d} \qquad \text{(A4.5)}$$

$$P = \frac{V_b}{x_e}(v_q \sin\delta - v_d \cos\delta) \tag{A4.6}$$

$$v_t = \sqrt{v_d^2 + v_q^2} \tag{A4.7}$$

$$|v_f| \leqslant 5.5 \text{ p.u.} \tag{A4.8}$$

10.4.2 A HIGHER ORDER SMIB MODEL

The equivalent circuits developed by Jackson and Winchester [71] demonstrate the complexity of the electrical behaviour in the rotor of a synchronous generator. The most detailed model which is used in this thesis has two equivalent rotor circuits in the direct axis and in the quadrature axis. The model is based on Hammons' representation 4, with an additional time-constant for the q-axis (see section 5.1). The d-axis and q-axis operational impedances are assumed to be:

$$x_d(p) = \frac{x_d(1 + pT'_d)(1 + pT''_d)}{(1 + pT'_{do})(1 + pT''_{do})} \tag{A4.9}$$

$$x_q(p) = \frac{x_q(1 + pT'_q)(1 + pT''_q)}{(1 + pT'_{qo})(1 + pT''_{qo})} \tag{A4.10}$$

In a similar manner to that employed by Hammons, these transfer functions are expressed in terms of transient and subtransient reactances and then variables v'_q, v''_q, v'_d and v''_d are defined such that the equations describing the generator are:

$$p\delta = 2\pi f_o(\omega_s - 1) \tag{A4.11}$$

$$2Hp\omega_s = P_m - P - D(\omega_s - 1) \tag{A4.12}$$

$$T'_{do}pv'_q = G'v_f - (x_d - x'_d)i_d - v'_q \tag{A4.13}$$

$$T''_{do}pv''_q = G''v_f - (x'_d - x''_d)i_d - v''_q + v'_q + T''_{do}pv'_q \tag{A4.14}$$

$$T'_{qo}pv'_d = (x_q - x'_q)i_q - v'_d \tag{A4.15}$$

$$T''_{qo}pv''_d = (x'_q - x''_q)i_q - v''_d + v'_d + T''_{qo}pv'_d \tag{A4.16}$$

$$P = v_d i_d + v_q i_q \tag{A4.17}$$

$$v_t^2 = v_d^2 + v_q^2 \tag{A4.18}$$

$$v_d = r_a i_d + v''_d + x''_q i_q \tag{A4.19}$$

$$v_q = r_a i_q + v''_q - x''_d i_d \tag{A4.20}$$

where $G' = \dfrac{T'_{do} - T_D}{T'_{do} - T''_{do}}$ and $G'' = \dfrac{T''_{do} - T_D}{T'_{do} - T''_{do}}$.

When the generator is connected to an infinite bus by a series impedance, the terminal voltages and currents are related by:

$$v_d - r_e i_d + x_e i_q = V_b \sin\delta \tag{A4.21}$$

$$v_q - x_e i_d - r_e i_q = V_b \cos\delta \tag{A4.22}$$

In order to ensure that the approximations made in deriving this state-space model from the transfer-function form have negligible effect on the dynamic behaviour, small signal responses from the following calculation methods were compared:

(1) Step by step integration of equations (A4.11) to (A4.22) using a Runge-Kutta algorithm.

(2) Analogue computer simulation of the transfer function based model in Figure 5.1.

(3) Step by step Runge-Kutta integration with a model formulated in terms of leakage reactances and resistances (e.g. Reichert [44]).

The results from these methods agreed closely indicating the absence of significant computational errors. The programme which was used to compute the eigenvalues in Chapter 5 is based on a linearized form of the above equations and was checked by comparing the results with time responses calculated by the above methods.

10.4.3 THE MODEL OF A FOUR MACHINE POWER SYSTEM

This appendix lists the linearized equations describing the four machine power system used in the examples in Chapter 8. The generators are numbered according to their buses and not as in Chapter 8. The rotor of generator 1 is taken as the angle reference for the system and accordingly there is no state corresponding to the angle of this generator (Undrill [26]).

<u>State equation for the infinite bus equivalent generator</u>

$$2H_1 p\Delta\omega_{s1} = -D_1\Delta\omega_{s1} + (2r_{a1}\bar{i}_{d1} + \bar{v}_{d1})\Delta i_{d1} - (2r_{a1}\bar{i}_{q1} + \bar{v}_{q1})\Delta i_{q1}$$

$$- \bar{i}_{d1}\Delta v_{d1} - \bar{i}_{q1}\Delta v_{q1} + \Delta u_{V1} + \Delta u_{S1} + \Delta u_{P1} \qquad \text{(A4.23)}$$

<u>State equations for generator #1 and its excitation controller</u>

$$p\Delta\delta_2 = 2\pi f_o(\Delta\omega_{s2} - \Delta\omega_{s1}) \qquad \text{(A4.24)}$$

$$2H_2 p\Delta\omega_{s2} = -D_2\Delta\omega_{s2} + (2r_{a2}\bar{i}_{d2} + \bar{v}_{d2})\Delta i_{d2} - (2r_{a2}\bar{i}_{q2} + \bar{v}_{q2})\Delta i_{q2}$$

$$- \bar{i}_{d2}\Delta v_{d2} - \bar{i}_{q2}\Delta v_{q2} \qquad \text{(A4.25)}$$

$$T'_{do2}p\Delta v'_{q2} = \Delta v_{f2} - \Delta v'_{q2} + (x'_{d2} - x_{d2})\Delta i_{d2} \qquad \text{(A4.26)}$$

$$T'_{qo2}p\Delta v'_{d2} = -\Delta v'_{d2} + (x_{q2} - x'_{q2})\Delta i_{q2} \qquad \text{(A4.27)}$$

$$T_{ex2}p\Delta v_{f2} = -\Delta v_{f2} + \left(1 - \frac{T_{vn}}{T_{vd}}\right)\Delta v_{LL} + \frac{T_{vn}}{T_{vd}}\Delta u_{v2} + \Delta u_{s2} + \Delta u_{f2} \qquad \text{(A4.28)}$$

$$T_{vd}p\Delta v_{LL} = -\Delta v_{LL} + \Delta u_{v2} \qquad \text{(A4.29)}$$

(Provision is made for a lag-lead filter in the voltage loop. For the examples in Chapter 8 its effect is removed by setting T_{vn} equal to T_{vd}.)

<u>State equations for generators #2 and #3 and their controllers</u>

$$p\Delta\delta_{s3} = 2\pi f_o(\Delta\omega_{s3} - \Delta\omega_{s1}) \tag{A4.30}$$

$$2H_3 p\Delta\omega_{s3} = -D_3\Delta\omega_{s3} + (2r_{a3}\overline{i}_{d3} + \overline{v}_{d3})\Delta i_{d3} - (2r_{a3}\overline{i}_{q3} + \overline{v}_{a3})\Delta i_{q3}$$
$$- \overline{i}_{d3}\Delta v_{d3} - \overline{i}_{q3}\Delta v_{q3} + \Delta P_{m3} \tag{A4.31}$$

$$T'_{do3}p\Delta v'_{q3} = G'_3\Delta v_{f3} - \Delta v'_{q3} + (x'_{d3} - x_{d3})\Delta i_{d3} \tag{A4.32}$$

$$T''_{do3}p\Delta v''_{q3} = (G'_3\frac{T''_{do3}}{T'_{do3}} - G''_3)\Delta v_{f3} + (1 - \frac{T''_{do3}}{T'_{do3}})\Delta v'_{q3} - \Delta v''_{q3}$$
$$+ (x''_{d3} - x'_{d3} + \frac{T''_{do3}}{T'_{do3}}(x'_{d3} - x_{d3}))\Delta i_{d3} \tag{A4.33}$$

$$T'_{qo3}p\Delta v'_{d3} = -\Delta v'_{d3} + (x_{q3} - x'_{q3})\Delta i_{q3} \tag{A4.34}$$

$$T''_{qo3}p\Delta v''_{d3} = (1 - \frac{T''_{qo3}}{T'_{qo3}})\Delta v'_{d3} - \Delta v''_{d3} + (x'_{q3} - x''_{q3}$$
$$+ \frac{T''_{qo3}}{T'_{qo3}}(x_{q3} - x'_{q3}))\Delta i_{q3} \tag{A4.35}$$

$$T_{ex3}p\Delta V_{f3} = -\Delta v_{f3} - \Delta v_{w3} + \Delta u_{v3} + \Delta u_{s3} + \Delta u_{p3} \tag{A4.36}$$

$$T_{w3}p\Delta V_{w3} = -\Delta v_{w3} + \Delta u_{p3} \tag{A4.37}$$

$$T_{t3}p\Delta P_{m3} = K_g\Delta w_{s3} - \Delta P_{m3} \tag{A4.38}$$

(The equations for generator 4 are simply obtained by replacing the "3" in each subscript by a "4".)

Equations relating electrical power output and terminal voltages and currents to state variables

$$\Delta v_{ti} = \frac{\bar{v}_{di}}{\bar{v}_{ti}} \Delta v_{di} + \frac{\bar{v}_{qi}}{\bar{v}_{ti}} \Delta v_{qi} \qquad i=1,2,3,4 \qquad \text{(A4.39)}$$

$$\Delta P_i = \bar{v}_{di}\Delta i_{di} + \bar{v}_{qi}\Delta i_{qi} + \bar{i}_{di}\Delta v_{di} + \bar{i}_{qi}\Delta v_{di} \qquad i=1,2,3,4 \qquad \text{(A4.40)}$$

$$\Delta v_{d1} - x_{q1}\Delta i_{q1} + r_{a1}\Delta i_{d1} = 0 \qquad \text{(A4.41)}$$

$$\Delta v_{q1} + x_{d1}\Delta i_{d1} + r_{a1}\Delta i_{q1} = 0 \qquad \text{(A4.42)}$$

$$\Delta v_{d2} - x'_{q2}\Delta i_{q2} + r_{a2}\Delta i_{d2} = \Delta v'_{d2} \qquad \text{(A4.43)}$$

$$\Delta v_{q2} + x'_{d2}\Delta i_{d2} + r_{a2}\Delta i_{q2} = \Delta v'_{q2} \qquad \text{(A4.44)}$$

$$\Delta v_{d3} - x''_{q3}\Delta i_{q3} + r_{a3}\Delta i_{d3} = \Delta v''_{d3} \qquad \text{(A4.45)}$$

$$\Delta v_{q3} + x''_{d3}\Delta i_{d3} + r_{a3}\Delta i_{q3} = \Delta v''_{q3} \qquad \text{(A4.45)}$$

Δu_{vi}, Δu_{si} and Δu_{pi} denote the signals input to the excitation systems from measurements terminal voltage, shaft speed and electrical power output. For generator 1, since there are no field or exciter dynamics, it is assumed that the signals affect the electrical power instantaneously; the existence of a fictitious input for this generator allows its behaviour to be viewed in an INA despite the fact that the "gain" must be zero.

No provision was made for the feedback of field voltage when the INA programme was written. The effect of this feedback may be incorporated by appropriately scaling the values of the exciter time-constant and the feedback gains. However, since the field voltage was not programmed as an output quantity, the INA showing the effect of changing this gain cannot be plotted.

The above equations have been used in the manner described in section 7.4 to calculate the INA and eigenvalues of Chapter 8. The close agreement of these results with the time responses calculated using a programme written by Dr. A.M. Parker verifies that there is no significant error in the derivation of the equations or their programming. The time response programme is based on a nonlinear model for the system and uses sparse matrix techniques for efficient step-by-step Runge-Kutta integration. The generator models in this programme only allow for the representation of one damper circuit in each axis. The provision of an extra q-axis rotor circuit would involve extensive revision of this programme so for units #2 and #3 the effects of the q-axis amortisseur are neglected and the q-axis rotor circuit is used to represent the effect of the rotor iron (T'_{qo}). The results of Chapter 5 suggest that this omission should have little effect and this is verified by the close agreement of the time responses with frequency domain predictions.

APPENDIX 10.5

Copy of the paper entitled "An Application of Multivariable Control Theory to the Study of Multi-machine Power System Dynamic Behaviour"

printed in the Electrical Engineering Transactions of the I.E.Aust., Vol. EE14, No. 2, pp. 53-58

Muttik, P. K. and Gibbard, M. J. (1978). An application of multivariable control theory to the study of multi-machine power system dynamic behaviour. *Electrical Engineering Transactions of the Institute of Engineers Australia, EE14*(2), 53-58.

NOTE:

This publication is included in the print copy
of the thesis held in the University of Adelaide Library.

APPENDIX 10.6

ALTERNATIVE METHODS OF CALCULATING THE INA

In applying INA methods to the analysis of power system dynamic behaviour, difficulties were encountered in deriving transfer function matrices from the state-space description of a high-order system. These difficulties led to the use of several methods of calculating the INA. The success of the various methods is briefly described in this appendix. Suppose that the state-space model of a system is

$$\underset{\sim}{x} = A\underset{\sim}{x} + B\underset{\sim}{u} \qquad \text{(A6.1)}$$

$$\underset{\sim}{y} = C\underset{\sim}{x} \qquad \text{(A6.2)}$$

and the transfer function is

$$Q(s) = C(sI - A)^{-1}B \qquad \text{(A6.3)}$$

Possible methods of evaluating the inverse transfer function matrix at a frequency s = jω are:

(a) <u>Calculation of the transfer function matrix, $Q(s)$</u>

The best known method of finding the transfer function matrix for a system given the matrices A, B and C is the Leverrier or Faddeev algorithm (Faddeev [73]). This method was successfully used to calculate the transfer function matrix for the system described in section 6.1.1. This method is unsuitable for systems of high order (Bosley [74]).

An alternative method (Daly [75]) was successfully used for the 25th order system described in Chapter 8. Once the transfer function matrix, $Q(s)$, has been found, the inverse transfer function matrix at the given frequency, $\hat{Q}(j\omega)$, may be calculated by evaluating the transfer function matrix, $Q(j\omega)$, and then finding its inverse.

Initially the multimachine INA program was written in a general form to allow sixth-order machine models and third-order governor and excitation system models to be used for each of the four generators. With the resulting 47th order system model, despite the use of Daly's algorithm, numerical instability occurred in the programme (written using double precision FORTRAN and run with a CYBER 173 digital computer). It appears that the error occurs in the calculation of the numerator coefficients because the eigenvalues calculated from the denominator coefficients agree closely with those found from the state-space description using the EISPACK subroutines. When the order of the system was reduced to 25, extensive testing failed to produce significant error.

(b) <u>Calculation of the inverse transfer function matrix $\hat{Q}(s)$</u>

It appears that finding coefficients of the inverse transfer function, $\hat{Q}(s)$, may be an efficient way of finding values for plotting the INA because the order of its elements $\hat{q}_{ij}(s)$ is generally lower than that of the $q_{ij}(s)$ in the transfer function matrix, $Q(s)$. Furthermore, no matrix inversion is needed after evaluation at the given frequency. The first method of finding $\hat{Q}(s)$ which was tried was that given by Kouvaritakis [76]. When the matrix CB has full rank, the inverse transfer function matrix is given by

$$\hat{Q}(s) = (CB)^{-1}[-CAM(sI - NAM)^{-1}NAB + sCB - CAB](CB)^{-1} \qquad (A6.4)$$

where N and M are matrices such that $CM = 0$, $NB = 0$ and $NM = I$. Although this method was successfully used to compute some inverse transfer function matrices for the low order TMIB system of section 6.1.1, finding the matrices N and M is not a simple task for a high order system. Furthermore, when CB does not have full rank, which occurs when speed is chosen as an output signal for one or more generators, the computation becomes even more complicated.

An alternative, easily programmable algorithm is given by Van Der Weiden [77]. This was successfully used to calculate all inverse transfer function matrices for the simple TMIB system. However, when the subroutine based on this algorithm was applied to the 25th order system of Chapter 8, numerical instability resulted. The reason for this failure has not been isolated.

(c) Direct calculation of the frequency response, $Q(j\omega)$

If $Q(s)$ is to be evaluated at the given frequency, ω, then the substitution of $s = j\omega$ into equation (A6.3) shows that the value of the forward transfer function is then

$$Q(j\omega) = C(j\omega I - A)^{-1}B \qquad (A6.5)$$

The inverse Nyquist array at the frequency ω is simply the inverse of this matrix of complex numbers. If the system is n^{th} order and has m inputs and outputs then Rogers [78] has shown that the computation required involves finding the inverse of an $n \times n$ real matrix and a $2m \times 2m$ real matrix. This method was not tried in the present study but may be a way to avoid the numerical instability problems encountered with the other techniques.

In the above investigations, methods of verifying the INA calculated had to be devised. One simple method to detect numerical error is to specify two identical generators at the same operating condition; clearly the transfer functions for each should be the same. Equation (7.1) provides another useful check because a change in feedback gain should simply cause a translation of one plot in the INA, even though all of the elements of $H(s)$ are altered.

One of the potential advantages of the INA method of analysis is its conciseness in presenting performance data for high-order systems because the size of the array depends on the number of inputs and outputs and not the order of the system. In order to fully exploit this potential and also to allow detailed models of generators and their controllers to be used, it is desirable that research into the possible calculation methods be undertaken to find one which gives acceptable accuracy with the minimum possible computing time for high-order systems.

APPENDIX 10.7

EFFECTS OF CHANGING SPEED OR POWER FEEDBACK GAIN ON THE ELEMENTS OF THE SPEED AND POWER INA

If the power loop INA before and after altering the shaft speed feedback gain for any given generator in a multimachine system are compared, it appears that the only element affected is that for the generator whose gain is perturbed. This appendix proves that this result is true for the case when there are no signals fed between different generators.

Figure A7.1 indicates the relationship between the speed and power loops of a generator in a multimachine system. $Q_p(s)$, the open-loop transfer function matrix for the power loops of the system may be expressed as:

$$Q_p(s) = G(s)K_p(s) \tag{A7.1}$$

where $G(s)$ has elements $g_{ij}(s)$ and $K_p(s)$ is a diagonal matrix with elements $k_{pi}(s)$. $Q_s(s)$, the open-loop transfer function matrix for the speed loop may be expressed as:

$$Q_s(s) = L(s)G(s)K_s(s) \tag{A7.2}$$

where $K_s(s)$ and $L(s)$ are diagonal matrices with $L(s)$ having elements $\ell_{ii}(s) = \dfrac{1}{gv_i(s) - D_i + 2H_i s}$. An expression relating $Q_p(s)$ and $Q_s(s)$ may be derived by combining equations (A7.1) and (A7.2).

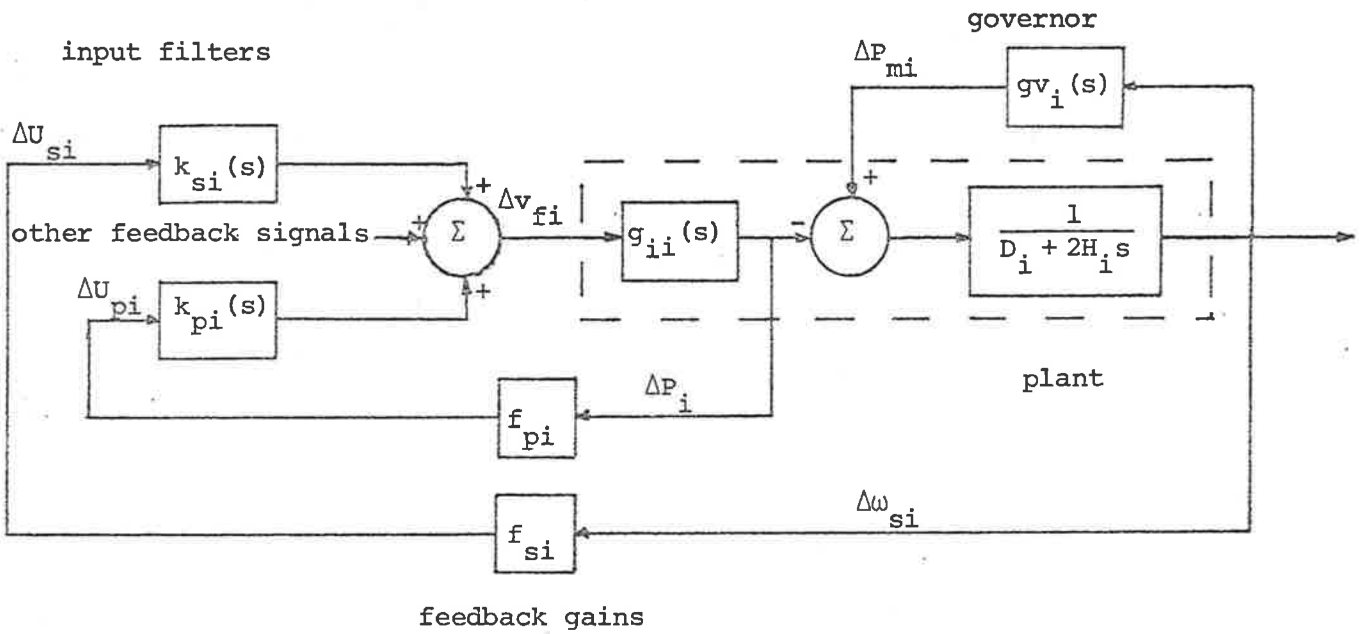

FIGURE A7.1 THE SPEED AND POWER LOOPS OF THE i^{th} GENERATOR IN A MULTIMACHINE POWER SYSTEM

$$Q_s(s) = L(s)Q_p(s)\hat{K}_p(s)K_s(s) \tag{A7.3}$$

A similar expression relating the inverse transfer function matrices $\hat{Q}_p(s)$ and $\hat{Q}_s(s)$ is obtained by inverting equation (A7.3).

$$\hat{Q}_s(s) = \hat{K}_s(s)K_p(s)\hat{Q}_p(s)\hat{L}(s) \tag{A7.4}$$

In the above derivation it is assumed that matrices $L(s)$, $K_s(s)$ and $K_p(s)$ are non-singular because each is a diagonal matrix with no zero diagonal element (speed or power feedbacks are removed by setting f_{si} or f_{pi} to zero and $k_{si}(s)$ or $k_{pi}(s)$ to unity).

Suppose speed feedback is applied to the j^{th} generator, then the new inverse speed transfer function matrix, $\hat{Q}'_s(s)$ differs from $\hat{Q}_s(s)$ only in the j^{th} diagonal element (equation (7.1) of Chapter 7).

$$\hat{Q}'_s(s) = \hat{Q}_s(s) + \text{diag}(0,\ldots,0,f_j,0,\ldots 0) \tag{A7.5}$$

where diag( ) denotes a diagonal matrix with the indicated diagonal elements. The new inverse power transfer function matrix, $\hat{Q}'_p(s)$ is found by applying equation (A7.4).

$$\begin{aligned}\hat{Q}'_p(s) &= \hat{K}_p(s)K_s(s)\hat{Q}'_s(s)L(s)\\ &= \hat{K}_p(s)K_s(s)\hat{Q}_s(s)L(s) + \hat{K}_p(s)K_s(s)\text{diag}(0,\ldots,f_j,\ldots 0)L(s)\\ &= \hat{Q}_p(s) + \text{diag}\left(0,0\ldots,0,\frac{f_j\ell_{jj}(s)\quad _{sj}(s)}{k_{pj}(s)},0\ldots,0\right)\end{aligned}$$

Because $L(s)$, $\hat{K}_p(s)$ and $K_s(s)$ are diagonal matrices, the adjusting of the speed gain of generator j affects only the

j^{th} diagonal element of the power INA. This means that the radii of the Gershgorin bands are not altered, even though the position of the j^{th} band has changed.

In a similar manner to the above, it may be demonstrated that the changing of a power feedback gain affects only the corresponding diagonal element of the speed INA. These results show that the width of the Gershgorin bands cannot be reduced by adjusting speed and power feedback gains. The fact that the radii of the bands are invariant may be useful in reducing the time taken to recompute the INA after modifying gain settings in an interactive design procedure to optimise the settings of subsidiary feedback gains using INA techniques.

BIBLIOGRAPHY

[1] G. Quazza and E. Ferrari, "Role of power station control in overall system operation", Proc. Symposium on real-time control of electric power systems, Baden, 1971, p. 242-251.

[2] M.M. Elmetwally and N. Dharma Rao, "Sensitivity analysis in power system dynamic stability studies", IEEE Trans., PAS-91, 1972, p. 1692.

[3] H.R. Outhred and F.J. Evans, "A model reference adaptive controller for turbo-alternators in large power systems", P.S.S.C., 1972.

[4] E. Irving et al., "A method to improve the power network 'steady state stability' and to reduce the unit stress. The multivariable adaptive control of generators", Proc. IFAC Symposium, Automatic control and protection of electrical power systems, Melbourne, 1977, p. 210.

[5] M. Venkata Rao and M.P. Dave, "Non-linear excitation stabilizer for a synchronous machine over wide range operating conditions", IEEE PES Winter Meeting 1976, paper A76, 139-6.

[6] M. Venkata Rao and M.P. Dave, "Stabilization of multi-machine system through nonlinear gain excitation control", IEEE PES Winter Meeting 1977, paper A77, 088-8.

[7] J.P. Bartlett, M.J. Gibbard and J.L. Woodward, "Performance of a 5 KVA synchronous generator with an optimal excitation regulator", Proc. IEE, 1973, vol. 120, p. 1250.

[8] Y.L. Abdel-Magid and G.W. Swift, "Variable structure power stabiliser to supplement static-excitation systems", Proc. IEE, 1976, vol. 123, p. 697.

[9] S. Raman and S.C. Kapoor, "Synthesis of optimal regulator for synchronous machine", Proc. IEE, 1972, vol. 119, p. 1383.

[10] H.A.M. Moussa and Y.N. Yu, "Optimal power system stabilization through excitation and/or governor control", IEEE Trans., PAS-91, 1972, p. 1166.

[11] A. Jameson, "Design of single-input systems for specified roots using output feedback", IEEE Trans., AC-15, 1970, p. 345.

[12] H. Seraji, "Design of pole shifting and optimal controllers for a synchronous generator", Ninth Universities Power Engineering Conference, University of Cambridge, 1974, p. 84.

[13] H. Glavitsch, "On the choice of control parameters of excitation systems for large turbogenerators", Brown Boveri Rev., vol. 61, 1974, p. 207.

[14] F.D. Galiana and H. Glavitsch, "State adaptation in power systems control", <u>IEEE PES Winter Meeting 1973</u>, paper T73, 100-5.

[15] J.F. Arnold and J.S. Packer, "Co-ordinating voltage regulator action during system transient disturbance", <u>I.E.(Aust.) Electrical Energy Conference</u>, 1978, p. 75.

[16] H.R. Outhred, A.C. Sullivan and R.H. Craven, "Design of alternator control systems incorporating stabilising signals", <u>IEEE PICA Conference</u>, New Orleans, 1975.

[17] F. Reggiani and F. Saccomanno, "Consideration upon stability margins with special regard to the effect of generator excitation system and voltage regulation characteristics", <u>CIGRÉ</u>, Paris, 1966, paper 330.

[18] A.S. Aldred, "Electronic analogue computer simulation of multi-machine power-system networks", <u>Proc. IEE</u>, vol. 109, Pt. A, 1962, p. 195.

[19] D.L. Johnson and J.B. Ward, "The solution of power system stability problems by means of digitial computers", <u>Trans. AIEE</u>, vol. 75, 1957, p. 1321.

[20] W.D. Humpage, "Structure for multinode-power-system dynamic-analysis methods", <u>Proc. IEE</u>, 1973, vol. 120, p. 853.

[21] F.J. Evans, R.B. Robinson and T. Wilson, "Model power systems", I.E.(Aust.) Trans., vol. EE6, 1970, p. 53.

[22] S.E. Blanch, K. Morsztyn and T. Dillon, "An electronic three phase turbo-generator model suitable for use in a hybrid configuration with a minicomputer", Int. J. Elect. Enging Educ., vol. 12, 1975, p. 338.

[23] F.P. Demello and C. Concordia, "Concepts of synchronous machine stability as affected by excitation control", IEEE Trans., vol. PAS-88, 1969, p. 316.

[24] H.A.M. Moussa and Y.N. Yu, "Dynamic interaction of multi-machine power system and excitation control", IEEE Trans., vol. PAS-93, 1974, p. 1150.

[25] A.M.A. Hamdan and F.M. Hughes, "Analysis and design of power system stabilisers", Int. J. Control, vol. 26, 1977, p. 769.

[26] J.M. Undrill, "Dynamic stability calculations for an arbitrary number of interconnected synchronous machines", IEEE Trans., vol. PAS-87, 1968, p. 835.

[27] C.A. Stapleton, "Root-locus study of synchronous machine regulation", Proc. IEE, vol. 111, 1964, p. 761

[28] V.A. Venikov, "Transient phenomena in electrical power systems", Pergamon, 1965.

[29] R.H. Craven, V.A. Stroev and H.R. Outhred, "Multi-machine stability analysis using the Newton-Raphson load flow and the domain separation method", Proc. 9th PICA Conf., New Orleans, 1975, p. 158.

[30] H. Goldstein, "Classical mechanics", Addison-Wellesley Publishing Co., Reading, Mass., 1950.

[31] C.A. Desoer, "Modes in linear circuits", IRE Trans. on Circuit Theory, vol. CT-7, 1960, p. 211.

[32] A.T. Wilson et al., "Investigation and control of the damping of power system oscillations", Proc. IFAC Symposium, automatic control and protection of electric power systems, Melbourne, 1977, p. 49.

[33] H.K. Messerle and R.W. Bruck, "Steady-state stability of synchronous generators as affected by regulators and governors", Proc. IEE, vol. 103C, 1956, p. 24.

[34] L.J. Jacovides and B. Adkins, "Effect of excitation regulation on synchronous-machine stability", Proc. IEE, vol. 113, 1966, p. 1021.

[35] A.G.J. MacFarlane, "A survey of some recent advances in linear multivariable feedback theory", Automatica, vol. 8, 1972, p. 455.

[36] H.H. Rosenbrock, "Computer-aided control system design", Academic Press, 1974.

[37] F.M. Hughes and A.M.A. Hamdan, "Design of turboalternator excitation controllers using multivariable frequency-response methods", Proc. IEE, vol. 123, 1976, p. 901.

[38] S.I. Ahson and H. Nickolson, "Improvement of turbo-alternator response using the inverse Nyquist array method", Int. J. Control, vol. 23, 1976, p. 657.

[39] J.R. Bumby and C. Preece, "Decoupling the transient dynamics of adjacent alternators", IEEE Trans., vol. PAS-94, 1975, p. 1147.

[40] P.K. Muttik and M.J. Gibbard, "An application of multivariable control theory to the study of multi-machine power system dynamic behaviour", I.E.(Aust.) Trans., vol. EE14, 1978, p.

[41] F. Fallside and H. Seraji, "Pole-shifting procedure for multivariable systems using output feedback", Proc. IEE, vol. 118, 1971, p. 1648.

[42] W.G. Heffron and R.A. Phillips, "Effect of modern amplidyne voltage regulators on underexcited operation of large turbine generators", AIEE Trans., vol. 71, 1952, p. 692.

[43] G. Shackshaft, "General purpose turbo-alternator model", Proc. IEE, vol. 110, 1963, p. 703.

[44] K. Reichert and N. Leon, "Computation methods and models for investigating the stability of large synchronous machines", Brown Boveri Rev., vol. 61, 1974, p. 480.

[45] Y.N. Yu and C. Siggers, "Stabilization and optimal control signals for a power system", IEEE Trans., vol. PAS-90, 1971, p. 1469.

[46] V.M. Raina, J.H. Anderson, W.J. Wilson and V.H. Quintana, "Optimal output feedback control of power systems with high speed excitation systems", IEEE Trans., vol. PAS-95, 1976, p. 677.

[47] A.L. Whiteley, "The theory of servo systems,with particular reference to stabilisation", J.IEE, vol. 93, pt. II, 1946, p. 353.

[48] D. Graham and R.C. Lathrop, "The synthesis of 'optimum' transient response: criteria and standard forms", AIEE Trans., vol. 72, pt. II, 1953, p. 273.

[49] B.J. Kabriel, "Choosing power-system voltage-regulator parameters by use of standard forms", Proc. IEE, vol. 117, 1970, p. 1809.

[50] V.A. Phung and M.J. Gibbard, "Practical implementation on a 5 KVA synchronous generator of an adaptive excitation controller strategy for a wide range of operating conditions", Proc. IEE, vol. 125, 1978, p. 1009.

[51] R. Kasturi and P. Doraju, "Sensitivity analysis of power systems", IEEE Trans., vol. PAS-88, 1969, p. 1521.

[52] W.J. Wilson, V.M. Raina and J.H. Anderson, "Nonlinear output feedback excitation controller design based on nonlinear optimal control and identification methods", IEEE PES Summer Meeting, 1976, paper A 76 343-4.

[53] A.S. Aldred and G. Shackshaft, "A frequency-response method for the predetermination of synchronous machine stability", Proc. IEE, vol. 107C, 1960, p. 2.

[54] G. Shackshaft, "Results of stability tests on an underexcited 120 MW generator", Proc. IEE, vol. 119, 1972, p. 175.

[55] R.P. Schulz, W.D. Jones, D.N. Ewart, "Dynamic models of turbine generators derived from solid rotor equivalent circuits", IEEE Trans., vol. PAS-92, 1973, p. 926.

[56] P.L. Dandeno, R.L. Hauth and R.P. Schulz, "Effects of synchronous machine modelling in large scale system studies", IEEE Trans., vol. PAS-92, 1973, p. 574.

[57] T. Wilson and V.J. Gosbell, "Stationary d.c. decay tests on a 50 MW turbogenerator to obtain q-axis parameters", IE(Aust.) Trans., vol. EE14, 1978, p. 97.

[58] G. Shackshaft, "Generator parameters for stability studies", CIGRÉ, Paris, 1976, paper 32-15.

[59] IEEE Committee Report, "Dynamic models for steam and hydro turbines in power system studies", IEEE Trans., vol. PAS-92, 1973, p. 1904.

[60] J.M. Stephenson and A.H.M.S. Ula, "Dynamic-stability analysis of synchronous machines including damper circuits, automatic voltage regulator and governor", Proc. IEE, vol. 124, 1977, p. 681.

[61] V.M. Raina, V.H. Quintana, M.A. Zhody and J.H. Anderson, "Excitation system stabiliser design through minimization techniques", IEEE PES Summer Meeting, 1975, paper A 75 456-4.

[62] V.M. Raina, J.H. Anderson, W.J. Wilson and V.H. Quintana, "Optimal output feedback control of power systems with high-speed excitation systems", IEEE Trans., vol. PAS-95, 1976, p. 677.

[63] L.K. Timothy and B.E. Bona, "State-space analysis: an introduction", McGraw Hill, 1968, pp. 180-187.

[64] Ö. Huseyin, A. Elmasli and E. Sezer, "Stability and control of a power system using inverse Nyquist array design technique", IFAC Symposium on Control in Power Electronics and Electrical Drives, Dusseldorf, 1974, p. 253.

[65] G.W. Stagg and A.H. El-Abiad, "Computer methods in power systems analysis", McGraw-Hill, 1968.

[66] O.I. Elgerd, "Electric energy systems theory: an introduction", McGraw-Hill, 1971.

[67] B.T. Smith et al., "Matrix eigensystem routines - EISPACK Guide", Springer, Berlin, 1974.

[68] R. Lamacraft, "LPPLOT - a line printer plotting package", (available from above author, C/- Waite Agricultural Research Institute, South Australia).

[69] R.H. Craven and H.R. Outhred, "The effects of load and machine modelling on small disturbance stability studies", IFAC Symposium, Melbourne, 1977.

[70] T.J. Hammons and D.J. Winning, "Comparisons of synchronous-machine models in the study of the transient behaviour of electrical power systems", Proc. IEE, vol. 118, 1971, p. 1442.

[71] W.B. Jackson and R.L. Winchester, "Direct- and quadrature-axis equivalent circuits for solid-rotor turbine generators", IEEE Trans., vol. PAS-88, 1969, p. 1121.

[72] G.A. Bekey and W.J. Karplus, "Hybrid Computation", Wiley, 1968.

[73] D.K. Faddeev and D.N. Fadeeva, "Computational methods of linear algebra", Freeman, 1963.

[74] M.J. Bosely et al., "The determination of transfer functions from state variable models", Automatica, vol. 8, 1972, p. 213.

[75] K.C. Daly, "A computational procedure for transfer-function evaluation", Int. J. Control, vol. 20, 1974, p. 569.

[76] B. Kouvaritakis, "A geometric approach to the inversion of multivariable systems", Int. J. Control, vol. 24, 1976, p. 609.

[77] A.J.J. Van Der Weiden, "Inversion of rational matrices", Int. J. Control, vol. 25, 1977, p. 393.

[78] G.J. Rogers and A.C. Ioannides, "Digital computation of frequency response", Proc. IEE, vol. 125, 1978, p. 244.

[79] H. Glavitsch, "Power system control and protection - the interaction of new and existing concepts in providing economic and reliable supply", Keynote address, IFAC Symposium control and protection of electric power systems, Melbourne, 1977.

[80] K.C. Daly and P.J. Mason, "Extended pseudodiagonalisation procedure for dominance improvement", Proc. IEE, vol. 126, 1979, p. 113.

[81] P.J. Nolan, N.K. Sinha and R.T.H. Alden, "Optimization of turbo-alternator dynamic response using state feedback decoupling", Int. J. Control, vol. 19, 1974, p. 1177.

[82] P.L. Falb and W.A. Wolovich, "Decoupling in the design and synthesis of multivariable control systems", IEEE Trans., vol. AC-12, 1967, p. 651.

[83] H.H. Rosenbrock, "State-space and multivariable theory", Nelson, 1970.

[84] G. D'Ans, H. Glavitsch and L.M. Panis, "An evaluation of present day excitation system control of turbo-generators", IFAC Symposium on the automatic control and protection of electric power system, Melbourne, 1977.

[85] E. Irving, J.P. Barret, C. Charcossey and J.P. Monville, "Improving Power Network Stability and Unit Stress with Adaptive Generator Control", Automatica, Vol. 15, 1979.